Theory of electronically nonadiabatic quantum reaction dynamics

Thesis by

Ravinder Abrol

In Partial Fulfillment of the Requirements

for the Degree of

Doctor of Philosophy

California Institute of Technology

Pasadena, California

2003

(Defended 26 November 2002)

Dedicated to my parents...

...for their boundless support and patience

Acknowledgements

My stay at Caltech has been a very fruitful, rewarding and enjoyable experience that I will cherish forever. This experience was made possible by the presence of a great set of people around me, who never let me feel that I was living so far away from my family. First and foremost, I would like to acknowledge the constant support and encouragement of my research adviser Professor Aron Kuppermann, who along with Roza treated me like family and took very good care of me. Interaction with Aron has not only helped me in my professional development, but also strengthened my belief in a satisfying scientific pursuit. At every stage of this work, he provided full intellectual freedom without making me loose sight of the big picture and made sure that all resources were available whenever needed. I thank him for being an excellent adviser and am already looking forward to working with him after I leave this place. My thesis committee members (besides Aron) Prof. Vince McKoy, Prof. Harry Gray and Prof. Rudy Marcus along with Prof. Mitchio Okumura have been excellent mentors and provided a lot of encouragement over the years.

The time I spent in the lab was made enjoyable by: Desheng Wang, who was always available for serious scientific discussions or just casual chat; Stephanie Rogers, who helped me when I joined the group and over the years; and finally Mark Wu and Ken Museth, both of whom helped me with many problems. Sharon Brunett from Center of Advanced Computing Research provided precious help with porting of our scattering code to MPI message passing system. It has been a pleasure to collaborate with Prof. David Yarkony (Johns Hopkins University), Prof. Laurent Wiesenfeld (University of Grenoble, France), Dr. Vidyasankar Sundaresan (The Scripps Research Institute), Dr. Rick Muller (Caltech) and Bruce Lambert (Caltech) on different projects over the years, some of which will continue even after I leave Caltech. The work in this thesis has been supported in part by NSF Grants

CHE-9810050 and CHE-0138091. I would also like to thank Dr. Prashant Purohit (Caltech) for suggesting the derivation given in Appendix 4.A of Chapter 4 of this thesis. Ms. Billie Tone has been a lot of fun to work and chat with over the years. Weitekamp group and Zewail group members have been great neighbours. Prof. N. Sathyamurthy (Indian Institute of Technology, Kanpur, India) has provided a lot of encouragement to my scientific ambitions.

Outside the lab, my experience has been made truely memorable by Tara, Sandeep, Vidya, Kirana, Goutam, Sulekha, Nitin, Amit, Ramesh, Shachi, MA, Suresh, Supraja, Ganesh, Anu, Jeetu, Nandita, Prakash, Swami, Ashish, Anu, Harish, Anitha, Sujata, Neha, Tejaswi, Pratip, Rajesh, Arjun, Prashant, Abhijit, Parandeh, Victoria, Dela, David, Hans Michael, Hsing, Stephanie Chow, Michael van Dam, Michael Fleming, Jim Kempf, Roni, Shervin, Office of International Student Programs and others. The cricket games, red-door coffee breaks, potlucks, international orientation, soccer games with the Chemistry team Kicking Buck and OASIS programs were times very well spent. My other friends in India/USA, who include Sushant, Sachchidanand, Anju, Suman, Sangeeta, Rajiv, Anjali, Monika, Aditya, Deepak, Manoj, Anand, Saurabh, Vishy, Kaustav, Neelanjana, Jonaki, Shankarshan and a few others provided great times chatting over the phone or in person whenever we met. Chhavi and her family never let me feel that I was living so far away from home and took very good care of me. She has provided tremendous support and encouragement every step of the way. The journey to the completion of this thesis would have been much harder without her.

Finally, my extended family back home receives all the kudos for their patience and constant encouragement over the years. My Shibu Mama and Sushma Mami have provided a rock solid foundation and support to me without which I wouldn't be here. My parents have taught me honesty and diligence and encouraged me to pursue anything that makes me happy. Their love and support has made me believe in myself and I dedicate this thesis to them and their life-long hard work.

Abstract

In most quantum descriptions of chemical reactions, the Born-Oppenheimer (BO) approximation is invoked that separates the motion of light electrons and heavy nuclei, thereby restricting the motion of those nuclei to a single adiabatic electronic state. Intersections between neighboring electronic states are more common in molecular systems of interest to chemistry and biology than in diatomic molecules. The picture is further complicated due to nonadiabatic couplings which can be present in these systems even in the absence of intersections between electronic states. These couplings are solely responsible for all nonadiabatic effects in chemical and biological processes. For understanding these nonadiabatic effects, the BO picture needs to be replaced by the general Born-Huang (BH) description, in which the nuclei can sample an arbitrary number of electronic states.

A general BH treatment is presented for a polyatomic system evolving on n adiabatic electronic states. All nonadiabatic couplings are considered in this adiabatic representation. These couplings can be singular for electronically degenerate nuclear geometries. The presence of these nonadiabatic couplings (even if not singular) can lead to numerical inefficiencies in the solution of the corresponding nuclear motion Schrödinger equation. This problem is circumvented by going to a diabatic representation, in which these couplings are not only never singular but are also minimized over the entire dynamically important nuclear configuration space. This BH description is applied to the benchmark triatomic system H_3 by obtaining an optimal diabatic representation of its lowest two adiabatic electronic states. A two-electronic-state quantum dynamics formulation is also presented, which, in addition to providing reaction cross sections over a broad energy range, will also enable a quantitative test of the validity of the BO approximation.

Contents

Chapter 1 Introduction

Electronic transitions (excitations or deexcitations) can take place during the course of a chemical reaction and have important consequences for its dynamics. The motions of electrons and nuclei were first analyzed in a quantum-mechanical framework by Born and Oppenheimer [1], who separated the motion of the light electrons from that of the heavy nuclei and assumed that the nuclei moved on a single adiabatic electronic state or potential energy surface (PES). This Born-Oppenheimer (BO) approximation can break down due to the presence of strong nonadiabatic couplings between degenerate electronic states (due to conical, parabolic or glancing intersections between those states) or between the near-degenerate ones (due to avoided crossings). These couplings allow for the motion of nuclei on coupled multiple adiabatic electronic states, with the BO approximation replaced by the Born-Huang expansion [2, 3] in which an arbitrary number of electronic states can be included. A recent volume of *Advances in Chemical Physics* [4] deals with understanding the issues surrounding the role played by degenerate electronic states in determining the mechanism and outcome of many chemical processes.

These nonadiabatic couplings that give rise to electronic transtions can be classified into two categories: (a) Radial couplings, which have been treated by Zener [5], Landau [6] and others [7–12], arise due to translational, vibrational and angular motions of the atomic or molecular species involved in the chemical process. These couplings allow for transitions to occur between electronic states of the same symmetry. (b) Rotational couplings, which have been studied by Kronig [13] and others [14–20], arise as a result of a transformation of molecular coordinates from a space-fixed (SF) frame to a body-fixed (BF) one due to the conservation of total electron plus nuclear angular momentum. These couplings allow for transitions between electronic states of the same as well as of different symmetries.

An important consequence of the presence of degenerate electronic states is the geometric phase effect. For a polyatomic system involving N atoms, where $N \geq 3$, any two adjacent adiabatic electronic states can be degenerate for a set of nuclear geometries even if those electronic states have the same symmetry and spin multiplicity [21]. These intersections occur more frequently in such polyatomic systems than in the diatomic world. The reason is that these systems possess three or more internal nuclear motion degrees of freedom, and only two independent relations between three electronic Hamiltonian matrix elements (in a simple two-electronic-state picture) are sufficient for the existence of doubly degenerate electronic energy eigenvalues. As a result, these relations can easily be satisfied explaining thereby the frequent occurrence of intersections. If the lowest order terms in the expansion of these elements in displacements away from the intersection geometry are linear (as is usually the case), these intersections are conical, the most common type of intersection. Assuming the adiabatic electronic wave functions of the two intersecting states to be real and as continuous as possible in nuclear coordinate space, if the polyatomic system is transported along a closed loop in that space (a so-called pseudorotation) that encircles one conical intersection geometry, these electronic wave functions must change sign [21, 22]. This change of sign requires the adiabatic nuclear wave functions to undergo a compensatory change of sign, known as the geometric phase (GP) effect [23–27], to keep the total wave function single-valued. This sign change of the nuclear wave function, which is a special case of Berry's geometric phase [26], is also referred to as the molecular Aharonov-Bohm effect [28] and has important consequences for the structure and dynamics of the polyatomic system being considered, as it greatly affects the nature of the solutions of the corresponding nuclear motion Schrödinger equation [27].

The dynamics of chemical reactions on a single ground adiabatic electronic PES has been studied extensively over the last few decades using accurate quantum-mechanical time-dependent and time-independent methods. These studies have been successfully applied to triatomic [29–31] and tetraatomic [32–34] reactions in the ab-

sence of conical intersections. In the last decade or so, these studies have included indirectly the effect of the first-excited adiabatic electronic state, that intersects conically with the ground state, by introducing the GP effect through appropriate boundary conditions on the adiabatic nuclear wave function corresponding to the ground electronic state [35–41]. The reaction rates (products of initial relative velocities by integral cross sections) for the D + H_2 reaction, obtained with the GP effect included [37], were in much better agreement with the experimental results [42–45] than those obtained with the GP effect excluded. Although the GP effect is certainly more pronounced at resonance energies [46], its importance for differential cross sections has been the topic of hot debate recently [40, 41].

Many studies have appeared in the last few years that include two or more excited electronic states and nonadiabatic couplings between them to study nonadiabatic behavior in chemical reactions. The effect of spin-orbit couplings on electronically nonadiabatic transitions has been demonstrated for many chemical systems [47–56]. The photodissociation of triatomic molecules like O_3 and H_2S has been studied on their conically intersecting potential energy surfaces (PESs) [57, 58]. The benchmark H + H_2 reaction has also been studied on its lowest two conically intersecting PESs, but only for total angular momentum quantum number $J = 0$ [59]. Most of these studies have been made possible due to the availability of realistic *ab initio* electronic PESs and their nonadiabatic couplings [60]. These nonadiabatic couplings have very interesting properties that have a forebearing on the behavior of molecular systems and are currently the topic of active interest [61]. The singular nature of these couplings at the conical intersections of two adiabatic electronic states introduces numerical difficulties in the solution of the corresponding coupled adiabatic nuclear motion Schrödinger equations. These difficulties can be circumvented by transforming the electronically adiabatic representation into a quasi-diabatic one [62–74], in which the nonadiabatic couplings still appear but are not singular.

In this thesis, a rigorous quantum-mechanical formalism is introduced for studying the dynamics of a polyatomic system (comprising of N atoms) on n electronically

adiabatic states, interacting due to the presence of nonadiabatic couplings. The spin-spin and spin-orbit interactions are not considered. These interactions can be introduced subsequently as perturbative corrections, if they are not too large. This formalism is then applied to a triatomic system in a two-electronic-state Born-Huang approximation. The overview of the thesis is as follows.

In Chapter 2, the adiabatic n-electronic-state coupled nuclear motion Schrödinger equations are presented for an N-body system and the properties of first-derivative and second-derivative nonadiabatic couplings are discussed. The presence of first-derivative couplings, that may be singular at electonically degenerate nuclear configurations, can lead to numerical inefficiencies in the solution of the adiabatic Schrödinger equations. A diabatic representation is defined through an adiabatic-to-diabatic transformation that minimizes the magnitude of the first-derivative nonadiabatic couplings in the diabatic nuclear motion Schrödinger equations. This formalism is applied in Chapters 3 through 5 to a triatomic system in the presence of two interacting electronic states.

In Chapter 3, accurate first-derivative nonadiabatic coupling vectors are presented for H_3 system that exhibits a conical intersection between its ground ($1\ ^2A'$) and its first-excited ($2\ ^2A'$) electronic states. These coupling vectors, which are singular at the conical intersection geometries, and the two electronic states they couple are fitted using their *ab initio* data and compared with their approximate analytical counterparts obtained by Varandas *et al.* [75] using the double many-body expansion (DMBE) method. Contour integrals of the *ab initio* first-derivative couplings, calculated along closed loops around the abovementioned conical intersection, contain important properties of these couplings besides information about possible interactions between the $2\ ^2A'$ and the second-excited ($3\ ^2A'$) states. The second-derivative couplings are approximated by using the abovementioned accurate first-derivative coupling vectors in a two-electronic-state model.

These coupling vectors between the corresponding electronically adiabatic states can be decomposed into longitudinal (*removable*) and transverse (*nonremovable*)

parts. This property is used in Chapter 4 to obtain a diabatic representation for the lowest two adiabatic electronic states of H_3, in which singular nonadiabatic couplings are replaced by non-singular ones. The adiabatic-to-diabatic transformation is achieved by solving a three-dimensional Poisson equation over the entire internal nuclear configuration space. The boundary conditions imposed on this solution minimize the magnitude of the *nonremovable* couplings that survive in the diabatic representation. This makes the diabatic language a convenient one for studying quantum reactive scattering on more than one interacting electronic states.

In Chapter 5, an electronically nonadiabatic reactive scattering formalism is presented for triatomic reactions involving two coupled adiabatic electronic states in adiabatic and diabatic languages. This formalism is an extension of the time-independent coupled-channel hyperspherical coordinate method [18] used in the past to study such reactions on a single adiabatic Born-Oppenheimer (BO) electronic state. Both adiabatic and diabatic representations lead to a set of coupled nuclear motion Schrödinger equations that can be solved to obtain scattering matrices, which then furnish the differential and integral cross sections. The advantages and disadvantages of the two languages are discussed. This formalism will not only provide reaction cross sections over a broad energy range (including those energies where the BO approximation breaks down), but will also enable a comparison with the cross sections obtained using only the ground adiabatic PES (with the geometric phase included), to estimate the validity of the one-electronic-state BO approximation as a function of energy.

Bibliography

[1] M. Born and J. R. Oppenheimer, Ann. Phys. (Leipzig) **84**, 457 (1927).

[2] M. Born, Nachr. Akad. Wiss. Gött. Math.-Phys. Kl. Article No. 6, 1 (1951).

[3] M. Born and K. Huang, *Dynamical Theory of Crystal Lattices* (Oxford University Press, Oxford, 1954), pp. 166-177 and 402-407.

[4] *The Role of Degenerate States in Chemistry: A Special Volume of Advances in Chemical Physics*, eds. M. Baer and G. D. Billing (Wiley-Interscience, New York, 2002), Vol. 124.

[5] C. Zener, Proc. R. Soc. London Ser. A **137**, 696 (1932).

[6] L. D. Landau, Phys. Z. Sowjetunion **2**, 46 (1932).

[7] E. C. G. Stuckelberg, Helv. Phys. Acta. **5**, 369 (1932).

[8] N. Rosen and C. Zener, Phys. Rev. **40**, 502 (1932).

[9] W. Lichten, Phys. Rev. **131**, 229 (1963).

[10] E. E. Nikitin, in *Chemische Elementarprozesse*, edited by H. Hartmann (Springer-Verlag, Berlin, 1968), 43.

[11] F. T. Smith, Phys. Rev. **179**, 111 (1969).

[12] M. S. Child, Mol. Phys. **20**, 171 (1971).

[13] R. de L Kronig, *Band Spectra and Molecular Structure*, Cambridge University Press, New York, 1930, 6.

[14] D. R. Bates, Proc. R. Soc. London Ser. A **240**, 437 (1957).

[15] D. R. Bates, Proc. R. Soc. London Ser. A **257**, 22 (1960).

[16] W. R. Thorson, J. Chem. Phys. **34**, 1744 (1961).

[17] D. J. Kouri and C. F. Curtiss, J. Chem. Phys. **44**, 2120 (1966).

[18] R. T. Pack and J. O. Hirschfelder, J. Chem. Phys. **49**, 4009 (1968).

[19] C. Gaussorgues, C. Le Sech, F. Mosnow-Seeuws, R. McCarroll and A. Riera, J. Phys. B **8**, 239 (1975).

[20] C. Gaussorgues, C. Le Sech, F. Mosnow-Seeuws, R. McCarroll and A. Riera, J. Phys. B **8** 253 (1975).

[21] G. Herzberg and H. C. Longuet-Higgins, Discussion Faraday Soc. **35**, 77 (1963).

[22] H. C. Longuet-Higgins, Proc. R. Soc. London A **344**, 147 (1975).

[23] H. C. Longuet-Higgins, Adv. Spectrosc. **2**, 429 (1961).

[24] C. A. Mead and D. G. Truhlar, J. Chem. Phys. **70**, 2284 (1979).

[25] C. A. Mead, Chem. Phys. **49**, 23 (1980).

[26] M. V. Berry, Proc. Roy. Soc. London, Ser. A **392**, 45 (1984).

[27] A. Kuppermann, in *Dynamics of Molecules and Chemical Reactions*, edited by R. E. Wyatt and J. Z. H. Zhang (Marcel Dekker, New York, 1996), pp. 411-472.

[28] Y. Aharonov and D. Bohm, Phys. Rev. **115**, 485 (1969).

[29] *Theory of Chemical Reaction Dynamics* Vols. I and II, edited by M. Baer (CRC Press, Boca Raton (Florida), 1985).

[30] *Dynamics of Molecules and Chemical Reactions*, edited by R. E. Wyatt and J. Z. H. Zhang (Marcel Dekker, New York, 1996).

[31] G. Nyman and H.-G. Yu, Rep. Prog. Phys. **63**, 1001 (2000).

[32] J. Z. H. Zhang, J. Q. Dai, and W. Zhu, J. Phys. Chem. A **101**, 2746 (1997).

[33] S. K. Pogrebnya, J. Palma, D. C. Clary, and J. Echave, Phys. Chem. Chem. Phys. **2**, 693 (2000).

[34] D. H. Zhang, M. A. Collins and S. Y. Lee, Science **290**, 961 (2000).

[35] Y.-S. M. Wu, A. Kuppermann, and B. Lepetit, Chem. Phys. Lett. **186**, 319 (1991).

[36] Y.-S. M. Wu and A. Kuppermann, Chem. Phys. Lett. **201**, 178 (1993).

[37] A. Kuppermann and Y.-S. M. Wu, Chem. Phys. Lett. **205**, 577 (1993).

[38] Y.-S. M. Wu and A. Kuppermann, Chem. Phys. Lett. **235**, 105 (1995).

[39] A. Kuppermann and Y.-S. M. Wu, Chem. Phys. Lett. **241**, 229 (1995).

[40] B. K. Kendrick, J. Chem. Phys. **112**, 5679 (2000); **114**, 4335 (2001) (E).

[41] A. Kuppermann and Y.-S. M. Wu, Chem. Phys. Lett. **349**, 537 (2001).

[42] D. A. V. Kliner, K. D. Rinen, and R. N. Zare, Chem. Phys. Lett. **166**, 107 (1990).

[43] D. A. V. Kliner, D. E. Adelman and R. N. Zare, J. Chem. Phys. **95**, 1648 (1991).

[44] D. Neuhauser, R. S. Judson, D. J. Kouri, D. E. Adelman, N. E. Shafer, D. A. V. Kliner and R. N. Zare, Science **257**, 519 (1992).

[45] D. E. Adelman, N. E. Shafer, D. A. V. Kliner and R. N. Zare, J. Chem. Phys. **97**, 7323 (1992).

[46] F. Fernandez-Alonso and R. N. Zare, Ann. Rev. Phys. Chem. **53**, 67 (2002).

[47] M. Gilbert and M. Baer, J. Phys. Chem. **98**, 12822 (1994).

[48] G. C. Schatz, J. Phys. Chem. **99**, 7522 (1995).

[49] C. S. Maierle, G. C. Schatz, M. S. Gordon, P. McCabe, and J. N. L. Connor, J. Chem. Soc. Faraday Trans. **93**, 709 (1997).

[50] G. C. Schatz, P. McCabe, and J. N. L. Connor, Faraday Discuss. **110**, 139 (1997).

[51] A. J. Dobbyn, J. N. L. Connor, N. A. Besley, P. J. Knowles, and G. C. Schatz, Phys. Chem. Chem. Phys. **2**, 549 (2000).

[52] T. W. J. Whiteley, A. J. Dobbyn, J. N. L. Connor and G. C. Schatz, Phys. Chem. Chem. Phys. **2**, 549 (2000).

[53] M. H. Alexander, H.-J. Werner, and D. E. Manolopoulos, J. Chem. Phys. **109**, 5710 (1998).

[54] M. H. Alexander, D. E. Manolopoulos and H.-J. Werner, J. Chem. Phys. **113**, 11084 (2000).

[55] T. Takayanagi and Y. Kurosaki, J. Chem. Phys. **113**, 7158 (2000).

[56] V. Aquilanti, S. Cavalli, D. De Fazio, and A. Volpi, Int. J. Quant. Chem. **85**, 368 (2001).

[57] H. Flöthmann, C. Beck, R. Schinke, C. Woywod and W. Domcke, J. Chem. Phys. **107**, 7296 (1997).

[58] D. Simah, B. Hartke and H.-J. Werner, J. Chem. Phys. **111**, 4523 (1999).

[59] S. Mahapatra, H. Köppel and L. S. Cederbaum, J. Phys. Chem. A **105**, 2321 (2001).

[60] B. H. Lengsfield and D.R. Yarkony, in State-selected and State-to-State Ion-Molecule Reaction Dynamics: Part 2 Theory, Vol. 82, edited by M. Baer and C.-Y. Ng (Wiley, New York, 1992), pp. 1-71.

[61] M. Baer, Phys. Rep. **358**, 75 (2002).

[62] T. Pacher, L. S. Cederbaum, and H. Köppel, J. Chem. Phys. **89**, 7367 (1988).

[63] T. Pacher, C. A. Mead, L. S. Cederbaum, and H. Köppel, J. Chem. Phys. **91**, 7057 (1989).

[64] V. Sidis, in *State-selected and State-to-State Ion-Molecule Reaction Dynamics*: Part 2 Theory, Vol. 82, edited by M. Baer and C.-Y. Ng (Wiley, New York, 1992), pp. 73-134.

[65] M. Baer and R. Englman, Mol. Phys. **75**, 293 (1992).

[66] K. Ruedenberg and G. J. Atchity, J. Chem. Phys. **99**, 3799 (1993).

[67] M. Baer and R. Englman, Chem. Phys. Lett. **265** 105 (1997).

[68] M. Baer, J. Chem. Phys. **107** 2694 (1997).

[69] B. K. Kendrick, C. A. Mead, and D. G. Truhlar, J. Chem. Phys. **110**, 7594 (1999).

[70] M. Baer, R. Englman, and A. J. C. Varandas, Mol. Phys. **97**, 1185 (1999).

[71] A. Thiel and H. Köppel, J. Chem. Phys. **110**, 9371 (1999).

[72] D. R. Yarkony, J. Chem. Phys. **112**, 2111 (2000).

[73] R. Abrol and A. Kuppermann, J. Chem. Phys. **116**, 1035 (2002).

[74] H. Nakamura and D. G. Truhlar, J. Chem. Phys. **117**, 5576 (2002).

[75] A. J. C. Varandas, F. B. Brown, C. A. Mead, D. G. Truhlar, and N. C. Blais, J. Chem. Phys. **86**, 6258 (1987).

Chapter 2 Born-Huang treatment of an N-body system

2.1 Introduction

Consider a polyatomic system consisting of N_{nu} nuclei (where $N_{nu} \geq 3$) and N_{el} electrons. In the absence of any external fields, we can rigorously separate the motion of the center of mass $\overline{G}$ of the whole system as its potential energy function V is independent of the position vector of $\overline{G}$ ($\mathbf{r}_{\overline{G}}$) in a laboratory-fixed frame with origin O. This separation introduces, besides $\mathbf{r}_{\overline{G}}$, the Jacobi vectors $\mathbf{R}'_\lambda \equiv (\mathbf{R}'_{\lambda_1}, \mathbf{R}'_{\lambda_2}, ..., \mathbf{R}'_{\lambda_{N_{nu}-1}})$ and $\mathbf{r}' \equiv (\mathbf{r}'_1, \mathbf{r}'_2, ..., \mathbf{r}'_{N_{el}})$ for nuclei and electrons, respectively [1]. These Jacobi vectors are simply related to the position vectors of those nuclei and electrons in the laboratory-fixed frame. λ refers to an arbitrary clustering scheme for the N_{nu} nuclei [2,3] and helps specify different product arrangement channels during a chemical reaction.

The kinetic energy operator $\widehat{T}_{\overline{G}}$ of the center of mass $\overline{G}$ can be omitted, since no external fields act on the system. The internal kinetic energy operator $\widehat{T}^{int}$ is given by

$$\widehat{T}^{int} = \widehat{T}^{int}_{nu} + \widehat{T}_{el}, \tag{2.1}$$

where $\widehat{T}^{int}_{nu}$ and $\widehat{T}_{el}$ are respectively internal nuclear and electronic kinetic energy operators in the Jacobi vectors mentioned above. If these Jacobi vectors $\mathbf{R}'_{\lambda_i}$ ($i = 1, 2, ..., N_{nu} - 1$) and $\mathbf{r}'_j$ ($j = 1, 2, ..., N_{el}$) are transformed to their mass-scaled counterparts [3] $\mathbf{R}_{\lambda_i}$ and $\mathbf{r}_j$, the kinetic energy operators have relatively simple expressions given by

$$\widehat{T}^{int}_{nu} = -\frac{\hbar^2}{2\mu}\nabla^2_{\mathbf{R}_\lambda} \quad \text{and} \quad \widehat{T}_{el} = -\frac{\hbar^2}{2\nu}\nabla^2_{\mathbf{r}} \tag{2.2}$$

where

$$\nabla^2_{\mathbf{R}_\lambda} \equiv \sum_{i=1}^{N_{nu}-1} \nabla^2_{\mathbf{R}_{\lambda_i}} \quad \text{and} \quad \nabla^2_{\mathbf{r}} \equiv \sum_{j=1}^{N_{el}} \nabla^2_{\mathbf{r}_j} \tag{2.3}$$

with the laplacians on the left of these equivalence relations being independent of the choice of the clustering scheme λ. The transformation of Jacobi vectors to the mass-scaled ones is defined by

$$\mathbf{R}_{\lambda_i} = \left(\frac{\mu_{\lambda_i}}{\mu}\right)^{1/2} \mathbf{R}'_{\lambda_i} \quad \text{and} \quad \mathbf{r}_j = \left(\frac{\nu_j}{\nu}\right)^{1/2} \mathbf{r}'_j, \tag{2.4}$$

where

$$\mu = \left(\frac{1}{M}\prod_{i=1}^{N_{nu}} M_i\right)^{1/(N_{nu}-1)} \quad \text{and} \quad \nu = m_{el}\left(\frac{M}{M+N_{el}m_{el}}\right)^{1/N_{el}} \tag{2.5}$$

are the effective reduced masses of the nuclei and electrons, respectively, with M_i being the mass of the i^{th} nucleus. μ_{λ_i} and ν_j in Eq. (2.4) are the effective masses [1] associated with the corresponding vectors $\mathbf{R}'_{\lambda_i}$ and $\mathbf{r}'_j$, with

$$\nu_j = \frac{[M+(j-1)m_{el}]m_{el}}{M+jm_{el}} \tag{2.6}$$

In Eqs. (2.5) and (2.6), M is the total mass of the nuclei and m_{el} is the mass of one electron. Using Eq. (2.2), the system's internal kinetic energy operator is given in terms of the mass-scaled Jacobi vectors by

$$\widehat{T}^{int} = -\frac{\hbar^2}{2\mu}\nabla^2_{\mathbf{R}_\lambda} - \frac{\hbar^2}{2\nu}\nabla^2_{\mathbf{r}} \tag{2.7}$$

If V is the total coulombic potential between all the nuclei and electrons in the system, then, in the absence of any spin-dependent terms, the electronic Hamiltonian $\widehat{H}^{el}$ is given by

$$\widehat{H}^{el}(\mathbf{r};\mathbf{q}_\lambda) = -\frac{\hbar^2}{2\nu}\nabla^2_{\mathbf{r}} + V(\mathbf{r};\mathbf{q}_\lambda), \tag{2.8}$$

where $\mathbf{q}_\lambda$ is a set of $3(N_{nu}-2)$ internal nuclear coordinates obtained by removing from the set $\mathbf{R}_\lambda$ three Euler angles which orient a nuclear body-fixed frame with

respect to the laboratory-fixed (or space-fixed) frame. Due to the small ratio of the electron mass to the total mass of the nuclei, $\nu \approx m_{el}$. This approximation is used in the *ab initio* electronic structure calculations that use the electronic Hamiltonian given in Eq. (2.8) but with the ν replaced by m_{el}. Figure 2.1 illustrates for a three-nuclei, 4-electron system, the corresponding non-mass-scaled Jacobi vectors. The nuclear center of mass G is distinct from the overall system's center of mass $\overline{G}$. This distinction of the centers of mass and the difference between ν and m_{el} is responsible for the so-called mass polarization effect in the electronic spectra of these systems that produces relative shifts in the energy levels of 10^{-4} or less. In actual scattering calculations, these differences are normally ignored as they introduce relative changes in the cross sections of the order of 10^{-4} or less [1].

The electronically adiabatic wave functions $\psi_i^{el,ad}(\mathbf{r};\mathbf{q}_\lambda)$ are defined as eigenfunctions of the electronic Hamiltonian $\widehat{H}^{el}$ with electronically adiabatic potential energies $\varepsilon_i^{ad}(\mathbf{q}_\lambda)$ as their eigenvalues:

$$\widehat{H}^{el}(\mathbf{r};\mathbf{q}_\lambda)\psi_i^{el,ad}(\mathbf{r};\mathbf{q}_\lambda) = \varepsilon_i^{ad}(\mathbf{q}_\lambda)\psi_i^{el,ad}(\mathbf{r};\mathbf{q}_\lambda) \tag{2.9}$$

The electronic Hamiltonian and the corresponding eigenfunctions and eigenvalues are independent of the orientation of the nuclear body-fixed frame with respect to the space-fixed one and hence depend only on $\mathbf{q}_\lambda$. The index i in Eq. (2.9) can span both discrete and continuous values. The $\psi_i^{el,ad}(\mathbf{r};\mathbf{q}_\lambda)$ form a complete orthonormal basis set and satisfy the orthonormality relations

$$\langle \psi_i^{el,ad}(\mathbf{r};\mathbf{q}_\lambda) | \psi_{i'}^{el,ad}(\mathbf{r};\mathbf{q}_\lambda) \rangle_{\mathbf{r}} = \begin{cases} \delta_{i,i'} & \text{for } i \text{ and } i' \text{ discrete} \\ \delta(i-i') & \text{for } i \text{ and } i' \text{ continuous} \\ 0 & \text{for } i \text{ discrete and } i' \text{ continuous or vice versa} \end{cases} \tag{2.10}$$

These electronic wave functions are used in a Born-Huang expansion of the electronuclear wave function, as presented in the next section.

2.2 Born-Huang expansion

The total orbital wave function for this system is given by an electronically adiabatic n-state Born-Huang expansion [4, 5] in terms of this electronic basis set $\psi_i^{el,ad}(\mathbf{r};\mathbf{q}_\lambda)$ as

$$\Psi^{\mathrm{O}}(\mathbf{r},\mathbf{R}_\lambda) = \sum\!\!\!\!\!\!\int_i \chi_i^{ad}(\mathbf{R}_\lambda)\psi_i^{el,ad}(\mathbf{r};\mathbf{q}_\lambda), \tag{2.11}$$

where $\sum\!\!\!\!\!\!\int_i$ is a sum over the discrete and an integral over the continuous values of i. The $\chi_i^{ad}(\mathbf{R}_\lambda)$, which are the coefficients in this expansion, are the adiabatic nuclear motion wave functions. The number of electronic states used in the Born-Huang expansion of Eq. (2.11) can, in most cases of interest, be restricted to a small number n of discrete states, and Eq. (2.11) replaced by

$$\Psi^{\mathrm{O}}(\mathbf{r},\mathbf{R}_\lambda) \approx \sum_{i=1}^{n} \chi_i^{ad}(\mathbf{R}_\lambda)\psi_i^{el,ad}(\mathbf{r};\mathbf{q}_\lambda) \tag{2.12}$$

where n is a small number. This corresponds to restricting the motion of nuclei to only those n electronic states. In particular, if those n states constitute a sub-Hilbert space that interacts very weakly with higher states [6], this would be a very good approximation. The orbital wave function Ψ^{O} satisfies the Schrödinger equation

$$\widehat{H}^{int}(\mathbf{r},\mathbf{R}_\lambda)\Psi^{\mathrm{O}}(\mathbf{r},\mathbf{R}_\lambda) = E\Psi^{\mathrm{O}}(\mathbf{r},\mathbf{R}_\lambda) \tag{2.13}$$

where

$$\widehat{H}^{int}(\mathbf{r},\mathbf{R}_\lambda) = \widehat{T}^{int}(\mathbf{r},\mathbf{R}_\lambda) + V(\mathbf{r};\mathbf{q}_\lambda) \tag{2.14}$$

is the internal Hamiltonian [Eq. (2.7)] of the system that excludes the motion of its center of mass and any spin-dependent terms and E is the system's total energy. The Eq. (2.12) through (2.14) are used next to get the n-electronic state nuclear motion Schrödinger equation.

2.2.1 Adiabatic nuclear motion Schrödinger equation

Let us define $\boldsymbol{\chi}^{ad}(\mathbf{R}_\lambda)$ as an n-dimensional nuclear motion column vector, whose components are $\chi_1^{ad}(\mathbf{R}_\lambda)$ through $\chi_n^{ad}(\mathbf{R}_\lambda)$. The n-electronic-state nuclear motion Schrödinger equation satisfied by $\boldsymbol{\chi}^{ad}(\mathbf{R}_\lambda)$ can be obtained by inserting Eqs. (2.12) and (2.14) into (2.13) and using Eqs. (2.7) through (2.10). The resulting Schrödinger equation can be expressed in compact matrix form as [1]

$$\left[-\frac{\hbar^2}{2\mu}\left\{\mathbf{I}\nabla^2_{\mathbf{R}_\lambda} + 2\mathbf{W}^{(1)ad}(\mathbf{R}_\lambda)\cdot\boldsymbol{\nabla}_{\mathbf{R}_\lambda} + \mathbf{W}^{(2)ad}(\mathbf{R}_\lambda)\right\} + \left\{\boldsymbol{\varepsilon}^{ad}(\mathbf{q}_\lambda) - E\mathbf{I}\right\}\right]\boldsymbol{\chi}^{ad}(\mathbf{R}_\lambda) = \mathbf{0}\,, \tag{2.15}$$

where $\mathbf{I}$, $\mathbf{W}^{(1)ad}$, $\mathbf{W}^{(2)ad}$, and $\boldsymbol{\varepsilon}^{ad}$ are $n \times n$ matrices and $\boldsymbol{\nabla}_{\mathbf{R}_\lambda}$ is the column vector gradient operator in the $3(N_{nu}-1)$-dimensional space-fixed nuclear configuration space. $\mathbf{I}$ is the identity matrix and $\boldsymbol{\varepsilon}^{ad}(\mathbf{q}_\lambda)$ is the diagonal matrix whose diagonal elements are the n electronically adiabatic PESs $\varepsilon_i^{ad}(\mathbf{q}_\lambda)$ $(i = 1, ..., n)$ being considered. All matrices appearing in this n-electronic state nuclear motion Schrödinger equation [Eq. (2.15)] are n-dimensional diagonal except for $\mathbf{W}^{(1)ad}$ and $\mathbf{W}^{(2)ad}$, which are respectively the first- and second-derivative [1, 7–13] nonadiabatic coupling matrices discussed below. These coupling matrices allow the nuclei to sample more than one adiabatic electronic state during a chemical reaction and hence alter its dynamics in an electronically nonadiabatic fashion. It should be stressed that the effect of the geometric phase on Eqs. (2.15) must be added by either appropriate boundary conditions [1, 25] or the introduction of an appropriate vector potential [1, 14, 15].

2.2.2 First-derivative coupling matrix

The matrix $\mathbf{W}^{(1)ad}(\mathbf{R}_\lambda)$ in Eq. (2.15) is an $n \times n$ adiabatic first-derivative coupling matrix whose elements are defined by

$$\mathbf{w}_{i,j}^{(1)ad}(\mathbf{R}_\lambda) = \langle\psi_i^{el,ad}(\mathbf{r};\mathbf{q}_\lambda) \mid \boldsymbol{\nabla}_{\mathbf{R}_\lambda}\psi_j^{el,ad}(\mathbf{r};\mathbf{q}_\lambda)\rangle_{\mathbf{r}} \qquad i,j = 1, ..., n \tag{2.16}$$

These coupling elements are $3(N_{nu}-1)$-dimensional vectors. If the cartesian components of $\mathbf{R}_\lambda$ in $3(N_{nu}-1)$ space-fixed nuclear congifuration space are $X_{\lambda 1}, X_{\lambda 2}, ..., X_{\lambda 3(N_{nu}-1)}$, the corresponding cartesian components of $\mathbf{w}^{(1)ad}_{i,j}(\mathbf{R}_\lambda)$ are

$$\left[\mathbf{w}^{(1)ad}_{i,j}(\mathbf{R}_\lambda)\right]_l = \langle \psi^{el,ad}_i(\mathbf{r};q_\lambda) \mid \frac{\partial}{\partial X_{\lambda l}} \psi^{el,ad}_i(\mathbf{r};q_\lambda)\rangle_{\mathbf{r}} \qquad l=1,2,...,3(N_{nu}-1) \quad (2.17)$$

The matrix $\mathbf{W}^{(1)ad}$ is in general skew-hermitian due to Eq. (2.10) and hence its diagonal elements $\mathbf{w}^{(1)ad}_{i,i}(\mathbf{R}_\lambda)$ are pure imaginary quantities. If we require that the $\psi^{el,ad}_i$ be real, then the matrix $\mathbf{W}^{(1)ad}$ becomes real and skew-symmetric with the diagonal elements equal to zero and the off-diagonal elements satisfying the relation

$$\mathbf{w}^{(1)ad}_{i,j}(\mathbf{R}_\lambda) = -\mathbf{w}^{(1)ad}_{j,i}(\mathbf{R}_\lambda) \qquad i \neq j \quad (2.18)$$

As with any vector, the above non-zero coupling vectors ($\mathbf{w}^{(1)ad}_{i,j}(\mathbf{R}_\lambda),\ i \neq j$) can be decomposed, due to an extension beyond three dimensions [1] of the Helmholtz theorem [16], into a longitudinal part $\mathbf{w}^{(1)ad}_{i,j,lon}(\mathbf{R}_\lambda)$ and a transverse one $\mathbf{w}^{(1)ad}_{i,j,tra}(\mathbf{R}_\lambda)$ according to

$$\mathbf{w}^{(1)ad}_{i,j}(\mathbf{R}_\lambda) = \mathbf{w}^{(1)ad}_{i,j,lon}(\mathbf{R}_\lambda) + \mathbf{w}^{(1)ad}_{i,j,tra}(\mathbf{R}_\lambda), \quad (2.19)$$

where by definition, the curl of $\mathbf{w}^{(1)ad}_{i,j,lon}(\mathbf{R}_\lambda)$ and the divergence of $\mathbf{w}^{(1)ad}_{i,j,tra}(\mathbf{R}_\lambda)$ vanish:

$$\text{curl } \mathbf{w}^{(1)ad}_{i,j,lon}(\mathbf{R}_\lambda) = \mathbf{0} \quad (2.20)$$

$$\boldsymbol{\nabla}_{\mathbf{R}_\lambda} \cdot \mathbf{w}^{(1)ad}_{i,j,tra}(\mathbf{R}_\lambda) = 0 \quad (2.21)$$

The curl in Eq. (2.20) is the skew-symmetric tensor of rank 2, whose k,l element is given by [1, 17]

$$\left[\text{curl } \mathbf{w}^{(1)ad}_{i,j,lon}(\mathbf{R}_\lambda)\right]_{k,l} = \frac{\partial}{\partial X_{\lambda l}}\left[\mathbf{w}^{(1)ad}_{i,j,lon}(\mathbf{R}_\lambda)\right]_k - \frac{\partial}{\partial X_{\lambda k}}\left[\mathbf{w}^{(1)ad}_{i,j,lon}(\mathbf{R}_\lambda)\right]_l \quad k,l=1,2,...,3(N_{nu}-1) \quad (2.22)$$

As a result of Eq. (2.20), a scalar potential $\alpha_{i,j}(\mathbf{R}_\lambda)$ exists for which

$$\mathbf{w}^{(1)ad}_{i,j,lon}(\mathbf{R}_\lambda) = \boldsymbol{\nabla}_{\mathbf{R}_\lambda}\alpha_{i,j}(\mathbf{R}_\lambda) \tag{2.23}$$

At conical intersection geometries, $\mathbf{w}^{(1)ad}_{i,j,lon}(\mathbf{R}_\lambda)$ is singular because of the $\mathbf{q}_\lambda$-dependence of $\psi^{el,ad}_i(\mathbf{r};\mathbf{q}_\lambda)$ and $\psi^{el,ad}_j(\mathbf{r};\mathbf{q}_\lambda)$ in the vicinity of those geometries and therefore so is the $\mathbf{W}^{(1)ad}(\mathbf{R}_\lambda)\cdot\boldsymbol{\nabla}_{\mathbf{R}_\lambda}$ term in Eq. (2.15). As a result of Eq. (2.19), $\mathbf{W}^{(1)ad}$ can be written as a sum of the corresponding skew-symmetric matrices $\mathbf{W}^{(1)ad}_{lon}$ and $\mathbf{W}^{(1)ad}_{tra}$, i.e.,

$$\mathbf{W}^{(1)ad}(\mathbf{R}_\lambda) = \mathbf{W}^{(1)ad}_{lon}(\mathbf{R}_\lambda) + \mathbf{W}^{(1)ad}_{tra}(\mathbf{R}_\lambda) \tag{2.24}$$

This decomposition into a longitudinal and a transverse part, as will be discussed in Sec. 2.3, plays a crucial role in going to a diabatic representation in which this singularity is completely removed. In addition, the presence of the first-derivative gradient term $\mathbf{W}^{(1)ad}(\mathbf{R}_\lambda)\cdot\boldsymbol{\nabla}_{\mathbf{R}_\lambda}\chi^{ad}(\mathbf{R}_\lambda)$ in Eq. (2.15), even for a non-singular $\mathbf{W}^{(1)ad}(\mathbf{R}_\lambda)$ (e.g., for avoided intersections), introduces numerical inefficiencies in the solution of that equation.

2.2.3 Second-derivative coupling matrix

The matrix $\mathbf{W}^{(2)ad}(\mathbf{R}_\lambda)$ in Eq. (2.15) is an $n\times n$ adiabatic second-derivative coupling matrix whose elements are defined by

$$\mathrm{w}^{(2)ad}_{i,j}(\mathbf{R}_\lambda) = \langle\psi^{el,ad}_i(\mathbf{r};\mathbf{q}_\lambda) \mid \nabla^2_{\mathbf{R}_\lambda}\psi^{el,ad}_j(\mathbf{r};\mathbf{q}_\lambda)\rangle_{\mathbf{r}} \qquad i,j=1,...,n \tag{2.25}$$

These coupling matrix elements are scalars due to the presence of the scalar laplacian $\nabla^2_{\mathbf{R}_\lambda}$ in Eq. (2.25). These elements are, in general, complex but if we require the $\psi^{el,ad}_i$ to be real, they become real. The matrix $\mathbf{W}^{(2)ad}(\mathbf{R}_\lambda)$, unlike its first-derivative counterpart, is neither skew-hermitian nor skew-symmetric.

The $\mathrm{w}^{(2)ad}_{i,j}(\mathbf{R}_\lambda)$ are also singular at conical intersection geometries. The decomposition of the first-derivative coupling vector, discussed in the preceding section, also

facilitates the removal of this singularity from the second-derivative couplings, as will be shown in Sec. 2.3. Being scalars, the second-derivative couplings can be easily included in the scattering calculations without any additional computational effort. It is interesting to note that in a one-electronic-state Born-Oppenheimer approximation, the first-derivative coupling element $\mathbf{w}_{1,1}^{(1)ad}(\mathbf{R}_\lambda)$ is rigorously zero (assuming real adiabatic electronic wave functions), but $\mathrm{w}_{1,1}^{(2)ad}(\mathbf{R}_\lambda)$ is not and might be important to predict sensitive quantum phenomena like resonances that can be experimentally verified.

2.3 Adiabatic-to-diabatic transformation

2.3.1 Electronically diabatic representation

As mentioned at the end of Sec. 2.2.2, the presence of the $\mathbf{W}^{(1)ad}(\mathbf{R}_\lambda) \cdot \boldsymbol{\nabla}_{\mathbf{R}_\lambda} \chi^{ad}(\mathbf{R}_\lambda)$ term in the n-adiabatic-electronic-state Schrödinger equation [Eq. (2.15)] introduces numerical inefficiencies in its solution, even if none of the elements of the $\mathbf{W}^{(1)ad}(\mathbf{R}_\lambda)$ matrix is singular.

This makes it desirable to define other representations in addition to the electronically adiabatic one [Eqs. (2.9) through (2.12)], in which the adiabatic electronic wave function basis set used in the Born-Huang expansion Eq. (2.12) is replaced by another basis set of functions of the electronic coordinates. Such a different electronic basis set can be chosen so as to minimize the abovementioned gradient term. This term can initially be neglected in the solution of the n-electronic-state nuclear motion Schrödinger equation and reintroduced later using perturbative or other methods, if desired. This new basis set of electronic wave functions can also be made to depend parametrically, like their adiabatic counterparts, on the internal nuclear coordinates $\mathbf{q}_\lambda$ that were defined after Eq. (2.8). This new electronic basis set is henceforth referred to as "diabatic" and, as is obvious, leads to an electronically diabatic representation that is not unique unlike the adiabatic one, which is unique by definition.

Let $\psi_n^{el,d}(\mathbf{r};\mathbf{q}_\lambda)$ refer to that alternate basis set. Assuming that it is complete in $\mathbf{r}$ and orthonormal in a manner similar to Eq. (2.10), we can use it to expand the total orbital wave function of Eq. (2.11) in the diabatic version of Born-Huang expansion as

$$\Psi^{\mathrm{O}}(\mathbf{r},\mathbf{R}_\lambda) = \sum\!\!\!\!\!\!\int_i \chi_i^d(\mathbf{R}_\lambda)\psi_i^{el,d}(\mathbf{r};\mathbf{q}_\lambda), \tag{2.26}$$

where the $\psi_i^{el,d}(\mathbf{r};\mathbf{q}_\lambda)$ form a complete orthonormal basis set in the electronic coordinates and the expansion coeffecients $\chi_i^d(\mathbf{R}_\lambda)$ are the diabatic nuclear wave functions.

As in Eq. (2.12), we also usually replace Eq. (2.26) by a truncated n-term version

$$\Psi^{\mathrm{O}}(\mathbf{r},\mathbf{R}_\lambda) \approx \sum_{i=1}^{n} \chi_i^d(\mathbf{R}_\lambda)\psi_i^{el,d}(\mathbf{r};\mathbf{q}_\lambda) \tag{2.27}$$

In the light of Eqs. (2.12) and (2.27), the diabatic electronic wave function column vector $\boldsymbol{\psi}^{el,d}(\mathbf{r};\mathbf{q}_\lambda)$ (with elements $\psi_i^{el,d}(\mathbf{r};\mathbf{q}_\lambda),\ i=1,...,n$) is related to the adiabatic one $\boldsymbol{\psi}^{el,ad}(\mathbf{r};\mathbf{q}_\lambda)$ (with elements $\psi_i^{el,ad}(\mathbf{r};\mathbf{q}_\lambda),\ i=1,...,n$) by an n-dimensional unitary transformation

$$\boldsymbol{\psi}^{el,d}(\mathbf{r};\mathbf{q}_\lambda) = \widetilde{\mathbf{U}}(\mathbf{q}_\lambda)\ \boldsymbol{\psi}^{el,ad}(\mathbf{r};\mathbf{q}_\lambda) \tag{2.28}$$

where

$$\mathbf{U}^\dagger(\mathbf{q}_\lambda)\ \mathbf{U}(\mathbf{q}_\lambda) = \mathbf{I} \tag{2.29}$$

$\mathbf{U}(\mathbf{q}_\lambda)$ is referred to as an adiabatic-to-diabatic transformation (ADT) matrix. Its mathematical structure is discussed in detail in Sec. 2.3.3. If the electronic wave functions in the adiabatic and diabatic representations are chosen to be real, as is normally the case, $\mathbf{U}(\mathbf{q}_\lambda)$ is orthogonal and therefore has $n(n-1)/2$ independent elements (or degrees of freedom). This transformation matrix $\mathbf{U}(\mathbf{q}_\lambda)$ can be chosen so as to yield a diabatic electronic basis set with desired properties, which can then be used to derive the diabatic nuclear motion Schrödinger equation. Using Eqs. (2.27) and (2.28) and the orthonormality of the diabatic and adiabatic electronic basis sets, we can relate the adiabatic and diabatic nuclear wave functions through the same

n-dimensional unitary transformation matrix $\mathbf{U}(\mathbf{q}_\lambda)$ according to

$$\boldsymbol{\chi}^d(\mathbf{R}_\lambda) = \widetilde{\mathbf{U}}(\mathbf{q}_\lambda)\ \boldsymbol{\chi}^{ad}(\mathbf{R}_\lambda) \tag{2.30}$$

In Eq. (2.30), $\boldsymbol{\chi}^{ad}(\mathbf{R}_\lambda)$ and $\boldsymbol{\chi}^d(\mathbf{R}_\lambda)$ are the column vectors with elements $\chi_i^{ad}(\mathbf{R}_\lambda)$ and $\chi_i^d(\mathbf{R}_\lambda)$, respectively, where $i = 1, ..., n$.

2.3.2 Diabatic nuclear motion Schrödinger equation

We will assume for the moment that we know the ADT matrix of Eqs. (2.28) and (2.30) $\mathbf{U}(\mathbf{q}_\lambda)$ and hence have a completely determined electronically diabatic basis set $\boldsymbol{\psi}^{el,d}(\mathbf{r}; \mathbf{q}_\lambda)$. Replacing Eq. (2.27) into Eq. (2.13) and using Eqs. (2.7) and (2.8) along with the orthonormality property of $\boldsymbol{\psi}^{el,d}(\mathbf{r}; \mathbf{q}_\lambda)$, we obtain for $\boldsymbol{\chi}^d(\mathbf{R}_\lambda)$ the n-electronic-state diabatic nuclear motion Schrödinger equation

$$\left[-\frac{\hbar^2}{2\mu}\left\{\mathbf{I}\nabla^2_{\mathbf{R}_\lambda} + 2\mathbf{W}^{(1)d}(\mathbf{R}_\lambda)\cdot\boldsymbol{\nabla}_{\mathbf{R}_\lambda} + \mathbf{W}^{(2)d}(\mathbf{R}_\lambda)\right\} + \left\{\boldsymbol{\varepsilon}^d(\mathbf{q}_\lambda) - E\mathbf{I}\right\}\right]\boldsymbol{\chi}^d(\mathbf{R}_\lambda) = \mathbf{0} \tag{2.31}$$

which is the diabatic counterpart of Eq. (2.15). $\boldsymbol{\varepsilon}^d(\mathbf{q}_\lambda)$ is an $n \times n$ diabatic electronic energy matrix which in general is nondiagonal (unlike its adiabatic counterpart) and has elements defined by

$$\varepsilon^d_{i,j}(\mathbf{q}_\lambda) = \langle \psi_i^{el,d}(\mathbf{r}; \mathbf{q}_\lambda) \mid \widehat{H}^{el}(\mathbf{r}; \mathbf{q}_\lambda) \mid \psi_j^{el,d}(\mathbf{r}; \mathbf{q}_\lambda)\rangle_{\mathbf{r}} \qquad i, j = 1, ..., n \tag{2.32}$$

$\mathbf{W}^{(1)d}(\mathbf{R}_\lambda)$ is an $n \times n$ diabatic first-derivative coupling matrix with elements defined using the diabatic electronic basis set as

$$\mathbf{w}^{(1)d}_{i,j}(\mathbf{R}_\lambda) = \langle \psi_i^{el,d}(\mathbf{r}; \mathbf{q}_\lambda) \mid \boldsymbol{\nabla}_{\mathbf{R}_\lambda} \psi_j^{el,d}(\mathbf{r}; \mathbf{q}_\lambda)\rangle_{\mathbf{r}} \qquad i, j = 1, ..., n \tag{2.33}$$

Requiring $\psi_i^{el,d}(\mathbf{r}; \mathbf{q}_\lambda)$ to be real, the matrix $\mathbf{W}^{(1)d}(\mathbf{R}_\lambda)$ becomes real and skew-symmetric (just like its adiabatic counterpart) with diagonal elements equal to zero. Similarly, $\mathbf{W}^{(2)d}(\mathbf{R}_\lambda)$ is an $n \times n$ diabatic second-derivative coupling matrix with

elements defined by

$$\mathrm{w}_{i,j}^{(2)d}(\mathbf{R}_\lambda) = \langle \psi_i^{el,d}(\mathbf{r};\mathbf{q}_\lambda) \mid \nabla_{\mathbf{R}_\lambda}^2 \psi_j^{el,d}(\mathbf{r};\mathbf{q}_\lambda)\rangle_{\mathbf{r}} \qquad i,j = 1,...,n \tag{2.34}$$

An equivalent form of Eq. (2.31) can be obtained by inserting Eq. (2.30) into Eq. (2.15). Comparison of the result with Eq. (2.31) furnishes the following relations between the adiabatic and diabatic coupling matrices:

$$\mathbf{W}^{(1)d}(\mathbf{R}_\lambda) = \widetilde{\mathbf{U}}(\mathbf{q}_\lambda)\left[\boldsymbol{\nabla}_{\mathbf{R}_\lambda}\mathbf{U}(\mathbf{q}_\lambda) + \mathbf{W}^{(1)ad}(\mathbf{R}_\lambda)\mathbf{U}(\mathbf{q}_\lambda)\right] \tag{2.35}$$

$$\mathbf{W}^{(2)d}(\mathbf{R}_\lambda) = \widetilde{\mathbf{U}}(\mathbf{q}_\lambda)\left[\nabla_{\mathbf{R}_\lambda}^2\mathbf{U}(\mathbf{q}_\lambda) + 2\mathbf{W}^{(1)ad}(\mathbf{R}_\lambda)\cdot\boldsymbol{\nabla}_{\mathbf{R}_\lambda}\mathbf{U}(\mathbf{q}_\lambda) + \mathbf{W}^{(2)ad}(\mathbf{R}_\lambda)\mathbf{U}(\mathbf{q}_\lambda)\right] \tag{2.36}$$

It also furnishes the following relation between the diagonal adiabatic energy matrix and the nondiagonal diabatic energy one:

$$\boldsymbol{\varepsilon}^d(\mathbf{q}_\lambda) = \widetilde{\mathbf{U}}(\mathbf{q}_\lambda)\boldsymbol{\varepsilon}^{ad}(\mathbf{q}_\lambda)\mathbf{U}(\mathbf{q}_\lambda) \tag{2.37}$$

It needs mentioning that the diabatic Schrödinger equation [Eq. (2.31)] also contains a gradient term $\mathbf{W}^{(1)d}(\mathbf{R}_\lambda)\cdot\boldsymbol{\nabla}_{\mathbf{R}_\lambda}\chi(\mathbf{R}_\lambda)$ like its adiabatic counterpart [Eq. (2.15)]. The presence of this term can also introduce numerical inefficiency problems in the solution of Eq. (2.31). Since the ADT matrix $\mathbf{U}(\mathbf{q}_\lambda)$ is arbitrary, it can be chosen to make Eq. (2.31) have desirable properties that Eq. (2.15) doesn't possess. $\mathbf{U}(\mathbf{q}_\lambda)$ can, for example, be chosen so as to automatically minimize $\mathbf{W}^{(1)d}(\mathbf{R}_\lambda)$ relative to $\mathbf{W}^{(1)ad}(\mathbf{R}_\lambda)$ everywhere in internal nuclear configuration space and incorporate the effect of the geometric phase. Next we will consider the structure of this ADT matrix for an n-electronic-state problem and a general evaluation scheme that minimizes the magnitude of $\mathbf{W}^{(1)d}(\mathbf{R}_\lambda)$.

2.3.3 Diabatization matrix

In the n-electronic-state adiabatic representation involving real electronic wave functions, the skew-symmetric first-derivative coupling vector matrix $\mathbf{W}^{(1)ad}(\mathbf{R}_\lambda)$ has $n(n-1)/2$ independent non-zero coupling vector elements $\mathbf{w}_{i,j}^{(1)ad}(\mathbf{R}_\lambda)$, $(i \neq j)$. The ones having the largest magnitudes are those that couple adjacent neighboring adiabatic PESs, and therefore the dominant $\mathbf{w}_{i,j}^{(1)ad}(\mathbf{R}_\lambda)$ are those for which $j = i \pm 1$, i.e., lying along the two off-diagonal lines adjacent to the main diagonal of zeroes. Each one of the $\mathbf{w}_{i,j}^{(1)ad}(\mathbf{R}_\lambda)$ elements is associated with a scalar potential $\alpha_{i,j}(\mathbf{R}_\lambda)$ through their longitudinal component (see Eqs. (2.19) and (2.23)). A convenient and general way of parametrizing the $n \times n$ orthogonal ADT matrix $\mathbf{U}(\mathbf{q}_\lambda)$ of Eqs. (2.28) and (2.30) is as follows. Since the coupling vector element $\mathbf{w}_{i,j}^{(1)ad}(\mathbf{R}_\lambda)$ couples the electronic states i and j, let us define an $n \times n$ orthogonal i,j-diabatization matrix ($\mathbf{u}_{i,j}(\mathbf{q}_\lambda)$, with $j > i$) whose row k and column l element $(k, l = 1, 2, ..., n)$ is designated by $\mathrm{u}_{i,j}^{k,l}(\mathbf{q}_\lambda)$ and is defined in terms of a set of diabatization angles $\beta_{i,j}(\mathbf{q}_\lambda)$ by the relations

$$\begin{aligned}
\mathrm{u}_{i,j}^{k,l}(\mathbf{q}_\lambda) &= \cos\beta_{i,j}(\mathbf{q}_\lambda) && \text{for } k = i \text{ and } l = i \\
&= \cos\beta_{i,j}(\mathbf{q}_\lambda) && \text{for } k = j \text{ and } l = j \\
&= -\sin\beta_{i,j}(\mathbf{q}_\lambda) && \text{for } k = i \text{ and } l = j \\
&= \sin\beta_{i,j}(\mathbf{q}_\lambda) && \text{for } k = j \text{ and } l = i \\
&= 1 && \text{for } k = l \neq i \text{ or } j \\
&= 0 && \text{for the remaining } k \text{ and } l
\end{aligned} \tag{2.38}$$

This choice of elements for the $\mathbf{u}_{i,j}(\mathbf{q}_\lambda)$ matrix will diabatize the adiabatic electronic states i and j while leaving the remaining states unaltered.

As an example, in a 4-electronic-state problem ($n = 4$) consider the electronic states $i = 2$ and $j = 4$ along with the first-derivative coupling vector element $\mathbf{w}_{2,4}^{(1)ad}(\mathbf{R}_\lambda)$ that couples those two states. The ADT matrix $\mathbf{u}_{2,4}(\mathbf{q}_\lambda)$ can then be

expressed in terms of the corresponding diabatization angle $\beta_{2,4}(\mathbf{q}_\lambda)$ as

$$\mathbf{u}_{2,4}(\mathbf{q}_\lambda) = \begin{pmatrix} 1 & 0 & 0 & 0 \\ 0 & \cos\beta_{2,4}(\mathbf{q}_\lambda) & 0 & -\sin\beta_{2,4}(\mathbf{q}_\lambda) \\ 0 & 0 & 1 & 0 \\ 0 & \sin\beta_{2,4}(\mathbf{q}_\lambda) & 0 & \cos\beta_{2,4}(\mathbf{q}_\lambda) \end{pmatrix} \tag{2.39}$$

This diabatization matrix only mixes the adiabatic states 2 and 4 leaving the states 1 and 3 unchanged.

In the n-electronic-state case, $n(n-1)/2$ such matrices $\mathbf{u}_{i,j}(\mathbf{q}_\lambda)$ ($j > i$ with $i = 1, 2, ..., n-1$ and $j = 2, ..., n$) can be defined using Eq. (2.38). The full ADT matrix $\mathbf{U}(\mathbf{q}_\lambda)$ is then defined as a product of these $n(n-1)/2$ matrices $\mathbf{u}_{i,j}(\mathbf{q}_\lambda)$ ($j > i$) as

$$\mathbf{U}(\mathbf{q}_\lambda) = \prod_{i=1}^{n-1} \prod_{j=i+1}^{n} \mathbf{u}_{i,j}(\mathbf{q}_\lambda) \tag{2.40}$$

which is the n-electronic-state version of the expression that has appeared earlier [18, 19] for three electronic states. This $\mathbf{U}(\mathbf{q}_\lambda)$ is orthogonal, as it is the product of orthogonal matrices. The matrices $\mathbf{u}_{i,j}(\mathbf{q}_\lambda)$ in Eq. (2.40) can be multiplied in any order without loss of generality. A different multiplication order leads to a different set of solutions for the diabatization angles $\beta_{i,j}(\mathbf{q}_\lambda)$. However, since the matrix $\mathbf{U}(\mathbf{q}_\lambda)$ is a solution of a set of Poisson-type equations with fixed boundary conditions, as will be discussed next, it is uniquely determined and therefore independent of this choice of the order of multiplication, i.e., all of these sets of $\beta_{i,j}(\mathbf{q}_\lambda)$ give the same $\mathbf{U}(\mathbf{q}_\lambda)$ [19]. It should be remembered, however, that these are purely formal considerations, which are useful for the truncated Born-Huang expansion as discussed after Eq. (2.46).

We want to choose the ADT matrix $\mathbf{U}(\mathbf{q}_\lambda)$ that either makes the diabatic first-derivative coupling vector matrix $\mathbf{W}^{(1)d}(\mathbf{R}_\lambda)$ zero if possible or that minimizes its magnitude in such a way that the gradient term $\mathbf{W}^{(1)d}(\mathbf{R}_\lambda) \cdot \boldsymbol{\nabla}_{\mathbf{R}_\lambda} \chi^d(\mathbf{R}_\lambda)$ in Eq. (2.31) can be neglected. Rewriting the relation between $\mathbf{W}^{(1)d}(\mathbf{R}_\lambda)$ and $\mathbf{W}^{(1)ad}(\mathbf{R}_\lambda)$ of

Eq. (2.35) as

$$\mathbf{W}^{(1)d}(\mathbf{R}_\lambda) = \widetilde{\mathbf{U}}(\mathbf{q}_\lambda)\left[\boldsymbol{\nabla}_{\mathbf{R}_\lambda}\mathbf{U}(\mathbf{q}_\lambda) + \mathbf{W}^{(1)ad}(\mathbf{R}_\lambda)\mathbf{U}(\mathbf{q}_\lambda)\right] \tag{2.41}$$

we see that all elements of the diabatic matrix $\mathbf{W}^{(1)d}(\mathbf{R}_\lambda)$ will vanish if and only if all elements of the matrix inside the square brackets in the right-hand side of this equation are zero, i.e.,

$$\boldsymbol{\nabla}_{\mathbf{R}_\lambda}\mathbf{U}(\mathbf{q}_\lambda) + \mathbf{W}^{(1)ad}(\mathbf{R}_\lambda)\mathbf{U}(\mathbf{q}_\lambda) = \mathbf{0} \tag{2.42}$$

The structure of $\mathbf{W}^{(1)ad}(\mathbf{R}_\lambda)$ discussed at the beginning of this section, will reflect itself in some interrelations between the $\beta_{i,j}(\mathbf{q}_\lambda)$ obtained by solving this equation. More importantly, this equation has a solution if and only if the elements of the matrix $\mathbf{W}^{(1)ad}(\mathbf{R}_\lambda)$ satisfy the following curl-condition [1, 20–23] for all values of $\mathbf{R}_\lambda$:

$$\left[\text{curl } \mathbf{w}^{(1)ad}_{i,j}(\mathbf{R}_\lambda)\right]_{k,l} = -\left[\mathbf{w}^{(1)ad}_{k}(\mathbf{R}_\lambda), \mathbf{w}^{(1)ad}_{l}(\mathbf{R}_\lambda)\right]_{i,j} \quad k,l = 1,2,...,3(N_{nu}-1) \tag{2.43}$$

In this equation, $\mathbf{w}^{(1)ad}_{p}(\mathbf{R}_\lambda)$ (with $p = k, l$) is the $n \times n$ matrix whose row i and column j element is the p cartesian component of the $\mathbf{w}^{(1)ad}_{i,j}(\mathbf{R}_\lambda)$ vector, i.e., $[\mathbf{w}^{(1)ad}_{i,j}(\mathbf{R}_\lambda)]_p$, and the square bracket on its right-hand side is the commutator of the two matrices within. This condition is satisfied for an $n \times n$ matrix $\mathbf{W}^{(1)ad}(\mathbf{R}_\lambda)$ when n samples the complete infinite set of adiabatic electronic states. In that case, we can rewrite Eq. (2.42) using the unitarity property [Eq. (2.29)] of $\mathbf{U}(\mathbf{q}_\lambda)$ as

$$\left[\boldsymbol{\nabla}_{\mathbf{R}_\lambda}\mathbf{U}(\mathbf{q}_\lambda)\right]\widetilde{\mathbf{U}}(\mathbf{q}_\lambda) = -\mathbf{W}^{(1)ad}(\mathbf{R}_\lambda) \tag{2.44}$$

This matrix equation can be expressed in terms of individual matrix elements on both sides as

$$\sum_k \left(\boldsymbol{\nabla}_{\mathbf{R}_\lambda} f_{i,k}[\boldsymbol{\beta}(\mathbf{q}_\lambda)]\right) f_{j,k}[\boldsymbol{\beta}(\mathbf{q}_\lambda)] = -\mathbf{w}^{(1)ad}_{i,j}(\mathbf{R}_\lambda) \tag{2.45}$$

where $\boldsymbol{\beta}(\mathbf{q}_\lambda) \equiv (\beta_{1,2}(\mathbf{q}_\lambda), ..., \beta_{1,n}(\mathbf{q}_\lambda), \beta_{2,3}(\mathbf{q}_\lambda), ..., \beta_{2,n}(\mathbf{q}_\lambda), ..., \beta_{n-1,n}(\mathbf{q}_\lambda))$ is a set of all

unknown diabatization angles and $f_{p,q}[\boldsymbol{\beta}(\mathbf{q}_\lambda)]$ with $p, q = i, j, k$ are matrix elements of the ADT matrix $\mathbf{U}(\mathbf{q}_\lambda)$, which are known trigonometric functions of the unknown $\boldsymbol{\beta}(\mathbf{q}_\lambda)$ due to Eqs. (2.38) and (2.40). Equations (2.45) are a set of coupled first-order partial differential equations in the unknown diabatization angles $\beta_{i,j}(\mathbf{q}_\lambda)$ in terms of the known first-derivative coupling vector elements $\mathbf{w}_{i,j}^{(1)ad}(\mathbf{R}_\lambda)$ obtained from *ab initio* electronic structure calculations [7]. This set of coupled differential equations can be solved in principle with some appropriate choice of boundary conditions for the angles $\beta_{i,j}(\mathbf{q}_\lambda)$.

The ADT matrix $\mathbf{U}(\mathbf{q}_\lambda)$ obtained in this way makes the diabatic first-derivative coupling matrix $\mathbf{W}^{(1)d}(\mathbf{R}_\lambda)$ that appears in the diabatic Schrödinger equation [Eq. (2.31)] rigorously zero. It also leads to a diabatic electronic basis set that is independent of $\mathbf{q}_\lambda$ [23], which, in agreement with the present formal considerations, can only be a correct basis set if it is complete, i.e., infinite. It can be proved using Eqs. (2.35), (2.36) and (2.42) that this choice of the ADT matrix also makes the diabatic second-derivative coupling matrix $\mathbf{W}^{(2)d}(\mathbf{R}_\lambda)$ appearing in Eq. (2.31) equal to zero. As a result, when n samples the complete set of adiabatic electronic states, the corresponding diabatic nuclear motion Schrödinger equation [Eq. (2.31)] reduces to the simple form

$$\left[-\frac{\hbar^2}{2\mu}\mathbf{I}\nabla^2_{\mathbf{R}_\lambda} + \left\{\boldsymbol{\varepsilon}^d(\mathbf{q}_\lambda) - E\mathbf{I}\right\}\right]\boldsymbol{\chi}^d(\mathbf{R}_\lambda) = \mathbf{0} \tag{2.46}$$

where the only term that couples the diabatic nuclear wave functions $\boldsymbol{\chi}^d(\mathbf{R}_\lambda)$ is the diabatic energy matrix $\boldsymbol{\varepsilon}^d(\mathbf{q}_\lambda)$.

The curl-condition given by Eq. (2.43) is in general not satisfied by the $n \times n$ matrix $\mathbf{W}^{(1)ad}(\mathbf{R}_\lambda)$, if n doesn't span the full infinite basis set of adiabatic electronic states and is truncated to include only a finite small number of these states. This truncation is extremely convenient from a physical as well as computational point of view. In this case, since Eq. (2.42) does not have a solution, let us consider instead the equation obtained from it by replacing $\mathbf{W}^{(1)ad}(\mathbf{R}_\lambda)$ by its longitudinal part:

$$\boldsymbol{\nabla}_{\mathbf{R}_\lambda}\mathbf{U}(\mathbf{q}_\lambda) + \mathbf{W}^{(1)ad}_{lon}(\mathbf{R}_\lambda)\mathbf{U}(\mathbf{q}_\lambda) = \mathbf{0} \tag{2.47}$$

This equation does have a solution, because in view of Eq. (2.20) the curl condition of Eq. (2.43) is satisfied when $\mathbf{W}^{(1)ad}(\mathbf{R}_\lambda)$ is replaced by $\mathbf{W}^{(1)ad}_{lon}(\mathbf{R}_\lambda)$.

We can now rewrite Eq. (2.47) using the orthogonality of $\mathbf{U}(\mathbf{q}_\lambda)$ as

$$[\boldsymbol{\nabla}_{\mathbf{R}_\lambda}\mathbf{U}(\mathbf{q}_\lambda)]\,\widetilde{\mathbf{U}}(\mathbf{q}_\lambda) = -\mathbf{W}^{(1)ad}_{lon}(\mathbf{R}_\lambda) \tag{2.48}$$

The quantity on the right-hand side of this equation is not completely specified since the decomposition of $\mathbf{W}^{(1)ad}(\mathbf{R}_\lambda)$ into its longitudinal and transverse parts given by Eq. (2.24) is not unique. Using that decomposition and the property of the transverse part $\mathbf{W}^{(1)ad}_{tra}(\mathbf{R}_\lambda)$ given by Eq. (2.21), we see that

$$\boldsymbol{\nabla}_{\mathbf{R}_\lambda}\cdot\mathbf{W}^{(1)ad}_{lon}(\mathbf{R}_\lambda) = \boldsymbol{\nabla}_{\mathbf{R}_\lambda}\cdot\mathbf{W}^{(1)ad}(\mathbf{R}_\lambda) \tag{2.49}$$

and since $\mathbf{W}^{(1)ad}(\mathbf{R}_\lambda)$ is assumed to have been previously calculated, $\boldsymbol{\nabla}_{\mathbf{R}_\lambda}\cdot\mathbf{W}^{(1)ad}_{lon}(\mathbf{R}_\lambda)$ is known. If we take the divergence of both sides of Eq. (2.48), we obtain (using Eq. (2.49))

$$\left[\nabla^2_{\mathbf{R}_\lambda}\mathbf{U}(\mathbf{q}_\lambda)\right]\widetilde{\mathbf{U}}(\mathbf{q}_\lambda) + [\boldsymbol{\nabla}_{\mathbf{R}_\lambda}\mathbf{U}(\mathbf{q}_\lambda)]\cdot\left[\boldsymbol{\nabla}_{\mathbf{R}_\lambda}\widetilde{\mathbf{U}}(\mathbf{q}_\lambda)\right] = -\boldsymbol{\nabla}_{\mathbf{R}_\lambda}\cdot\mathbf{W}^{(1)ad}(\mathbf{R}_\lambda) \tag{2.50}$$

Using the parameterization of $\mathbf{U}(\mathbf{q}_\lambda)$ given by Eqs. (2.38) and (2.40) for a finite n, this matrix equation can be expressed in terms of the matrix elements on both sides as

$$\sum_k\left[\left(\nabla^2_{\mathbf{R}_\lambda}f_{i,k}[\boldsymbol{\beta}(\mathbf{q}_\lambda)]\right)f_{j,k}[\boldsymbol{\beta}(\mathbf{q}_\lambda)] + \left(\boldsymbol{\nabla}_{\mathbf{R}_\lambda}f_{i,k}[\boldsymbol{\beta}(\mathbf{q}_\lambda)]\right)\cdot\left(\boldsymbol{\nabla}_{\mathbf{R}_\lambda}f_{j,k}[\boldsymbol{\beta}(\mathbf{q}_\lambda)]\right)\right] = -\boldsymbol{\nabla}_{\mathbf{R}_\lambda}\cdot\mathbf{w}^{(1)ad}_{i,j}(\mathbf{R}_\lambda) \tag{2.51}$$

where $f_{p,q}$ are the same as defined after Eq. (2.45). Equation (2.51) is a set of coupled Poisson-type equations in the unknown angles $\beta_{i,j}(\mathbf{q}_\lambda)$. For $n = 2$ this becomes Eq. (4.30), as shown in Chapter 4. The structure of this set of equations is again dependent on the order of multiplication of matrices $\mathbf{u}_{i,j}(\mathbf{q}_\lambda)$ in Eq. (2.40). Each choice of the order of multiplication will give a different set of $\beta_{i,j}(\mathbf{q}_\lambda)$ as before but

the same ADT matrix $\mathbf{U}(\mathbf{q}_\lambda)$ after they are solved using the same set of boundary conditions.

Using the fact that for a finite number of adiabatic electronic states n, we choose a $\mathbf{U}(\mathbf{q}_\lambda)$ that satisfies Eq. (2.47) (rather than Eq. (2.42) that has no solution), Eq. (2.35) now reduces to

$$\mathbf{W}^{(1)d}(\mathbf{R}_\lambda) = \widetilde{\mathbf{U}}(\mathbf{q}_\lambda)\mathbf{W}^{(1)ad}_{tra}(\mathbf{R}_\lambda)\mathbf{U}(\mathbf{q}_\lambda) \tag{2.52}$$

This can be used to rewrite the diabatic nuclear motion Schrödinger equation for an incomplete set of n electronic states as

$$\left[-\frac{\hbar^2}{2\mu}\left\{\mathbf{I}\nabla^2_{\mathbf{R}_\lambda} + 2\widetilde{\mathbf{U}}(\mathbf{q}_\lambda)\mathbf{W}^{(1)ad}_{tra}(\mathbf{R}_\lambda)\mathbf{U}(\mathbf{q}_\lambda)\cdot\boldsymbol{\nabla}_{\mathbf{R}_\lambda} + \mathbf{W}^{(2)d}(\mathbf{R}_\lambda)\right\} + \left\{\boldsymbol{\varepsilon}^d(\mathbf{q}_\lambda) - E\mathbf{I}\right\}\right]\boldsymbol{\chi}^d(\mathbf{R}_\lambda) = \mathbf{0} \tag{2.53}$$

In this equation, the gradient term $\widetilde{\mathbf{U}}(\mathbf{q}_\lambda)\mathbf{W}^{(1)ad}_{tra}(\mathbf{R}_\lambda)\mathbf{U}(\mathbf{q}_\lambda)\cdot\boldsymbol{\nabla}_{\mathbf{R}_\lambda}\boldsymbol{\chi}^d(\mathbf{R}_\lambda) = \mathbf{W}^{(1)d}(\mathbf{R}_\lambda)\cdot\boldsymbol{\nabla}_{\mathbf{R}_\lambda}\boldsymbol{\chi}^d(\mathbf{R}_\lambda)$ still appears and, as mentioned before, introduces numerical inefficiencies in its solution. Even though a truncated Born-Huang expansion was used to obtain Eq. (2.53), $\mathbf{W}^{(1)ad}_{tra}(\mathbf{R}_\lambda)$, although no longer zero, has no poles at conical intersection geometries (as opposed to the full $\mathbf{W}^{(1)ad}(\mathbf{R}_\lambda)$ matrix).

The set of coupled Poisson equations [Eq. (2.50)] can, in principle, be solved with any appropriate choice of boundary conditions for $\beta_{i,j}(\mathbf{q}_\lambda)$. There is one choice, however, for which the magnitude of $\mathbf{W}^{(1)ad}_{tra}(\mathbf{R}_\lambda)$ is minimized. If at the boundary surfaces $\mathbf{R}^{\mathrm{b}}_\lambda$ of the nuclear configuration space spanned by $\mathbf{R}_\lambda$ (and the corresponding subset of boundary surfaces $\mathbf{q}^{\mathrm{b}}_\lambda$ in the internal configuration space spanned by $\mathbf{q}_\lambda$), one imposes the following mixed Dirichlet-Neumann condition (based on Eq. (2.48)),

$$\left[\boldsymbol{\nabla}_{\mathbf{R}^{\mathrm{b}}_\lambda}\mathbf{U}(\mathbf{q}^{\mathrm{b}}_\lambda)\right]\widetilde{\mathbf{U}}(\mathbf{q}^{\mathrm{b}}_\lambda) = -\mathbf{W}^{(1)ad}(\mathbf{R}^{\mathrm{b}}_\lambda) \tag{2.54}$$

it minimizes the average magnitude of the vector elements of the transverse coupling matrix $\mathbf{W}^{(1)ad}_{tra}(\mathbf{R}_\lambda)$ over the entire internal nuclear configuration space and hence the magnitude of the gradient $\mathbf{W}^{(1)d}(\mathbf{R}_\lambda)\cdot\boldsymbol{\nabla}_{\mathbf{R}_\lambda}\boldsymbol{\chi}^d(\mathbf{R}_\lambda)$, as will be shown for the $n = 2$ case [24] in Chapter 4. To a first very good approximation, this term can be neglected

in the diabatic Schrödinger Eq. (2.53) resulting in a simpler equation

$$\left[-\frac{\hbar^2}{2\mu}\left\{\mathbf{I}\nabla^2_{\mathbf{R}_\lambda}+\mathbf{W}^{(2)d}(\mathbf{R}_\lambda)\right\}+\left\{\boldsymbol{\varepsilon}^d(\mathbf{q}_\lambda)-E\mathbf{I}\right\}\right]\boldsymbol{\chi}^d(\mathbf{R}_\lambda)=\mathbf{0} \tag{2.55}$$

In this diabatic Schrödinger equation, the only terms that couple the nuclear wave functions $\chi_i^d(\mathbf{R}_\lambda)$ are the elements of the $\mathbf{W}^{(2)d}(\mathbf{R}_\lambda)$ and $\boldsymbol{\varepsilon}^d(\mathbf{q}_\lambda)$ matrices. The $-\frac{\hbar^2}{2\mu}\mathbf{W}^{(2)d}(\mathbf{R}_\lambda)$ matrix does not have poles at conical intersection geometries (as opposed to $\mathbf{W}^{(2)ad}(\mathbf{R}_\lambda)$) and furthermore it only appears as an additive term to the diabatic energy matrix $\boldsymbol{\varepsilon}^d(\mathbf{q}_\lambda)$ and doesn't increase the computational effort for the solution of Eq. (2.55). Since the neglected gradient term is expected to be small, it can be reintroduced as a first order perturbation afterwards, if desired.

In the following chapters, this theory will be applied to a two-electronic-state triatomic problem and results presented for the H_3 system.

Bibliography

[1] A. Kuppermann, in *Dynamics of Molecules and Chemical Reactions*, edited by R. E. Wyatt and J. Z. H. Zhang (Marcel Dekker, New York, 1996), pp. 411-472.

[2] L. M. Delves, Nucl. Phys. **9**, 391 (1959).

[3] L. M. Delves, Nucl. Phys. **20**, 275 (1960).

[4] M. Born, Nachr. Akad. Wiss. Gött. Math.-Phys. Kl. Article No. 6, 1 (1951).

[5] M. Born and K. Huang, *Dynamical Theory of Crystal Lattices* (Oxford University Press, Oxford, 1954), pp. 166-177 and 402-407.

[6] M. Baer, Chem. Phys. Lett. **322**, 520 (2000).

[7] B. H. Lengsfield and D.R. Yarkony, in State-selected and State-to-State Ion-Molecule Reaction Dynamics: Part 2 Theory, Vol. 82, edited by M. Baer and C.-Y. Ng (Wiley, New York, 1992), pp. 1-71.

[8] R. J. Buenker, G. Hirsch, S. D. Peyerimhoff, P. J. Bruna, J. Römelt, M. Bettendorff, and C. Petrongolo, in *Current Aspects of Quantum Chemistry*, Elsevier, New York, 1981, pp. 81-97.

[9] M. Desouter-Lecomte, C. Galloy, J. C. Lorquet, and M. V. Pires, J. Chem. Phys. **71**, 3661 (1979).

[10] B. H. Lengsfield, P. Saxe, and D. R. Yarkony, J. Chem. Phys. **81**, 4549 (1984).

[11] P. Saxe, B. H. Lengsfield, and D. R. Yarkony, Chem. Phys. Lett. **113**, 159 (1985).

[12] B. H. Lengsfield, and D. R. Yarkony, J. Chem. Phys. **84**, 348 (1986).

[13] J. O. Jensen and D. R. Yarkony, J. Chem. Phys. **89**, 3853 (1988).

[14] C. A. Mead and D. G. Truhlar, J. Chem. Phys. **70**, 2284 (1979).

[15] B. Kendrick and R. T. Pack, J. Chem. Phys. **104**, 7475 (1996).

[16] P. M. Morse and H. Feshbach, *Methods of Theoretical Physics* (McGraw-Hill, New York, 1953), pp. 52-54, 1763.

[17] H. Margenau and G. M. Murphy, *The Mathematics of Physics and Chemistry* (Van Nostrand, New York, 1943), p. 192.

[18] M. Baer (Ed.), *Theory of Chemical Reaction Dynamics* Vol. II, (CRC Press, Boca Raton (Florida), 1985), chapter 4.

[19] A. Alijah and M. Baer, J. Phys. Chem. A **104**, 389 (2000).

[20] M. Baer and R. Englman, Mol. Phys. **75**, 293 (1992).

[21] M. Baer, Chem. Phys. Lett. **35**, 112 (1975).

[22] M. Baer, Chem. Phys. **15**, 49 (1976).

[23] C. A. Mead and D. G. Truhlar, J. Chem. Phys. **77**, 6090 (1982).

[24] R. Abrol and A. Kuppermann, J. Chem. Phys. **116**, 1035 (2002).

[25] Y.-S. M. Wu, A. Kuppermann, and B. Lepetit, Chem. Phys. Lett. **186**, 319 (1991).

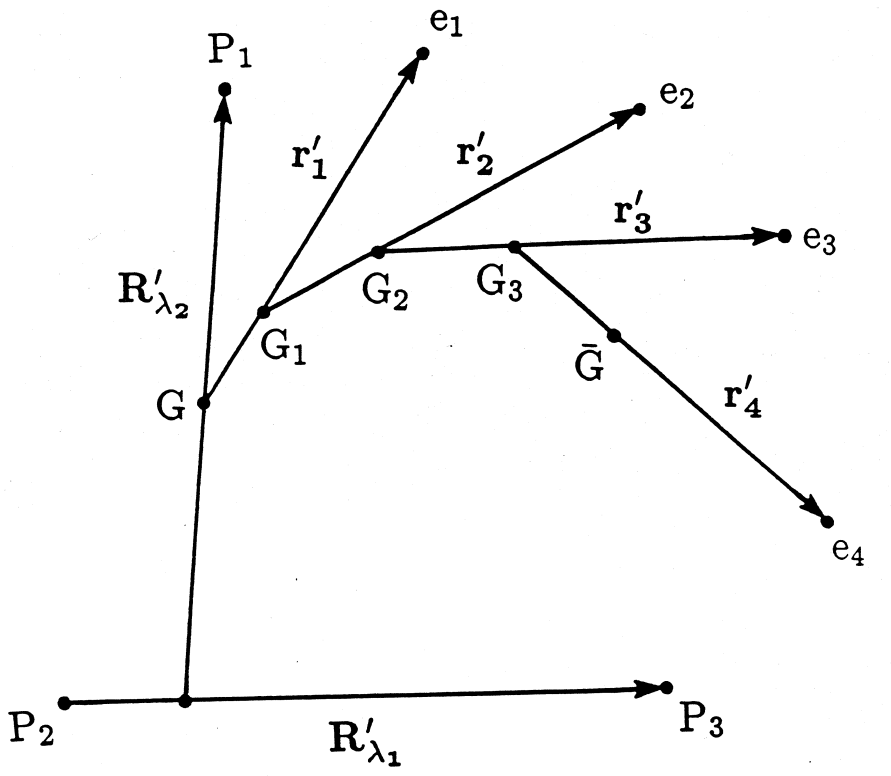

Figure 2.1: Jacobi vectors for a three-nuclei, four-electron system. The nuclei are P_1, P_2, P_3 and the electrons are e_1, e_2, e_3, e_4.

Chapter 3 Accurate first-derivative nonadiabatic couplings for H_3 system

3.1 Introduction

For any polyatomic system involving three or more atoms, the ground and the first-excited adiabatic electronic PESs can intersect even if the corresponding states have the same symmetry and spin multiplicity [1]. These intersections, which are usually conical, occur quite frequently in polyatomic systems. The reason is that these polyatomic systems possess three or more internal nuclear motion degrees of freedom, and only two independent relations between three electronic Hamiltonian matrix elements are sufficient for the existence of doubly degenerate electronic energy eigenvalues. As a result, these relations between those matrix elements are easily satisfied and explain the frequent occurrence of conical intersections. Assuming the adiabatic electronic wave functions to be real and as continuous as possible in the nuclear coordinate space, if the polyatomic system is transported around a closed loop in that space (a so-called pseudorotation) that encircles a conical intersection geometry, these electronic wave functions must change sign [1,2]. This change of sign has consequences for the structure and dynamics of the polyatomic system, as it requires the corresponding nuclear wave functions to undergo a compensatory change of sign, known as the geometric phase (GP) effect [3–7], to keep the total wave function single-valued. This sign change is a special case of Berry's geometric phase [6], and is also referred to as the molecular Aharonov-Bohm effect [8]. It greatly affects the nature of the solutions of the corresponding nuclear motion Schrödinger equation [7, 9]. Accurate quantum-mechanical reactive scattering calculations (on the ground electronic PES), with and without the GP effect included, have been carried out for the H + H_2 system and

its isotopic variants (D + H_2 and H + D_2) [9–13] to obtain differential and integral cross sections. The cross sections obtained with the GP effect included were in much better agreement with the experimental results [14–17] than those obtained with the GP effect excluded. Hence, the GP effect is an important factor in accurate quantum scattering calculations done on the ground adiabatic electronic PES.

A review of the one- and two-electronic-state Born-Huang [18, 19] (also usually called Born-Oppenheimer) approximations has been given in detail elsewhere [7] and only the features pertinent to this chapter are summarized here. In the one-electronic-state approximation, the GP effect has to be imposed on the adiabatic nuclear wave functions in order to obtain accurate results at low energies. At energies above the conical intersection energy, when this approximation breaks down, the effect of the first-excited electronic PES has to be included explicitly in the scattering calculations to obtain accurate results. In the adiabatic representation, the GP effect still has to be imposed on each of the two state nuclear wave functions. In this two-electronic-state approximation [7], the nuclear motion Schrödinger equation for an N-atom system [Eq. (2.15)] becomes

$$\left[-\frac{\hbar^2}{2\mu}\left\{\mathbf{I}\nabla^2_{\mathbf{R}_\lambda}+2\mathbf{W}^{(1)ad}(\mathbf{R}_\lambda)\cdot\boldsymbol{\nabla}_{\mathbf{R}_\lambda}+\mathbf{W}^{(2)ad}(\mathbf{R}_\lambda)\right\}+\left\{\boldsymbol{\varepsilon}^{ad}(\mathbf{q}_\lambda)-E\mathbf{I}\right\}\right]\boldsymbol{\chi}^{ad}(\mathbf{R}_\lambda)=\mathbf{0}, \tag{3.1}$$

where $\mathbf{R}_\lambda$ is a set of $3(N-1)$ nuclear coordinates (remaining after the removal of the center of mass coordinates), and $\mathbf{q}_\lambda$ is a set of $3(N-2)$ internal nuclear coordinates obtained by removing from the set $\mathbf{R}_\lambda$ three Euler angles which orient a nuclear body-fixed frame with respect to a space-fixed one. As an example, for a triatomic system $\mathbf{R}_\lambda$ can be a set of principal axes of inertia body-fixed symmetrized hyperspherical coordinates $(\rho, \theta, \phi_\lambda, a_\lambda, b_\lambda, c_\lambda)$ [7, 9], and $\mathbf{q}_\lambda$ is then comprised of ρ, θ, and ϕ_λ since the remaining $a_\lambda, b_\lambda, c_\lambda$, are Euler angles. It is shown in Appendix 3.A that for a triatomic system, $\mathbf{W}^{(1)ad}(\mathbf{R}_\lambda)\cdot\boldsymbol{\nabla}_{\mathbf{R}_\lambda}$ of Eq. (3.1) can be replaced by $\mathbf{W}^{(1)ad}(\mathbf{q}_\lambda)\cdot\boldsymbol{\nabla}_{\mathbf{R}_\lambda}$. The matrix $\mathbf{W}^{(2)ad}(\mathbf{R}_\lambda)$ can also be replaced by $\mathbf{W}^{(2)ad}(\mathbf{q}_\lambda)$ as the electronic wave functions don't depend on the three Euler angles mentioned above. So Eq. (3.1)

becomes

$$\left[-\frac{\hbar^2}{2\mu}\left\{\mathbf{I}\nabla^2_{\mathbf{R}_\lambda}+2\mathbf{W}^{(1)ad}(\mathbf{q}_\lambda)\cdot\boldsymbol{\nabla}_{\mathbf{R}_\lambda}+\mathbf{W}^{(2)ad}(\mathbf{q}_\lambda)\right\}+\left\{\boldsymbol{\varepsilon}^{ad}(\mathbf{q}_\lambda)-E\mathbf{I}\right\}\right]\boldsymbol{\chi}^{ad}(\mathbf{R}_\lambda)=\mathbf{0} \tag{3.2}$$

In addition, $\mathbf{I}$ is a 2×2 identity matrix,

$$\boldsymbol{\chi}^{ad}(\mathbf{R}_\lambda)=\begin{pmatrix}\chi_1^{ad}(\mathbf{R}_\lambda)\\ \\ \chi_2^{ad}(\mathbf{R}_\lambda)\end{pmatrix} \tag{3.3}$$

is a 2×1 column vector whose elements are the ground ($\chi_1^{ad}(\mathbf{R}_\lambda)$) and the first-excited ($\chi_2^{ad}(\mathbf{R}_\lambda)$) adiabatic nuclear motion wave functions, and

$$\boldsymbol{\varepsilon}^{ad}(\mathbf{q}_\lambda)=\begin{pmatrix}\varepsilon_1^{ad}(\mathbf{q}_\lambda) & 0\\ \\ 0 & \varepsilon_2^{ad}(\mathbf{q}_\lambda)\end{pmatrix} \tag{3.4}$$

is a diagonal matrix whose diagonal elements are the ground ($\varepsilon_1^{ad}(\mathbf{q}_\lambda)$) and the first-excited ($\varepsilon_2^{ad}(\mathbf{q}_\lambda)$) adiabatic electronic PESs.

$\mathbf{W}^{(1)ad}(\mathbf{q}_\lambda)$ and $\mathbf{W}^{(2)ad}(\mathbf{q}_\lambda)$ are respectively the first-derivative [20–23] and second-derivative [20, 24, 25] nonadiabatic coupling matrix elements between the ground and first-excited adiabatic electronic PESs. For the two-electronic-state approximation they are 2×2 matrices, whose elements are defined by

$$\mathbf{W}^{(1)ad}_{m,n}(\mathbf{q}_\lambda) = \langle\psi_m^{ad}(\mathbf{r};\mathbf{q}_\lambda)\mid\boldsymbol{\nabla}_{\mathbf{R}_\lambda}\psi_n^{ad}(\mathbf{r};\mathbf{q}_\lambda)\rangle_{\mathbf{r}} \quad \text{and} \tag{3.5}$$

$$\mathrm{W}^{(2)ad}_{m,n}(\mathbf{q}_\lambda) = \langle\psi_m^{ad}(\mathbf{r};\mathbf{q}_\lambda)\mid\nabla^2_{\mathbf{R}_\lambda}\psi_n^{ad}(\mathbf{r};\mathbf{q}_\lambda)\rangle_{\mathbf{r}}, \tag{3.6}$$

where $\mathbf{r}$ is a set of electronic coordinates, and m and n refer to the ground or the first-excited electronic PESs. $\psi_n^{ad}(\mathbf{r};\mathbf{q}_\lambda)$ is an eigenfunction of the electronic Hamiltonian and satisfies the electronic Schrödinger equation

$$\left[\hat{H}^{el}-\varepsilon_n^{ad}(\mathbf{q}_\lambda)\right]\psi_n^{ad}(\mathbf{r};\mathbf{q}_\lambda)=0. \tag{3.7}$$

$\psi_n^{ad}(\mathbf{r};\mathbf{q}_\lambda)$ and $\varepsilon_n^{ad}(\mathbf{q}_\lambda)$ depend only on the internal nuclear coordinates $\mathbf{q}_\lambda$ because the coulombic interaction potential between the (N-atom) system's particles (nuclei and electrons), which appears in $\hat{H}^{el}$, depends only on their relative distances and hence these quantities depend on $\mathbf{q}_\lambda$ but not on the three Euler angles which orient the nuclear frame with respect to a space-fixed one. This introduces small rotational coupling terms that are two orders of magnitude or more smaller than the remaining coupling terms and can be neglected. This leads to a subtle but important point implicit in Eqs. (3.5) and (3.6): although the right-hand sides of these equations contain $\mathbf{R}_\lambda$, the left-hand sides contain only $\mathbf{q}_\lambda$. Also, since $\boldsymbol{\nabla}_{\mathbf{R}_\lambda}$ and $\nabla^2_{\mathbf{R}_\lambda}$ are respectively the gradient and laplacian operators, $\mathbf{W}^{(1)ad}_{m,n}(\mathbf{q}_\lambda)$ is a vector quantity and $\mathrm{W}^{(2)ad}_{m,n}(\mathbf{q}_\lambda)$ is a scalar quantity.

The matrix $\mathbf{W}^{(1)ad}(\mathbf{q}_\lambda)$ is skew-hermitian, and if we choose $\psi_1^{ad}(\mathbf{r};\mathbf{q}_\lambda)$ and $\psi_2^{ad}(\mathbf{r};\mathbf{q}_\lambda)$ to be real, it is skew-symmetric and $\mathbf{W}^{(1)ad}_{1,1}(\mathbf{q}_\lambda)$ and $\mathbf{W}^{(1)ad}_{2,2}(\mathbf{q}_\lambda)$ are identically zero. Furthermore, the off-diagonal elements, $\mathbf{W}^{(1)ad}_{1,2}(\mathbf{q}_\lambda)$ and $\mathbf{W}^{(1)ad}_{2,1}(\mathbf{q}_\lambda)$, satisfy the relation

$$\mathbf{W}^{(1)ad}_{1,2}(\mathbf{q}_\lambda) = -\mathbf{W}^{(1)ad}_{2,1}(\mathbf{q}_\lambda). \tag{3.8}$$

The presence of the first-derivative term $\mathbf{W}^{(1)ad}(\mathbf{q}_\lambda)\cdot\boldsymbol{\nabla}_{\mathbf{R}_\lambda}$ in Eq. (3.2) introduces inefficiencies in the numerical solution of this equation. A diabatic representation [7,26] of this equation is introduced to circumvent this problem, since in that representation the first-derivative coupling element is minimized. It has been shown [27, 28] that in general a perfect diabatic basis that makes that first term vanish for all nuclear geometries does not exist for a polyatomic system, and hence a finite part of the first-derivative coupling cannot be totally removed even in the diabatic representation. This part is referred to in literature as the *nonremovable* part. For systems having a conical intersection, $\mathbf{W}^{(1)ad}_{1,2}(\mathbf{q}_\lambda)$ has a singularity at conical intersection geometries [29]. This singularity along with some finite part of the coupling is *removable* upon an adiabatic to diabatic transformation and is hence referred to as the *removable* part. Mead and Truhlar [28] have shown how to calculate the *removable* part, but their approach is difficult to implement [30]. Over the years, a number of formalisms

involving (quasi-)diabatic basis have also been put forward [30–40].

This chapter focuses on the calculation of high-quality *ab initio* ground and first-excited electronic energies and the first-derivative couplings between them. The second-derivative couplings are generally assumed to be negligible as compared to the other terms in the Hamiltonian [Eq. (3.2)], except at the conical intersection [41]. These accurate energies and first-derivative couplings will be used for transforming the two-state adiabatic problem expressed by Eq. (3.2) to a (quasi-)diabatic representation and will be incorporated into the quantum scattering formalism to calculate the effect of conical intersections on the dynamics of the chemical reactions at energies for which a minimum of two electronic states is required to obtain accurate results.

The H + H_2 system is being used for this work because it is the simplest of the chemical reactions for which the concurrent bond breaking and bond formation can be studied in detail both experimentally and theoretically. Many quantum scattering calculations have been performed on this system [9,10,42–45]. The equilateral triangle (C_{3v}) configuration of H_3 corresponds to a conical intersection between the ground and the first-excited electronic states of the system. This conical intersection induces a GP that is important in studying the reactive scattering in the ground state [7, 9–13, 46, 47]. With the breakdown of the one electronic state Born-Oppenheimer approximation near 2.75 eV, which corresponds to the minimum of the first-excited PES [48], both surfaces must be used in a scattering calculation for an accurate result to be obtained. Such two-state calculations should be performed and compared with the recent quantum scattering calculations [9,10] done with and without the inclusion of the GP effect. This comparison is expected to provide an upper limit to the energy at which the ground state PES by itself, with an incorporation of the GP effect, is capable of furnishing a quantitative description of the reaction dynamics of the H_3 system and its isotopomers.

In this chapter, we present the first-derivative nonadiabatic couplings between the ground and the first-excited PESs for the H + H_2 system obtained from high-quality *ab initio* wave functions and analytic gradient techniques over the entire nuclear

internal configuration space. We also present a fit to the corresponding ground and first-excited electronic PESs and analyze the regions of that space for which the first-derivative couplings could affect the dynamics of the H + H_2 reaction. For comparison, we also present the first-derivative couplings and the lowest two electronic PESs obtained analytically from the double many-body expansion (DMBE) method of Varandas *et al.* [49], as the DMBE couplings are designed to be accurate only in the vicinity of the conical intersection.

In Sec. 3.2, we describe the methods used to obtain the first-derivative couplings and introduce their contour integrals. In Sec. 3.3, we present a fit to the *ab initio* energies corresponding to the lowest two electronic PESs and compare them to the DMBE ones. We present and compare the *ab initio* and DMBE first-derivative couplings in Sec. 3.4, which is concluded by an analysis of the contour integrals of the *ab initio* couplings.

3.2 Theory and numerical methods

3.2.1 *Ab initio* couplings and electronic energies

The first-derivative couplings are determined using an analytic gradient technique summarized in Ref. [50]. This technique is a significant improvement over the finite-difference techniques introduced previously [20, 51–54] and has been used recently in a number of problems to obtain electronic energies and first-derivative couplings [37, 55–58]. Using it, the first-derivative couplings are first evaluated in terms of six atom-centered displacements [50] in the H_3 molecular plane and then transformed to standard internal mass-scaled Jacobi coordinates $(R_\lambda, r_\lambda, \gamma_\lambda)$. In addition to the derivative couplings associated with these coordinates, the coupling due to rotation in the molecular plane is also determined. This rotational coupling must equal the interstate matrix element of the z component of total electronic orbital angular momentum operator, L_z^e [59, 60]. This equivalence provides a measure of the precision

of the derivative couplings presented in this chapter and the two approaches agree to 1×10^{-6} bohr^{-1}.

In this work, the first-derivative couplings and the ground (E_1) and first-excited (E_2), electronic PESs for H_3 were determined on a grid of 784 geometry points picked in the symmetrized hyperspherical coordinates ($\mathbf{q}_\lambda$:$\rho, \theta, \phi_\lambda$) used previously [7,9] and defined in detail in Sec. 3.3. The adiabatic wave functions, first-derivative couplings, and electronic energies were determined from second-order CI [61–63] wave functions based on a three-electron, three-orbital, active space. The molecular orbitals were determined from a complete active space [64–66] state-averaged multiconfiguration self-consistent field procedure [67, 68], in which two $^2A'$ states were averaged with weights (0.505,0.495) based on ($6s3p1d$) contracted Gaussian basis sets on the hydrogens.

After being evaluated in nuclear mass-scaled Jacobi coordinates as mentioned above, the first-derivative couplings are transformed to the $\mathbf{q}_\lambda$ coordinates $(\rho, \theta, \phi_\lambda)$ to obtain the first-derivative coupling vector

$$\mathbf{W}_{1,2}^{(1)ad}(\mathbf{q}_\lambda) = \langle \psi_1^{ad}(\mathbf{r}; \mathbf{q}_\lambda) \mid \boldsymbol{\nabla}_{\mathbf{q}_\lambda} \psi_2^{ad}(\mathbf{r}; \mathbf{q}_\lambda) \rangle_{\mathbf{r}}, \tag{3.9}$$

whose components in the ρ, θ and ϕ_λ unit vector directions are defined as

$$\mathrm{W}_{1,2,\rho}^{(1)ad}(\rho, \theta, \phi_\lambda) = \langle \psi_1^{ad}(\mathbf{r}; \rho, \theta, \phi_\lambda) \mid \frac{\partial}{\partial \rho} \psi_2^{ad}(\mathbf{r}; \rho, \theta, \phi_\lambda) \rangle_{\mathbf{r}}, \tag{3.10}$$

$$\mathrm{W}_{1,2,\theta}^{(1)ad}(\rho, \theta, \phi_\lambda) = \langle \psi_1^{ad}(\mathbf{r}; \rho, \theta, \phi_\lambda) \mid \frac{1}{\rho} \frac{\partial}{\partial \theta} \psi_2^{ad}(\mathbf{r}; \rho, \theta, \phi_\lambda) \rangle_{\mathbf{r}}, \quad \text{and} \tag{3.11}$$

$$\mathrm{W}_{1,2,\phi_\lambda}^{(1)ad}(\rho, \theta, \phi_\lambda) = \langle \psi_1^{ad}(\mathbf{r}; \rho, \theta, \phi_\lambda) \mid \frac{1}{\rho \sin\theta} \frac{\partial}{\partial \phi_\lambda} \psi_2^{ad}(\mathbf{r}; \rho, \theta, \phi_\lambda) \rangle_{\mathbf{r}}. \tag{3.12}$$

The values of the $\mathbf{q}_\lambda$ coordinates $(\rho, \theta, \phi_\lambda)$ are limited to the ranges

$$0 \le \rho < \infty \qquad 0 \le \theta \le \pi/2 \qquad 0 \le \phi_\lambda < 2\pi \tag{3.13}$$

$\theta = 0^\circ$ corresponds to conical intersection geometries. As seen from Eq. (3.12) and the

behavior of $\psi_1^{ad}(\mathbf{r};\rho,\theta,\phi_\lambda)$ and $\psi_2^{ad}(\mathbf{r};\rho,\theta,\phi_\lambda)$ in the vicinity of the conical intersection (see Eq. (116) of Ref. [7]), $\mathrm{W}_{1,2,\phi_\lambda}^{(1)ad}$ has a pole at those geometries.

A three-dimensional cubic spline [69] interpolation of the components of the first-derivative coupling vector is performed using all 784 geometries. The vector resulting from this interpolation is presented and discussed in Sec. 3.4. The adiabatic electronic energies for the ground and first-excited states are fitted by a method that will be described in Section 3.3.

According to Mead and Truhlar [28], the first-derivative coupling vector can be partitioned (using the Helmholtz decomposition theorem [70]) as

$$\mathbf{W}_{1,2}^{(1)ad}(\mathbf{q}_\lambda) = \mathbf{W}_{1,2,lon}^{(1)ad}(\mathbf{q}_\lambda) + \mathbf{W}_{1,2,tra}^{(1)ad}(\mathbf{q}_\lambda) \tag{3.14}$$

where $\mathbf{W}_{1,2,lon}^{(1)ad}(\mathbf{q}_\lambda)$ is the curl-free longitudinal (*removable*) part and $\mathbf{W}_{1,2,tra}^{(1)ad}(\mathbf{q}_\lambda)$ is the divergence-free transverse (*nonremovable*) part of the coupling vector. Although $\mathbf{W}_{1,2}^{(1)ad}(\mathbf{q}_\lambda)$ is singular, the Helmholtz theorem is still valid in this case because the singularity can be removed analytically [71] from $\mathrm{W}_{1,2,\phi_\lambda}^{(1)ad}$. For a strictly diabatic two-electronic-state basis, $\mathbf{W}_{1,2,tra}^{(1)ad}(\mathbf{q}_\lambda)$ is identically zero. In the present two-adiabatic-electronic-state approximation, $\mathbf{W}_{1,2,tra}^{(1)ad}(\mathbf{q}_\lambda)$ is not zero due to the presence of contributions to $\mathbf{W}_{1,2}^{(1)ad}(\mathbf{q}_\lambda)$ from other non-negligible derivative couplings with states outside this two-state space (see Eq. (28) of Ref [28]). Since $\mathbf{W}_{1,2,lon}^{(1)ad}(\mathbf{q}_\lambda)$ is curl-free, an angular potential $\beta(\mathbf{q}_\lambda)$ exists for which

$$\mathbf{W}_{1,2,lon}^{(1)ad}(\mathbf{q}_\lambda) = \boldsymbol{\nabla}_{\mathbf{q}_\lambda}\beta(\mathbf{q}_\lambda) \tag{3.15}$$

This equation can be solved by integration along paths $\mathcal{L}$ in the nuclear configuration space [27, 37, 72]

$$\beta(\mathbf{q}_\lambda) = \int_{\mathcal{L}\ \mathbf{q}_{\mathbf{0}\lambda}}^{\mathbf{q}_\lambda} \mathbf{W}_{1,2,lon}^{(1)ad}(\mathbf{q}'_\lambda)\cdot d\mathbf{q}'_\lambda \tag{3.16}$$

where $\mathbf{q}_{\mathbf{0}\lambda}$ is a point along $\mathcal{L}$ at which we take $\beta(\mathbf{q}_{\mathbf{0}\lambda}) = 0$. β defined in this way is a particular diabatization angle that transforms an adiabatic basis to a diabatic

basis. It should be noted that because of Eq. (3.15), this integral depends on $\mathbf{q}_\lambda$ and $\mathbf{q}_{\mathbf{0}\lambda}$, but not on the path $\mathcal{L}$. In addition, if the integral in Eq. (3.16) is carried along a closed loop enclosing one or no conical intersections, due to the geometric phase theorem β should change by π or zero, respectively [6, 37, 55]. We can define another angular potential $\Phi(\mathbf{q}_\lambda, \mathbf{q}_{\mathbf{0}\lambda}; \mathcal{L})$ corresponding to the $\mathbf{W}_{1,2}^{(1)ad}(\mathbf{q}_\lambda)$ analog of Eq. (3.16) by

$$\Phi(\mathbf{q}_\lambda, \mathbf{q}_{\mathbf{0}\lambda}; \mathcal{L}) = \int_{\mathcal{L}\ \mathbf{q}_{\mathbf{0}\lambda}}^{\mathbf{q}_\lambda} \mathbf{W}_{1,2}^{(1)ad}(\mathbf{q}'_\lambda) \cdot d\mathbf{q}'_\lambda \tag{3.17}$$

This angle is called the open-path phase if $\mathbf{q}_\lambda \neq \mathbf{q}_{\mathbf{0}\lambda}$ [73]. It is also convenient to define the corresponding closed path phase Φ_T, called the topological phase [74]:

$$\Phi_\mathsf{T}(\mathcal{L}) = \oint_{\mathcal{L}} \mathbf{W}_{1,2}^{(1)ad}(\mathbf{q}'_\lambda) \cdot d\mathbf{q}'_\lambda \tag{3.18}$$

Since $\mathbf{W}_{1,2}^{(1)ad}(\mathbf{q}_\lambda)$ does not in general satisfy Eq. (3.15), these path integrals are no longer independent of the path $\mathcal{L}$. It is also convenient to define the angle $\eta(\mathcal{L})$ by

$$\eta(\mathcal{L}) = \Phi_\mathsf{T}(\mathcal{L}) - p\pi \tag{3.19}$$

where $p = 0$ if $\mathcal{L}$ does not enclose any conical intersection and $p = 1$ if it encloses one conical intersection. This angle is the closed path integral of the transverse part of the first-derivative coupling. A necessary but insufficient condition for the first-derivative coupling to be purely longitudinal is that $\eta(\mathcal{L})$ should vanish [71]. Since conical intersections produce large derivative couplings, large $\eta(\mathcal{L})$ have been interpreted in the past as indicating the existence of conical intersections with the first excluded state [37] or even to locate such intersections [75]. In Sec. 3.4, we present values of the topological phase between the first two states of H_3 over the entire nuclear configuration space and discuss the results.

3.2.2 DMBE couplings and electronic energies

Varandas *et al.* [49] have reported an analytical representation of the lowest electronic PES ($1\ ^2A'$) of H + H_2 based on the DMBE method. For the DMBE fit, they used 267 *ab initio* points of Liu and Siegbahn [76,77], 31 points from Blomberg and Liu [78] and 18 new *ab initio* points. Their *ab initio* calculations employed a primitive ($9s3p1d$) basis set contracted to [$4s3p1d$]. They first perfomed a complete-active-space-self-consistent-field (CASSCF) calculation [64] with the three active orbitals to obtain eight configurations. It was followed by a multireference CI calculation with all single and double excitations out of that eight configuration reference space (MR-CISD). The fundamental form used for the DMBE fit has correct analytical properties [79–82] for a PES exhibiting a C_{3v} conical intersection and is analytically continued to the first-excited electronic PES ($2\ ^2A'$). In the process, it yields a good representation of the first-derivative couplings in the vicinity of the conical intersection. In fact, it gives the leading terms of the longitudinal part of the first-derivative coupling vector, $\mathbf{W}^{(1)ad}_{1,2,lon}(\mathbf{q}_\lambda)$. Varandas *et al.* [49] also mention that these leading terms (of the longitudinal part) can be determined from the adiabatic PESs, but the transverse part ($\mathbf{W}^{(1)ad}_{1,2,tra}(\mathbf{q}_\lambda)$) cannot be completely determined. Besides, in the vicinity of the conical intersection, $\mathbf{W}^{(1)ad}_{1,2,lon}(\mathbf{q}_\lambda)$ diverges but the $\mathbf{W}^{(1)ad}_{1,2,tra}(\mathbf{q}_\lambda)$ part stays finite and small. Hence, the leading terms that provide the longitudinal part give a good representation of the first-derivative couplings in the vicinity of the conical intersection.

Using the DMBE method, it has been shown [49,80] that the longitudinal part and hence the total DMBE first-derivative coupling vector can be approximated (assuming the transverse part to be zero over the entire configuration space) as

$$\mathbf{W}^{(1)ad,\mathrm{DMBE}}_{1,2}(\mathbf{q}_\lambda) \sim \mathbf{W}^{(1)ad,\mathrm{DMBE}}_{1,2,lon}(\mathbf{q}_\lambda) = \boldsymbol{\nabla}_{\mathbf{q}_\lambda}\beta^{\mathrm{DMBE}}(\mathbf{q}_\lambda) \tag{3.20}$$

where

$$\beta^{\mathrm{DMBE}}(\mathbf{q}_\lambda) = \frac{1}{2}\left[\phi_\lambda - \tan^{-1}\frac{g_0(\rho)\sin\theta\sin 3\phi_\lambda}{f_0(\rho) + g_0(\rho)\sin\theta\cos 3\phi_\lambda + f_1(\rho)\sin^2\theta}\right] \tag{3.21}$$

Eqs. (3.20) and (3.21) have been obtained in our hyperspherical coordinates by replacing s by $\sin\theta$ and ϕ by our ϕ_λ in Eq. (48) of Ref. [49]. $g_0(\rho)$, $f_0(\rho)$, and $f_1(\rho)$ are some factors that depend only on the hyperradius ρ. The original DMBE code was used in this work to obtain these longitudinal couplings and the two lowest PESs for H_3. In the vicinity of the conical intersection, these longitudinal couplings are expected to be quite close to the *ab initio* first-derivative couplings. Using this criterion, a systematic mismatch in sign was found in those couplings and was removed by flipping the sign of $g_0(\rho)$ in the DMBE code. These DMBE couplings are presented and compared with the *ab initio* ones in Sec. 3.4. In Sec. 3.3, the two lowest DMBE PESs for H_3 are compared to the PESs obtained from the fits of the *ab initio* energies.

3.3 *Ab initio* and DMBE electronic energies

3.3.1 Fitting method

Any PES fitting procedure is expected to be reasonably simple, result in good agreement with the *ab initio* data and have a physically realistic mathematical form to minimize the number of *ab initio* geometries needed to obtain a surface with correct features and topology [83, 84]. We have used a DMBE plus single-polynomial (DSP) fitting method based on the recent [85] generalized London-Eyring-Polanyi-Sato double-polynomial (GLDP) method as it satisfies most of the abovementioned criteria for fitting methods. The DSP method uses data from the DMBE fit to the lowest two adiabatic electronic PESs for H_3. Since the original DMBE fit is explained in detail in Ref. [49], we will only describe the DSP method here.

The DSP mathematical form used for the lowest two PESs for H_3 is the sum of two terms

$$E_n^{\mathrm{DSP}} = E_n^{\mathrm{DMBE}} + E_n^{\mathrm{POLY}}, \tag{3.22}$$

where $n = 1$ or 2 for the ground or first-excited PES, respectively. The first term is the DMBE potential [49], as it gives a good physical description of the two PESs.

The second term is a single high-order polynomial multiplied by a switching function and modifies the initial DMBE potential to provide greater accuracy. With the three H atoms in H_3 labelled A_α, A_β, or A_γ, this polynomial term is defined by

$$E_n^{\mathrm{POLY}} = S_n(\mathbf{q}_\lambda) \left(\sum_{i+j+k=0}^{t_n} c_{n,ijk} (R_{\alpha\beta} - a_n)^i (R_{\beta\gamma} - a_n)^j (R_{\gamma\alpha} - a_n)^k \right) \tag{3.23}$$

where $R_{\lambda\nu}$ is the distance between A_λ and A_ν ($\lambda\nu = \alpha\beta, \beta\gamma, \gamma\alpha$). The $c_{n,ijk}$ are coefficients and $S_n(\mathbf{q}_\lambda)$ are the switching functions. The switching function S is used to turn the single polynomial in E_n^{POLY} on and off in different regions of the internal nuclear configuration space. Terms up to fifth-order ($t_1 = 5$) are used in the above polynomial for the ground state PES and up to sixth-order ($t_2 = 6$) for the first-excited PES. The sum extends over all possible sets of i, j, k satisfying the condition $i + j + k \leq t_n$. The switching function S is defined by

$$S_n(\mathbf{q}_\lambda) = s(y_{n,\alpha\beta}) s(y_{n,\beta\gamma}) s(y_{n,\gamma\alpha}) \tag{3.24}$$

where

$$s(y_{n,\lambda\nu}) = 1 - \tanh(y_{n,\lambda\nu}) \tag{3.25}$$

in which

$$y_{n,\lambda\nu} = \gamma_n (R_{\lambda\nu} - a_n), \quad \lambda\nu = \alpha\beta, \beta\gamma, \gamma\alpha \tag{3.26}$$

The $c_{n,ijk}$, a_n, and γ_n are variational parameters determined by the fitting method. The $s(y_{n,\lambda\nu})$ terms in Eq. (3.25) turn the E_n^{POLY} term off for the asymptotic geometries. As a result, the asymptotic regions of the PESs have the correct diatomic behavior, included in the E_n^{DMBE} term. The slope parameter, γ_n, having dimensions of a reciprocal length controls how rapidly E_n^{POLY} is made to vanish, whereas a_n is a reference internuclear distance.

The DSP mathematical form is fitted to the *ab initio* data using a *linear* least-squares method to obtain the set of variational parameters (a_n and γ_n) that minimize the root-mean-square (rms) error. Using an initial estimate of the parameters, the

$c_{n,ijk}$ and the corresponding root-mean square (rms) error ϵ are determined by a linear variational procedure. a_n and γ_n are then varied and the determination of $c_{n,ijk}$ and ϵ is repeated until that error is minimized. This procedure is carried out for both the ground and first-excited PESs, and the resulting PESs are examined with the help of equipotential contour plots in the corresponding two-internuclear-distance cartesian space at fixed bond angles for any spurious features in these PESs. No such features were detected. The fitted ground PES 1 $^2A'$ ($E_1^{\rm DSP}$) has an rms error with respect to the *ab initio* data of 0.31 kcal/mol and the corresponding error for the fitted first-excited PES 2 $^2A'$ ($E_2^{\rm DSP}$) is 1.12 kcal/mol. The optimized parameters (a_n and γ_n) are given in Table 3.I and the corresponding optimized coefficients ($c_{n,ijk}$) are given in Table 3.II. These fitted DSP PESs are also examined in hyperspherical coordinates with the help of equipotential contour plots at fixed hyperradii, as discussed in the next subsection and compared with the corresponding contour plots for the DMBE PESs.

3.3.2 DSP and DMBE potential energy surfaces

Equatorial projection plots (Figs. 3.1 and 3.2) of potential energy surfaces in internal symmetrized hyperspherical coordinates $(\rho, \theta, \phi_\lambda)$ [7, 9, 86] provide useful information for reactive scattering calculations that use these coordinates. These plots are obtained as follows. Let the arrangement channel $A_\lambda + A_\nu A_\kappa$ be called the λ arrangement channel, where $\lambda\nu\kappa$ is a cyclic permutation of $\alpha\beta\gamma$. Let $\mathbf{R}'_\lambda, \mathbf{r}'_\lambda$ be the Jacobi vectors associated with this arrangement channel, where $\mathbf{r}'_\lambda$ is the vector from A_ν to A_κ and $\mathbf{R}'_\lambda$ the vector from the center of mass of $A_\nu A_\kappa$ to A_λ. Let $\mathbf{R}_\lambda, \mathbf{r}_\lambda$ be the corresponding mass-scaled Jacobi coordinates [86–90] defined by

$$\mathbf{R}_\lambda = \left(\frac{\mu_{\lambda,\nu\kappa}}{\mu}\right)^{1/2} \mathbf{R}'_\lambda \qquad\qquad \mathbf{r}_\lambda = \left(\frac{\mu_{\nu\kappa}}{\mu}\right)^{1/2} \mathbf{r}'_\lambda \tag{3.27}$$

where $\mu_{\nu\kappa}$ is the reduced mass of $A_\nu A_\kappa$, $\mu_{\lambda,\nu\kappa}$ the reduced mass of the A_λ,$A_\nu A_\kappa$ pair, and μ the system's overall reduced mass given by

$$\mu = \left(\frac{m_\alpha m_\beta m_\gamma}{m_\alpha + m_\beta + m_\gamma} \right)^{1/2}$$

m_λ being the mass of atom A_λ ($\lambda = \alpha, \beta, \gamma$). We now define a set of symmetrized hyperspherical coordinates $\rho, \omega_\lambda, \gamma_\lambda$ [86, 91] by

$$\rho = \left(R_\lambda^2 + r_\lambda^2 \right)^{1/2} \tag{3.28}$$

and

$$R_\lambda = \rho \cos \tfrac{\omega_\lambda}{2} \qquad r_\lambda = \rho \sin \tfrac{\omega_\lambda}{2} \qquad 0 \le \omega_\lambda \le \pi \tag{3.29}$$

where ρ is independent of the arrangement channel [87, 88]. The corresponding internal configuration space cartesian coordinates are defined by

$$X_\lambda = \rho \, \sin\omega_\lambda \, \cos\gamma_\lambda \tag{3.30}$$

$$Y = \rho \, \sin\omega_\lambda \, \sin\gamma_\lambda \tag{3.31}$$

$$Z_\lambda = \rho \, \cos\omega_\lambda \tag{3.32}$$

where γ_λ is the angle between $\mathbf{R}_\lambda$ and $\mathbf{r}_\lambda$ (or $\mathbf{R}'_\lambda$ and $\mathbf{r}'_\lambda$) in the 0 to π range and $\omega_\lambda, \gamma_\lambda$ are the polar angles of a point in this space. The alternate internal configuration space symmetrized hyperspherical coordinates θ, ϕ_λ are defined as the polar angles associated with the interchanged axes $\mathsf{O}\overline{X}_\lambda = \mathsf{O}Z_\lambda$, $\mathsf{O}\overline{Y}_\lambda = \mathsf{O}X_\lambda$, and $\mathsf{O}\overline{Z}_\lambda = \mathsf{O}Y_\lambda$ for which we have

$$\overline{X}_\lambda = Z_\lambda = \rho \, \sin\theta \, \cos\phi_\lambda \tag{3.33}$$

$$\overline{Y}_\lambda = X_\lambda = \rho \, \sin\theta \, \sin\phi_\lambda \tag{3.34}$$

$$\overline{Z} = Y = \rho \, \cos\theta \tag{3.35}$$

with θ and ϕ_λ limited to the ranges given in Eq. (3.13).

The coordinates used for Figs. 3.1 and 3.2 correspond to a mapping [86,92] of the points P of a constant ρ hemisphere in the $\mathsf{O}X_\lambda Y Z_\lambda$ space onto a plane tangent to that hemisphere at the intersection T of the $\mathsf{O}Y$ axis with it (Fig. 3.3). Let $\mathsf{T}x_\lambda$ and $\mathsf{T}y_\lambda$ be respectively the intersection of the $\mathsf{O}Z_\lambda Y$ and $\mathsf{O}X_\lambda Y$ planes with that tangent plane. The corresponding x_λ and y_λ of the map Q of the point P onto the tangent plane are then

$$x_\lambda = \rho\ \theta\ \cos\phi_\lambda \tag{3.36}$$

$$y_\lambda = \rho\ \theta\ \sin\phi_\lambda \tag{3.37}$$

This mapping of P onto Q is not a perpendicular projection, but is one in whch the length of the arc PT of the circle of center O on the constant ρ hemisphere is equal to the length of the straight line TQ on the tangent plane.

To obtain such maps, we start out with a configuration of the molecule defined by the 3 internuclear distances $R_{\alpha\beta}$, $R_{\beta\gamma}$, and $R_{\gamma\alpha}$ and then calculate R'_λ (the magnitude of $\mathbf{R}'_\lambda$), r'_λ (the magnitude of $\mathbf{r}'_\lambda$), and γ_λ. From the first two we calculate the mass-scaled distances R_λ and r_λ and then, with the help of Eqs. (3.28) and (3.29) we obtain ρ and ω_λ. Using Eqs. (3.30) through (3.35) and (3.13) we then calculate θ and ϕ_λ and finally we obtain x_λ and y_λ from Eqs. (3.36) and (3.37), respectively.

This mapping of the PES onto the x_λ, y_λ tangent plane is called the equatorial view because it corresponds to a non-perpendicular arc-length preserving projection of the constant hyperradius hemisphere on a plane tangent to it at the point on its equator defined by $\omega_\lambda = \gamma_\lambda = \pi/2$. This permits the viewing of all three possible atom-diatom arrangement channels (for the triatomic reaction) as well as the regions for which the three atoms are at comparable distances from each other, for a fixed hyperradius ρ. Maps of this kind have been used before [85, 86, 93].

In Figs. 3.1 and 3.2, we present the equatorial views for the lowest two PESs for H_3 obtained by the DSP and DMBE fits. The plots display the C_{3v} symmetry of the H_3 system. Also, the circle at the edge of each plot corresponds to collinear geometries

($\theta = \pi/2$) and the center of each plot corresponds to a conical intersection geometry ($\theta = 0$). Figs. 3.1 (a) through (d) show the equatorial views of the equipotential contours of the 1 $^2A'$ surface for the DSP fit ($E_1^{\rm DSP}$) to the *ab initio* data at constant values of the hyperradius ρ. Figs. 3.1 (e) through (h) show the corresponding contours for the DMBE fit ($E_1^{\rm DMBE}$). Figs. 3.2 (a) through (h) show the corresponding equatorial views for the first-excited (2 $^2A'$) surface. The DSP and DMBE fits are extremely similar for the ground PES (1 $^2A'$), but show some differences in the first-excited PES (2 $^2A'$).

For the ground PES (1 $^2A'$) at $\rho = 2$ bohr (Fig. 3.1 (a)), there are no contours below 3.5 eV suggesting that at energies below 3.5 eV regions for which ρ is smaller than 2 bohr will not be dynamically important. For all other ρ (Fig. 3.1 (b, c, d)), contours as low as 0.5 eV exist suggesting the dynamical importance of these higher ρ regions. In going from $\rho = 4$ bohr (Fig. 3.1 (b)) to $\rho = 6$ bohr (Fig. 3.1 (c)) to $\rho =$ 8 bohr (Fig. 3.1 (d)), we are considering triatomic configurations whose overall size is increasing. For $\rho = 4$ bohr the region near to the center of the figure corresponds to E_1 between 2.5 eV and a value less than 4.0 eV, whereas for $\rho = 6$ bohr that energy lies between 4.0 eV and a value close to the dissociation limit of 4.75 eV and for $\rho =$ 8 bohr it is between 4.5 eV and that dissociation limit. This indicates that for large ρ and stretched configurations of the system, which those regions correspond to, the system approaches dissociation, as expected. The first-excited PES (2 $^2A'$) is similar for both the DSP and DMBE PESs at $\rho = 2$ bohr (Figs. 3.2 (a) and (e)) and at ρ = 8 bohr (Figs. 3.2 (d) and (h)). At $\rho = 4$ bohr, the DSP PES (Fig. 3.2 (b)) has a 6 eV contour that spreads over the entire surface, whereas this contour is closed for the DMBE PES (Fig. 3.2 (f)). On the other hand at $\rho = 6$ bohr, the 5 eV contour spreads over the entire surface for the DMBE PES (Fig. 3.2 (g)) but is closed for the DSP one (Fig. 3.2 (b)).

For the ground PES, DSP fit ($\rm E_1^{DSP}$) has a rms deviation of 1.15 kcal/mol relative to the Liu-Siegbahn-Truhlar-Horowitz (LSTH) PES [94] ($\rm E_1^{LSTH}$) and of 1.03 kcal/mol relative to the DMBE one ($\rm E_1^{DMBE}$) for energies below 5 eV. For the first-excited

PES, DSP fit (E_2^{DSP}) has a rms deviation of 1.19 kcal/mol relative to the DMBE one (E_2^{DMBE}) for energies below 5 eV and of 2.97 kcal/mol for energies below 10 eV. E_1^{DSP} stays greater than E_1^{LSTH} and E_1^{DMBE} for most geometries (except for large geometries with ρ greater than 6 bohr near the conical intersection with θ smaller than 10°) in the internal nuclear configuration space, whereas E_2^{DSP} stays greater than E_2^{DMBE} only for compact geometries (ρ less than 4 bohr) near and slightly away from the conical intersection (θ less than 40°). This is due to the fact that *ab initio* electronic structure calculations were performed to obtain good representative ground and first-excited state energies used in the E_1^{DSP} and E_2^{DSP} fits. This leads to a slightly higher E_1^{DSP} than it would be, if the basis set used was chosen to optimize the ground state energies only. Since E_2^{DMBE} PES is an analytic continuation of the E_1^{DMBE} PES, E_2^{DSP} PES is lower than E_2^{DMBE} for most nuclear geometries.

Overall, for the ground PES, the DMBE PES is accurate over the entire internal configuration space, but for the first-excited state PES, the similarities between DSP and DMBE PESs at $\rho = 2$ bohr and 8 bohr and the differences between them at $\rho = 4$ bohr and 6 bohr indicate that the DMBE PES is accurate in the compact and asymptotic regions, but not in the strong interaction regions.

3.4 Results and discussion

3.4.1 *Ab initio* and DMBE first-derivative couplings

The first-derivative coupling vector ($\mathbf{W}_{1,2}^{(1)ad}(\mathbf{q}_\lambda)$) obtained using Eq. (3.9) had its three components defined in the ρ, θ, and ϕ_λ unit vector directions by Eqs. (3.10) through (3.12). These internal hyperspherical coordinates ($\mathbf{q}_\lambda$: ρ, θ, ϕ_λ) defined in Sec. 3.2 are identical to ordinary spherical polar coordinates except for the range of θ which is 0 to $\pi/2$ for the former [Eq. (3.13)] compared to 0 to π for the latter. These internal hyperspherical coordinates span half a sphere (compared to the full sphere spanned by ordinary spherical polar coordinates). This property facilitates

the visualization of the first-derivative coupling vector in the associated internal 3-D cartesian coordinate configuration space. The transformation of this vector into its cartesian counterpart, which has components $\mathrm{W}^{(1)ad}_{1,2,x}$, $\mathrm{W}^{(1)ad}_{1,2,y}$, and $\mathrm{W}^{(1)ad}_{1,2,z}$ in the x, y, and z unit vector directions, is defined as

$$\begin{pmatrix} \mathrm{W}^{(1)ad}_{1,2,x} \\ \mathrm{W}^{(1)ad}_{1,2,y} \\ \mathrm{W}^{(1)ad}_{1,2,z} \end{pmatrix} = \begin{pmatrix} \sin\theta\cos\phi_\lambda & \cos\theta\cos\phi_\lambda & -\sin\phi_\lambda \\ \sin\theta\sin\phi_\lambda & \cos\theta\sin\phi_\lambda & \cos\phi_\lambda \\ \cos\theta & -\sin\theta & 0 \end{pmatrix} \begin{pmatrix} \mathrm{W}^{(1)ad}_{1,2,\rho} \\ \mathrm{W}^{(1)ad}_{1,2,\theta} \\ \mathrm{W}^{(1)ad}_{1,2,\phi_\lambda} \end{pmatrix} \tag{3.38}$$

In the central panels of Figs. 3.4 through 3.7, we present a perpective view of the three-dimensional *ab initio* first-derivative coupling vector at points in this space with varying values of the hyperangle ϕ_λ, for fixed values of the hyperradius ρ and hyperangle θ. In cartesian language, this is equivalent to varying x and y and keeping z fixed, as indicated by the dotted horizontal circles in those figures. The cartesian components of this vector were obtained from Eq. (3.38). The leftmost panels contain the corresponding DSP ground state electronic energies plotted as vertical lines such that the energies can be read off from the length of those vertical lines. The rightmost panels contain the DSP first-excited state electronic energies plotted in the same way as the ground state electronic energies. Figs. 3.8 through 3.11 present the same physical quantities but obtained by the DMBE method. The cartesian components of the longitudinal part of the DMBE first-derivative coupling vector are also obtained from Eq. (3.38). Figs. 3.4, 3.5, 3.6, and 3.7 correspond to the fixed hyperradii of 2 bohr, 4 bohr, 6 bohr, and 8 bohr respectively. The same is the case for Figs. 3.8, 3.9, 3.10, and 3.11. In all figures (3.4 through 3.11), panel (a) (the first row of plots) corresponds to $\theta = 1^\circ$ (a value very close to the conical intersection geometries of $\theta = 0^\circ$), panel (b) corresponds to $\theta = 30^\circ$, panel (c) to $\theta = 60^\circ$, and panel (d) to $\theta = 90^\circ$ (collinear geometries). The tail end of the vectors lies on a circle that corresponds to a fixed θ on the hemisphere in hyperspherical coordinate space defined

by a fixed hyperradius ρ. This circle maps the full ϕ_λ range of 0° to 360° and is shown on the bottom face of all E_1 and E_2 panels. The coupling vectors shown in the central panels correspond to the configurations being mapped by this circle. Above each of these central panels two scales are given. The one in units of bohr corresponds to the internal nuclear configuration space corresponding to the full 0° to 360° ϕ_λ range spanned on the xy plane. The second one in units of bohr^{-1} corresponds to the three-dimensional space sampled by the x, y, and z components of the coupling vector. The two spaces co-exist on the xy plane. In addition, in all figures the ground-state energies (E_1) have been cut off at 10 eV and the first-excited state electronic energies (E_2) at 15 eV.

The first-derivative coupling vector plots at $\theta = 1°$ (panel (a) in all figures) have been included to show their behavior near the conical intersection. The $\theta = 90°$ (panel (d) in all figures) case has been included, as it corresponds to collinear geometries for the triatomic system. This case is important for lower energies due to the collinear dominance of the H + H_2 reaction at those energies, as will be discussed in the next subsection. The $\theta = 30°$ and $\theta = 60°$ cases (panels (b) and (c) respectively in all figures) have been included to gauge the importance of the coupling vector away from the conical intersection as well as the collinear geometries.

For the DMBE case, the total first-derivative coupling vector ($\mathbf{W}_{1,2}^{(1)ad,\mathrm{DMBE}}(\mathbf{q}_\lambda)$) is equal to its longitudinal part ($\mathbf{W}_{1,2,lon}^{(1)ad,\mathrm{DMBE}}(\mathbf{q}_\lambda)$) because the transverse part ($\mathbf{W}_{1,2,tra}^{(1)ad,\mathrm{DMBE}}(\mathbf{q})_\lambda$) was neglected over the entire internal configuration space. Figs. 3.8 through 3.11 show the DMBE's total (or longitudinal) first-derivative coupling vector and the corresponding ground and first-excited DMBE energies for comparison with the *ab initio* first-derivative coupling vector plots. In the next subsection, the comparison between DMBE and *ab initio* first-derivative coupling vectors is discussed, based upon their magnitudes and the corresponding ground and first-excited energies. This discussion will help locate the regions of the internal hyperspherical configuration space for the H + H_2 reaction, for which the first-derivative couplings may affect the dynamics of that reaction.

3.4.2 The topological phase

In Sec. 3.2.1 we mentioned how we can get some qualitative indication of possible non-negligible derivative couplings between the 2 $^2A'$ and 3 $^2A'$ PESs of H_3. This involves calculating the topological phase $\Phi_{\mathsf{T}}(\mathcal{L})$ from Eq. (3.18) along closed loops around the conical intersection between the 1 $^2A'$ and 2 $^2A'$ states. A non-zero $\eta(\mathcal{L})$ (defined by Eq. (3.19)) is indicative of such non-negligible couplings (see Sec. 3.2.1).

In our symmetrized hyperspherical coordinates, $\mathbf{q}_\lambda$ is a set of the three coordinates ρ, θ, and ϕ_λ. The abovementioned original conical intersection between the 1 $^2A'$ and 2 $^2A'$ states lies along $\theta = 0°$ for all values of ρ. ϕ_λ is undefined at $\theta = 0°$. To evaluate the integral in Eq. (3.17) along an open loop around that conical intersection, we take a circular path $\mathcal{L}$ given by a fixed value of $\theta \neq 0°$, a fixed ρ, and ϕ_λ varying along that path from 0 to an arbitrary value, according to

$$\Phi(\phi_\lambda, 0; \rho, \theta) = \int_0^{\phi_\lambda} \mathrm{W}^{(1)ad}_{1,2,\phi_\lambda}(\rho, \theta, \phi'_\lambda)\ \rho \sin\theta\ d\phi'_\lambda \tag{3.39}$$

where $\mathrm{W}^{(1)ad}_{1,2,\phi_\lambda}(\rho, \theta, \phi'_\lambda)$ is defined in Eq. (3.12). These integrals are evaluated using the standard Simpson numerical integration quadrature. From here on, we will drop the 0 in $\Phi(\phi_\lambda, 0; \rho, \theta)$ and just refer to it as $\Phi(\phi_\lambda; \rho, \theta)$.

In Fig. 3.12 we show the open-path phase $\Phi(\phi_\lambda; \rho, \theta)$ as a function of ϕ_λ evaluated using Eq. (3.39) for four values of ρ (2, 4, 6, and 8 bohr) and four values of θ (1°, 30°, 60°, and 90°). For each ρ and θ we then calculate the closed-loop integral (or the topological phase) Φ_{T}. This corresponds to a complete loop around the conical intersection ($\phi_\lambda = 2\pi$ in Eq. (3.39)) and is expressed as

$$\Phi_{\mathsf{T}}(\rho, \theta) = \oint \mathrm{W}^{(1)ad}_{1,2,\phi_\lambda}(\rho, \theta, \phi'_\lambda)\ \rho \sin\theta\ d\phi'_\lambda \tag{3.40}$$

In Fig. 3.13 we display this topological phase as a function of ρ and θ for the entire (ρ, θ) space considered in this chapter.

3.4.3 Discussion

As mentioned in Sec. 3.4.1, Figs. 3.4 through 3.7 display the *ab initio* first-derivative coupling vector and the corresponding DSP ground and first-excited electronic state energies for $\rho = 2$ bohr through 8 bohr, in steps of 2 bohr. Each of the figures has 4 sets of panels: (a) $\theta = 1^\circ$ (triatomic geometries near conical intersection), (b) $\theta = 30^\circ$, (c) $\theta = 60^\circ$, and (d) $\theta = 90^\circ$ (collinear triatomic geometries).

Fig. 3.4 (a) ($\rho = 2$ bohr and $\theta = 1^\circ$) corresponds to a very compact set of geometries near the conical intersection. Being near the conical intersection (where the two electronic states are degenerate), the ground (E_1) and the first-excited (E_2) state energies are close to each other and stay around 3.3 eV as a function of ϕ_λ. The first-derivative coupling vector has a large magnitude (between 10 and 15 bohr^{-1}) but its z-component is very small compared to its length, due to a singularity at the conical intersection geometries. This dominance of the x- and y- components translates into a strong dominance of the ϕ_λ-component of the first-derivative coupling vector near the conical intersection. Fig. 3.4 (b) ($\rho = 2$ bohr and $\theta = 30^\circ$) corresponds to a compact set of geometries further away from the conical intersection (but with the largest bond angle in the range 106° to 120° and the smallest bond length around 1.5 bohr, as seen in Table 3.III). This manifests itself in the fact that for this θ the E_1 and E_2 energies are quite different from each other, the former staying above 3.1 eV and varying slowly between 3.1 and 3.5 eV as a function of ϕ_λ with the latter staying around 6 eV and varying even more slowly with ϕ_λ. The coupling vector is smaller in magnitude (with a maximum around 1 bohr^{-1} and an average around 0.5 bohr^{-1}) than for Fig. 3.4 (a) due to its greater distance from the conical intersection configurations.

Fig. 3.4 (c) ($\rho = 2$ bohr and $\theta = 60^\circ$) corresponds to compact geometries (with the largest bond angle in the range 140° to 150° and the smallest bond length in the range 0.56−1.14 bohr, as seen in Table 3.III) even further removed from the conical intersection. The E_1 and E_2 energies are again quite different from each other, and vary more rapidly with ϕ_λ than before (Fig. 3.4 (b)). The E_1 energies vary between 4 eV and some value higher than 10 eV as a function of ϕ_λ, while the E_2 energies

vary between 7 eV and some value higher than 15 eV with ϕ_λ. Both E_1 and E_2 display maxima at $\phi_\lambda = 0°$, 120°, and 240°. The coupling vector is again smaller in magnitude (with a maximum around 0.5 bohr^{-1} and averaging around 0.3 bohr^{-1}) than for $\theta = 1°$ (Fig. 3.4 (a)) but varies more rapidly with ϕ_λ as compared to the $\theta = 30°$ case (Fig. 3.4 (b)). The x-, y-, and z-components are comparable with each other contrary to the $\theta = 1°$ (Fig. 3.4 (a)) and $\theta = 30°$ (Fig. 3.4 (b)) cases. Fig. 3.4 (d) (ρ = 2 bohr and $\theta = 90°$) corresponds to compact collinear geometries with the smallest bond length in the range 0 to 1 bohr. The E_1 and E_2 energies are again quite different from each other, and vary even more rapidly with ϕ_λ than before (Fig. 3.4 (c)) with minima around 5 eV and 8 eV, respectively. Both E_1 and E_2 have maxima at ϕ_λ = 0°, 120°, and 240° as for the $\theta = 30°$ case (Fig. 3.4 (c)), as at these configurations two out of three atoms are superimposed on each other. The coupling vector is small (averaging around 0.5 bohr^{-1}) as compared to the $\theta = 1°$ case (Fig. 3.4 (a)), and has a negligible z-component compared to the $\theta = 30°$ (Fig. 3.4 (b)) and $\theta = 60°$ (Fig. 3.4 (c)) cases. Both E_1 and E_2 energies over the entire $\rho = 2$ bohr configuration (compact geometries) space are 3.1 eV or higher and are expected to be of dynamical importance only at energies slightly below that value or higher.

Figure 3.5 presents the first-derivative coupling vector and the E_1 and E_2 energies for $\rho = 4$ bohr. This hyperradius is of dynamical importance for energies significantly below the lowest conical intersection energy of 2.75 eV (which occurs at $\rho_{min} \equiv 2.6$ bohr for the DMBE PES [49]), and is also expected to be of importance at that energy and above since the conical intersection energy increases rather slowly with with ρ above ρ_{min}. The $\theta = 1°$ case (Fig. 3.5 (a)) is similar to the one for $\rho = 2$ bohr (Fig. 3.4 (a)). E_1 and E_2 are close to each other and are approximately equal to 3.6 eV. The coupling vector has large x- and y-components (10 bohr^{-1}) and a negligible z-component, again translating into a strong dominance of its ϕ_λ-component near the conical intersection. At $\theta = 30°$ (Fig. 3.5 (b)), E_1 is as low as 1.5 eV, E_2 is 5 eV or larger, and the coupling vector has a smaller magnitude than for $\theta = 1°$ (Fig. 3.5 (a)). At $\theta = 60°$ (Fig. 3.5 (c)), E_1 is as small as 0.25 eV, E_2 is 6 eV or larger, and the

coupling vector has about the same magnitude as that at $\theta = 30°$ (Fig. 3.5 (b)). At $\theta = 90°$ (Fig. 3.5 (d)), which corresponds to collinear geometries, E_1 can be as low as 0.2 eV and varies rapidly with ϕ_λ than for smaller values of θ and E_2 is again 6 eV or larger. The coupling vector has a larger z-component than for the lower values of θ discussed. Collinear geometries are important for low collision energies [42]. Their importance at energies close to and above conical intersection energies is likely to be significantly smaller or perhaps negligible but this remains to be determined by future scattering calculations.

For the $\rho = 6$ bohr (Fig. 3.6) and 8 bohr (Fig. 3.7) cases, which correspond to triatomic large sized geometries (see Table 3.III), the electronic energies are fairly similar to the $\rho = 4$ bohr case (Fig. 3.5). In both these cases, E_1 can be as low as 0.2 eV. The coupling vector magnitudes on the the other hand are smaller on average and have sharper maxima compared to the $\rho = 4$ bohr case at around $\phi_\lambda = 60°$, 180°, and 300°. They all have negligible z-components, but their maxima occur in low energy regions. The coupling vectors presented in Figs. 3.6 and 3.7 may also affect the dynamics of the H + H_2 reaction depending on their magnitudes.

A similar detailed analysis of the DMBE first-derivative coupling vectors (Figs. 3.8 through 3.11) leads to the following conclusions. For $\rho = 2$ bohr (Fig. 3.8), the coupling vector has a z-component which is negligible in the vicinity of the conical intersection ($\theta = 1°$) and at the collinear geometries ($\theta = 90°$) but non-negligible in the intermediate regions. For all other values of the hyperradii ($\rho = 4$ bohr, 6 bohr, and 8 bohr), that z-component is negligible over the entire θ, ϕ_λ space (Figs. 3.9, 3.10, and 3.11), which indicates the dominance of the ϕ_λ-component. This stems from the fact that the DMBE coupling vector is purely longitudinal and given by Eqs. (3.20) and (3.21). A comparison of the DMBE first-derivative coupling vectors with the corresponding *ab initio* couplings confirms the previously stated fact that the DMBE's coupling vector has the right physical and quantitative behaviour in the vicinity of the conical intersection. The differences between these two vectors, which occur even at low energies, stem mainly from the fact that the *ab initio* couplings

include both a longitudinal part and a transverse part, whereas the DMBE couplings only include a longitudinal part, which is a good approximation to the *ab initio* longitudinal part in the vicinity of a conical intersection.

Fig. 3.12 shows the open-path phase $\Phi(\phi_\lambda; \rho, \theta)$ for four values of θ (1°, 30°, 60°, and 90°) and four values of ρ ((a) 2 bohr, (b) 4 bohr, (c) 6 bohr, and (d) 8 bohr) as a function of ϕ_λ as defined by Eq. (3.39). It shows how the open-path phase Φ increases with ϕ_λ along a loop around the conical intersection between the $1\ ^2A'$ and $2\ ^2A'$ electronic states. For the $\theta = 1°$ case (solid line in all four panels), to a very good approximation (0.2 % or smaller difference) Φ is equal to $\phi_\lambda/2$ for all values of ρ considered. This is clearly expected because $\theta = 1°$ is a region very close to the conical intersection and the $\phi_\lambda/2$ is a leading term of the diabatization angle in that region. For other values of θ, Φ fluctuate around some mean value proportional to ϕ_λ. The deviation of this mean value from $\phi_\lambda/2$ is dependent both on ρ and θ. Also, Φ returns to its mean value at regular intervals of 60° in ϕ_λ. As a result, we can approximate Φ by a sum of two terms, the first one being proportional to ϕ_λ and the second more complicated one possessing the C_{3v} symmetry (of H_3) via a $\sin 3\phi_\lambda$ dependence. The fluctuations in Φ about the mean value arise only from this second term and have an amplitude which increases monotonically with ρ between $\rho = 2$ bohr and $\rho = 8$ bohr. This seems to stem from the fact that for a large value of ρ, the length of the circular loop around the conical intersection is large, which leads to a large phase accumulation in these fluctuations.

Fig. 3.13 shows the topological phase $\Phi_\mathsf{T}(\rho, \theta)$ (defined by Eq. (3.40)) as a function of ρ and θ over the ρ space of 2 bohr to 10 bohr and the θ space of 1° to 90°. $\Phi_\mathsf{T} = 180°$ values correspond to a purely longitudinal first-derivative coupling vector. Any deviation of $\Phi_\mathsf{T}(\rho, \theta)$ from this value suggests a non-zero transverse (*nonremovable*) part of the coupling vector [37,56]. On the bottom part of Fig. 3.13 we show contours corresponding to fixed values of $\Phi_\mathsf{T}(\rho, \theta)$ ranging from 150° to 225° every 15°. The 180° contour has been shown in bold lines and its different segments labelled $\mathbf{S}_1$, $\mathbf{S}_2$, and $\mathbf{S}_3$. For small values of θ and all ρ, the values of $\Phi_\mathsf{T}(\rho, \theta)$ stay reasonably constant

and equal to 180°. This is expected because these small values of θ correspond to regions near the conical intersection, where the transverse component of the first-derivative coupling vector is expected to be negligible. This flat portion of the Φ_{T} surface is quite narrow at small ρ and gets wider as ρ increases. Also, for small values of ρ ($<$ 6 bohr) $\Phi_{\mathsf{T}}(\rho,\theta)$ first increases and then drops as a function of θ. Beyond ρ = 6 bohr, $\Phi_{\mathsf{T}}(\rho,\theta)$ first drops somewhat and then increases slightly to a value under 180° as a function of θ.

The phase $\Phi_{\mathsf{T}}(\rho,\theta)$ plotted in Fig. 3.13 gives an indication of the presence of non-negligible derivative couplings in the regions of (ρ,θ) space where it is different from 180°. In the present work, we have computed this phase over the entire dynamically important part of configuration space. In the absence of additional electronic state calculations, no method exists, to the best of our knowledge, that quantitatively correlates the deviation of this phase from 180° (over the whole configuration space) with the non-negligible derivative couplings that arise from nonadiabatic interactions involving states outside the two-adiabatic-state space. The 180° contour segments $\mathbf{S}_2$ and $\mathbf{S}_3$ in Fig. 3.13 are embedded in regions of (ρ,θ) configuration space, where $\Phi_{\mathsf{T}}(\rho,\theta)$ deviates substantially from 180° and hence are not expected to contain information about any glancing interaction or conical intersections between the 2 $^2A'$ and 3 $^2A'$ states of H_3. Such is not the case for the $\mathbf{S}_1$ segment. In Fig. 3.14, we display this segment in two representations. Fig. 3.14 (a) shows it in the $X_\lambda Y$ plane of Fig. 3.3 and Fig. 3.14 (b) in the regular ρ-θ plane. The points corresponding to ρ greater than 8 bohr have been indicated as dashed lines because they are a result of an extrapolation of the computed couplings and hence should not be used to draw any conclusions. Points below the solid curves correspond to extended regions of configuration space for which $\Phi_{\mathsf{T}}(\rho,\theta)$ deviates from 180° and indicates that the value of $\mathbf{W}^{(1)ad}_{1,2,tra}$ is non-negligible in those regions. These solid curves seem to suggest the presence of intersection lines or avoided intersections between the 2 $^2A'$ and 3 $^2A'$ PESs in the $(\rho,\theta,\phi_\lambda)$ space, where ϕ_λ might correspond to three possible sets of C_{2v} configurations. It can either be the $(0°, 120°, 240°)$ set or the $(60°, 180°, 300°)$ set, or

even both. A possible conical intersection between the 2 $^2A'$ and 3 $^2A'$ states was suggested by Yarkony [37] earlier for H_3. An alternate explanation may be that, at the values of ρ of relevance to Fig. 3.14, the curl of $\mathbf{W}_{1,2}^{(1)ad}$ (or, equivalently, of its transverse part) is large [95].

Calculations of the energy of the 3 $^2A'$ state of H_3 and of its first-derivative couplings with the 2 $^2A'$ state are needed to help establish a quantitative correlation between possible conical intersections involving those two states and the topological phase between the 1 $^2A'$ and 2 $^2A'$ states. The regions of nuclear configuration space, where the effect of nonadiabatic couplings (between the 2 $^2A'$ and 3 $^2A'$ states) is being felt, have many low energy regions, suggesting that the *nonremovable* part of the nonadiabatic couplings (between the 1 $^2A'$ and 2 $^2A'$ states) cannot be ignored and may play a significant role in the dynamics of the H + H_2 reaction, due to its presence in the diabatic nuclear motion Schrödinger equation [7].

The vector $\mathsf{w}^{(1)ad}(\mathbf{q}_\lambda)$ (or $\mathsf{w}_{1,2}^{(1)ad}(\mathbf{q}_\lambda)$) can also provide a good first approximation to the second-derivative coupling matrix $\mathsf{W}^{(2)ad}(\mathbf{q}_\lambda)$, which in a two-electronic-state approximation is given by

$$\mathsf{W}^{(2)ad}(\mathbf{q}_\lambda) = \begin{pmatrix} \mathsf{w}_{1,1}^{(2)ad}(\mathbf{q}_\lambda) & \mathsf{w}_{1,2}^{(2)ad}(\mathbf{q}_\lambda) \\ \\ \mathsf{w}_{2,1}^{(2)ad}(\mathbf{q}_\lambda) & \mathsf{w}_{2,2}^{(2)ad}(\mathbf{q}_\lambda) \end{pmatrix} \tag{3.41}$$

In the two-electronic-state Born-Huang expansion, the full Hilbert space of adiabatic electronic states is approximated by the lowest two states and furnishes for the corresponding electronic wave functions the approximate closure relation

$$\mid \psi_1^{el,ad}(\mathbf{r};\mathbf{q}_\lambda)\rangle\langle\psi_1^{el,ad}(\mathbf{r};\mathbf{q}_\lambda) \mid + \mid \psi_2^{el,ad}(\mathbf{r};\mathbf{q}_\lambda)\rangle\langle\psi_2^{el,ad}(\mathbf{r};\mathbf{q}_\lambda) \mid \approx 1 \tag{3.42}$$

Using this equation and the fact that for real electronic wave functions the diagonal

elements of $\mathsf{W}^{(1)ad}(\mathbf{q}_\lambda)$ vanish, it can be shown that

$$\begin{aligned} \mathsf{w}_{1,1}^{(2)ad}(\mathbf{q}_\lambda) = \mathsf{w}_{2,2}^{(2)ad}(\mathbf{q}_\lambda) &= -\,\mathsf{w}_{1,2}^{(1)ad}(\mathbf{q}_\lambda)\cdot\mathsf{w}_{1,2}^{(1)ad}(\mathbf{q}_\lambda) \\ \mathsf{w}_{1,2}^{(2)ad}(\mathbf{q}_\lambda) = \mathsf{w}_{2,1}^{(2)ad}(\mathbf{q}_\lambda) &= 0 \end{aligned} \tag{3.43}$$

For the H_3 system, since $\mathsf{w}_{1,2}^{(1)ad}(\mathbf{q}_\lambda)$ is known over the entire $\mathbf{q}_\lambda$ space [96], Eq. (3.43) can be used to obtain the two equal non-zero diagonal elements of the $\mathsf{W}^{(2)ad}(\mathbf{q}_\lambda)$ matrix. Since this matrix appears with a multiplicative factor of $(-\hbar^2/2\mu)$ in the adiabatic nuclear motion Schrödinger equation giving it the units of energy, both $(-\hbar^2/2\mu)\ \mathsf{w}_{1,1}^{(2)ad}(\mathbf{q}_\lambda)$ and $(-\hbar^2/2\mu)\ \mathsf{w}_{2,2}^{(2)ad}(\mathbf{q}_\lambda)$ can be labelled as $\varepsilon^{(2)ad}$. In Fig. 3.15, this quantity is displayed in units of kcal mol^{-1} for several values of ρ as a function of θ and ϕ_λ. It shows the singular behavior of the diagonal elements of $\mathsf{W}^{(2)ad}(\mathbf{q}_\lambda)$ at conical intersection geometries ($\theta = 0^\circ$). Being a repulsive correction to the adiabatic energies, this singular behavior would prevent any hopping of the nuclei from one electronic state to another at and extremely close to the conical intersection.

Appendix 3.A - First-derivative coupling vector for triatomic reactions

As discussed in Sec. 2.1, the adiabatic electronic wave functions $\psi_i^{el,ad}$ and $\psi_j^{el,ad}$ depend on the nuclear coordinates $\mathbf{R}_\lambda$ only through the subset $\mathbf{q}_\lambda$ (which in the triatomic case consists of a nuclear coordinate hyperradius ρ and a set of two internal hyperangles $\boldsymbol{\xi}_\lambda$), this permits one to relate the six-dimensional vector $\mathbf{w}^{(1)ad}(\mathbf{R}_\lambda)$ to another one $\mathsf{w}^{(1)ad}(\mathbf{q}_\lambda)$ that is three-dimensional. For a triatomic system, let $\mathbf{a}^{I\lambda} \equiv (a^{I\lambda}, b^{I\lambda}, c^{I\lambda})$ be the Euler angles that rotate the space-fixed cartesian frame into the body-fixed principal axis of inertia frame $I\lambda$, and let $\boldsymbol{\nabla}_{\mathbf{R}_\lambda}^{I\lambda}$ be the six-dimensional gradient vector in this rotated frame. The relation between the space-fixed $\boldsymbol{\nabla}_{\mathbf{R}_\lambda}$ and $\boldsymbol{\nabla}_{\mathbf{R}_\lambda}^{I\lambda}$ is given by

$$\boldsymbol{\nabla}_{\mathbf{R}_\lambda} = \tilde{\mathcal{R}}(\mathbf{a}^{I\lambda})\ \boldsymbol{\nabla}_{\mathbf{R}_\lambda}^{I\lambda} \tag{3.44}$$

where $\mathcal{R}(\mathbf{a}^{I\lambda})$ is a 6×6 block-diagonal matrix whose 2 diagonal blocks are both equal to the 3×3 rotational matrix $\mathsf{R}(\mathbf{a}^{I\lambda})$. The $\boldsymbol{\nabla}_{\mathbf{R}_\lambda}^{I\lambda}$ operator can be written as [97]

$$\boldsymbol{\nabla}_{\mathbf{R}_\lambda}^{I\lambda} = \mathbf{G}^{I\lambda}(\boldsymbol{\xi}_\lambda)\hat{\mathbf{p}}^{I\lambda}(\mathbf{q}_\lambda) + \mathbf{H}^{I\lambda}(\boldsymbol{\xi}_\lambda)\hat{\mathbf{J}}^{I\lambda}(\mathbf{a}^{I\lambda}) \tag{3.45}$$

In this expression, $\mathbf{G}^{I\lambda}$ and $\mathbf{H}^{I\lambda}$ are both 6×3 rectangular matrices whose elements are known functions of the internal hyperangles $\boldsymbol{\xi}_\lambda$. $\hat{\mathbf{p}}^{I\lambda}$ is a 3×1 column vector operator whose elements contain first-derivatives with respect to the three $\mathbf{q}_\lambda$ coordinates and $\hat{\mathbf{J}}^{I\lambda}$ is the 3×1 column vector operator whose elements are the components $\hat{J}_x^{I\lambda}$, $\hat{J}_y^{I\lambda}$ and $\hat{J}_z^{I\lambda}$ of the system's nuclear motion angular momentum operator $\hat{\mathbf{J}}$ in the $I\lambda$ frame. From these properties it can be shown that

$$\mathbf{w}^{(1)ad}(\mathbf{R}_\lambda) = \mathcal{R}(\mathbf{a}^{I\lambda})\widetilde{\mathbf{G}}^{I\lambda}(\boldsymbol{\xi}_\lambda)\mathsf{w}^{(1)ad}(\mathbf{q}_\lambda) \tag{3.46}$$

and that

$$\mathbf{W}^{(1)ad}(\mathbf{R}_\lambda) \cdot \boldsymbol{\nabla}_{\mathbf{R}_\lambda}\boldsymbol{\chi}^{ad}(\mathbf{R}_\lambda) = \widetilde{\mathbf{G}}^{I\lambda}(\xi_\lambda)\mathsf{W}^{(1)ad}(\mathbf{q}_\lambda) \cdot \boldsymbol{\nabla}_{\mathbf{R}_\lambda}^{I\lambda}\boldsymbol{\chi}^{ad}(\mathbf{R}_\lambda) \tag{3.47}$$

where

$$\mathsf{w}^{(1)ad}(\mathbf{q}_\lambda) = \langle \psi_1^{el,ad}(\mathbf{r};\mathbf{q}_\lambda) \mid \hat{\mathbf{p}}^{I\lambda}(\mathbf{q}_\lambda)\psi_2^{el,ad}(\mathbf{r};\mathbf{q}_\lambda)\rangle_{\mathbf{r}} \tag{3.48}$$

is a three-dimensional column vector and $\mathsf{W}^{(1)ad}(\mathbf{q}_\lambda)$ is a 2×2 skew-symmetric matrix whose only non-zero element is the $\mathsf{w}^{(1)ad}(\mathbf{q}_\lambda)$ vector. The effect of $\mathbf{G}^{I\lambda}(\xi_\lambda)$ can be built into the $\boldsymbol{\nabla}^{I\lambda}_{\mathbf{R}_\lambda}$ operator leading to

$$\mathbf{W}^{(1)ad}(\mathbf{R}_\lambda)\cdot\boldsymbol{\nabla}_{\mathbf{R}_\lambda}\boldsymbol{\chi}^{ad}(\mathbf{R}_\lambda) = \mathsf{W}^{(1)ad}(\mathbf{q}_\lambda)\cdot\boldsymbol{\nabla}_{\mathbf{R}_\lambda}\boldsymbol{\chi}^{ad}(\mathbf{R}_\lambda) \tag{3.49}$$

where

$$\boldsymbol{\nabla}_{\mathbf{R}_\lambda} = \hat{\mathbf{p}}^{I\lambda}(\mathbf{q}_\lambda) + \widetilde{\mathbf{G}}^{I\lambda}(\xi_\lambda)\mathbf{H}^{I\lambda}(\boldsymbol{\xi}_\lambda)\hat{\mathbf{J}}^{I\lambda}(\mathbf{a}^{I\lambda}) \tag{3.50}$$

Using the symmetrized hyperspherical coordinates defined in Sec. 3.3 for a triatomic system, the elements of $\hat{\mathbf{p}}^{I\lambda}$ are the spherical polar components of the three-dimensional gradient associated with the polar coordinates ρ,θ,ϕ_λ [96]:

$$\hat{\mathbf{p}}^{I\lambda} = \begin{pmatrix} \dfrac{\partial}{\partial\rho} \\ \dfrac{1}{\rho}\dfrac{\partial}{\partial\theta} \\ \dfrac{1}{\rho\sin\theta}\dfrac{\partial}{\partial\phi_\lambda} \end{pmatrix} \tag{3.51}$$

The corresponding cartesian gradient $\boldsymbol{\nabla}_{\mathbf{q}_\lambda}$ is given by

$$\boldsymbol{\nabla}_{\mathbf{q}_\lambda} = \begin{pmatrix} \sin\theta\cos\phi_\lambda & \cos\theta\cos\phi_\lambda & -\sin\phi_\lambda \\ \sin\theta\sin\phi_\lambda & \cos\theta\sin\phi_\lambda & \cos\phi_\lambda \\ \cos\theta & -\sin\theta & 0 \end{pmatrix} \hat{\mathbf{p}}^{I\lambda} \tag{3.52}$$

in a space whose polar coordinates are ρ,θ,ϕ_λ.

Bibliography

[1] G. Herzberg and H. C. Longuet-Higgins, Discussion Faraday Soc. **35**, 77 (1963).

[2] H. C. Longuet-Higgins, Proc. R. Soc. London A **344**, 147 (1975).

[3] H. C. Longuet-Higgins, Adv. Spectrosc. **2**, 429 (1961).

[4] C. A. Mead and D. G. Truhlar, J. Chem. Phys. **70**, 2282 (1979).

[5] C. A. Mead, Chem. Phys. **49**, 23 (1980).

[6] M. V. Berry, Proc. Roy. Soc. London A **392**, 45 (1984).

[7] A. Kuppermann, in *Dynamics of Molecules and Chemical Reactions*, edited by R. E. Wyatt and J. Z. H. Zhang (Marcel Dekker, New York, 1996), pp. 411-472.

[8] Y. Aharonov and D. Bohm, Phys. Rev. **115**, 485 (1969).

[9] Y.-S. M. Wu, A. Kuppermann, and B. Lepetit, Chem. Phys. Lett. **186**, 319 (1991).

[10] Y.-S. M. Wu and A. Kuppermann, Chem. Phys. Lett. **201**, 178 (1993).

[11] A. Kuppermann and Y.-S. M. Wu, Chem. Phys. Lett. **205**, 577 (1993).

[12] Y.-S. M. Wu and A. Kuppermann, Chem. Phys. Lett. **235**, 105 (1995).

[13] A. Kuppermann and Y.-S. M. Wu, Chem. Phys. Lett. **241**, 229 (1995).

[14] D. A. V. Kliner, K. D. Rinen, and R. N. Zare, Chem. Phys. Lett. **166**, 107 (1990).

[15] D. A. V. Kliner, D. E. Adelman, and R. N. Zare, J. Chem. Phys. **95**, 1648 (1991).

[16] D. Neuhauser, R. S. Judson, D. J. Kouri, D. E. Adelman, N. E. Shafer, D. A. V. Kliner, and R. N. Zare, Science **257**, 519 (1992).

[17] D. E. Adelman, N. E. Shafer, D. A. V. Kliner, and R. N. Zare, J. Chem. Phys. **97**, 7323 (1992).

[18] M. Born, Nachr. Akad. Wiss. Goett. Math. Phys. **2**, 6 (1951).

[19] M. Born and K. Huang, *Dynamical Theory of Crystal Lattices* (Oxford University Press, Oxford, 1954), pp. 166-177 and 402-407.

[20] R. J. Buenker, G. Hirsch, S. D. Peyerimhoff, P. J. Bruna, J. Römelt, M. Bettendorff, and C. Petrongolo, in *Current Aspects of Quantum Chemistry*, Elsevier, New York, 1981, pp. 81-97.

[21] M. Desouter-Lecomte, C. Galloy, J. C. Lorquet, and M. V. Pires, J. Chem. Phys. **71**, 3661 (1979).

[22] B. H. Lengsfield, P. Saxe, and D. R. Yarkony, J. Chem. Phys. **81**, 4549 (1984).

[23] P. Saxe, B. H. Lengsfield, and D. R. Yarkony, Chem. Phys. Lett. **113**, 159 (1985).

[24] B. H. Lengsfield, and D. R. Yarkony, J. Chem. Phys. **84**, 348 (1986).

[25] J. O. Jensen and D. R. Yarkony, J. Chem. Phys. **89**, 3853 (1988).

[26] V. Sidis, in *State-selected and State-to-State Ion-Molecule Reaction Dynamics Part 2, Theory*, Vol. 82, edited by M. Baer and C.-Y. Ng (Wiley, New York, 1992), pp. 73-134.

[27] M. Baer, Chem. Phys. Lett. **35**, 112 (1975).

[28] C. A. Mead and D. G. Truhlar, J. Chem. Phys. **77**, 6090 (1982).

[29] C. A. Mead, J. Chem. Phys. **78**, 807 (1983).

[30] T. Pacher, L. S. Cederbaum, and H. Köppel, J. Chem. Phys. **89**, 7367 (1988).

[31] E. Mercier and G. Chambaud, J. Phys. B **20**, 4659 (1987).

[32] T. Pacher, C. A. Mead, L. S. Cederbaum, and H. Köppel, J. Chem. Phys. **91**, 7057 (1989).

[33] T. Pacher, H. Köppel, and L. S. Cederbaum, J. Chem. Phys. **95**, 6668 (1991).

[34] M. Baer and R. Englman, Mol. Phys. **75**, 293 (1992).

[35] I. D. Petsalakis, G. Theodorakopoulos, and C. A. Nicolaides, J. Chem. Phys. **97**, 7623 (1992).

[36] K. Ruedenberg and G. J. Atchity, J. Chem. Phys. **99**, 3799 (1993).

[37] D. R. Yarkony, J. Chem. Phys. **105**, 10456 (1996).

[38] R. Thurwachter and P. Halvick, Chem. Phys. **221**, 33 (1997).

[39] V. M. Garcia, M. Reguero, R. Caballol and J. P. Malrieu, Chem. Phys. Lett. **281**, 161 (1997).

[40] H. Nobutoki, Int. J. Quantum Chem. **74**, 745 (1999).

[41] D. R. Yarkony, J. Chem. Phys. **114**, 2601 (2001).

[42] G. C. Schatz and A. Kuppermann, J. Chem. Phys. **65**, 4668 (1976).

[43] W. H. Miller and J. Z. H. Zhang, J. Phys. Chem. **95**, 12 (1991).

[44] R. T. Pack and G. A. Parker, J. Chem. Phys. **87**, 3888 (1987).

[45] F. Webster and J. C. Light, J. Chem. Phys. **90**, 300 (1989).

[46] C. A. Mead, J. Chem. Phys. **72**, 3839 (1980).

[47] B. Lepetit and A. Kuppermann, Chem. Phys. Lett. **166**, 581 (1990).

[48] Z. Peng, Ph. D. Thesis, California Institute of Technology, Pasadena, CA, USA (1991).

[49] A. J. C. Varandas, F. B. Brown, C. A. Mead, D. G. Truhlar, and N. C. Blais, J. Chem. Phys. **86**, 6258 (1987).

[50] B. H. Lengsfield and D.R. Yarkony, in State-selected and State-to-State Ion-Molecule Reaction Dynamics: Part 2 Theory, Vol. 82, edited by M. Baer and C.-Y. Ng (Wiley, New York, 1992), pp. 1-71.

[51] C. Galloy and J. C. Lorquet, J. Chem. Phys. **67**, 4672 (1971).

[52] H. J. Werner and W. Meyer, J. Chem. Phys. **74**, 5802 (1981).

[53] D. Dehareng, X. Chapuisat, J. C. Lorquet, C. Galloy, and G. Raseev, J. Chem. Phys. **78**, 1246 (1983).

[54] H. J. Werner, B. Follmeg, and M. H. Alexander, J. Chem. Phys. **89**, 3139 (1988).

[55] D. R. Yarkony, J. Phys. Chem. A **101**, 4263 (1997).

[56] N. Matsunaga and D. R. Yarkony, J. Chem. Phys. **107**, 7825 (1997).

[57] N. Matsunaga and D. R. Yarkony, Mol. Phys. **93**, 79 (1998).

[58] D. R. Yarkony, Mol. Phys. **93**, 971 (1998).

[59] D. R. Yarkony, J. Chem. Phys. **84**, 3206 (1986).

[60] J. O. Jensen and D. R. Yarkony, J. Chem. Phys. **90**, 1657 (1989).

[61] H. J. Silverstone and O. Sinanoglu, J. Chem. Phys. **44**, 1899 (1966).

[62] I. Shavitt, *Modern Theoretical Chemistry*, Plenum Press, New York, 1976, Vol. 3.

[63] H. J. Werner, in *Advances in Chemical Physics* Vol. 69, edited by K. P. Lawley (Wiley, New York, 1987), p. 1.

[64] B. O. Roos, P. R. Taylor, and P. E. M. Siegbahn, Chem. Phys. **48**, 157 (1980).

[65] B. O. Roos, Int. J. Quantum Chem. Symp. **14**, 175 (1980).

[66] P. Siegbahn, A. Heiberg, B. Roos, and B. Levy, Phys. Scr. **21**, 323 (1980).

[67] H. J. Werner and W. Meyer, J. Chem. Phys. **74**, 5794 (1981).

[68] B. H. Lengsfield, J. Chem. Phys. **77**, 4073 (1982).

[69] W. H. Press, S. A. Teukolsky, W. T. Vetterling, and B. P. Flannery, *Numerical Recipes in Fortran: The Art of Scientific Computing*, Cambridge University Press, Cambridge, 1992, pp. 116-122.

[70] P. M. Morse and H. Feshbach, *Methods of Theoretical Physics*, McGraw-Hill, New York, 1953, pp. 52-54, 1763.

[71] R. G. Sadygov and D. R. Yarkony, J. Chem. Phys. **109**, 20 (1998).

[72] M. Baer, Chem. Phys. **15**, 49 (1976).

[73] R. Englman, A. Yahalom, and M. Baer, Eur. Phys. J. D **8**, 1 (2000).

[74] R. Englman and M. Baer, J. Phys. Cond. Matt. **11**, 1059 (1999).

[75] A. M. Mebel, M. Baer, V. M. Rozenbaum, and S. H. Lin, Chem. Phys. Lett. **336**, 135 (2001).

[76] B. Liu, J. Chem. Phys. **58**, 1925 (1973).

[77] P. Siegbahn and B. Liu, J. Chem. Phys. **68**, 2457 (1978).

[78] M. R. A. Blomberg and B. Liu, J. Chem. Phys. **82**, 1050 (1985).

[79] R. N. Porter, R. M. Stevens, and M. Karplus, J. Chem. Phys. **49**, 5163 (1968).

[80] T. C. Thompson and C. A. Mead, J. Chem. Phys. **82**, 2408 (1985).

[81] T. C. Thompson, G. Izmirlian Jr., S. J. Lemon, D. G. Truhlar, and C. A. Mead, J. Chem. Phys. **82**, 5597 (1985).

[82] K. D. Jordan, Chem. Phys. **9**, 199 (1975).

[83] T. Ho and H. Rabitz, J. Chem. Phys. **104**, 2584 (1996).

[84] A. Frishman, D. K. Hoffman, and D. J. Kouri, J. Chem. Phys. **107**, 804 (1997).

[85] S. Rogers, D. Wang, S. Walch, and A. Kuppermann, J. Phys. Chem. A **104**, 2308 (2000).

[86] A. Kuppermann, Chem. Phys. Lett. **32**, 374 (1975).

[87] L. M. Delves, Nucl. Phys. **9**, 391 (1959).

[88] L. M. Delves, Nucl. Phys. **20**, 275 (1960).

[89] D. Jepsen and J. O. Hirschfelder, Proc. Natl. Acad. Sci. U.S.A. **45**, 249 (1959).

[90] F. T. Smith, J. Math. Phys. **3**, 735 (1962).

[91] A. Kuppermann, in *Advances in Molecular Vibrations and Collision Dynamics*, edited by J. Bowman (JAI Press, Greenwich, CT, 1994), Vol. 2B, p. 117-186.

[92] R. T. Ling and A. Kuppermann, in *Electronic and Atomic Collisions, Abstract of the 9th International Conference on the Physics of Electronic and Atomic Collisions, Seattle, Washington, 24-30 July 1975*, Vol. 1, edited by J. S. Riley and R. Geballe (Univ. Washington Press, Seattle, 1975), pp. 353-354.

[93] Y.-S. M. Wu, A. Kuppermann, and J. B. Anderson, Phys. Chem. Chem. Phys. **6**, 929 (1999).

[94] D. G. Truhlar and C. J. Horowitz, J. Chem. Phys. **68**, 2466 (1978); **71**, 1514 (1979) (E).

[95] R. G. Sadygov and D. R. Yarkony, J. Chem. Phys. **110**, 3639 (1999).

[96] R. Abrol, A. Shaw, A. Kuppermann and D. R. Yarkony, J. Chem. Phys. **115**, 4640 (2001).

[97] A. Kuppermann, unpublished results.

Table 3.I: Switching Function Parameters[a]

parameter	$1\ ^2A'$	$2\ ^2A'$
a_n/bohr	0.00	2.00
γ_n/bohr^{-1}	0.17	0.20

[a] These parameters are used for S_n, as described in Eqs. (3.23)-(3.26)

Table 3.II: Coefficients[b] $c_{1,ijk}$ and $c_{2,ijk}$ corresponding to E_1^{DSP} and E_2^{DSP}, respectively (as defined in Eq. (3.23))[c]

i	j	k	$c_{1,ijk}$	$c_{2,ijk}$
0	0	0	0.3699	-0.2274
1	0	0	-0.4927	0.0255
2	0	0	0.4726	0.0996
1	1	0	0.0237	0.2025
3	0	0	-0.2590	-0.2606
2	1	0	0.1258	0.1934
1	1	1	-0.4795	-1.2400
4	0	0	0.0398	0.0845
3	1	0	-0.0156	0.0075
2	1	1	0.0299	0.2397
2	2	0	-0.0162	-0.2428
5	0	0	-0.0018	-0.0070
4	1	0	0.0006	-0.0155
3	2	0	0.0005	0.0332
2	2	1	-0.0006	-0.0378
3	1	1	-0.0009	-0.0044
6	0	0	-	0.0000
5	1	0	-	0.0013
4	2	0	-	-0.0015
3	3	0	-	-0.0013
3	2	1	-	-0.0001
4	1	1	-	0.0006
2	2	2	-	0.0062

[b] $c_{1,ijk} = c_{1,jki} = c_{1,kij}$ and $c_{2,ijk} = c_{2,jki} = c_{2,kij}$

[c] With these $c_{n,ijk}$ coefficients used in Eq. (3.23) and $R_{AB}, R_{BC}, \text{and} R_{CA}$ given in bohr, the E_n^{DSP} are given in eV and are referred to the minimum of an isolated H_2 molecule as the origin of energy.

Table 3.III: Range of the largest and smallest internuclear distances and largest bond angle over the full 0 to 2π range of ϕ_λ

		$\rho = 2$ bohr		$\rho = 4$ bohr	
θ	γ_λ^{max}	$R_{\lambda\nu}^{min}$	$R_{\lambda\nu}^{max}$	$R_{\lambda\nu}^{min}$	$R_{\lambda\nu}^{max}$
1°	90.5-91.0°	1.50-1.51	1.52-1.53	3.01-3.03	3.05-3.07
30°	106.1-120.0°	1.07-1.32	1.70-1.86	2.15-2.63	3.40-3.72
60°	130.9-150.0°	0.56-1.14	1.82-2.08	1.11-2.29	3.64-4.15
90°	180.0-180.0°	0.00-1.07	1.86-2.15	0.00-2.15	3.72-4.30

		$\rho = 6$ bohr		$\rho = 8$ bohr	
θ	γ_λ^{max}	$R_{\lambda\nu}^{min}$	$R_{\lambda\nu}^{max}$	$R_{\lambda\nu}^{min}$	$R_{\lambda\nu}^{max}$
1°	90.5-91.0°	4.52-4.54	4.58-4.60	6.03-6.05	6.11-6.13
30°	106.1-120.0°	3.22-3.95	5.10-5.58	4.30-5.26	6.80-7.44
60°	130.9-150.0°	1.67-3.43	5.46-6.23	2.23-4.58	7.28-8.30
90°	180.0-180.0°	0.00-3.22	5.58-6.45	0.00-4.30	7.44-8.60

FIGURE CAPTIONS

Fig. 3.1 Ground electronic state (E_1) energy contours in eV for the H_3 system in an equatorial view (see text for definition): (a) DSP E_1 at $\rho = 2$ bohr, (b) DSP E_1 at $\rho = 4$ bohr, (c) DSP E_1 at $\rho = 6$ bohr,(d) DSP E_1 at $\rho = 8$ bohr, (e) DMBE E_1 at $\rho = 2$ bohr,(f) DMBE E_1 at $\rho = 4$ bohr (g) DMBE E_1 at $\rho = 6$ bohr,(h) DMBE E_1 at $\rho = 8$ bohr. The solid circle depicts collinear geometries ($\theta = 90°$) and the dotted circles are lines of constant θ. The radial dotted lines correspond to the constant values of ϕ_λ, in degrees, displayed outside the solid circle.

Fig. 3.2 First-excited electronic state (E_2) energy contours in eV for the H_3 system in an equatorial view (see text for definition): (a) DSP E_2 at $\rho = 2$ bohr, (b) DSP E_2 at $\rho = 4$ bohr, (c) DSP E_2 at $\rho = 6$ bohr,(d) DSP E_2 at $\rho = 8$ bohr, (e) DMBE E_2 at $\rho = 2$ bohr,(f) DMBE E_2 at $\rho = 4$ bohr (g) DMBE E_2 at $\rho = 6$ bohr,(h) DMBE E_2 at $\rho = 8$ bohr. The solid circle depicts collinear geometries ($\theta = 90°$) and the dotted circles are lines of constant θ. The radial dotted lines correspond to the constant values of ϕ_λ, in degrees, displayed outside the solid circle.

Fig. 3.3 Mapping of the point P of a constant ρ hemisphere in the $\mathsf{O}X_\lambda Y Z_\lambda$ space onto a point Q on a plane tangent to that hemisphere at the intersection T of the $\mathsf{O}Y$ axis with it, such that the length of the arc(TP) = TQ. The point P has θ, ϕ_λ polar angles in the $\mathsf{O}X_\lambda Y Z_\lambda$ space and $\omega_\lambda, \gamma_\lambda$ in the $\mathsf{O}\overline{X}_\lambda \overline{Y}_\lambda \overline{Z}$ space. $\overline{\mathsf{P}}$ is the projection of point P on the $\mathsf{O}X_\lambda Y$ plane.

Fig. 3.4 *Ab initio* nonadiabatic coupling vector, $\mathbf{W}_{1,2}^{(1)ad}$, ground state energy (E_1) and first-excited state energy (E_2) for $\rho = 2$ bohr and (a) $\theta = 1°$; (b) $\theta = 30°$; (c) $\theta = 60°$; (d) $\theta = 90°$ (collinear). The scale in bohr^{-1} refers to coupling vectors, and that in bohr to the cartesian coordinates associated with the middle column plots (see Sec. 3.4.1).

Fig. 3.5 Same as Fig. 3.4 for $\rho = 4$ bohr.

Fig. 3.6 Same as Fig. 3.4 for $\rho = 6$ bohr.

Fig. 3.7 Same as Fig. 3.4 for $\rho = 8$ bohr.

Fig. 3.8 DMBE nonadiabatic coupling vector, $\mathbf{W}_{1,2}^{(1)ad,\mathrm{DMBE}}$, ground state energy ($E_1$) and first-excited state energy (E_2) for $\rho = 2$ bohr and (a) $\theta = 1°$; (b) $\theta = 30°$; (c) $\theta = 60°$; (d) $\theta = 90°$ (collinear). The scales have the same meaning as in Fig. 3.4.

Fig. 3.9 Same as Fig. 3.8 for $\rho = 4$ bohr.

Fig. 3.10 Same as Fig. 3.8 for $\rho = 6$ bohr.

Fig. 3.11 Same as Fig. 3.8 for $\rho = 8$ bohr.

Fig. 3.12 Phase $\Phi(\phi_\lambda; \rho, \theta)$ as a function of ϕ_λ evaluated using Eq. (3.39) for four values of θ: 1° (solid line), 30° (dashed line), 60° (dotted line), and 90° (dash-dotted line) for each of the four values of ρ: (a) 2 bohr, (b) 4 bohr, (c) 6 bohr, and (d) 8 bohr.

Fig. 3.13 Topological phase $\Phi_\mathsf{T}(\rho, \theta)$ as a function of ρ and θ evaluated using Eq. (3.40). The contours on the bottom face correspond to $\Phi_\mathsf{T}(\rho, \theta)$ values ranging from 150° to 225° every 15°. The three 180° contours have been shown in bold and labelled as $\mathbf{S}_1$, $\mathbf{S}_2$, and $\mathbf{S}_3$.

Fig. 3.14 (a) The 180° $\mathbf{S}_1$ contour of Fig. 3.13 shown in the $X_\lambda Y$ plane of Fig. 3.3. (b) The same contour shown in the regular (ρ, θ) plane. (The dashed points correspond to values of ρ greater than 8 bohr).

Fig. 3.15 Second-derivative coupling term $\varepsilon^{(2)ad}(\mathbf{q}_\lambda)$, defined after Eq. (3.43), for the H_3 system at: (a) $\rho = 2$ bohr, (b) $\rho = 4$ bohr, (c) $\rho = 6$ bohr, and (d) $\rho = 8$ bohr. The following contours are displayed: 0 to 0.1 kcal mol^{-1} every 0.01 kcal mol^{-1}, 0.1 to 1.0 kcal mol^{-1} every 0.1 kcal mol^{-1} and 1.0 to 10.0 kcal mol^{-1} every 0.5 kcal mol^{-1}.

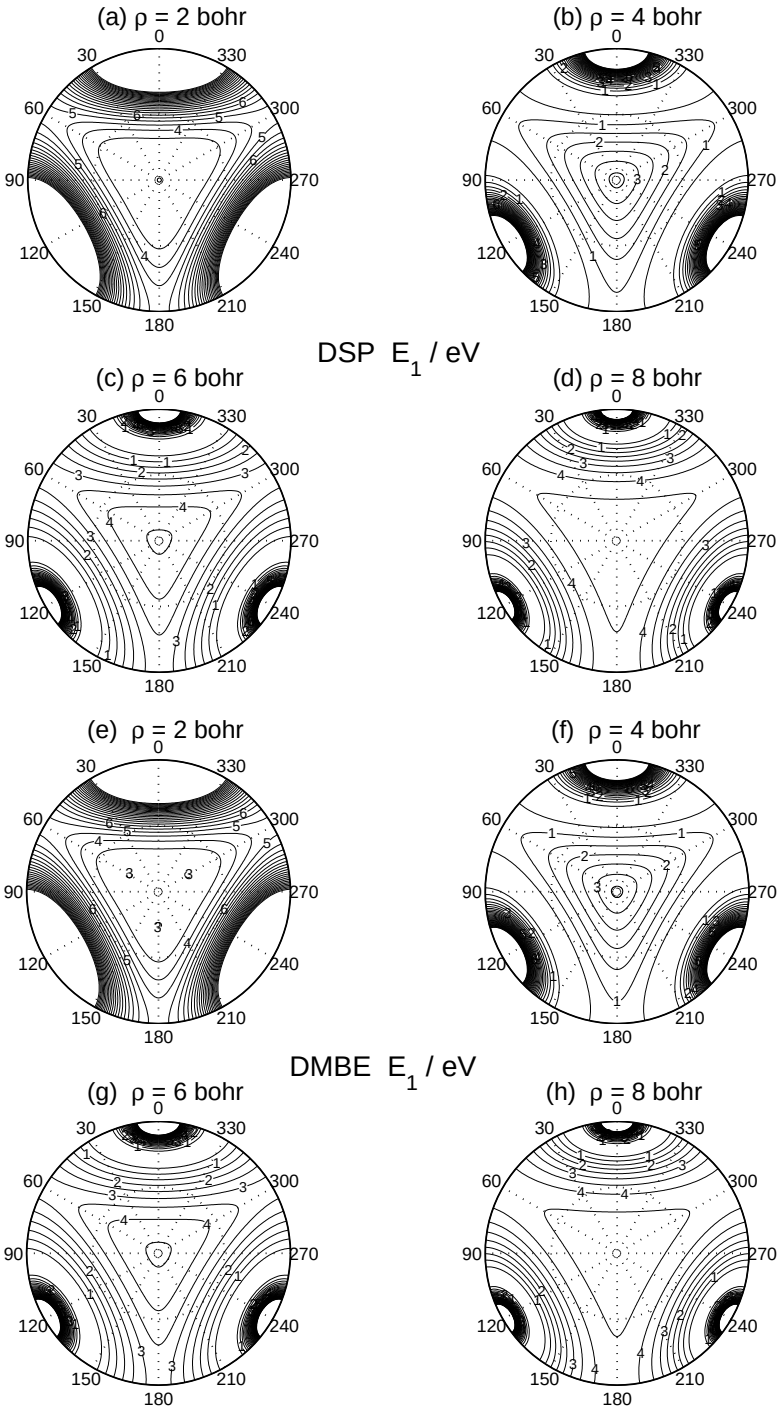
(a) ρ = 2 bohr
(b) ρ = 4 bohr
DSP E1 / eV
(c) ρ = 6 bohr
(d) ρ = 8 bohr
(e) ρ = 2 bohr
(f) ρ = 4 bohr
DMBE E1 / eV
(g) ρ = 6 bohr
(h) ρ = 8 bohr
0
30
60
90
120
150
180
210
240
270
300
330

Figure 3.1:

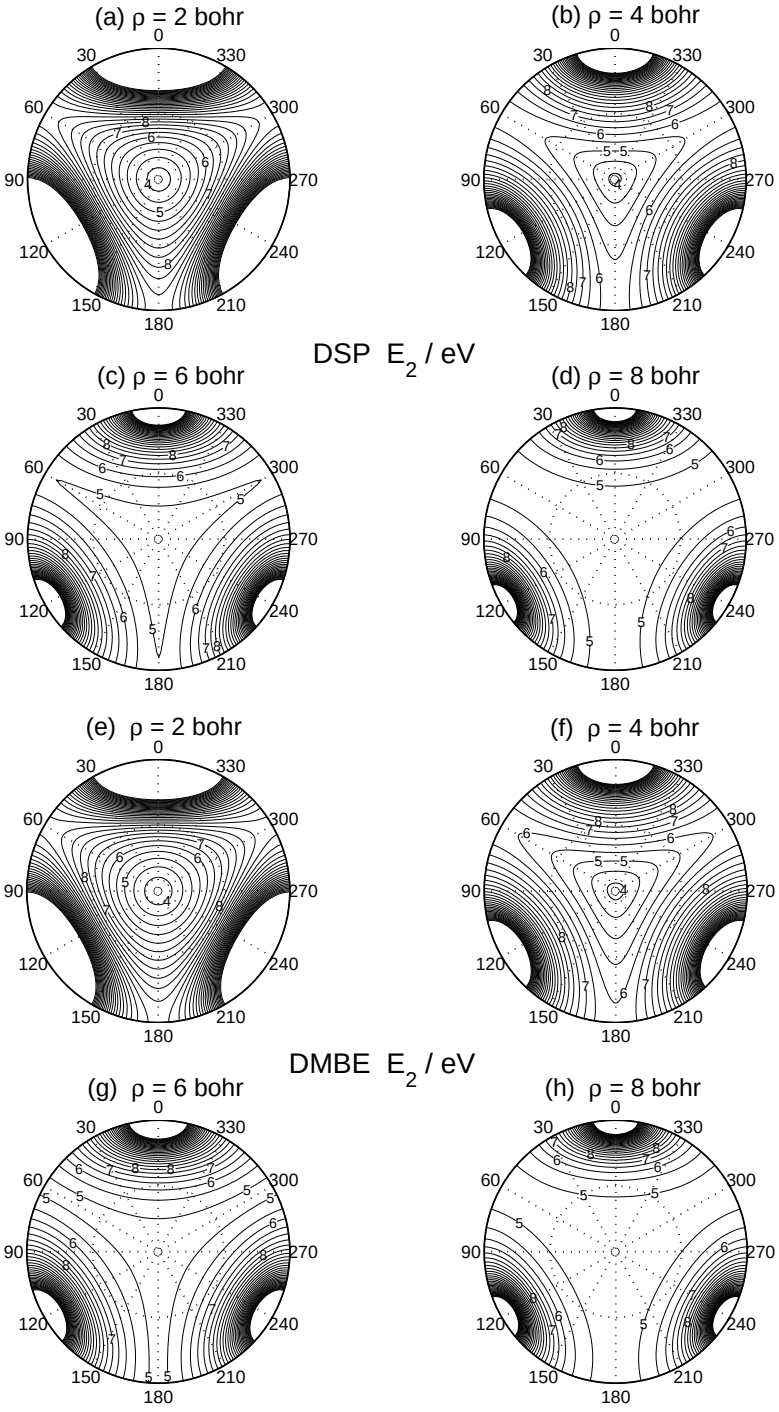
(a) ρ = 2 bohr
(b) ρ = 4 bohr
DSP E2 / eV
(c) ρ = 6 bohr
(d) ρ = 8 bohr
(e) ρ = 2 bohr
(f) ρ = 4 bohr
DMBE E2 / eV
(g) ρ = 6 bohr
(h) ρ = 8 bohr
0
30
330
60
300
90
270
120
240
150
210
180

Figure 3.2:

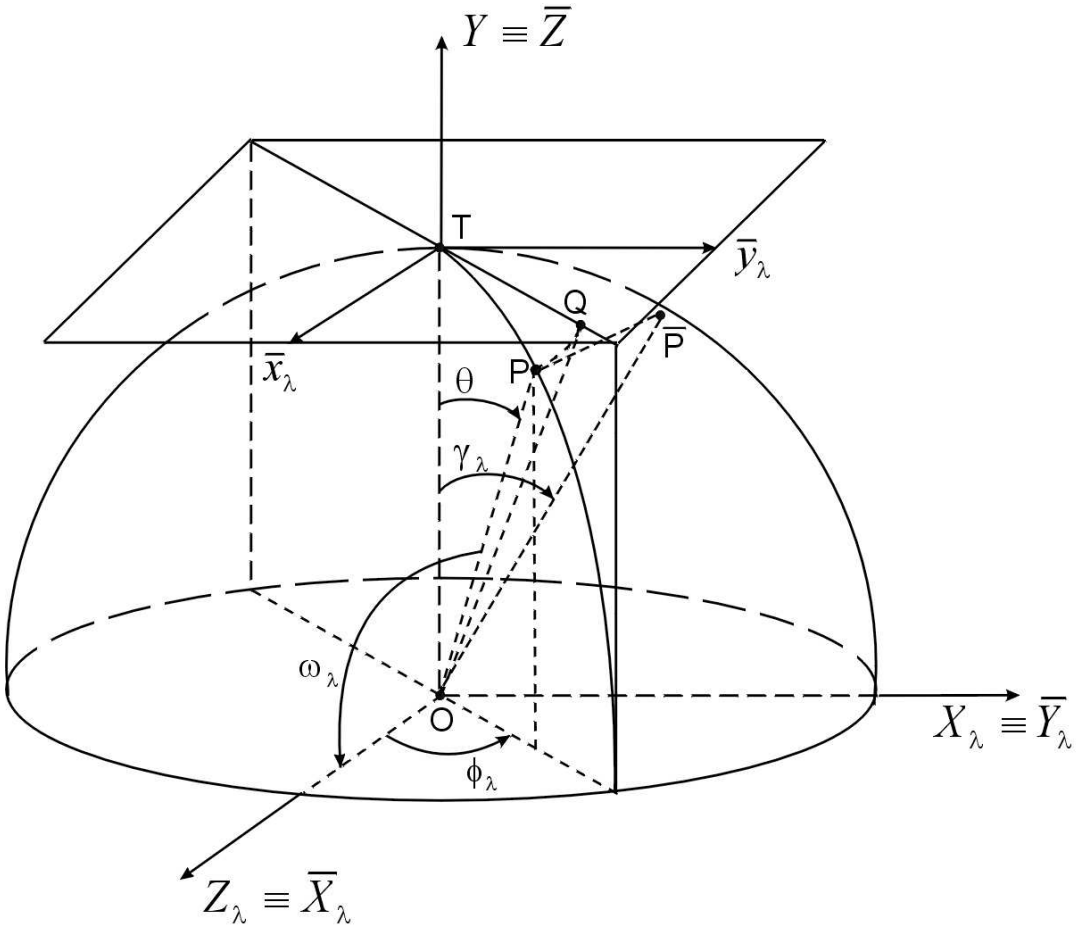
$Y \equiv \overline{Z}$
T
$\overline{y}_\lambda$
Q
$\overline{P}$
$\overline{x}_\lambda$
P
θ
γ_λ
ω_λ
O
$X_\lambda \equiv \overline{Y}_\lambda$
ϕ_λ
$Z_\lambda \equiv \overline{X}_\lambda$

Figure 3.3:

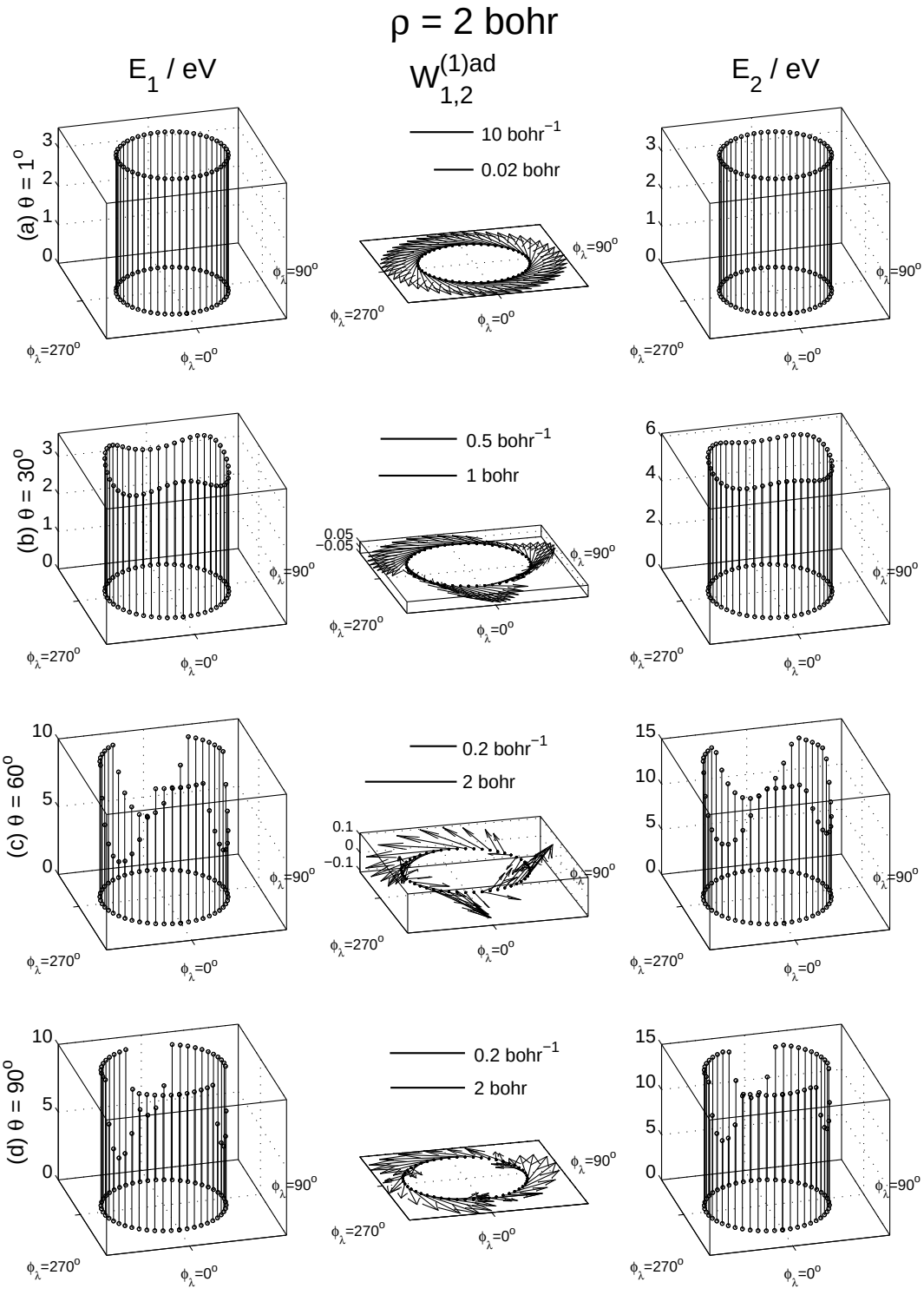
ρ = 2 bohr
E1 / eV
W(1)ad 1,2
E2 / eV
(a) θ = 1°
(b) θ = 30°
(c) θ = 60°
(d) θ = 90°
10 bohr−1
0.02 bohr
0.5 bohr−1
1 bohr
0.2 bohr−1
2 bohr
0.2 bohr−1
2 bohr
φλ=90°
φλ=270°
φλ=0°

Figure 3.4:

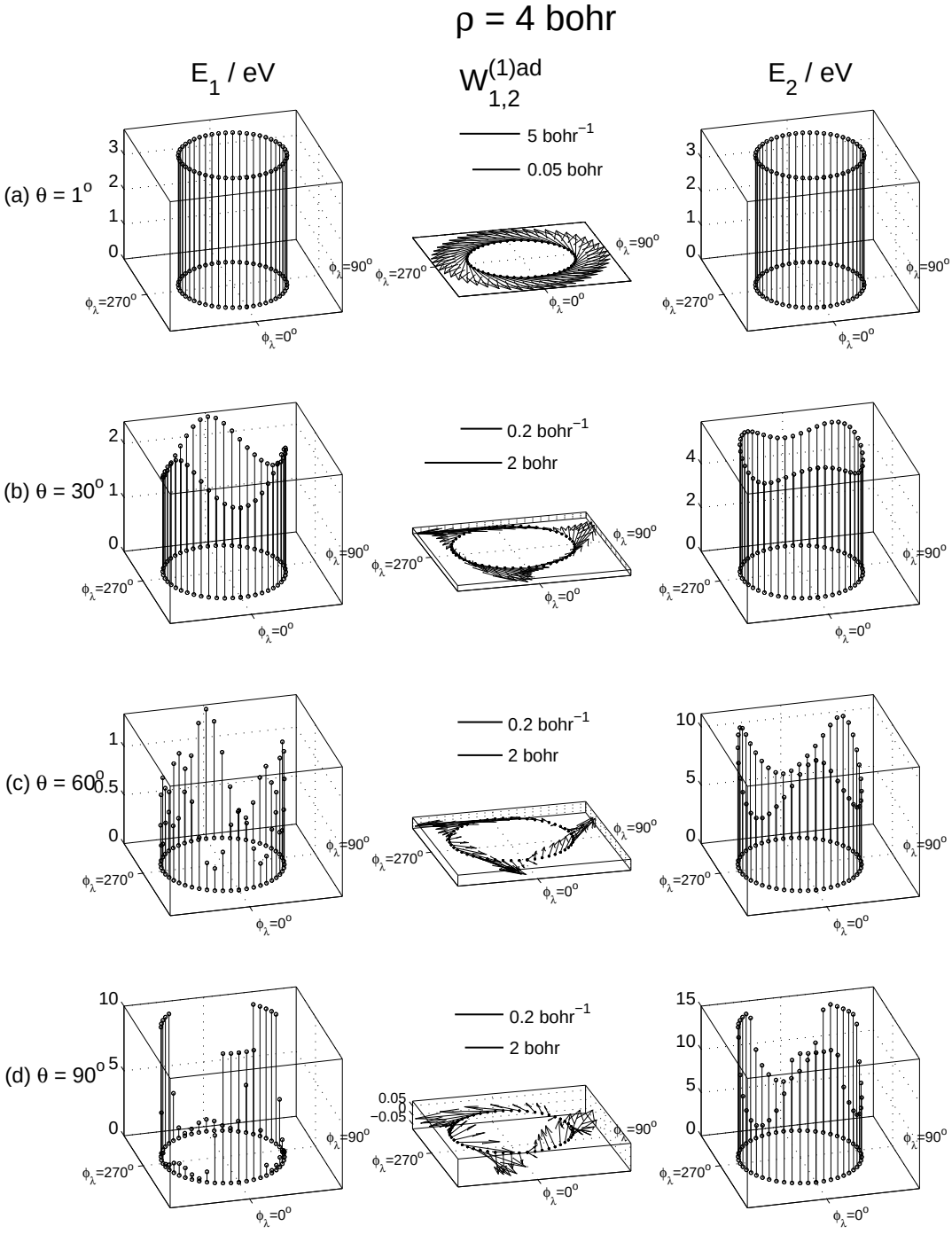
ρ = 4 bohr
E1 / eV
W(1)ad 1,2
E2 / eV
5 bohr−1
0.05 bohr
0.2 bohr−1
2 bohr
(a) θ = 1o
(b) θ = 30o
(c) θ = 60o
(d) θ = 90o
φλ=0o
φλ=90o
φλ=270o

Figure 3.5:

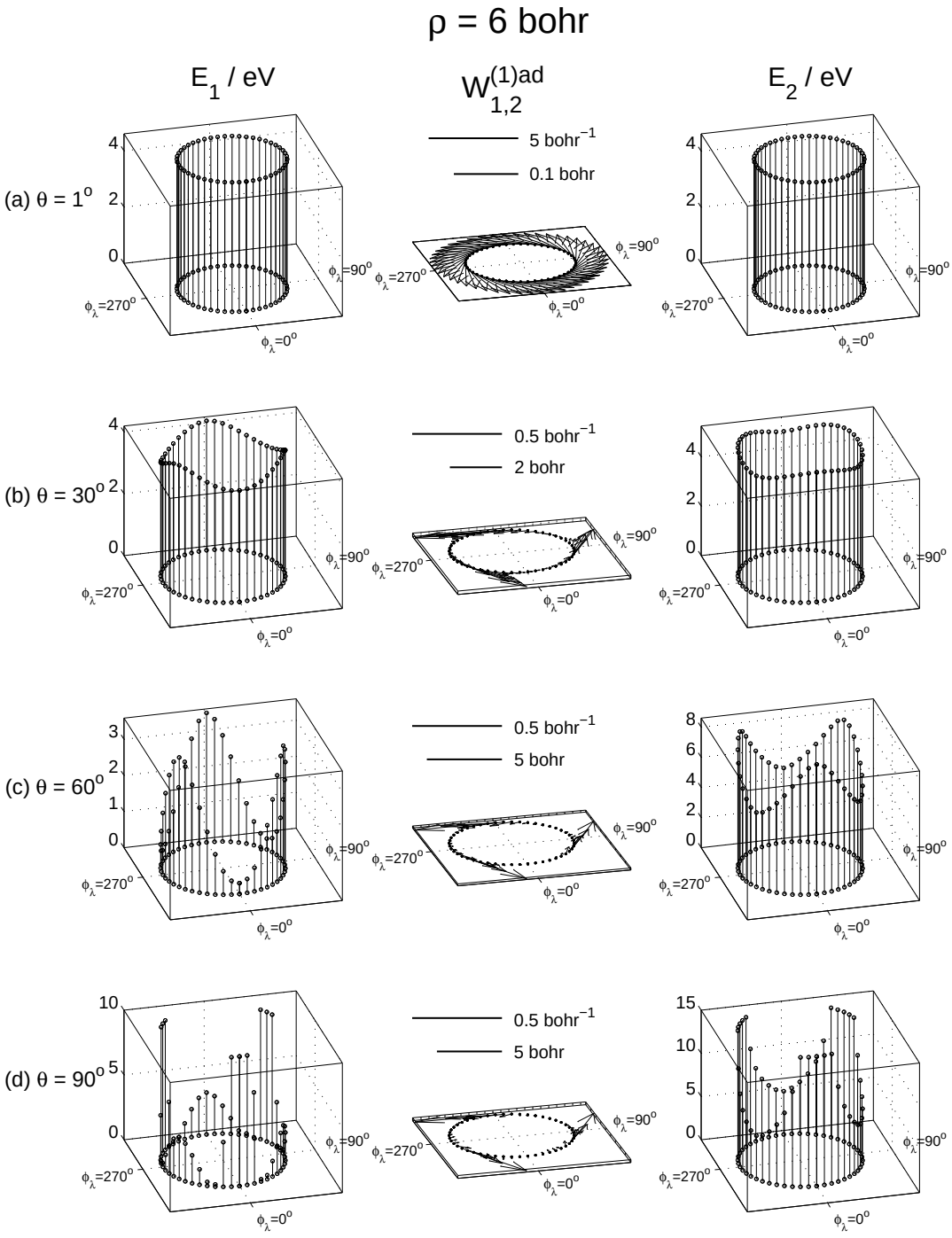
ρ = 6 bohr
E1 / eV
W(1)ad 1,2
E2 / eV
5 bohr−1
0.1 bohr
0.5 bohr−1
2 bohr
0.5 bohr−1
5 bohr
0.5 bohr−1
5 bohr
(a) θ = 1o
(b) θ = 30o
(c) θ = 60o
(d) θ = 90o
φλ=0o
φλ=90o
φλ=270o

Figure 3.6:

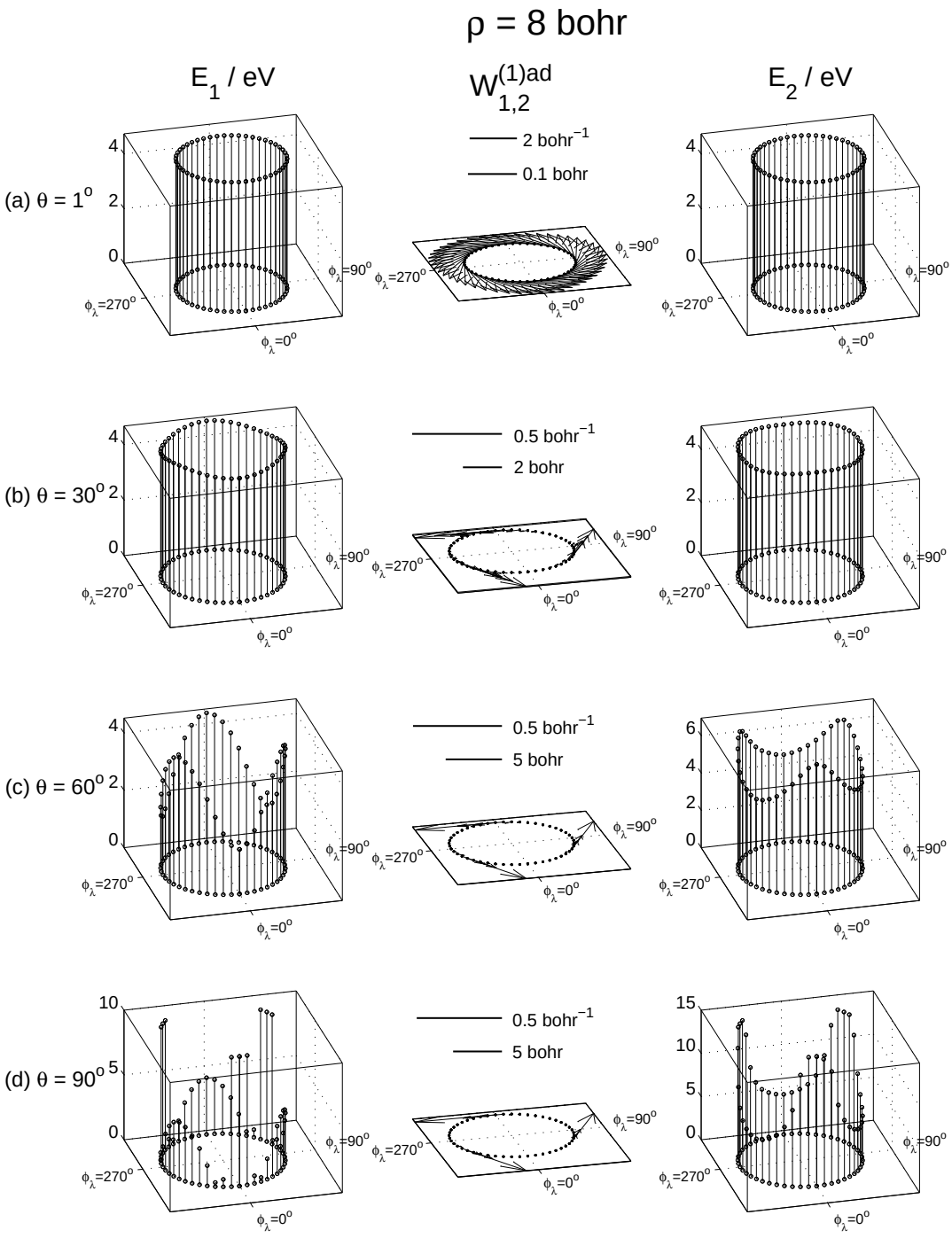
ρ = 8 bohr
E1 / eV
W(1)ad 1,2
E2 / eV
2 bohr−1
0.1 bohr
0.5 bohr−1
2 bohr
0.5 bohr−1
5 bohr
0.5 bohr−1
5 bohr
(a) θ = 1o
(b) θ = 30o
(c) θ = 60o
(d) θ = 90o
φλ=0o
φλ=90o
φλ=270o

Figure 3.7:

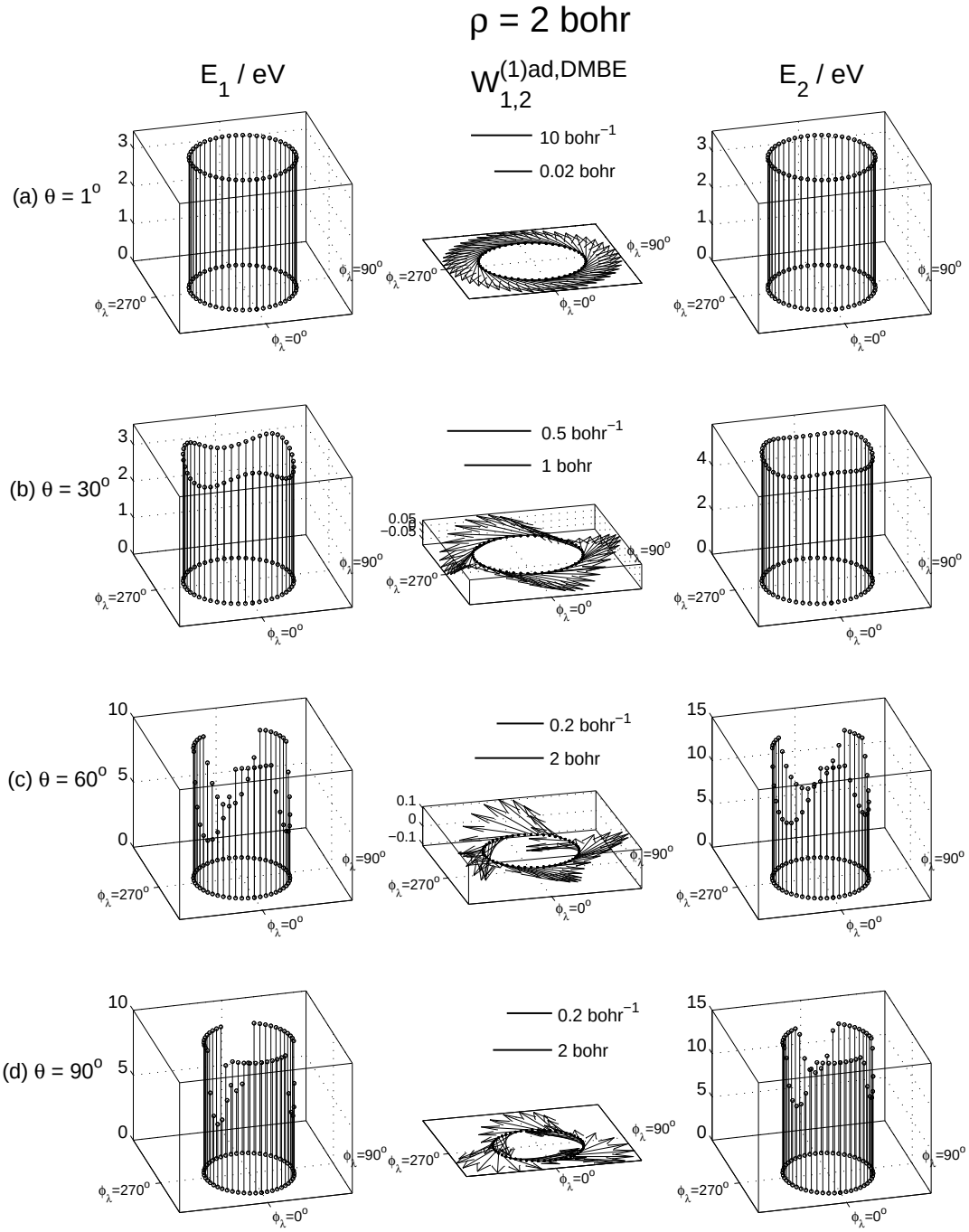
ρ = 2 bohr
E1 / eV
W(1)ad,DMBE 1,2
E2 / eV
(a) θ = 1o
10 bohr−1
0.02 bohr
(b) θ = 30o
0.5 bohr−1
1 bohr
(c) θ = 60o
0.2 bohr−1
2 bohr
(d) θ = 90o
0.2 bohr−1
2 bohr
ϕλ=0o
ϕλ=90o
ϕλ=270o

Figure 3.8:

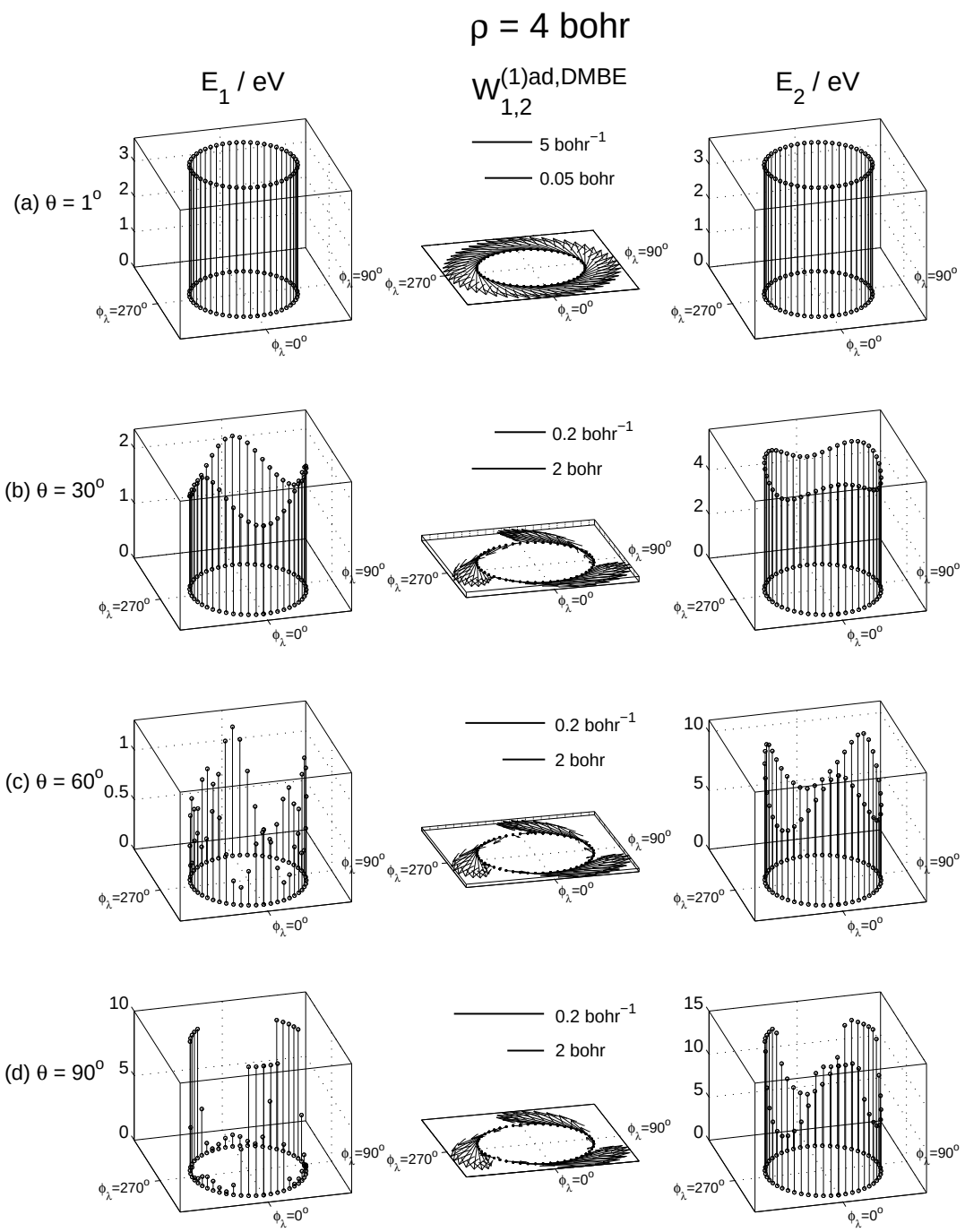
ρ = 4 bohr
E1 / eV
W(1)ad,DMBE 1,2
E2 / eV
5 bohr−1
0.05 bohr
0.2 bohr−1
2 bohr
0.2 bohr−1
2 bohr
0.2 bohr−1
2 bohr
(a) θ = 1o
(b) θ = 30o
(c) θ = 60o
(d) θ = 90o
φλ=90o
φλ=270o
φλ=0o

Figure 3.9:

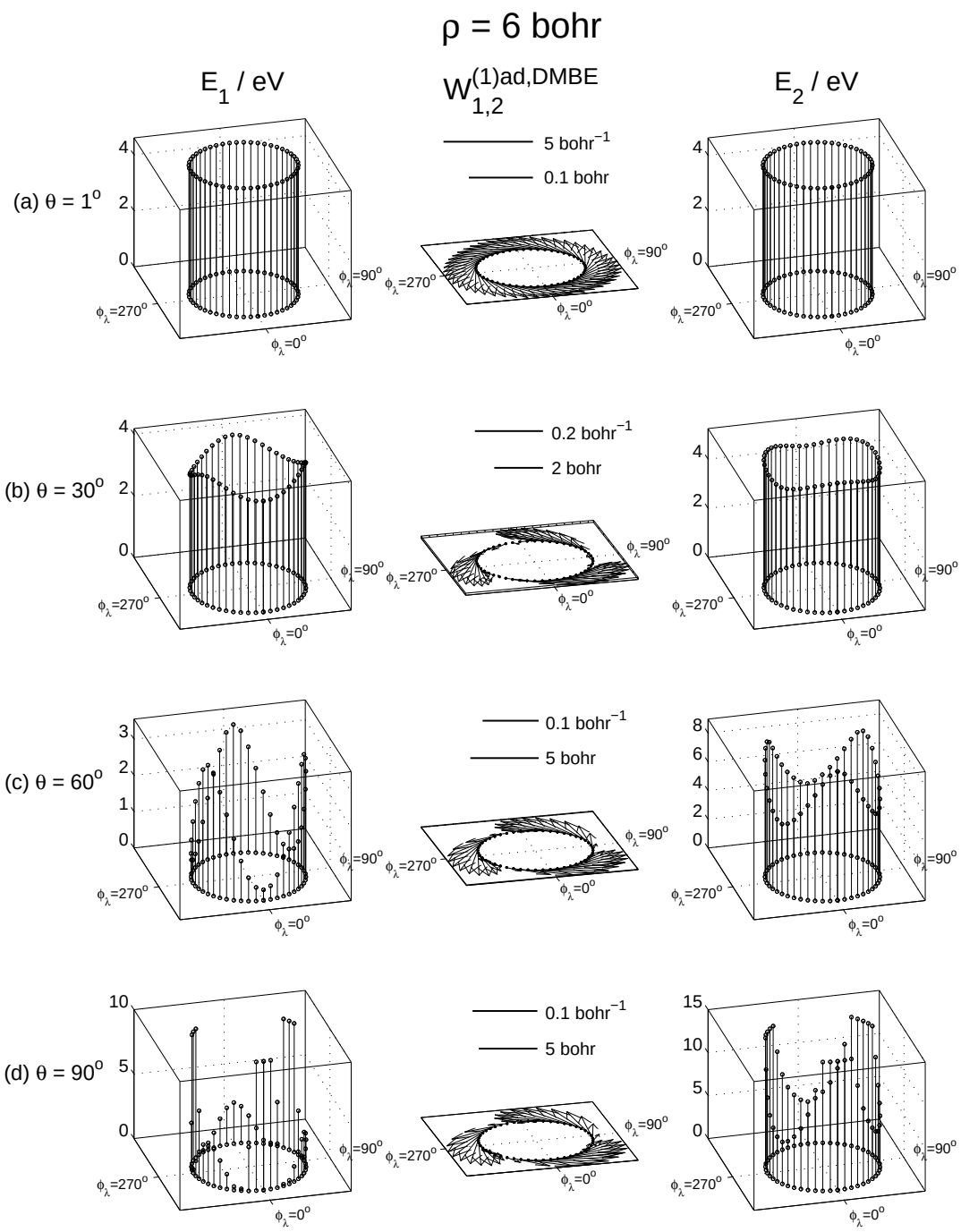
ρ = 6 bohr
E1 / eV
W(1)ad,DMBE 1,2
E2 / eV
(a) θ = 1o
5 bohr−1
0.1 bohr
(b) θ = 30o
0.2 bohr−1
2 bohr
(c) θ = 60o
0.1 bohr−1
5 bohr
(d) θ = 90o
0.1 bohr−1
5 bohr
φλ=0o
φλ=90o
φλ=270o

Figure 3.10:

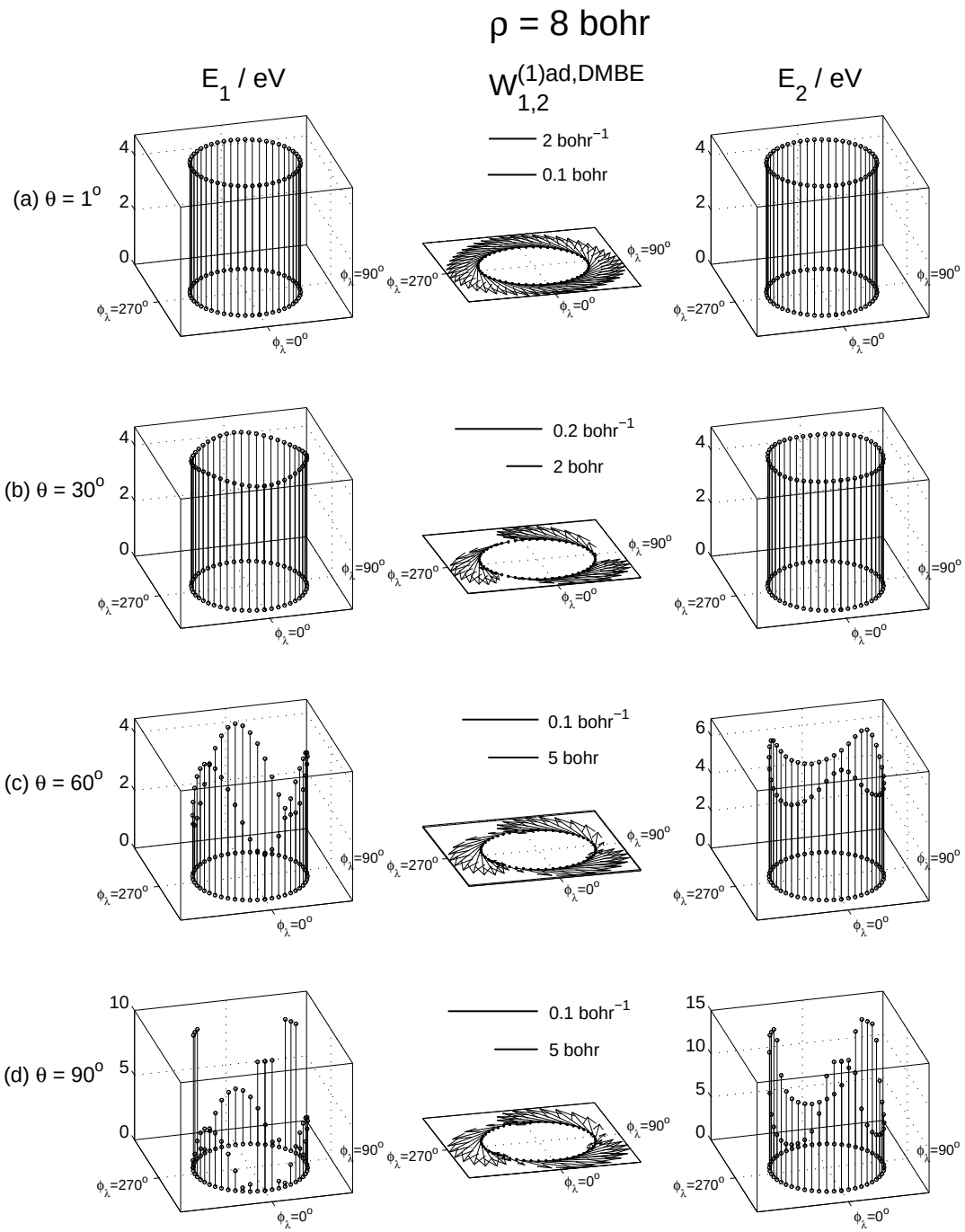
ρ = 8 bohr
E1 / eV
W(1)ad,DMBE 1,2
E2 / eV
(a) θ = 1°
2 bohr−1
0.1 bohr
(b) θ = 30°
0.2 bohr−1
2 bohr
(c) θ = 60°
0.1 bohr−1
5 bohr
(d) θ = 90°
0.1 bohr−1
5 bohr
φλ=0°
φλ=90°
φλ=270°

Figure 3.11:

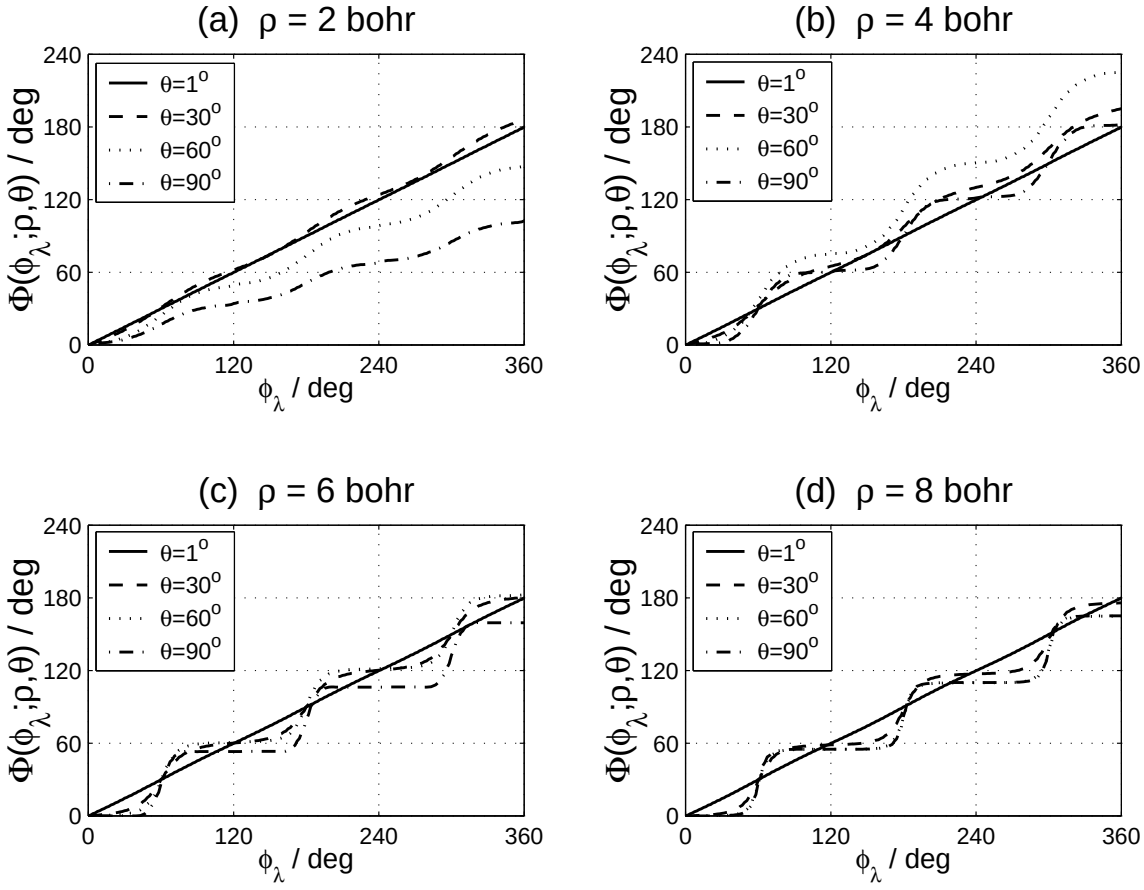
(a) ρ = 2 bohr
(b) ρ = 4 bohr
(c) ρ = 6 bohr
(d) ρ = 8 bohr
θ=1°
θ=30°
θ=60°
θ=90°
Φ(φλ;ρ,θ) / deg
φλ / deg
0
60
120
180
240
360

Figure 3.12:

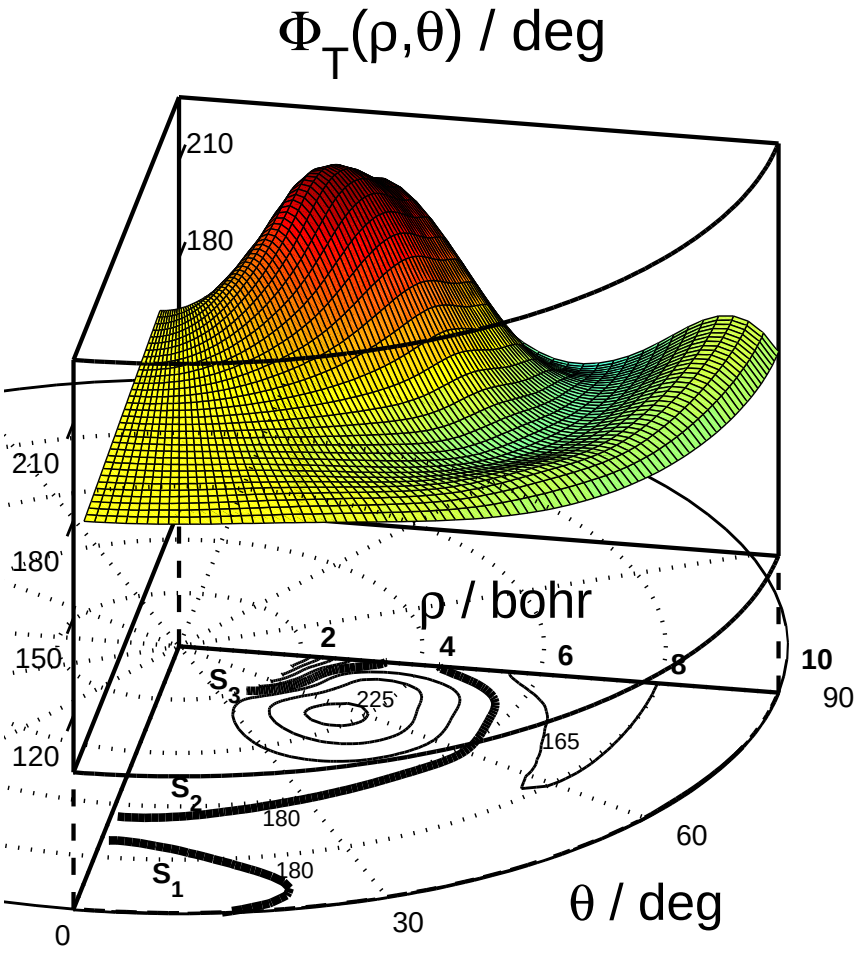
$\Phi_T(\rho,\theta)$ / deg
210
180
210
180
150
120
ρ / bohr
2
4
6
8
10
90
S_3
225
165
S_2
180
S_1
180
60
θ / deg
0
30

Figure 3.13:

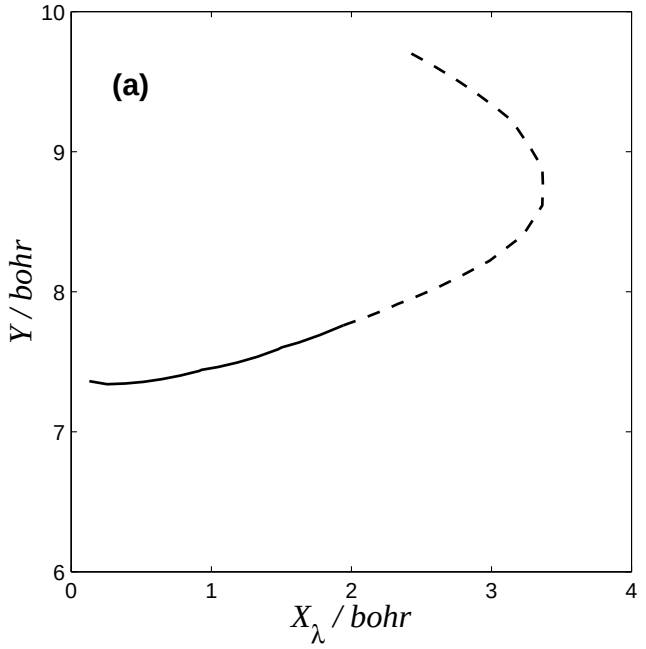

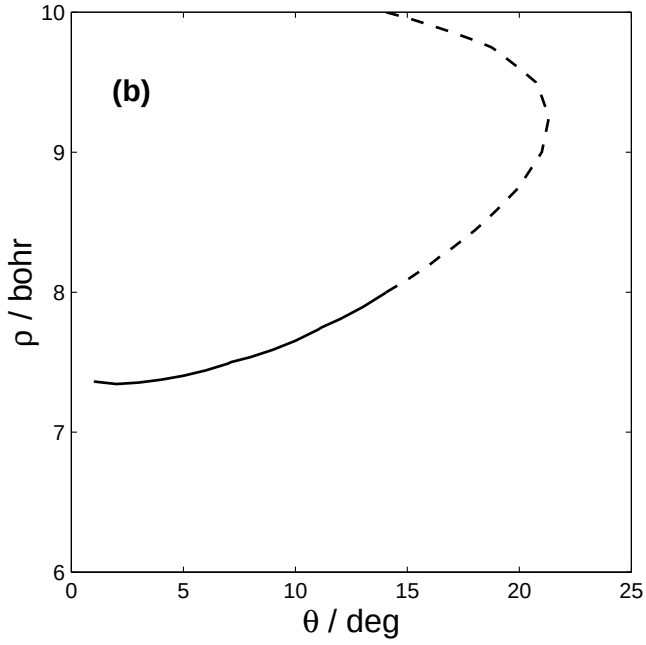

Figure 3.14:

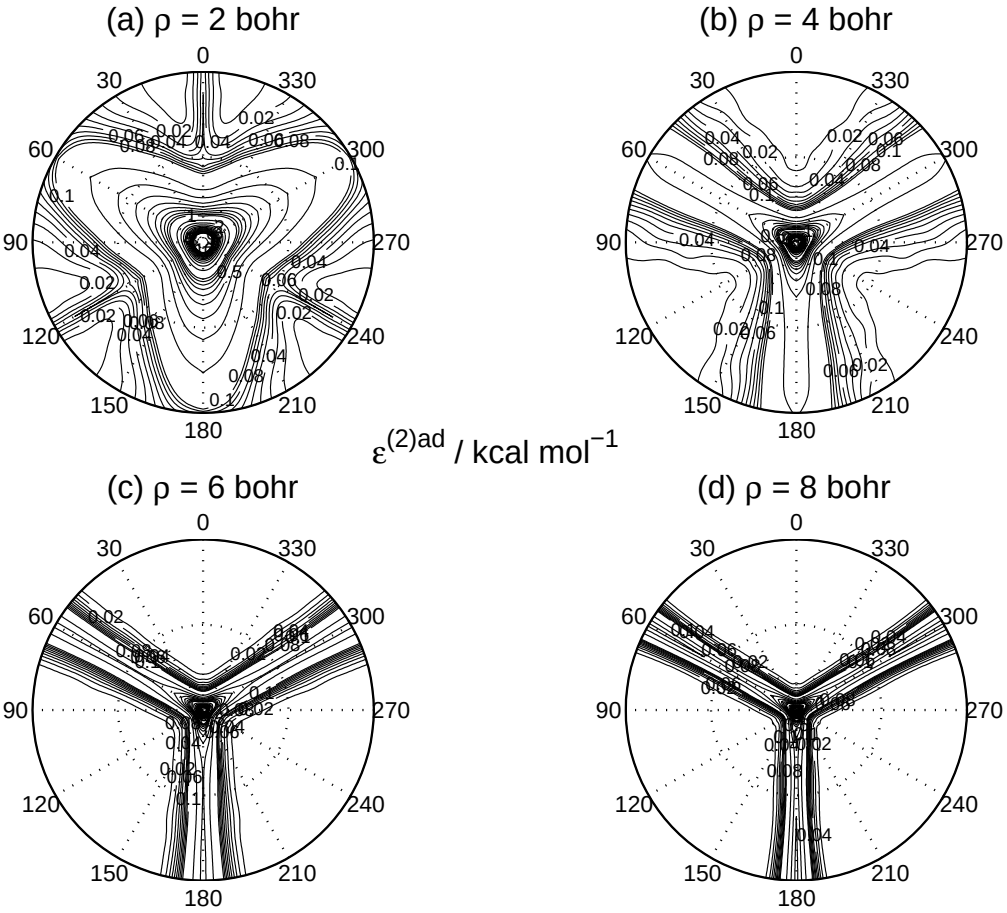
(a) ρ = 2 bohr
(b) ρ = 4 bohr
(c) ρ = 6 bohr
(d) ρ = 8 bohr
ε(2)ad / kcal mol−1
0
30
330
60
300
90
270
120
240
150
210
180

Figure 3.15:

Chapter 4 An optimal diabatization of the lowest two states of H_3

4.1 Introduction

A detailed review of the adiabatic and diabatic representation of polyatomic molecules is given in Chapter 1 and we will only summarize below the main aspects needed for the present chapter. We neglect all spin-spin and spin-orbit terms in the molecular Hamiltonian. Consider a polyatomic system with electronic coordinates $\mathbf{r}$ and nuclear coordinates $\mathbf{R}_\lambda$. The total wave function for this system is given by the Born-Huang expansion [1, 2]

$$\Psi(\mathbf{r};\mathbf{R}_\lambda) = \sum_n \chi_n^{ad}(\mathbf{R}_\lambda)\psi_n^{ad}(\mathbf{r};\mathbf{R}_\lambda) \tag{4.1}$$

where $\psi_n^{ad}(\mathbf{r};\mathbf{R}_\lambda)$ are the adiabatic electronic wave functions satisfying the electronic Schrödinger equation

$$\widehat{H}^{el}(\mathbf{r};\mathbf{R}_\lambda)\psi_n^{ad}(\mathbf{r};\mathbf{R}_\lambda) = \varepsilon_n^{ad}(\mathbf{R}_\lambda)\psi_n^{ad}(\mathbf{r};\mathbf{R}_\lambda), \tag{4.2}$$

n is a complete set of quantum numbers needed to specify them and $\chi_n^{ad}(\mathbf{R}_\lambda)$ are the adiabatic nuclear wave functions. $\varepsilon_n^{ad}(\mathbf{R}_\lambda)$ are the electronically adiabatic potential energy surfaces (PESs). If two of these surfaces, labelled $n = i$ and $n = j$, exhibit a single conical intersection and the ψ_n^{ad} are required to be real, then according to the geometric phase (GP) theorem [3–7],

$$\psi_n^{ad}(\mathbf{r};\mathbf{R}_\lambda) \rightarrow -\psi_n^{ad}(\mathbf{r};\mathbf{R}_\lambda) \qquad n = i, j \tag{4.3}$$

and

$$\chi_n^{ad}(\mathbf{R}_\lambda) \rightarrow -\chi_n^{ad}(\mathbf{R}_\lambda) \qquad n = i, j \tag{4.4}$$

when the polyatomic system traverses a closed loop in nuclear configuration space $\mathcal{Q}$ around that conical intersection (a so called pseudorotation). As a result, the $\psi_n^{ad}(\mathbf{r}; \mathbf{R}_\lambda)$ are not single-valued functions of $\mathbf{R}_\lambda$. Alternatively, if the electronic wave functions are allowed to be complex, they may be required to be single-valued [8]. For example, we may express them as

$$\overline{\psi}_n^{ad}(\mathbf{r}; \mathbf{R}_\lambda) = e^{iA_n(\mathbf{R}_\lambda)} \psi_n^{ad}(\mathbf{r}; \mathbf{R}_\lambda) \qquad n = i, j \tag{4.5}$$

and require that the $e^{iA_n(\mathbf{R}_\lambda)}$ $(n = i, j)$ change sign (i.e., that $A_n(\mathbf{R}_\lambda)$ change by π) upon a pseudorotation. The $A_n(\mathbf{R}_\lambda)$ are the geometric phases that appear in the corresponding modified adiabatic nuclear motion Schrödinger equation [7–11]. In this chapter, we will require the electronic wave functions to be real.

In a two-electronic-state representation of the system involving electronically adiabatic states i and j, Eq. (4.1) is written as

$$\Psi(\mathbf{r}; \mathbf{R}_\lambda) = \chi_i^{ad}(\mathbf{R}_\lambda) \psi_i^{ad}(\mathbf{r}; \mathbf{R}_\lambda) + \chi_j^{ad}(\mathbf{R}_\lambda) \psi_j^{ad}(\mathbf{r}; \mathbf{R}_\lambda) \tag{4.6}$$

Let us define $\boldsymbol{\chi}^{ad}(\mathbf{R}_\lambda)$ as a two-dimensional column vector whose components are $\chi_i^{ad}(\mathbf{R}_\lambda)$ and $\chi_j^{ad}(\mathbf{R}_\lambda)$. The Schrödinger equation satisfied by $\boldsymbol{\chi}^{ad}(\mathbf{R}_\lambda)$ is

$$\left[-\frac{\hbar^2}{2\mu} \left\{ \mathbf{I} \nabla^2_{\mathbf{R}_\lambda} + 2\mathbf{W}^{(1)ad}(\mathbf{q}_\lambda) \cdot \boldsymbol{\nabla}_{\mathbf{R}_\lambda} + \mathbf{W}^{(2)ad}(\mathbf{q}_\lambda) \right\} + \left\{ \boldsymbol{\varepsilon}^{ad}(\mathbf{q}_\lambda) - E\mathbf{I} \right\} \right] \boldsymbol{\chi}^{ad}(\mathbf{R}_\lambda) = \mathbf{0} \tag{4.7}$$

where $\mathbf{q}_\lambda$ represents a set of internal nuclear coordinates of the system, whereas $\mathbf{R}_\lambda$ includes both $\mathbf{q}_\lambda$ and the external coordinates that orient the system in space, but excludes the system's center of mass coordinates. The $\mathbf{R}_\lambda$ symbol represents a set of nuclear coordinates that locate the N nuclei of the molecule in a center of mass frame, and μ is an overall reduced mass. $\mathbf{I}$, $\mathbf{W}^{(1)ad}$, $\mathbf{W}^{(2)ad}$, and $\boldsymbol{\varepsilon}^{ad}$ are 2×2 matrices and $\boldsymbol{\nabla}_{\mathbf{R}_\lambda}$ is a gradient operator in the $3(N-1)$-dimensional nuclear configuration

space. $\mathbf{I}$ is the identity matrix and $\boldsymbol{\varepsilon}^{ad}$ is the diagonal matrix whose diagonal elements are the potential energy surfaces ε_i^{ad} and ε_j^{ad} of the two electronically adiabatic states being considered. The matrices $\mathbf{W}^{(1)ad}$ and $\mathbf{W}^{(2)ad}$ are the the first- and second-derivative [9, 12–17] 2×2 coupling matrices whose elements are defined by

$$\left.\begin{aligned} \mathbf{W}_{m,n}^{(1)ad}(\mathbf{q}_\lambda) &= \langle \psi_m^{ad}(\mathbf{r};\mathbf{q}_\lambda) \mid \boldsymbol{\nabla}_{\mathbf{R}_\lambda} \psi_n^{ad}(\mathbf{r};\mathbf{q}_\lambda) \rangle_{\mathbf{r}} \\ \mathrm{W}_{m,n}^{(2)ad}(\mathbf{q}_\lambda) &= \langle \psi_m^{ad}(\mathbf{r};\mathbf{q}_\lambda) \mid \nabla_{\mathbf{R}_\lambda}^2 \psi_n^{ad}(\mathbf{r};\mathbf{q}_\lambda) \rangle_{\mathbf{r}} \end{aligned}\right\} m,n = i,j \tag{4.8}$$

and are respectively $3(N-2)$-dimensional vectors ($\mathbf{W}_{m,n}^{(1)ad}(\mathbf{q}_\lambda)$) [18] and scalars ($\mathrm{W}_{m,n}^{(2)ad}(\mathbf{q}_\lambda)$). The matrix $\mathbf{W}^{(1)ad}$ is in general skew-hermitian and, due to the requirement that the ψ_n^{ad} be real, is real and skew-symmetric and can be written as

$$\mathbf{W}^{(1)ad}(\mathbf{q}_\lambda) = \begin{pmatrix} 0 & \mathbf{W}_{1,2}^{(1)ad}(\mathbf{q}_\lambda) \\ -\mathbf{W}_{1,2}^{(1)ad}(\mathbf{q}_\lambda) & 0 \end{pmatrix} \tag{4.9}$$

For a triatomic system, $\mathbf{W}_{1,2}^{(1)ad}$ is a three-dimensional vector that from here on will be labeled $\mathbf{w}^{(1)ad}$. As any three-dimensional vector, it can be expressed, according to the Helmholtz theorem [19], as a sum of a longitudinal part $\mathbf{w}_{lon}^{(1)ad}(\mathbf{q}_\lambda)$ and a transverse one $\mathbf{w}_{tra}^{(1)ad}(\mathbf{q}_\lambda)$ according to

$$\mathbf{w}^{(1)ad}(\mathbf{q}_\lambda) = \mathbf{w}_{lon}^{(1)ad}(\mathbf{q}_\lambda) + \mathbf{w}_{tra}^{(1)ad}(\mathbf{q}_\lambda) \tag{4.10}$$

where by definition, the curl of $\mathbf{w}_{lon}^{(1)ad}(\mathbf{q}_\lambda)$ and the divergence of $\mathbf{w}_{tra}^{(1)ad}(\mathbf{q}_\lambda)$ vanish:

$$\boldsymbol{\nabla}_{\mathbf{q}_\lambda} \times \mathbf{w}_{lon}^{(1)ad}(\mathbf{q}_\lambda) = 0 \tag{4.11}$$

$$\boldsymbol{\nabla}_{\mathbf{q}_\lambda} \cdot \mathbf{w}_{tra}^{(1)ad}(\mathbf{q}_\lambda) = 0 \tag{4.12}$$

As a result of these equations, a scalar potential $\beta(\mathbf{q}_\lambda)$ and a vector potential $\mathbf{A}(\mathbf{q}_\lambda)$ (not to be confused with the scalar geometric phase $A_n(\mathbf{q}_\lambda)$ of Eq. (4.5)) exist for

which

$$\mathbf{w}_{lon}^{(1)ad}(\mathbf{q}_\lambda) = \boldsymbol{\nabla}_{\mathbf{q}_\lambda}\beta(\mathbf{q}_\lambda) \tag{4.13}$$

and

$$\mathbf{w}_{tra}^{(1)ad}(\mathbf{q}_\lambda) = \boldsymbol{\nabla}_{\mathbf{q}_\lambda} \times \mathbf{A}(\mathbf{q}_\lambda) \tag{4.14}$$

At conical intersection geometries, $\mathbf{w}_{lon}^{(1)ad}(\mathbf{q}_\lambda)$ is singular because of the $\mathbf{q}_\lambda$ dependence of $\psi_i^{ad}(\mathbf{r};\mathbf{q}_\lambda)$ and $\psi_j^{ad}(\mathbf{r};\mathbf{q}_\lambda)$ in their vicinity and therefore so is the $\mathbf{W}^{(1)ad}(\mathbf{q}_\lambda)\cdot\boldsymbol{\nabla}_{\mathbf{R}_\lambda}$ term in Eq. (4.7). For the same reason, $\mathrm{W}_{1,1}^{(2)ad}(\mathbf{q}_\lambda)$ and $\mathrm{W}_{2,2}^{(2)ad}(\mathbf{q}_\lambda)$ are also singular at such geometries. Replacing Eq. (4.10) into Eq. (4.9), $\mathbf{W}^{(1)ad}$ can be written as a sum of the corresponding skew-symmetric matrices $\mathbf{W}_{lon}^{(1)ad}$ and $\mathbf{W}_{tra}^{(1)ad}$. In addition, the presence of a first-derivative term of this type, even if not singular (for intersections that are not conical or for nearly avoided intersections), introduces inefficiencies in the numerical solution of that equation. This makes it desirable to switch to a diabatic electronic basis [9, 20, 21], $\psi_n^d(\mathbf{r};\mathbf{R}_\lambda)$, which in the two-electronic-state case is given by

$$\begin{pmatrix} \psi_i^d(\mathbf{r};\mathbf{R}_\lambda) \\ \\ \psi_j^d(\mathbf{r};\mathbf{R}_\lambda) \end{pmatrix} = \widetilde{\mathbf{U}}[\beta(\mathbf{q}_\lambda)] \begin{pmatrix} \psi_i^{ad}(\mathbf{r};\mathbf{R}_\lambda) \\ \\ \psi_j^{ad}(\mathbf{r};\mathbf{R}_\lambda) \end{pmatrix} \tag{4.15}$$

where $\widetilde{\mathbf{U}}[\beta(\mathbf{q}_\lambda)]$ is the transpose of the matrix

$$\mathbf{U}[\beta(\mathbf{q}_\lambda)] = \begin{pmatrix} \cos\beta(\mathbf{q}_\lambda) & -\sin\beta(\mathbf{q}_\lambda) \\ \\ \sin\beta(\mathbf{q}_\lambda) & \cos\beta(\mathbf{q}_\lambda) \end{pmatrix} \tag{4.16}$$

and $\beta(\mathbf{q}_\lambda)$ is called the diabatization or mixing angle. In terms of the diabatic electronic basis, Eq. (4.6) becomes

$$\Psi(\mathbf{r};\mathbf{R}_\lambda) = \chi_i^d(\mathbf{R}_\lambda)\psi_i^d(\mathbf{r};\mathbf{R}_\lambda) + \chi_j^d(\mathbf{R}_\lambda)\psi_j^d(\mathbf{r};\mathbf{R}_\lambda) \tag{4.17}$$

where the relation between the $\chi_n^{ad}(\mathbf{R}_\lambda)$ and $\chi_n^d(\mathbf{R}_\lambda)$ is

$$\boldsymbol{\chi}^d(\mathbf{R}_\lambda) = \widetilde{\mathbf{U}}[\beta(\mathbf{q}_\lambda)]\boldsymbol{\chi}^{ad}(\mathbf{R}_\lambda) \tag{4.18}$$

where in analogy to $\boldsymbol{\chi}^{ad}(\mathbf{R}_\lambda)$, $\boldsymbol{\chi}^{d}(\mathbf{R}_\lambda)$ is the two-dimensional column vector whose two elements are $\chi_i^d(\mathbf{R}_\lambda)$ and $\chi_j^d(\mathbf{R}_\lambda)$. Replacement of Eq. (4.18) into Eq. (4.7) yields the diabatic nuclear motion scattering equation

$$\left[-\frac{\hbar^2}{2\mu}\left\{\mathbf{I}\nabla^2_{\mathbf{R}_\lambda}+2\mathbf{W}^{(1)d}(\mathbf{q}_\lambda)\cdot\boldsymbol{\nabla}_{\mathbf{R}_\lambda}+\mathbf{W}^{(2)d}(\mathbf{q}_\lambda)\right\}+\left\{\boldsymbol{\varepsilon}^{d}(\mathbf{q}_\lambda)-E\mathbf{I}\right\}\right]\boldsymbol{\chi}^{d}(\mathbf{R}_\lambda)=\mathbf{0}. \tag{4.19}$$

where

$$\mathbf{W}^{(1)d}(\mathbf{q}_\lambda)=\mathbf{W}^{(1)ad}_{tra}(\mathbf{q}_\lambda) \tag{4.20}$$

The elements of the first-derivative $\mathbf{W}^{(1)d}(\mathbf{q}_\lambda)$ and second-derivative $\mathbf{W}^{(2)d}(\mathbf{q}_\lambda)$ coupling diabatic matrices are analogous to their adiabatic counterparts and given by Eq. (4.8) with the ψ_n^{ad} $(n=i,j)$ replaced by the ψ_n^d. In addition, $\boldsymbol{\varepsilon}^d(\mathbf{q}_\lambda)$ is the 2×2 matrix defined by

$$\boldsymbol{\varepsilon}^{d}(\mathbf{q}_\lambda)=\widetilde{\mathbf{U}}[\beta(\mathbf{q}_\lambda)]\;\boldsymbol{\varepsilon}^{ad}(\mathbf{q}_\lambda)\;\mathbf{U}[\beta(\mathbf{q}_\lambda)] \tag{4.21}$$

The adiabatic to diabatic transformation eliminates the poles in both the first- and second-derivative coupling matrices. $\mathbf{W}^{(1)d}(\mathbf{q}_\lambda)$ does not appear explicitly in Eq. (4.19) but is equal to $\mathbf{W}^{(1)ad}_{tra}(\mathbf{q}_\lambda)$, as can be shown by using Eq. (4.15) in the definition of $\mathbf{W}^{(1)d}(\mathbf{q}_\lambda)$ together with Eqs. (4.10) through (4.14). Elements of the diabatic matrix $\mathbf{W}^{(2)d}$ are usually small in the vicinity of a conical intersection and can be added to $\boldsymbol{\varepsilon}^d$ to give a corrected diabatic matrix. An approximate estimate of the magnitude of the elements of this matrix is made at the end of the results section. As can be seen, whereas in Eq. (4.7) $\mathbf{W}^{(1)ad}$ contains both the singular matrix $\mathbf{W}^{(1)ad}_{lon}$ and the non-singular one $\mathbf{W}^{(1)ad}_{tra}$, Eq. (4.19) contains only the latter. Nevertheless, the residual first-derivative coupling term $\mathbf{W}^{(1)ad}_{tra}\cdot\boldsymbol{\nabla}_{\mathbf{R}_\lambda}$ does not vanish.

A "perfect" diabatic basis would be one for which the first-derivative coupling $\mathbf{W}^{(1)d}$ vanishes [22]. From the abovementioned considerations, we conclude, as is well known [9,23,24], that a "perfect" diabatic basis cannot exist for a polyatomic system (except when the complete infinite set of electronic adiabatic functions is included [23, 27]), which means that $\mathbf{W}^{(1)ad}(\mathbf{q}_\lambda)$ cannot be transformed away to zero. As a result, the longitudinal and transverse parts of the first-derivative coupling vector are referred

to as *removable* and *nonremovable* parts respectively. Over the years, a number of formulations of approximate or quasi-diabatic or "locally rigorous" diabatic states [20, 25–33] have appeared. Only very recently [34–39] have there been attempts to use high-quality *ab initio* wave functions to consider the magnitude of the *nonremovable* part of the first-derivative coupling vector. In one such attempt [38], a quasi-diabatic basis was reported for the HeH_2 system by solving a two-dimensional Poisson equation on the plane in three-dimensional configuration space passing through the conical intersection configuration of smallest energy. It seems that no attempt has been made to get an optimal diabatization over the entire configuration space for a triatomic system, to facilitate accurate two-electronic-state scattering dynamics calculations. Conical intersections being omnipresent, such scattering calculations will permit a test of the validity of the one-electronic-state Born-Oppenheimer approximation as a function of energy in the presence of conical intersections, by comparing the results of these two kinds of calculations.

We report here an approach to obtain an optimal diabatic basis over the entire internal nuclear configuration space, based on the knowledge of the first-derivative coupling vector over the entire dynamically important part U of that space and appropriately chosen boundary conditions. We have applied this approach to the simplest triatomic system, H_3, which has a conical intersection between the $1\ ^2A'$ and $2\ ^2A'$ electronic potential energy surfaces (PESs) at equilateral triangle geometries. The corresponding conical intersection line induces a geometric phase effect, important for the reaction properties of the ground electronic state [9, 40–46]. The lowest conical intersection configuration energy occurs at 2.75 eV [47]. As a result, for energies in the vicinity of this value and above, the one-electronic-state Born-Oppenheimer approximation breaks down and a scattering calculation involving both these states and their couplings must be used to obtain accurate scattering results for this system. In this approach, first an adiabatic to diabatic transformation is obtained by calculating the diabatization angle $\beta(\mathbf{q}_\lambda)$ (appearing in Eq. (4.16)) from the first-derivative couplings ($\mathbf{W}^{(1)ad}(\mathbf{q}_\lambda)$). This calculation involves solving a three-dimensional Poisson

equation with boundary conditions that minimize the average value of the magnitude of $\mathbf{W}_{tra}^{(1)ad}$ over U. This will allow an initial neglect of the term containing $\mathbf{W}_{tra}^{(1)ad}$ in Eq. (4.19) and a later reintroduction of this term followed by a solution using perturbative or other methods.

Another check of the existence of a non-zero transverse part ($\mathbf{W}_{tra}^{(1)ad}$ or equivalently $\mathbf{w}_{tra}^{(1)ad}$) is the evaluation of line integrals of first-derivative couplings $\mathbf{w}^{(1)ad}$ along loops around conical intersection geometries. If these integrals are carried along open paths $\mathcal{L}$ in nuclear configuration space, an angular potential $\Phi(\mathbf{q}_\lambda, \mathbf{q_0}_\lambda; \mathcal{L})$ with $\mathbf{q}_\lambda = \mathbf{q_0}_\lambda$ can be defined by [18, 23, 34, 48]

$$\Phi(\mathbf{q}_\lambda, \mathbf{q_0}_\lambda; \mathcal{L}) = \int_{\mathcal{L}\ \mathbf{q_0}_\lambda}^{\mathbf{q}_\lambda} \mathbf{w}^{(1)ad}(\mathbf{q}'_\lambda) \cdot d\mathbf{q}'_\lambda \tag{4.22}$$

where $\mathbf{q_0}_\lambda$ locates the initial point on $\mathcal{L}$. This angle is called the open-path phase [49]. It is also convenient to define the corresponding closed path phase Φ_T, called the topological phase [50]:

$$\Phi_\mathsf{T}(\mathcal{L}) = \oint_{\mathcal{L}} \mathbf{w}^{(1)ad}(\mathbf{q}'_\lambda) \cdot d\mathbf{q}'_\lambda \tag{4.23}$$

In light of Eq. (4.10), we can define two more angular potentials $\Phi_{lon}(\mathbf{q}_\lambda, \mathbf{q_0}_\lambda; \mathcal{L})$ and $\Phi_{tra}(\mathbf{q}_\lambda, \mathbf{q_0}_\lambda; \mathcal{L})$, by replacing $\mathbf{w}^{(1)ad}$ in Eq. (4.22) by $\mathbf{w}_{lon}^{(1)ad}$ and $\mathbf{w}_{tra}^{(1)ad}$, respectively. The corresponding topological phases $\Phi_{\mathsf{T},lon}(\mathcal{L})$ and $\Phi_{\mathsf{T},tra}(\mathcal{L})$ can be likewise defined using Eq. (4.23) in lieu of Eq. (4.22):

$$\Phi_{\mathsf{T},lon}(\mathcal{L}) = \oint_{\mathcal{L}} \mathbf{w}_{lon}^{(1)ad}(\mathbf{q}'_\lambda) \cdot d\mathbf{q}'_\lambda \tag{4.24}$$

$$\Phi_{\mathsf{T},tra}(\mathcal{L}) = \oint_{\mathcal{L}} \mathbf{w}_{tra}^{(1)ad}(\mathbf{q}'_\lambda) \cdot d\mathbf{q}'_\lambda \tag{4.25}$$

According to the geometric phase theorem [6, 34, 35]

$$\Phi_{\mathsf{T},lon}(\mathcal{L}) = p\pi \tag{4.26}$$

where $p = 0$ if $\mathcal{L}$ does not enclose any conical intersection and $p = 1$ if it encloses one conical intersection. Using this and Eq. (4.10), we have

$$\Phi_{\mathsf{T},tra}(\mathcal{L}) = \Phi_{\mathsf{T}}(\mathcal{L}) - p\pi \tag{4.27}$$

As a result, a necessary but insufficient condition for the first-derivative coupling to be purely longitudinal is that $\Phi_{\mathsf{T},tra}(\mathcal{L})$ vanish [38]. Non-zero $\Phi_{\mathsf{T},tra}(\mathcal{L})$ and hence a non-zero $\mathbf{w}_{tra}^{(1)ad}$ correspond to the existence of non-zero derivative couplings involving electronic states outside the two-electronic-state sub-Hilbert space [24] being considered in the present chapter.

In Sec. 4.2, we present an approach to obtain an optimal diabatic basis by using a Poisson equation obtained from Eqs. (4.10) through (2.21), similar to that used previously [38], and a special set of boundary conditions. The present Poisson equation differs from the latter, however, in that it extends over the entire three-dimensional U domain of configuration space and uses very different boundary conditions. In Sec. 4.3, we present the results of the diabatization angle calculation and the longitudinal as well as transverse parts of the first-derivative coupling vector and discuss the possible implications of dropping the transverse part in two-electronic-state quantum scattering calculations. The open-path phases Φ_{lon} and Φ_{tra} and topological (closed-path) phases $\Phi_{\mathsf{T},lon}$ and $\Phi_{\mathsf{T},tra}$ are evaluated, which confirm the presence of a non-zero transverse part. We also present the diabatic PESs (elements of the 2×2 diabatic energy matrix $\boldsymbol{\varepsilon}^d(\mathbf{q}_\lambda)$) corresponding to this optimal diabatic basis and discuss their features.

4.2 Methodology

4.2.1 Coordinate system

For any triatomic system, the internal nuclear coordinate space $\mathcal{Q}$ spanned by $\mathbf{q}_\lambda$ is three-dimensional. We adopt the symmetrized hyperspherical coordinates $\mathbf{q}_\lambda \equiv$

$(\rho, \theta, \phi_\lambda)$ used previously [9,42–46,51]. The ranges of these coordinates are as follows:

$$0 \leq \rho < \infty \qquad 0 \leq \theta \leq \pi/2 \qquad 0 \leq \phi_\lambda < 2\pi \tag{4.28}$$

For a constant hyperradius ρ, these coordinates span a hemisphere whereas ordinary spherical polar coordinates span a full sphere.

The H_3 system exhibits a conical intersection between the $1\ ^2A'$ and $2\ ^2A'$ electronic PESs for equilateral triangle geometries, which corresponds to $\theta = 0$ and all values of ρ and ϕ_λ. Collinear geometries of H_3 are mapped by $\theta = \pi/2$ for all values of ρ and ϕ_λ.

Projection plots of physical quantities in internal configuration space cartesian coordinates $(X_\lambda, Y, Z_\lambda)$, which are related to these symmetrized hyperspherical coordinates, provide valuable information for reactive scattering calculations that use these physical quantities and hyperspherical coordinates. As mentioned above, for a constant hyperradius ρ the hyperspherical coordinates span a hemisphere. Fig. 4.1 shows this hemisphere for a constant ρ (the radius of this hemisphere) and a point P on this hemisphere which has θ, ϕ_λ polar angles in the $\mathsf{O}\overline{X}_\lambda\overline{Y}_\lambda\overline{Z}$ frame and another related set of polar angles $\omega_\lambda, \gamma_\lambda$ in the associated $\mathsf{O}X_\lambda Y Z_\lambda$ frame. γ_λ is the angle between mass-scaled jacobi coordinates. $\gamma_\lambda = 0°$ or $180°$ (equivalent to $\theta = 90°$) corresponds to collinear configurations of the H_3 system and $\gamma_\lambda = 90°$ to configurations for which the H atom is on the perpendicular bisector of the H−H line. All these coordinates and their interrelations have been discussed elsewhere [18,52–58].

4.2.2 The Poisson equation

Replacing Eq. (4.13) into Eq. (4.10) results in

$$\mathbf{w}^{(1)ad}(\mathbf{q}_\lambda) = \boldsymbol{\nabla}_{\mathbf{q}_\lambda}\beta(\mathbf{q}_\lambda) + \mathbf{w}_{tra}^{(1)ad}(\mathbf{q}_\lambda), \tag{4.29}$$

Taking the divergence of both sides of this equation and using Eq. (4.14) together with the known property that the divergence of a curl of a three-dimensional vector vanishes, we get

$$\nabla^2_{\mathbf{q}_\lambda}\beta(\mathbf{q}_\lambda) = \sigma(\mathbf{q}_\lambda) \tag{4.30}$$

where

$$\sigma(\mathbf{q}_\lambda) = \nabla_{\mathbf{q}_\lambda} \cdot \mathbf{w}^{(1)ad}(\mathbf{q}_\lambda) \tag{4.31}$$

is known because $\mathbf{w}^{(1)ad}(\mathbf{q}_\lambda)$ has been accurately calculated and fitted over the entire $\mathcal{Q}$ space of interest [18]. Eq. (4.30) is the Poisson equation for $\beta(\mathbf{q}_\lambda)$. Once the boundary conditions associated with it are chosen, this equation can be solved numerically. Replacing the solution into Eq. (4.29) then furnishes $\mathbf{w}^{(1)ad}_{tra}(\mathbf{q}_\lambda)$ and therefore the first-derivative transverse coupling matrix

$$\mathbf{W}^{(1)ad}_{tra}(\mathbf{q}_\lambda) = \begin{pmatrix} 0 & \mathbf{w}^{(1)ad}_{tra}(\mathbf{q}_\lambda) \\ -\mathbf{w}^{(1)ad}_{tra}(\mathbf{q}_\lambda) & 0 \end{pmatrix} \tag{4.32}$$

which appears in the diabatic nuclear motion scattering Eq. (4.19). As a result, the flexibility provided by the selection of these boundary conditions injects an element of flexibility in the determination of $\mathbf{W}^{(1)ad}_{tra}(\mathbf{q}_\lambda)$.

In the next section we discuss the nature of the effect of the boundary conditions on this determination and how to select these conditions so as to result in an optimal diabatization.

4.2.3 Boundary conditions for solving the Poisson equation

The Poisson equation [Eq. (4.30)], being a second-order partial differential equation, has an infinite set of solutions because of the infinite choice of boundary conditions that can be imposed on it. Any of these solutions results in a $\beta(\mathbf{q}_\lambda)$ that removes the singularity in $\mathbf{W}^{(1)ad}(\mathbf{q}_\lambda)$ at the conical intersection geometries upon the adiabatic to diabatic transformation defined by Eqs. (4.18) and (4.16). If $\sigma(\mathbf{q}_\lambda)$ goes to zero at

infinity, a formal solution that also goes to zero at infinity is [9, 19, 59]

$$\beta(\mathbf{q}_\lambda) = -\int \frac{\sigma(\mathbf{q}'_\lambda)}{4\pi|\mathbf{q}_\lambda - \mathbf{q}'_\lambda|} d\mathbf{q}'_\lambda \tag{4.33}$$

This is, however, not the only boundary condition possible. To pick an optimal set of boundary conditions we need to look at the individual terms in the diabatic nuclear motion Schrödinger equation [Eq. (4.19)].

It is customary in two-electronic-state problems to introduce two approximations into this equation. The first is to assume that the $\mathbf{W}^{(2)d}(\mathbf{q}_\lambda)\boldsymbol{\chi}^d(\mathbf{R}_\lambda)$ term is negligible compared to the remaining ones. This term vanishes for a complete diabatic electronic basis set but not for a two-diabatic electronic basis set. The second is to assume that the $\mathbf{W}^{(1)ad}_{tra}(\mathbf{q}_\lambda) \cdot \boldsymbol{\nabla}_{\mathbf{R}_\lambda}\boldsymbol{\chi}^d(\mathbf{R}_\lambda)$ term is negligible compared to the remaining ones. This assumption is justifiable if $\mathbf{W}^{(1)ad}_{tra}(\mathbf{q}_\lambda)$ is sufficiently small in the entire internal nuclear configuration space $\mathcal{Q}$ and, in particular, in the neighborhood of the conical intersection. This suggests that we select the boundary conditions satisfied by Eq. (4.30) so as to minimize as much as possible this transverse part in this space.

We will select a domain V in configuration space $\mathcal{Q}$, enclosed by a boundary surface S, within which the Poisson equation is to be solved. This domain includes the dynamically important part of $\mathcal{Q}$. The definitions of V and S are given in Sec. 4.2.4. As shown in that section, the choice of a reference surface at which the adiabatic and diabatic wave functions are equal, together with the condition that the adiabatic to diabatic transformation should reflect the P_3 permutation symmetry of the H_3 system, as well as the change of sign under pseudorotations given by Eq. (4.4), fixes the value of $\beta(\mathbf{q}_\lambda)$ on parts of S. On the remaining parts, we pick the following boundary condition (using Eq. (4.29)),

$$[\boldsymbol{\nabla}_{\mathbf{q}_\lambda}\beta(\mathbf{q}_\lambda)]_{\mathsf{S}} = \left[\mathbf{w}^{(1)ad}(\mathbf{q}_\lambda)\right]_{\mathsf{S}} \tag{4.34}$$

The reason for this choice is that if we make the transverse part zero on some parts of the boundary surface S, Eq. (4.29) leads directly to Eq. (4.34) on those parts. This

equation corresponds to a Neumann boundary condition for the Poisson equation and, as proved in Appendix 4.A, minimizes the average value of the magnitude of this transverse part over the domain V. Using this condition tends to decrease the magnitude of the $\mathbf{W}_{tra}^{(1)ad}(\mathbf{q}_\lambda) \cdot \boldsymbol{\nabla}_{\mathbf{R}_\lambda} \boldsymbol{\chi}^d(\mathbf{R}_\lambda)$ term in Eq. (4.19). This is therefore an optimal boundary condition. It is quite different from setting $\beta(\mathbf{q}_\lambda) = 0$ at the boundary, as will be shown in Sec. 4.2.4. In order to assess the effect of $\mathbf{W}_{tra}^{(1)ad}$ on the dynamics, one can first solve Eq. (4.19) omitting that term and then reintroduce it using perturbation theory or other methods.

4.2.4 Numerical solution of the Poisson equation

We express the Poisson equation in terms of the internal hyperspherical coordinates $\rho, \theta, \phi_\lambda$ as

$$\left[\frac{\partial^2}{\partial\rho^2} + \frac{2}{\rho}\frac{\partial}{\partial\rho} + \frac{1}{\rho^2}\left(\frac{\partial^2}{\partial\theta^2} + \cot\theta\frac{\partial}{\partial\theta} + \frac{1}{\sin^2\theta}\frac{\partial^2}{\partial\phi_\lambda^2}\right)\right]\beta(\rho,\theta,\phi_\lambda) = \sigma(\rho,\theta,\phi_\lambda) \quad (4.35)$$

For the H_3 system, we change the dependent variable β to γ by the transformation

$$\beta(\rho,\theta,\phi_\lambda) = \frac{\phi_\lambda}{2} - \gamma(\rho,\theta,3\phi_\lambda). \quad (4.36)$$

The dependence of γ on $3\phi_\lambda$ (rather than on ϕ_λ simply) is due to the P_3 permutation symmetry of the H_3 system. It should be noted that although the P_3 group is isomorphic with C_{3v}, the configurations we are considering are only equilateral triangles for $\theta = 0°$. The term $\phi_\lambda/2$ is responsible for the singularity in the first-derivative coupling vector at conical intersection ($\theta = 0°$) configurations. When ϕ_λ changes by 2π radians during a pseudorotation (which encircles the conical intersection), γ does not change but β changes by π. As pointed out in the beginning of the introduction, under such a pseudorotation $\boldsymbol{\chi}^{ad}$ changes sign and as a result of Eqs. (4.18) and (4.16) $\boldsymbol{\chi}^d$ is unchanged and is single-valued. This is a useful property of the diabatic representation. An approximate analytical expression for $\beta(\rho,\theta,\phi_\lambda)$ was obtained by Varandas *et al* [47] using a double many-body expansion (DMBE) of the two lowest

electronic PESs for H_3, and is given by

$$\beta^{\mathrm{DMBE}}(\rho,\theta,\phi_\lambda) = \frac{\phi_\lambda}{2} - \gamma^{\mathrm{DMBE}}(\rho,\theta,3\phi_\lambda) \tag{4.37}$$

where

$$\gamma^{\mathrm{DMBE}}(\rho,\theta,3\phi_\lambda) = \frac{1}{2}\tan^{-1}\frac{g_0(\rho)\sin\theta\sin 3\phi_\lambda}{f_0(\rho)+g_0(\rho)\sin\theta\cos 3\phi_\lambda + f_1(\rho)\sin^2\theta} \tag{4.38}$$

and $g_0(\rho)$, $f_0(\rho)$, and $f_1(\rho)$ are functions that depend only on the hyperradius ρ. $\beta^{\mathrm{DMBE}}(\rho,\theta,\phi_\lambda)$ is accurate close to conical intersection geometries, i.e.,

$$\beta^{\mathrm{DMBE}}(\rho,\theta,\phi_\lambda) \underset{\theta\to 0}{\longrightarrow} \beta(\rho,\theta,\phi_\lambda) \tag{4.39}$$

In the DMBE treatment, the transverse part of the first-derivative coupling vector is assumed to be negligible (especially near the conical intersection) as compared to the longitudinal part. In this approximation $\mathbf{w}^{(1)ad}_{tra,\mathrm{DMBE}}(\mathbf{q}_\lambda)$ is required to vanish at all $\mathbf{q}_\lambda$, i.e.,

$$\mathbf{w}^{(1)ad}_{\mathrm{DMBE}}(\mathbf{q}_\lambda) = \boldsymbol{\nabla}_{\mathbf{q}_\lambda}\beta^{\mathrm{DMBE}}(\mathbf{q}_\lambda). \tag{4.40}$$

To test the validity of Eq. (4.39), since we know $\beta^{\mathrm{DMBE}}(\rho,\theta,\phi_\lambda)$ analytically, we compared $\mathbf{w}^{(1)ad}_{\mathrm{DMBE}}(\mathbf{q}_\lambda)$ with our *ab initio* first-derivative coupling vector $\mathbf{w}^{(1)ad}(\mathbf{q}_\lambda)$ in regions near the conical intersection and found a systematic mismatch in sign that was removed by changing the sign of $g_0(\rho)$ in the DMBE code. After making this change these first-derivative coupling vectors agreed quite well in these regions. Rewriting the Poisson Eq. (4.35) in terms of $\gamma(\rho,\theta,3\phi_\lambda)$ by using Eq. (4.36), we get

$$-\left[\frac{\partial^2}{\partial\rho^2}+\frac{2}{\rho}\frac{\partial}{\partial\rho}+\frac{1}{\rho^2}\left(\frac{\partial^2}{\partial\theta^2}+\cot\theta\frac{\partial}{\partial\theta}+\frac{1}{\sin^2\theta}\frac{\partial^2}{\partial\phi_\lambda^2}\right)\right]\gamma(\rho,\theta,3\phi_\lambda) = \sigma(\rho,\theta,3\phi_\lambda). \tag{4.41}$$

This equation was solved using the MUDPACK [60, 61] library of subroutines. This library permits the solution of two- and three-dimensional linear elliptic partial differential equations with any combination of periodic, Dirichlet (for which the unknown

function is specified on the boundary), Neumann (for which a derivative of the unknown function at the boundary is specified) and mixed Dirichlet-Neumann boundary conditions. The solution of Eq. (4.41) was obtained on the following restricted domain V of nuclear configuration space:

$$1.5 \text{ bohr} \leq \rho \leq 10 \text{ bohr} \qquad 0.1^\circ \leq \theta \leq 90^\circ \qquad 0^\circ \leq \phi_\lambda \leq 60^\circ \tag{4.42}$$

The full domain $\mathsf{U} \equiv 6\mathsf{V}$ has the same ρ and θ ranges as in Eq. (4.42) but the full ϕ_λ range of 0° to 360°. The solution over V leads directly to a solution over U with the help of the P_3 symmetry properties of the system. The use of 1.5 bohr for the minimum value of ρ required a small extrapolation of the *ab initio* first-derivative couplings available in the 2 bohr to 8 bohr interval. At 2 bohr, the lowest energy point on the ground adiabatic DSP PES [18] is about 3 eV. The corresponding lowest energy point for $\rho = 1.5$ bohr is greater than 5 eV and hence regions of configuration space for which $\rho < 1.5$ bohr (very compact nuclear geometries) will not be important for scattering dynamics at energies less than 5 eV, approximately. The 10 bohr value was chosen as the maximum ρ because at this hyperradius the H + H_2 interaction energy is too small to affect reaction cross sections of interest to this chapter. The lowest value used for θ was 0.1° because the Poisson equation solver in MUDPACK library for spherical polar coordinates is unstable for values of θ below that value. Besides, at such small values of θ, both β and γ are known since the DMBE representation [47] [Eqs. (4.37) and (4.38)] is quite accurate in these regions.

Let us consider the internal configuration space frame $\mathsf{O}\overline{X}_\lambda\overline{Y}_\lambda\overline{Z}$ of Fig. 4.1 in which an internal nuclear configuration $\mathbf{q}_\lambda$ is represented by a point whose spherical polar coordinates are ρ, θ, ϕ_λ. Fig. 4.2 depicts in this frame the boundary surface S that encloses the domain V defined by Eq. (4.42). It is comprised of 6 pieces:

a) S_1, the surface defined by $\phi_\lambda = 0^\circ$, $0.1^\circ \leq \theta \leq 90^\circ$ and 1.5 bohr $\leq \rho \leq$ 10 bohr. It lies on the positive $\overline{X}_\lambda$ and $\overline{Z}$ quadrant of the $\mathsf{O}\overline{X}_\lambda\overline{Z}$ plane. Its vertices are points A, B, C and D.

b) S_2, the surface defined by $\phi_\lambda = 60°$, $0.1° \leq \theta \leq 90°$ and 1.5 bohr $\leq \rho \leq$ 10 bohr. It is analogous to S_1, but lies on a plane containing the $\mathsf{O}\overline{Z}$ axis and making an angle of 60° with the $\mathsf{O}\overline{X}_\lambda\overline{Z}$ plane (measured counterclockwise from the latter as viewed from a point on the latter having $\overline{Z} > 0$). Its vertices are points E, F, G and H.

c) S_3, the surface defined by $\theta = 0.1°$, $0° \leq \phi \leq 60°$ and 1.5 bohr $\leq \rho \leq$ 10 bohr. It is a piece of a narrow conical surface whose vertices are B, C, H and E.

d) S_4, the surface defined by $\theta = 90°$, $0° \leq \phi \leq 60°$ and 1.5 bohr $\leq \rho \leq$ 10 bohr. It lies on the $\mathsf{O}\overline{X}_\lambda\overline{Y}_\lambda$ plane. Its vertices are A, D, G and F.

e) S_5, the surface defined by $\rho = 1.5$ bohr, $0.1° \leq \theta \leq 90°$ and $0° \leq \phi \leq 60°$. It is a portion of a spherical surface of radius 1.5 bohr having as edges the intersections with S_1, S_2, S_3 and S_4. Its vertices are C, D, G and H.

f) S_6, the surface defined by $\rho = 10$ bohr, $0.1° \leq \theta \leq 90°$ and $0° \leq \phi \leq 60°$. It is a portion of a spherical surface of radius 10 bohr having as edges the intersections with S_1, S_2, S_3 and S_4. Its vertices are A, B, E and F.

The boundary conditions adopted on S were the following:

a) On S_1,

$$\beta(\mathsf{S}_1) = \gamma(\mathsf{S}_1) = 0 \tag{4.43}$$

for all points on this surface. From Eqs. (4.16), (4.18) and (4.36), this condition results in the relation

$$\chi^d(\mathsf{S}_1) = \chi^{ad}(\mathsf{S}_1) \tag{4.44}$$

In other words, S_1 is chosen as the surface on which the diabatic and adiabatic representations coincide. This is a natural Dirichlet boundary condition.

b) On S_2,

$$\beta(\mathsf{S}_2) = \pi/6 \quad \text{and} \quad \gamma(\mathsf{S}_2) = 0 \tag{4.45}$$

for all points on this surface. This condition is a consequence of Eq. (4.43) and the P_3 symmetry of the H_3 system and forces γ to be single valued upon a pseudorotation of the system around the conical intersection line between the 1 $^2A'$ and 2 $^2A'$ states of H_3, i.e., to have the same value at $\phi_\lambda = 0°$ and $\phi_\lambda = 360°$. This in turn forces $\beta(\rho, \theta, \phi_\lambda)$ [Eq. (4.36)] to change by π upon such a pseudorotation, as required. This is also a natural Dirichlet boundary condition that follows from the one on S_1.

c) On S_3,

$$\beta(\mathsf{S}_3) = \phi_\lambda/2 \quad \text{and} \quad \gamma(\mathsf{S}_3) = 0 \tag{4.46}$$

for all points on this surface. This is a consequence of the fact that, close to the conical intersection ($\theta = 0.1°$ in the present case), the electronic wave functions $\psi_i^{ad}(\mathbf{r}; \mathbf{q}_\lambda)$ and $\psi_j^{ad}(\mathbf{r}; \mathbf{q}_\lambda)$ are, to first order in θ, independent of θ and depend on $\mathbf{q}_\lambda$ only through ρ and ϕ_λ [9]. This is a mandatory Dirichlet boundary condition.

For boundary surfaces S_4 through S_6 we chose Neumann boundary conditions which force the θ-component of $\mathbf{w}_{tra}^{(1)ad}$ to vanish at the S_4 boundary and the ρ-component of this vector to vanish at the S_5 and S_6 boundaries. As proved in Appendix 4.A, these choices minimize the average value of the magnitude of $\mathbf{w}_{tra}^{(1)ad}$ over the space enclosed by S. Specifically, the boundary conditions on S_4 through S_6 are as follows:

d) On S_4,

$$\left(\frac{\partial \beta}{\partial \theta}\right)_{\mathsf{S}_4} = -\left(\frac{\partial \gamma}{\partial \theta}\right)_{\mathsf{S}_4} = \rho \; \mathrm{w}_\theta^{(1)ad}(\rho, \theta = 90°, \phi_\lambda) \tag{4.47}$$

for all points on this surface. This condition results in the property

$$\mathrm{w}_{tra,\theta}^{(1)ad}(\rho, \theta = 90^{\circ}, \phi_{\lambda}) = 0 \tag{4.48}$$

i.e., the θ-component of $\mathbf{w}_{tra}^{(1)ad}$ is forced to vanish on this surface.

e) On S_5,

$$\left(\frac{\partial \beta}{\partial \rho}\right)_{\mathsf{S}_5} = -\left(\frac{\partial \gamma}{\partial \rho}\right)_{\mathsf{S}_5} = \mathrm{w}_{\rho}^{(1)ad}(\rho = 1.5 \text{ bohr}, \theta, \phi_{\lambda}) \tag{4.49}$$

which results in

$$\mathrm{w}_{tra,\rho}^{(1)ad}(\rho = 1.5 \text{ bohr}, \theta, \phi_{\lambda}) = 0 \tag{4.50}$$

f) On S_6,

$$\left(\frac{\partial \beta}{\partial \rho}\right)_{\mathsf{S}_6} = -\left(\frac{\partial \gamma}{\partial \rho}\right)_{\mathsf{S}_6} = \mathrm{w}_{\rho}^{(1)ad}(\rho = 10 \text{ bohr}, \theta, \phi_{\lambda}) \tag{4.51}$$

which results in

$$\mathrm{w}_{tra,\rho}^{(1)ad}(\rho = 10 \text{ bohr}, \theta, \phi_{\lambda}) = 0 \tag{4.52}$$

The calculation using the boundary conditions above will henceforth be designated as $\mathbf{b}_0$.

The number of grid points used in the ρ, θ and ϕ_{λ} directions in the MUDPACK equation solver was 513, 257 and 65, respectively, for a total of about 8.6 million grid points. The relative number of points for the three variables was found to optimize the accuracy of the solution. The grid spacings associated with ρ and θ were smaller than that associated with ϕ_{λ} because the Neumann boundary conditions for S_4 through S_6 and the associated evaluation of numerical derivatives required such finer grids.

$\gamma(\rho, \theta, 3\phi_{\lambda})$, obtained by the solution of the Poisson equation [Eq. (4.41)] with the boundary conditions just described, was used in Eq. (4.36) to obtain the diabatization angle, $\beta(\rho, \theta, \phi_{\lambda})$. This angle was then used in Eq. (4.29) to obtain the transverse part of the first-derivative coupling vector. As a check of the self-consistency of the

calculations performed, we also employed the values of γ obtained at the boundary surfaces S_4 through S_6 as Dirichlet starting conditions in a new solution of the Poisson equation involving only Dirichlet conditions. As expected, the new results were identical to the previous ones within the numerical accuracy of the calculation.

To obtain a quantitative estimate of the sensitivity of the solution of the Poisson equation to the boundary conditions used, we generated solutions for the following additional sets of boundary conditions:

1. Neumann conditions on S_3 through S_6 and Dirichlet conditions on S_1 and S_2. The Neumann condition on S_3 is given by

$$\left(\frac{\partial\beta}{\partial\theta}\right)_{\mathsf{S}_3} = -\left(\frac{\partial\gamma}{\partial\theta}\right)_{\mathsf{S}_3} = \rho\ \mathrm{w}_{\theta}^{(1)ad}(\rho, \theta = 0.1^\circ, \phi_\lambda) \tag{4.53}$$

which results in the property

$$\mathrm{w}_{tra,\theta}^{(1)ad}(\rho, \theta = 0.1^\circ, \phi_\lambda) = 0 \tag{4.54}$$

This property is consistent with the boundary condition Eq. (4.46) (at $\theta = 0.1^\circ$ but not necessarily at other small θ) and as a result we should expect this calculation to yield results very close to those obtained in the $\mathbf{b}_0$ calculation. That did indeed turn out to be the case, the results of the two calculations differing only slightly near the conical intersection (for $\theta \lesssim 3^\circ$) and being identical (within calculation accuracy) away from it. The ratio ξ_1 defined by Eq. (4.56), differed from unity by less than 10^{-4}.

2. Dirichlet conditions $\gamma = 0$ on all six boundaries S_1 through S_6. This calculation without any Neumann boundary condition is expected to give results that most differ from the optimal $\mathbf{b}_0$ (3 Dirichlet and 3 Neumann) boundary conditions.

3. Neumann conditions on S_4 and S_5 and $\gamma = 0$ Dirichlet conditions on the other S_i.

4. Neumann conditions on S_4 and S_6 and $\gamma = 0$ Dirichlet conditions on the other S_i.

5. Neumann conditions on S_5 and S_6 and $\gamma = 0$ Dirichlet conditions on the other S_i.

6. Neumann conditions on S_4 and $\gamma = 0$ Dirichlet conditions on the other S_i.

7. Neumann conditions on S_5 and $\gamma = 0$ Dirichlet conditions on the other S_i.

8. Neumann conditions on S_6 and $\gamma = 0$ Dirichlet conditions on the other S_i.

The Neumann conditions referred to in 3. to 8. above are those given by Eqs. (4.47), (4.49) and (4.51). The calculations specified in 1. through 8. above will henceforth be designated as $\mathbf{b}_1$ through $\mathbf{b}_8$, respectively. They were all performed using the same grid parameters as for $\mathbf{b}_0$, described after Eq. (4.52).

In order to compare results of calculations $\mathbf{b}_0$ through $\mathbf{b}_8$, we calculated for each the corresponding root-mean-square average magnitude of the transverse coupling vector, over the full domain U of configuration space, defined by

$$\langle \mathrm{w}_{tra}^{(1)ad} \rangle_i = \left[\frac{\int_{\mathsf{U}} |\mathbf{w}_{tra}^{(1)ad}(\mathbf{q}_\lambda)|^2 d\mathbf{q}_\lambda}{\int_{\mathsf{U}} d\mathbf{q}_\lambda} \right]^{1/2} \qquad i = 0 \text{ through } 8 \tag{4.55}$$

where $d\mathbf{q}_\lambda$ is the volume element of the domain U. We also obtained the ratios

$$\xi_i = \frac{\langle \mathrm{w}_{tra}^{(1)ad} \rangle_i}{\langle \mathrm{w}_{tra}^{(1)ad} \rangle_0} \qquad i = 0 \text{ through } 8 \tag{4.56}$$

which will be useful for comparing the results of these $\mathbf{b}_i$ calculations. The larger ξ_i is, the larger is the deviation of the corresponding $\langle \mathrm{w}_{tra}^{(1)ad} \rangle_i$ from the minimum value $\langle \mathrm{w}_{tra}^{(1)ad} \rangle_0$. These quantities will permit an assessment of the magnitude of the minimization achieved in the latter and of the relative importance of using Neumann

boundary conditions on S_4, S_5 and S_6.

In the next section, we present the results obtained for the diabatization angle as well as those for the longitudinal and transverse parts of the first-derivative coupling vector. We will also discuss the magnitude of the transverse part in the dynamically relevant regions of nuclear configuration space, the importance of the Neumann boundary conditions used in its determination, and its possible effect on scattering calculations upon its reintroduction as a perturbation.

4.3 Results and discussion

4.3.1 Diabatization angle

The function $\sigma(\rho, \theta, 3\phi_\lambda)$, needed to solve the Poisson equation, is displayed in Fig. 4.3, with a multiplicative factor of $\sin^2\theta$, as a function of θ and ϕ_λ for $\rho = 2$ bohr, 4 bohr, 6 bohr and 8 bohr. This factor is used to cancel out the pole behavior of σ associated with its $1/\sin^2\theta$ dependence. This source term also displays the permutation symmetry of the H_3 system. For $\rho = 2$ bohr (panel (a)), it ($\sin^2\theta\ \sigma$) has sharp minima of about 0.75 bohr^{-2} at $\phi_\lambda = 0°$, 120° and 240° while displaying small oscillations around a flat value in other regions. For $\rho = 8$ bohr (panel (d)), it displays sharp maxima of about 0.45 bohr^{-2} at $\phi_\lambda = 60°$, 180° and 300° while staying flat with no oscillations in other regions. Both these extrema (sharp minima for $\rho = 2$ bohr and sharp maxima for $\rho = 8$ bohr) occur for all values of θ with the most pronounced behavior occuring at $\theta = 90°$ (collinear configurations). Its characteristics at $\rho = 4$ bohr (panel (b)) are midway between those at $\rho = 2$ bohr and $\rho = 8$ bohr, with no sharp features. Besides, at this hyperradius it has oscillations which show minima around $\phi_\lambda = 0°$, 120° and 240° and maxima around $\phi_\lambda = 60°$, 180° and 300°. At $\rho = 6$ bohr (panel (c)), its behavior is similar to that at $\rho = 8$ bohr. In panels (e) through (h) we depict equatorial views of $\sin^2\theta\ \sigma(\rho, \theta, 3\phi_\lambda)$ contours and their mapping onto the $\bar{x}_\lambda \bar{y}_\lambda$ tangent plane of Fig. 4.1. This mapping is called the

equatorial view because it corresponds to a non-perpendicular arc-length-preserving projection of the constant hyperradius hemisphere on a plane tangent to it at the point on its equator, defined by $\omega_\lambda = \gamma_\lambda = \pi/2$. This permits the viewing of all three possible atom-diatom arrangement channel regions (for the triatomic reaction) as well as the regions for which the three atoms are at comparable distances from each other, for a fixed hyperradius ρ. Maps of this kind have been used before [18, 52, 65, 66]. This view of $\sin^2\theta\ \sigma(\rho, \theta, 3\phi_\lambda)$ contours confirms the sharp minima behavior for $\rho =$ 2 bohr and sharp maxima behavior for $\rho = 8$ bohr in different regions of the ϕ_λ space. They also confirm the flat regions of 0 bohr^{-2} for $\rho = 6$ bohr and $\rho =$ 8 bohr around $\phi_\lambda = 0°$, 120° and 240° regions of configuration space. Analysis of $\mathbf{w}^{(1)ad}$ at these hyperradii (using their plots from Chapter 3) shows that in and around these regions of configuration space the coupling vector is about two orders of magnitude smaller than in the regions of space around $\phi_\lambda = 60°$, 180° and 300°. This is also evident in the corresponding plots of $\mathbf{w}_{lon}^{(1)ad}$ (Fig. 4.9) and $\mathbf{w}_{tra}^{(1)ad}$ (Fig. 4.10) discussed in Sec. 4.3.4, since their sum gives the total coupling vector $\mathbf{w}^{(1)ad}$. In the three ϕ_λ regions mentioned above, the dominant $\mathbf{w}_{lon}^{(1)ad}$ is much smaller than in other regions. This negligibly small magnitude of the coupling vector leads to its negligible divergence as indicated by the source term $\sigma(\rho, \theta, 3\phi_\lambda)$ plotted in panels (c), (d), (g) and (h) of Fig. 4.3.

Solution of the Poisson Eq. (4.41), subject to the boundary condition of Eq. (4.43) and Eqs. (4.45) through (4.52) and the source term discussed above, furnishes $\gamma(\rho, \theta, 3\phi_\lambda)$ in the domain of internal nuclear configuration space defined by Eq. (4.42), which is the entire ρ and θ space but one-sixth of the full ϕ_λ space due to the P_3 symmetry of H_3. This can be extended to the full $0 \leq \phi_\lambda < 2\pi$ space by symmetry considerations. The diabatization angle $\beta(\rho, \theta, \phi_\lambda)$ is then obtained over the full domain U by using $\gamma(\rho, \theta, 3\phi_\lambda)$ together with Eq. (4.36).

Fig. 4.4 (panels (a) through (d)) depicts the diabatization angle $\beta(\rho, \theta, \phi_\lambda)$ as a function of θ and ϕ_λ for four different hyperradii. Panels (a), (b), (c) and (d) correspond to the fixed hyperradii of 2 bohr (tight geometries), 4 bohr, 6 bohr, and

8 bohr (asymptotic geometries), respectively. Panels (e) through (h) display the equatorial views of β contours corresponding to panels (a) through (d) through their mapping onto the $\bar{x}_\lambda \bar{y}_\lambda$ tangent plane of Fig. 4.1. Since near conical intersection geometries and even at other geometries $\beta(\rho, \theta, \phi_\lambda)$ is dominated by the $\phi_\lambda/2$ term, we plot in Fig. 4.5 (panels (a) through (d)) $\gamma(\rho, \theta, 3\phi_\lambda)$ as a function of θ and ϕ_λ for the same hyperradii as before and the corresponding equatorial views in panels (e) through (h), respectively. In each of the panels in Figs. 4.4 and 4.5, the hyperradius ρ is kept fixed and the hyperangle ϕ_λ is varied from 0 to 2π along the circle shown at the bottom. In addition, the hyperangle θ is varied from 0 to $\pi/2$, from the center of that circle (corresponding to $\theta = 0$ or conical intersection geometries) to its edge (corresponding to $\theta = \pi/2$ or collinear geometries).

Panels (a) through (d) of Fig. 4.6 display cuts of the $\gamma(\rho, \theta, 3\phi_\lambda)$ plots shown in panels (a) through (d), respectively of Fig. 4.5 at three values of θ (5°, 45°, and 90°) for the same four values of ρ. The corresponding DMBE angle, $\gamma^{\text{DMBE}}(\rho, \theta, 3\phi_\lambda)$, is displayed in panels (e) through (h) of Fig. 4.6 for the same θ cuts and hyperradii. Since $\gamma^{\text{DMBE}}(\rho, \theta, 3\phi_\lambda)$ is accurate in the vicinity of the conical intersection, a quantity Δ_γ is defined as the maximum difference between γ and γ^{DMBE} over all values of ϕ_λ, keeping the values of ρ and θ fixed:

$$\Delta_\gamma(\rho, \theta) = max\left[\gamma(\rho, \theta, 3\phi_\lambda) - \gamma^{\text{DMBE}}(\rho, \theta, 3\phi_\lambda)\right]_{\phi_\lambda} \tag{4.57}$$

In Fig. 4.7, Δ_γ is depicted as a function of θ for the same four values of the hyperradius ρ, since it provides an indication of the ρ-dependent difference between γ^{DMBE} and γ as a function of θ. As the latter increases from 0° to 90°, the corresponding configuration moves away from the conical intersection. Fig. 4.8 depicts γ_{6D} obtained from the 6 Dirichlet boundary conditions calculation $\mathbf{b}_2$ described in Sec. 4.2.4. Figs. 4.4 through 4.8 are further discussed in Sec. 4.3.4.

4.3.2 Longitudinal and transverse parts of the first-derivative coupling vector

The gradient of $\beta(\rho, \theta, \phi_\lambda)$ furnishes $\mathbf{w}_{lon}^{(1)ad}(\mathbf{q}_\lambda)$, and Eq. (4.29) then gives $\mathbf{w}_{tra}^{(1)ad}(\mathbf{q}_\lambda)$. We have calculated in Chapter 3 the components of $\mathbf{w}^{(1)ad}(\mathbf{q}_\lambda)$ in the directions of the unit vectors associated with ρ, θ, and ϕ_λ. We can now calculate the corresponding hyperspherical components of $\mathbf{w}_{lon}^{(1)ad}$ and $\mathbf{w}_{tra}^{(1)ad}$. The corresponding $\mathcal{Q}$ space cartesian components of $\mathbf{w}_{lon}^{(1)ad}$ are given by

$$\begin{pmatrix} \mathrm{w}_{lon,x}^{(1)ad} \\ \mathrm{w}_{lon,y}^{(1)ad} \\ \mathrm{w}_{lon,z}^{(1)ad} \end{pmatrix} = \begin{pmatrix} \sin\theta\cos\phi_\lambda & \cos\theta\cos\phi_\lambda & -\sin\phi_\lambda \\ \sin\theta\sin\phi_\lambda & \cos\theta\sin\phi_\lambda & \cos\phi_\lambda \\ \cos\theta & -\sin\theta & 0 \end{pmatrix} \begin{pmatrix} \mathrm{w}_{lon,\rho}^{(1)ad} \\ \mathrm{w}_{lon,\theta}^{(1)ad} \\ \mathrm{w}_{lon,\phi_\lambda}^{(1)ad} \end{pmatrix} \tag{4.58}$$

and those of $\mathbf{w}_{tra}^{(1)ad}$ by an analogous expression.

In Fig. 4.9, we present perspective plots of the longitudinal part of first-derivative coupling vector ($\mathbf{w}_{lon}^{(1)ad}$) as a function of the hyperangle ϕ_λ, at a fixed hyperradius ρ (4 bohr, 6 bohr and 8 bohr) and a fixed hyperangle θ. In cartesian language, this is equivalent to varying x and y on a circle and keeping z fixed. The corresponding adiabatic ground state and first-excited state electronic energies are displayed in Figs. 3.5 through 3.7 of Chapter 3. Fig. 4.10 presents the corresponding perspective plots of the transverse part ($\mathbf{w}_{tra}^{(1)ad}$) of the first-derivative coupling vector. In both Figs. 4.9 and 4.10, the panel (a) corresponds to $\theta = 1^\circ$ (a value very close to the conical intersection geometries of $\theta = 0^\circ$), panel (b) to $\theta = 30^\circ$, panel (c) to $\theta = 60^\circ$, and the panel (d) to $\theta = 90^\circ$ (collinear geometries). The origin of the coupling vectors lies on a circle that corresponds to a fixed θ on the hyperspherical coordinate hemisphere for the indicated value of ρ. This circle maps the full ϕ_λ range of 0° to 360°. The coupling vectors shown in these two figures correspond to the hyperspherical space being mapped by this circle. Above each of the panels two scales are given. The one in units of bohr corresponds to the internal nuclear configuration space corresponding

to the full 0° to 360° ϕ_λ range spanned on the xy plane. The second one, in units of bohr^{-1}, corresponds to the three-dimensional space sampled by the x, y, and z components of the coupling vector. The two spaces co-exist on the xy plane.

The $\mathbf{w}_{lon}^{(1)ad}$ and $\mathbf{w}_{tra}^{(1)ad}$ plots at $\theta = 1°$ (panel (a) in Figs. 4.9 and 4.10) have been included to show their behavior near the conical intersection. The $\theta = 90°$ case (panel (d) in these two figures), corresponds to collinear geometries for the triatomic system. This case is important for lower energies due to the collinear dominance of the H + H_2 reaction at those energies, as will be discussed in Sec. 4.3.4. The $\theta = 30°$ and $\theta = 60°$ cases (panels (b) and (c), respectively) have been included to gauge the importance of the coupling vector away from the conical intersection as well as from the collinear geometries. Fig. 4.11 displays the corresponding perpective plots of the $\mathbf{w}_{tra,6D}^{(1)ad}$ vector, obtained in the $\mathbf{b}_2$ calculation described in Sec. 4.2.4 using 6 Dirichlet boundary conditions, at $\rho = 4$ bohr, 6 bohr and 8 bohr. It has been provided to permit a comparison of the magnitude of this vector with that obtained from the optimal calculation (shown in Fig. 4.10).

We can now check whether the $\mathbf{w}_{lon}^{(1)ad}$ and $\mathbf{w}_{tra}^{(1)ad}$ described above satisfy Eq. (4.26) and Eq. (4.27), which are consequences of the geometric phase theorem. This is a numerical self-consistency check. Writing Eq. (4.26) explicitly in terms of $\mathbf{w}_{lon}^{(1)ad}$ and the symmetrized hyperspherical coordinates, and taking for path $\mathcal{L}$ a closed loop around the conical intersection between the 1 $^2A'$ and 2 $^2A'$ states of H_3, we get for the longitudinal topological phases [Eq. (4.25)] the expression

$$\Phi_{\mathsf{T},lon}(\rho,\theta) = \oint \mathrm{w}_{lon,\phi_\lambda}^{(1)ad}(\rho,\theta,\phi'_\lambda)\ \rho\sin\theta\ d\phi'_\lambda \tag{4.59}$$

where $\mathrm{w}_{lon,\phi_\lambda}^{(1)ad}$ is the ϕ_λ-component of $\mathbf{w}_{lon}^{(1)ad}$ vector. Similarly, the transverse topological phase [Eq. (4.25)], can be written in terms of $\mathbf{w}_{tra}^{(1)ad}$ as

$$\Phi_{\mathsf{T},tra}(\rho,\theta) = \oint \mathrm{w}_{tra,\phi_\lambda}^{(1)ad}(\rho,\theta,\phi'_\lambda)\ \rho\sin\theta\ d\phi'_\lambda \tag{4.60}$$

where $\mathrm{w}_{tra,\phi_\lambda}^{(1)ad}$ is the ϕ_λ-component of $\mathbf{w}_{tra}^{(1)ad}$ vector. The corresponding longitudinal

and transverse open-path phases associated with Eq. (4.22) can be expressed in the symmetrized hyperspherical coordinates as

$$\Phi_{lon}(\phi_\lambda;\rho,\theta) = \int_0^{\phi_\lambda} \mathrm{w}^{(1)ad}_{lon,\phi_\lambda}(\rho,\theta,\phi'_\lambda)\ \rho\sin\theta\ d\phi'_\lambda \tag{4.61}$$

and

$$\begin{aligned}\Phi_{tra}(\phi_\lambda;\rho,\theta) &= \int_0^{\phi_\lambda} \mathrm{w}^{(1)ad}_{tra,\phi_\lambda}(\rho,\theta,\phi'_\lambda)\ \rho\sin\theta\ d\phi'_\lambda \\ &= \int_0^{\phi_\lambda} \mathrm{w}^{(1)ad}_{\phi_\lambda}(\rho,\theta,\phi'_\lambda)\ \rho\sin\theta\ d\phi'_\lambda\ -\ \pi \end{aligned} \tag{4.62}$$

where $p = 1$ is used along with Eq. (4.27), since $\mathcal{L}$ encircles the one conical intersection mentioned above. The relation between these open-path phases and the corresponding topological phases is obviously

$$\Phi_{\mathsf{T},lon}(\rho,\theta) = \Phi_{lon}(2\pi;\rho,\theta) \tag{4.63}$$

$$\Phi_{\mathsf{T},tra}(\rho,\theta) = \Phi_{tra}(2\pi;\rho,\theta) \tag{4.64}$$

In Fig. 4.12 (panels (a) through (d)), we display $\Phi_{lon}(\phi_\lambda;\rho,\theta)$ as a function of ϕ_λ evaluated using Eq. (4.61) for four values of ρ (2 bohr through 8 bohr every 2 bohr, respectively) and four values of θ (1°, 30°, 60°, and 90°). In Fig. 4.12 (panels (e) through (h)) we depict $\Phi_{tra}(\phi_\lambda;\rho,\theta)$ as a function of ϕ_λ evaluated using Eq. (4.62) at the same values of ρ and θ. The values of the corresponding topological phases $\Phi_{\mathsf{T},lon}(\rho,\theta)$ and $\Phi_{\mathsf{T},tra}(\rho,\theta)$ can be read off these panels by taking the open-path phases at $\phi_\lambda = 2\pi$ (or 360°). The results shown in Figs. 4.9 through 4.12 are analyzed in Sec. 4.3.4.

4.3.3 Diabatic potential energy surfaces

Once the diabatization angle $\beta(\mathbf{q}_\lambda)$ is known from the solution of Poisson equation, the diabatic energy matrix $\boldsymbol{\varepsilon}^d(\mathbf{q}_\lambda)$ can be evaluated using Eq. (4.21) which in extended

form is:

$$\boldsymbol{\varepsilon}^d(\mathbf{q}_\lambda) = \begin{pmatrix} \varepsilon^d_{11}(\mathbf{q}_\lambda) & \varepsilon^d_{12}(\mathbf{q}_\lambda) \\ \\ \varepsilon^d_{21}(\mathbf{q}_\lambda) & \varepsilon^d_{22}(\mathbf{q}_\lambda) \end{pmatrix} = \widetilde{\mathbf{U}}[\beta(\mathbf{q}_\lambda)] \begin{pmatrix} \varepsilon^{ad}_1(\mathbf{q}_\lambda) & 0 \\ \\ 0 & \varepsilon^{ad}_2(\mathbf{q}_\lambda) \end{pmatrix} \mathbf{U}[\beta(\mathbf{q}_\lambda)] \quad (4.65)$$

where $\mathbf{U}[\beta(\mathbf{q}_\lambda)]$ is given by Eq. (4.16). $\varepsilon^{ad}_1(\mathbf{q}_\lambda)$ and $\varepsilon^{ad}_2(\mathbf{q}_\lambda)$ are respectively the adiabatic ground and first-excited PESs which have been fitted earlier to the *ab intio* energies using the DMBE-Single-Polynomial (DSP) method [18]. From this expression we get

$$\begin{aligned} \varepsilon^d_{11}(\mathbf{q}_\lambda) &= \cos^2\beta(\mathbf{q}_\lambda)\ \varepsilon^{ad}_1(\mathbf{q}_\lambda) + \sin^2\beta(\mathbf{q}_\lambda)\ \varepsilon^{ad}_2(\mathbf{q}_\lambda) \\ \varepsilon^d_{22}(\mathbf{q}_\lambda) &= \sin^2\beta(\mathbf{q}_\lambda)\ \varepsilon^{ad}_1(\mathbf{q}_\lambda) + \cos^2\beta(\mathbf{q}_\lambda)\ \varepsilon^{ad}_2(\mathbf{q}_\lambda) \\ \varepsilon^d_{12}(\mathbf{q}_\lambda) &= \varepsilon^d_{21}(\mathbf{q}_\lambda) = \cos\beta(\mathbf{q}_\lambda)\ sin\beta(\mathbf{q}_\lambda)\ \left[\varepsilon^{ad}_2(\mathbf{q}_\lambda) - \varepsilon^{ad}_1(\mathbf{q}_\lambda)\right] \end{aligned} \quad (4.66)$$

Fig. 4.15 and panels (a) and (b) of Figs. 4.13 and 4.14 show the adiabatic and diabatic PES contours in the $X_\lambda Z_\lambda$ plane of Fig. 4.1, which corresponds to the $\gamma_\lambda = 0°$ and 180° cuts. Panels (c) and (d) in Figs. 4.13 and 4.14 show these contours in the YZ_λ plane of Fig. 4.1 corresponding to the $\gamma_\lambda = 90°$ cut. Fig. 4.16 depicts the conical intersection energies, corresponding to equilateral triangle configurations, as a function of ρ for four sets of electronically adiabatic *ab initio* PES calculations: DSP [18], LSTH [62–64], DMBE [47] and EQMC [66]. The DSP curve corresponds to the $Z_\lambda = 0$ energies in panels (c) and (d) of Fig. 4.13. Figs. 4.17 through 4.19 show equatorial views (described in the first paragraph of Sec. 4.3.1) of the PES contours through their mapping onto the $\bar{x}_\lambda \bar{y}_\lambda$ tangent plane of Fig. 4.1. In the next section we will discuss the features of the adiabatic and diabatic PESs through their contours displayed in Figs. 4.13 through 4.15 and 4.17 through 4.19.

4.3.4 Discussion

Fig. 4.4 (panels (a) through (d)) displays the diabatization angle $\beta(\rho, \theta, \phi_\lambda)$ for four fixed values of the hyperradius ρ. In all these panels, the dominance of the $\phi_\lambda/2$ part of β is clearly visible: as ϕ_λ increases from 0 to 2π, β varies from a value close to 0 to a value close to π. Besides this behavior, some small variations are visible in the ϕ_λ-dependence of β. Due to the dominance of the $\phi_\lambda/2$ term, it is hard to distinguish the β at $\rho = 2$ bohr (corresponding to a compact set of geometries) from that at $\rho = 8$ bohr (corresponding to a near-asymptotic set of geometries), except for the small variations mentioned above which become slightly more prominent as ρ increases from 2 bohr to 8 bohr.

Panels (e) through (h) of Fig. 4.4 depict the equatorial view of the contours corresponding to the β panels (a) through (d). In these equatorial views, the three atom-diatom arrangement channels lie along the $\phi_\lambda = 0°$, 120° and 240° lines. These panels show that their contour lines are mainly radial, independently of the value of ρ. This is a consequence of having set $\gamma = 0°$ at $\phi_\lambda = 0°$ and 60° (the S_1 and S_2 boundary surfaces), for the reasons given in Sec. 4.2.4. They also show clearly the $\phi_\lambda/2$ dependence of β with the contour values increasing with an increase in ϕ_λ. Hence, although in this view the β contours seem to have P_3 symmetry they actually don't, due to this $\phi_\lambda/2$ dependence. The feature that is clear in these contours of β that was not very obvious in panels (a) through (d) of Fig. 4.4 is that β increases sharply with an increase in ϕ_λ around the $\phi_\lambda = 60°$, 180° and 300° lines and increases slowly in other regions. This sharp increase becomes sharper with an increase in ρ as we go from panel (e) ($\rho = 2$ bohr) to panel (h) ($\rho = 8$ bohr). In each panel, the line corresponding to $\phi_\lambda = 0°$ and 180° is interesting because on the $\phi_\lambda = 0°$ line β is zero and on the 180° line it is 90°. This has the following effect on the behavior of diabatic surfaces ε^d_{11}, ε^d_{22} and ε^d_{12} (using Eqs. (4.66) discussed in Sec. 4.3.3) and on the diabatic nuclear wavefunctions χ^d_1 and χ^d_2 (using Eqs. (4.18) and (4.16) discussed in the introduction section): (a) the coupling PES ε^d_{12} is zero on both these ϕ_λ lines; (b) on the $\phi_\lambda = 0°$ line, $\varepsilon^d_{11} = \varepsilon^{ad}_1$ and $\varepsilon^d_{22} = \varepsilon^{ad}_2$ which means that the adiabatic and

diabatic nuclear wavefunctions coincide on this line; and (c) on the $\phi_\lambda = 180°$ line, $\varepsilon^d_{11} = \varepsilon^{ad}_2$ and $\varepsilon^d_{22} = \varepsilon^{ad}_1$ which means that the adiabatic nuclear wavefunctions are switched in the diabatic representation on this line with one of them switching the sign also, i.e., $\chi^d_1 = \chi^{ad}_2$ and $\chi^d_2 = -\chi^{ad}_1$. This provides good physical insight into the behavior of the diabatic PESs and diabatic nuclear wavefunctions in terms of their adiabatic counterparts on the ϕ_λ = constant half-planes in configuration space just considered. Other interesting ϕ_λ half-planes are those corresponding to 45° and 135° because along them ε^d_{11} and ε^d_{22} coincide.

It is hard to see any quantitative variation in β as a function of the hyperangle θ. To make this and previously mentioned distinctions clear, panels (a) through (d) of Fig. 4.5 display the $\gamma(\rho, \theta, 3\phi_\lambda)$ part of the diabatization angle, which doesn't contain the dominant $\phi_\lambda/2$ term. In all these panels, the P_3 symmetry is visible, as γ repeats itself every $2\pi/3$ radians. For $\rho = 2$ bohr, γ fluctuates as a function of ϕ_λ between -5° and +5°. As a function of θ (looking from the center of the bottom circle to its edge), it starts from 0° at $\theta = 0°$ and increases (or decreases) to its maximum (or minimum) value at $\theta = 90°$. For $\rho = 4$ bohr (which is dynamically an important region), the oscillations of γ with ϕ_λ are sharper (as compared to the $\rho = 2$ bohr case), and have a larger amplitude staying between -16° and +16°. As θ is varied, γ has the same behavior as that for the $\rho = 2$ bohr case. For $\rho = 6$ bohr and 8 bohr γ displays sharper oscillations and amplitudes that stay between -20° and +20°. This indicates that it is approaching the asymptotic limit as ρ increases. Their θ-dependence of γ is similar to that for the $\rho = 2$ bohr and 4 bohr cases. Since the diabatization matrix $\mathbf{U}[\beta(\mathbf{q}_\lambda)]$ elements are sines and cosines of β (see Eq. (4.16)), the dominance of the $\phi_\lambda/2$ term manifests itself as a change in the sign of the electronic and the nuclear adiabatic wave functions and forces the diabatic wave functions to be single-valued, as discussed previously after Eq. (4.36). The γ term in that equation will be important in determining the characteristics of the diabatic PESs that appear in Eq. (4.19).

Panels (e) through (h) of Fig. 4.5 depict equatorial views of γ contours corresponding to panels (a) through (d), respectively. These panels show the expected P_3

symmetry. Again, the contour lines have a strong radial behavior for all values of ρ due to the choice of boundary conditions on S_1 and S_2 just mentioned. In addition, the sharp rise observed in the β panels discussed earlier around $\phi_\lambda = 60°$, 180° and 300° lines is manifested in these γ contours with the sharpness rising with an increase with ρ as we go from panel (e) ($\rho = 2$ bohr) to panel (h) ($\rho = 8$ bohr). Across these ϕ_λ lines γ goes from a large positive value to a large negative value, the absolute value of which also increases with ρ.

Three constant-θ cuts of γ plots in Fig. 4.5, which provide additional insight into the features of γ, are shown in Fig. 4.6 (panels (a) through (d)). In each of these panels, the $\theta = 5°$ cut (shown as a solid line) depicts the behavior of γ in the vicinity of equilateral triangle geometries. $\theta = 90°$ cut (dotted line) shows it for collinear geometries and 45° cut (dash-dotted line) shows it for a set of intermediate geometries. For all three cuts the amplitude of the oscillations in γ is smallest for $\rho =$ 2 bohr and increases as ρ increases to 8 bohr. The increase in this amplitude is largest in going from $\rho = 2$ bohr to 4 bohr and tapers off by 8 bohr. Another interesting feature not very clear in the γ plots of Fig. 4.5 is that γ, which repeats itself every $2\pi/3$ radians with a maximum in the first half and a minimum in the second half of any $2\pi/3$ radians period in ϕ_λ, doesn't display that maximum (or minimum) at the exact middle of those halves but is skewed towards the middle of those full $2\pi/3$ radians periods. The corresponding cuts for γ^{DMBE} are shown in Fig. 4.6 (panels (e) through (h)) for comparison. For $\rho = 2$ bohr, γ^{DMBE} shows a maximum, where γ shows a minimum and vice versa. For all other ρ, it shows the qualitatively correct behavior but with the absolute value of its maximum (or minimum) always smaller than that of γ. Also, for all ρ, the agreement between γ^{DMBE} and γ gets worse as θ is increased. To make this comparison more quantitative, we show in Fig. 4.7 the quantity $\Delta_\gamma(\rho, \theta)$ defined by Eq. (4.57) as a function of θ for fixed values of ρ. As expected, γ^{DMBE} agrees in general with the present optimal γ only close to the conical intersection ($\theta = 0°$). In the vicinity of $\rho = 4$ bohr, this agreement is very good up to about $\theta = 30°$. This analysis shows that even if the transverse part of the *ab initio* first-derivative

coupling is ignored, as was done in the DMBE treatment [47], γ^{DMBE} and hence β^{DMBE} agrees with the current γ only in the vicinity of the conical intersection, as expected, and should not be used to construct diabatic states and nuclear wavefunctions for accurate two-electronic-state scattering calculations.

Fig. 4.8 displays γ_{6D} obtained from the Poisson equation solution using only Dirichlet boundary conditions. Comparison of panels (a) through (d) of this figure with panels (a) through (d) of Fig. 4.5 shows that the maximum magnitude of γ_{6D} is on average half that of the optimal γ. This can be qualitatively explained by the fact that γ_{6D} is made to be zero at all six boundaries and hence it doesn't increase enough in magnitude inside the enclosed region to become smaller than the corresponding optimal γ. In addition, the maxima and minima in γ_{6D} occur in the same ϕ_λ regions as those of the corresponding optimal γ. Comparing the contours of γ_{6D} (Fig. 4.8 panels (e) through (h)) with those of the optimal γ (Fig. 4.5 panels (e) through (h)) highlights the qualitative similarity in the sharp rises around $\phi_\lambda = 60°$, 180° and 300°.

As mentioned in Sec. 4.3.2, Fig. 4.9 displays the longitudinal part ($\mathbf{w}_{lon}^{(1)ad}$) of the first-derivative coupling vector for $\rho = 4$ bohr, 6 bohr and 8 bohr. It has four sets of panels: (a) $\theta = 1°$ (triatomic geometries near the conical intersection), (b) $\theta = 30°$, (c) $\theta = 60°$, and (d) $\theta = 90°$ (collinear triatomic geometries). Fig. 4.10 displays the corresponding plots for the transverse part ($\mathbf{w}_{tra}^{(1)ad}$) of that coupling vector.

The panels in the leftmost column of Fig. 4.9 present the $\mathbf{w}_{lon}^{(1)ad}$ vector for $\rho =$ 4 bohr, which is expected to be of high dynamical importance for the H + H_2 reaction. For the $\theta = 1°$ case (Fig. 4.9 (a), $\rho = 4$ bohr), the longitudinal vector has a magnitude of about 5 bohr^{-1} and a negligible z-component, translating into a strong dominance of its ϕ_λ-component near the conical intersection. The adiabatic energies (E_1 and E_2, see Fig. 3.5 in Chapter 3) are comparable and stay around 3.6 eV in this region. At $\theta = 30°$ (Fig. 4.9 (b), $\rho = 4$ bohr), values of E_1 as low as 1.5 eV occur, E_2 is 5 eV or larger and $\mathbf{w}_{lon}^{(1)ad}$ has a smaller magnitude as compared to the $\theta = 1°$ case (Fig. 4.9 (a), $\rho = 4$ bohr). At $\theta = 60°$ (Fig. 4.9 (c), $\rho = 4$ bohr), values of E_1 as low as 0.25 eV

occur, E_2 is 6 eV or larger, and $\mathbf{w}_{lon}^{(1)ad}$ shows a sharper variation with ϕ_λ than before (Fig. 4.9 (b), $\rho = 4$ bohr) around $\phi_\lambda = 60°$, 180°, and 300°. At $\theta = 90°$ (Fig. 4.9 (d), $\rho = 4$ bohr), which corresponds to collinear geometries, E_1 energies as low as 0.2 eV occur and this PES varies more rapidly with ϕ_λ than for the smaller values of θ, and E_2 is again 6 eV or larger. $\mathbf{w}_{lon}^{(1)ad}$ is comparable to the previous $\theta = 60°$ case. For the $\rho = 6$ bohr (panels in the central column of Fig. 4.9) and 8 bohr (panels in the rightmost column of Fig. 4.9) cases, which correspond to triatomic large sized geometries, the electronic energies as well as the longitudinal vectors have general characteristics that are analogous to the $\rho = 4$ bohr case. In both these cases, E_1 energies as low as 0.2 eV occur and $\mathbf{w}_{lon}^{(1)ad}$ has comparable or larger magnitudes with maxima around $\phi_\lambda = 60°$, 180°, and 300°.

The panels in the leftmost column of Fig. 4.10 display $\mathbf{w}_{tra}^{(1)ad}$, the transverse part of the coupling vector for $\rho = 4$ bohr, where we observe very small absolute magnitudes near the conical intersection ($\theta = 1°$, Fig. 4.10 (a)). For this value of ρ, as we move away from the conical intersection, the magnitude of $\mathbf{w}_{tra}^{(1)ad}$ increases to between 0.05 bohr^{-1} and 0.1 bohr^{-1}. There is also an initial increase (up to around $\theta = 60°$, Fig. 4.10 (c)) and a final decrease in the relative magnitude of its z-component. The θ-component ($w_{tra,\theta}^{(1)ad}$) of the transverse coupling vector at $\theta = 90°$ should be zero (due to the Neumann condition imposed at this boundary by Eq. (4.48)). This should manifest itself in the z-component of the transverse vector being zero (due to Eq. (4.58)). Fig. 4.10 panel (d) (for $\rho = 4$ bohr) shows that it is close to zero (less than 0.001 bohr^{-1}) everywhere except at $\phi_\lambda = 0°$, 120° and 240°, where it is of the order of 0.030 bohr^{-1}. This is due to the Dirichlet boundary condition imposed on γ at $\phi_\lambda = 0°$ (due to Eq. 4.43)) and by symmetry at 120° and 240°. A look at the adiabatic energies in these regions (see Fig. 3.5 in Chapter 3) indicates that these energies remain higher than 10 eV in these regions, so these regions will not be accessible for scattering at or below 5 eV. For $\rho = 6$ bohr (central column of Fig. 4.10) and $\rho = 8$ bohr (rightmost column of Fig. 4.10), nothing unusual happens except for the fact that away from the conical intersection the magnitudes of $\mathbf{w}_{tra}^{(1)ad}$ increase to

the 0.01 bohr^{-1} to 0.02 bohr^{-1} range.

A comparison of the transverse coupling vectors (Fig. 4.10) with their longitudinal counterparts (Fig. 4.9) leads to the following conclusions. For all hyperradii shown, the transverse vectors have similar magnitude x, y, and z components, where the x and y components are smaller in general than their longitudinal counterparts. Comparing Figs. 4.9 (a) and 4.10 (a) for $\rho = 4$ bohr, both of which correspond to $\theta = 1^\circ$ (near-conical intersection geometries), the transverse (or *nonremovable*) vector is three orders of magnitude smaller than its longitudinal counterpart, a typical situation near the conical intersection. Analogously, comparing Figs. 4.9 (d) and 4.10 (d) for this hyperradius, both of which correspond to $\theta = 90^\circ$ (collinear geometries), the magnitudes of the transverse and longitudinal vectors are similar to each other but at least an order of magnitude smaller than the magnitude of the longitudinal vector near the conical intersection. These conclusions are valuable due to the dynamical importance of $\rho = 4$ bohr. Near the conical intersection ($\theta = 1^\circ$), ground (E_1) and first-excited (E_2) adiabatic PESs are very close to each other (see Fig. 3.5 in Chapter 3), so one expects that there will be maximum hopping of the nuclei between these PESs. In this region, the transverse (*nonremovable*) part is quite small (around 0.005 bohr^{-1} or less) and so this part is expected to have only a small effect on the reactive scattering. Near the collinear geometry regions, $\theta = 90^\circ$, the E_1 and E_2 adiabatic PESs are separated by around 5 eV, so although the transverse vector is not that much smaller than the longitudinal vector, the separation between the surfaces is big enough that it should prevent any noticable hopping of nuclei from one surface to the other. The same analysis for $\rho = 6$ bohr and 8 bohr leads to similar conclusions. The main points of difference are as follows. As we go from the conical intersection region, $\theta = 1^\circ$, to the collinear region, $\theta = 90^\circ$, the transverse vector remains at least an order of magnitude smaller than the longitudinal vector, whenever the two surfaces are closer than 5 eV. The transverse part becomes comparable to the longitudinal part only in regions where the two surfaces are separated by 5 eV or more.

Fig. 4.11 depicts the transverse vector $\mathbf{w}_{tra,6D}^{(1)ad}$ obtained by the all-Dirichlet Poisson equation calculation $\mathbf{b}_2$ described in Sec. 4.2.4. Its leftmost column ($\rho = 4$ bohr) compared with the optimal $\mathbf{w}_{tra}^{(1)ad}$ (leftmost column of Fig. 4.10) shows that the magnitudes of the former are 2 to 4 times those of the latter. The middle column of Fig. 4.11 ($\rho = 6$ bohr), compared with the corresponding column of Fig. 4.10, shows that $\mathbf{w}_{tra,6D}^{(1)ad}$ is 5 to 10 times larger in magnitude than $\mathbf{w}_{tra}^{(1)ad}$. A similar comparison of the rightmost column ($\rho = 8$ bohr) shows its magnitude to be 10 to 50 times larger than that of the optimal $\mathbf{w}_{tra}^{(1)ad}$ vector. To make this comparison quantitative over the full domain U we evaluated, using Eq. (4.55), the average magnitude of both transverse parts and found them to be 0.0208 bohr^{-1} for the optimal transverse vector and 0.0981 bohr^{-1} for the full-Dirichlet $\mathbf{w}_{tra,6D}^{(1)ad}$ transverse vector, resulting in a value of the ratio defined by Eq. (4.56) of $\xi_2 = 4.7$, i.e., the $\mathbf{w}_{tra,6D}^{(1)ad}$ vector is in average nearly five times larger than the optimal one. This shows that the minimization provided by the three-Neumann boundary conditions of the optimal calculation $\mathbf{b}_0$ is very significant. Since it is the transverse part that is retained in the diabatic equations describing the nuclear motion, and has been minimized over the entire important domain U of nuclear configuration space, it will be interesting to determine by a perturbative treatment how and in what regions of that space it will affect the scattering dynamics for the H_3 system at energies of the order of 5 eV and below.

The values of the $\langle \mathrm{w}_{tra}^{(1)ad} \rangle_i$ for the calculations $\mathbf{b}_3$ through $\mathbf{b}_8$ were 0.0856 bohr^{-1}, 0.0236 bohr^{-1}, 0.0683 bohr^{-1}, 0.0863 bohr^{-1}, 0.0978 bohr^{-1} and 0.0687 bohr^{-1}, respectively, resulting in corresponding values of ξ_i of 4.1, 1.1, 3.3, 4.1, 4.7 and 3.3. Two important conclusions are as follows:

a) The $\mathbf{b}_4$ calculation (Neumann conditions on S_4 and S_6 and Dirichlet conditions $\gamma = 0$ at other S_i) is almost as good as the optimal $\mathbf{b}_0$ calculation.

b) The order of importance of using Neumann boundary conditions to minimize $\langle \mathrm{w}_{tra}^{(1)ad} \rangle$ is S_6 first, followed by S_4 and S_5.

Fig. 4.12 shows the longitudinal $\Phi_{lon}(\phi_\lambda; \rho, \theta)$ and transverse $\Phi_{tra}(\phi_\lambda; \rho, \theta)$ open-

path phases as a function of ϕ_λ for four values of θ and four values of ρ evaluated using Eqs. (4.61) and (4.62). For the $\theta = 1^\circ$ case, to a very good approximation (0.2 % or smaller difference) Φ_{lon} is equal to $\phi_\lambda/2$ for all the values of ρ considered. This is clearly expected because this value of θ corresponds to a region of configuration space very close to the conical intersection and $\phi_\lambda/2$ is a leading term of the diabatization angle β, γ being very small in that region. For other values of θ, Φ_{lon} fluctuates around this $\phi_\lambda/2$ value and returns to it at regular intervals of 60° in ϕ_λ. As a result, we can approximate Φ_{lon} by a sum of two terms, the first one being $\phi_\lambda/2$ and the second more complicated one possessing the P_3 symmetry (of H_3) via a $\sin 3\phi_\lambda$ dependence. This second term is the γ term of the diabatization angle β given by Eq. (4.36), since from Eqs. (4.13) and (4.61) we have $\Phi_{lon} \equiv \beta$. The fluctuations in Φ_{lon} about $\phi_\lambda/2$ are due to this second term and have an amplitude which increases monotonically with ρ between $\rho = 2$ bohr and $\rho = 8$ bohr. This seems to stem from the fact that for a large value of ρ, the length of the circular loop around the conical intersection is large, which leads to a large phase accumulation in these fluctuations. As mentioned in Sec. 4.3.2, the corresponding topological phases (closed-loop line integrals, $\Phi_{\mathsf{T},lon}$) can be read off these panels by looking at the value of Φ_{lon} at $\phi_\lambda = 2\pi$. It can be seen that for all values of ρ and θ considered in Fig. 4.12 (panels (a) through (d)), $\Phi_{\mathsf{T},lon} = \pi$, satisfying the condition given by Eq. (4.26) for $p = 1$ since we are encircling only one conical intersection, the one between the $1\ ^2A'$ and $2\ ^2A'$ states of H_3.

The transverse open-path phase $\Phi_{tra}(\phi_\lambda; \rho, \theta)$ was evaluated as a function of ϕ_λ by using both the middle part and the right-hand side of Eq. (4.62) for the same four values each of ρ and θ, used for Φ_{lon}. Both evaluations give identical result, which is shown in panels (e) through (h) of Fig. 4.12. This again is consistent with the fact that we are encircling one conical intersection. For the $\theta = 1^\circ$ case, Φ_{tra} is nearly zero, which, is expected due to the dominance of $\mathbf{w}_{lon}^{(1)ad}$ over $\mathbf{w}_{tra}^{(1)ad}$ in this region close to the conical intersection. In general, for each θ, Φ_{tra} is the sum of a linear term in ϕ_λ, whose slope can be positive, negative or zero, plus an oscillatory term of period $2\pi/3$.

Also, the corresponding topological phases $\Phi_{\mathsf{T},tra}$ (Φ_{tra} at $\phi_\lambda = 2\pi$) show a value close to zero not only for $\theta = 1^\circ$ and all four values of ρ, but also for $\theta = 90^\circ$ (i.e., collinear geometries) at $\rho = 4$ bohr. Examination of the $\mathbf{w}_{tra}^{(1)ad}$ vector (Fig. 4.10) at these geometries shows that its magnitude is comparable to its value at other geometries where $\Phi_{\mathsf{T},tra}$ is significantly different from zero. We conclude that the vanishing of $\Phi_{\mathsf{T},tra}$ is a necessary but insufficient condition for the the first-derivative coupling vector to be purely longitudinal.

Using the diabatization angle β obtained as described in Sec. 4.3.1 and discussed in the first two paragraphs of the present section, and the adiabatic ground and first-excited DSP PESs obtained previously [18], we have calculated, using Eq. (4.65), the diagonal and off-diagonal elements of the diabatic energy matrix $\boldsymbol{\varepsilon}^d$. Fig. 4.13 shows the cuts of the adiabatic ground (ε_1^{ad}) and first-excited (ε_2^{ad}) PESs with the $X_\lambda Z_\lambda$ and $Y Z_\lambda$ planes as explained in Sec. 4.3.3. Panels (a) and (b) correspond to collinear configurations and show the three atom-diatom channels. For such configurations, the lowest value of ε_1^{ad} is 0.013 eV (close to the H + H_2 limit) and that of ε_2^{ad} is 4.62 eV (close to the H + H + H limit). In addition, since the intersection between these two PESs occurs for equilateral triangle ($\theta = 0^\circ$) geometries, the collinear ($\theta = 90^\circ$) cuts of these panels do not intersect. Panels (c) and (d) correspond to perpendicular configurations, which for $Z_\lambda = 0$ are equilateral triangles and hence conical intersection configurations. Therefore, the dashed horizontal lines in these panels (at $Z_\lambda = 0$) correspond to the conical intersection lines for which $\varepsilon_1^{ad} = \varepsilon_2^{ad}$. The minimum value of this conical intersection energy for the DSP PESs [18] also used in the present calculation is 2.85 eV and occurs for $\rho = Y$ =2.6 bohr. The corresponding point is located in panel (d) inside the 3 eV contour. The hyperspherical coordinates don't span negative values of Y, but these are nevertheless included for convenience. The highest energy contour for ε_1^{ad} depicted in panel (c) is for 2.4 eV and the lowest energy contour for ε_2^{ad} depicted in panel (d) is for 3.0 eV. The conical intersection energies (corresponding to $Z_\lambda = 0$ in panels (c) and (d)) are displayed in Fig. 4.16 as a function of ρ for the DSP, DMBE, LSTH, and EQMC PESs. The minima of

the latter three are 2.75 eV, 2.76 eV and 2.73 eV, respectively. The minimum DSP conical intersection energy of 2.85 eV mentioned above is slightly higher than that for the latter three PESs. This is due to the fact that *ab initio* electronic energies used for fitting the DSP PESs were gotten from calculations performed to obtain good representative ground and first-excited state energies. This leads to a slightly higher DSP energy than it would be, if the basis set used was chosen to optimize the ground state energies only [18].

Fig. 4.14 depicts the diagonal elements (ε^d_{11} and ε^d_{22}) of the diabatic energy matrix on the same cuts as Fig. 4.13. For the collinear configurations (panels (a) and (b)), lowest ε^d_{11} and ε^d_{22} contours occur for 0.5 eV but in different regions of the internal configuration space. The ε^d_{11} minimum occurs in the positive Z_λ region for some values of X_λ at which ε^{ad}_1 contours also show a minimum. The ε^d_{22} minimum however occurs in the negative Z_λ region for some values of X_λ at which ε^{ad}_1 contours also show a minimum. Interestingly, the saddle point at $X_\lambda = 0$ in ε^{ad}_1 (Fig. 4.13(a)) transforms to a well roughly 2.0 eV deep for ε^d_{22}. The behavior of ε^d_{11} in this region is very similar to that of ε^{ad}_2 (Fig. 4.13(b)). The ε^d_{11} and ε^d_{22} PESs display an intersection at collinear geometries at about 4.5 eV. No intersection is present for such geometries between the ε^{ad}_1 and ε^{ad}_2 PESs. For the perpendicular configurations (panels (c) and (d)), the relation of ε^d_{11} and ε^d_{22} with ε^{ad}_1 and ε^{ad}_2 is similar to that for the collinear case. Also for these configurations, the ε^d_{11} and ε^d_{22} PESs display an intersection at around 2.85 eV, similar to the one between the adiabatic PESs. Fig. 4.15 shows the off-diagonal element ε^d_{12} of the diabatic energy matrix for collinear configurations. This element vanishes for perpendicular configurations. From Eqs. (4.66) and (4.36) it can be easily shown that in general ε^d_{12} is antisymmetric with respect to $\phi_\lambda = 0°$ and $\phi_\lambda = 180°$, i.e., the YZ_λ plane, for which $X_\lambda = 0$. Fig. 4.15 corresponds to $Y = 0$. As a result, this antisymmetry manifests itself in that figure with respect to the $X_\lambda = 0$ axis. This translates into ε^d_{12} being attractive for $X_\lambda > 0$ and repulsive for $X_\lambda < 0$. Since ε^d_{12} is of the same order of magnitude as ε^d_{11} and ε^d_{22} and it is the largest term that couples the two nuclear motion scattering equations in the two-electronic-

state diabatic representation of Eq. (4.19), it should be of major importance for the dynamics of the H + H_2 reaction at energies for which the two PESs participate.

Fig. 4.17 displays the adiabatic PESs in equatorial views for four values of the hyperradii ρ (2, 4, 6, and 8 bohr). These PESs have been discussed in the last chapter and are repeated here only for comparison with the corresponding views of the diabatic PESs. Fig. 4.18 depicts the diagonal ε^d_{11} and ε^d_{22} PESs in the equatorial view for the same four values of ρ. The P_3 symmetry of the adiabatic PESs is lost in the diabatic representation due to the $\phi_\lambda/2$ term in β (see Eq. (4.36)) which doesn't have the required $3\phi_\lambda$ dependence. For $\rho = 2$ bohr, the lowest contour displayed for both the ε^d_{11} and ε^d_{22} PESs is the 3.5 eV contour. For $\rho = 4$ bohr, 6 bohr and 8 bohr it is the 0.5 eV contour. A close look at all panels in Fig. 4.18 indicates that the top half circle of ε^d_{11} looks like ε^{ad}_1 and the bottom half looks like ε^{ad}_2. Similarly, the top half of ε^d_{22} looks like ε^{ad}_2 and the bottom half looks like ε^{ad}_1. This is closely related to the discussion involving Fig. 4.4, where for the $\phi_\lambda = 0^\circ$ line (lying in the top half circle) $\beta = 0^\circ$ making $\varepsilon^d_{11} = \varepsilon^{ad}_1$ and $\varepsilon^d_{22} = \varepsilon^{ad}_2$ and for the $\phi_\lambda = 180^\circ$ line (lying in the bottom half circle) $\beta = 90^\circ$ which makes $\varepsilon^d_{11} = \varepsilon^{ad}_2$ and $\varepsilon^d_{22} = \varepsilon^{ad}_1$. Fig. 4.19 shows the off-diagonal ε^d_{12} term of the diabatic energy matrix in an equatorial view for the same four values of ρ. As in Fig. 4.15, the contours are antisymmetric with respect to the $\phi_\lambda = 0^\circ, 180^\circ$ (i.e., the YZ_λ plane), one half of the ε^d_{12} PES being repulsive and the other half attractive. It displays a large flat region of 0 eV around the $\phi_\lambda = 0^\circ, 180^\circ$ lines suggesting negligible coupling in these regions. It will be interesting to see how this antisymmetric property of ε^d_{12} affects the scattering dynamics in the regions for energies of interest (less than 5 eV).

Using the diabatic version of the closure relation [Eq. (3.42)], and Eq. (4.20), the elements of the diabatic second-derivative coupling matrix $\mathsf{W}^{(2)d}(\mathbf{q}_\lambda)$ of Eq. (4.19) can be expressed as

$$\begin{aligned} \mathsf{w}^{(2)d}_{1,1}(\mathbf{q}_\lambda) = \mathsf{w}^{(2)d}_{2,2}(\mathbf{q}_\lambda) &= -\,\mathsf{w}^{(1)ad}_{1,2,tra}(\mathbf{q}_\lambda)\cdot\mathsf{w}^{(1)ad}_{1,2,tra}(\mathbf{q}_\lambda) \\ \mathsf{w}^{(2)d}_{1,2}(\mathbf{q}_\lambda) = \mathsf{w}^{(2)d}_{2,1}(\mathbf{q}_\lambda) &= 0 \end{aligned} \tag{4.67}$$

where both $(-\hbar^2/2\mu)\ \mathsf{w}_{1,1}^{(2)d}(\mathbf{q}_\lambda)$ and $(-\hbar^2/2\mu)\ \mathsf{w}_{2,2}^{(2)d}(\mathbf{q}_\lambda)$ can be labelled as $\varepsilon^{(2)d}(\mathbf{q}_\lambda)$. The values of this (approximate) $\varepsilon^{(2)d}(\mathbf{q}_\lambda)$ calculated from this equation, using the $\mathsf{w}_{1,2,tra}^{(1)ad}(\mathbf{q}_\lambda)$ vector obtained in this chapter, are smaller than 0.08 kcal mol^{-1} over the entire nuclear configuration space involved, and to a very good approximation can be neglected.

We conclude, from the discussion in this section, that neglecting the transverse (*nonremovable*) part of $\mathbf{w}^{(1)ad}$ in the diabatic nuclear Schrödinger equation should be a good approximation in the first step of an accurate two-state scattering calculation. As we have already computed this nonremovable part, we can add it as a perturbation to the scattering results in a second step. Use of the global optimal diabatic basis reported here is underway in the implementation of a two-electronic-state scattering calculation for H_3.

Appendix 4.A - Optimal boundary conditions for the diabatization angle Poisson equation

Consider the Helmholtz decomposition of the first-derivative coupling vector $\mathbf{w}^{(1)ad}(\mathbf{q})$ given by Eq. (4.29) after dropping the subscript λ from $\mathbf{q}_\lambda$, as the following discussion doesn't depend on it:

$$\mathbf{w}^{(1)ad}(\mathbf{q}) = \boldsymbol{\nabla}_{\mathbf{q}}\beta(\mathbf{q}) + \mathbf{w}^{(1)ad}_{tra}(\mathbf{q}) \tag{4.68}$$

where the diabatization angle $\beta(\mathbf{q})$ is the solution of the Poisson equation [Eq. (4.30)]

$$\nabla^2_{\mathbf{q}}\beta(\mathbf{q}) = \sigma(\mathbf{q}) \tag{4.69}$$

the source term $\sigma(\mathbf{q})$ being defined by

$$\sigma(\mathbf{q}) = \nabla_{\mathbf{q}} \cdot \mathbf{w}^{(1)ad}(\mathbf{q}) \tag{4.70}$$

Let $\beta_0(\mathbf{q})$ and $\beta_1(\mathbf{q})$ be solutions of Eq. (4.69) subject to boundary conditions specified by the functions $\mathrm{B}_0(\mathbf{q}_\mathsf{S})$ and $\mathrm{B}_1(\mathbf{q}_\mathsf{S})$, respectively and to be given in greater detail below. $\mathbf{q}_\mathsf{S}$ designates values of $\mathbf{q}$ on the boundary surface S that encloses the domain V in which Eq. (4.69) is to be solved. In the symmetrized hyperspherical coordinates $\mathbf{q}$ $(\rho, \theta, \phi_\lambda)$, that domain is given by $\rho_{min} \leq \rho \leq \rho_{max}$, $\theta_{min} \leq \theta \leq \theta_{max}$ and $\phi_{\lambda min} \leq \phi_\lambda \leq \phi_{\lambda max}$. S is comprised of 6 parts S_i ($i = 1$ through 6) described in Sec. 4.2.4. Dirichlet conditions are used on the S_1, S_2 and S_3 parts of S for the reasons described after Eqs. (4.43), (4.45) and (4.46). As a result of these equations and Eq. (4.36) we have

$$\begin{aligned}
&\beta_0(\mathsf{S}_1) = 0 \qquad && \beta_1(\mathsf{S}_1) = 0 \\
&\beta_0(\mathsf{S}_2) = \pi/6 \qquad && \beta_1(\mathsf{S}_2) = \pi/6 \\
&\beta_0(\mathsf{S}_3) = \phi_\lambda/2 \qquad && \beta_1(\mathsf{S}_3) = \phi_\lambda/2
\end{aligned} \tag{4.71}$$

This leaves the three remaining boundary surfaces S_4 through S_6 on which Neumann, Dirichlet or mixed boundary conditions may be adopted.

Let us define a residue function $E(\beta(\mathbf{q}))$ that measures the square of the average magnitude of $\mathbf{w}_{tra}^{(1)ad}(\mathbf{q})$ over the domain V

$$E(\beta(\mathbf{q})) = \int_{\mathsf{V}} \left[\mathbf{w}^{(1)ad}(\mathbf{q}) - \boldsymbol{\nabla}_{\mathbf{q}}\beta(\mathbf{q})\right]^2 d\mathbf{q} \tag{4.72}$$

In addition, let

$$\Delta\beta(\mathbf{q}) = \beta_1(\mathbf{q}) - \beta_0(\mathbf{q}) \tag{4.73}$$

We now impose the condition that $\beta_0(\mathbf{q})$ be the solution of the Poisson equation that minimizes the average value of $|\mathbf{w}_{tra}^{(1)ad}(\mathbf{q})|$ over V. This condition can be expressed as

$$\left\{\frac{\partial}{\partial\epsilon} E\left[\beta_0(\mathbf{q}) + \epsilon\Delta\beta(\mathbf{q})\right]\right\}(\epsilon = 0) = 0 \tag{4.74}$$

This minimization condition will result in a specification of the boundary function $\mathrm{B}_0(\mathbf{q}_\mathsf{S})$ and of the nature of the associated boundary condition (Neumann, Dirichlet or mixed), as described below.

In light of the Dirichlet conditions represented by Eqs. (4.71), the quantity $\Delta\beta(\mathbf{q})$ is given by

$$\begin{aligned} \Delta\beta(\mathsf{S}_1) &= 0 \\ \Delta\beta(\mathsf{S}_2) &= 0 \\ \Delta\beta(\mathsf{S}_3) &= 0 \end{aligned} \tag{4.75}$$

on the two ϕ_λ boundary surfaces S_1 and S_2 and the minimum θ boundary surface S_3. Replacement of Eq. (4.72) into Eq. (4.74) results in

$$\left\{\frac{\partial}{\partial\epsilon}\int_{\mathsf{V}} \left[\mathbf{w}^{(1)ad}(\mathbf{q}) - \boldsymbol{\nabla}_{\mathbf{q}}\beta_0(\mathbf{q}) - \epsilon\boldsymbol{\nabla}_{\mathbf{q}}\Delta\beta(\mathbf{q})\right]^2 d\mathbf{q}\right\}(\epsilon = 0) = 0 \tag{4.76}$$

Since $\mathbf{q}$ and ϵ are independent variables, we can interchange the order of differentiation

and integration in this expression to get

$$\int_{\mathsf{V}} \left[\mathbf{w}^{(1)ad}(\mathbf{q}) - \boldsymbol{\nabla}_{\mathbf{q}}\beta_0(\mathbf{q})\right] \cdot \boldsymbol{\nabla}_{\mathbf{q}}\Delta\beta(\mathbf{q})d\mathbf{q} = 0 \tag{4.77}$$

With the help of the identity

$$\mathbf{u} \cdot \boldsymbol{\nabla}_{\mathbf{q}} v = \boldsymbol{\nabla}_{\mathbf{q}} \cdot (v\mathbf{u}) - v(\boldsymbol{\nabla}_{\mathbf{q}} \cdot \mathbf{u}) \tag{4.78}$$

where v and $\mathbf{u}$ are arbitrary scalar and vector functions of $\mathbf{q}$, Eq. (4.77) furnishes

$$\int_{\mathsf{V}} \boldsymbol{\nabla}_{\mathbf{q}} \cdot \left\{\Delta\beta(\mathbf{q}) \left[\mathbf{w}^{(1)ad}(\mathbf{q}) - \boldsymbol{\nabla}_{\mathbf{q}}\beta_0(\mathbf{q})\right]\right\} d\mathbf{q} - \int_{\mathsf{V}} \Delta\beta(\mathbf{q}) \left[\boldsymbol{\nabla}_{\mathbf{q}} \cdot \mathbf{w}^{(1)ad}(\mathbf{q}) - \nabla^2_{\mathbf{q}}\beta_0(\mathbf{q})\right] d\mathbf{q} = 0 \tag{4.79}$$

Using the Gauss divergence theorem in the first term and Eq. (4.70) in the second term of this equation, we get

$$\int_{\mathsf{S}} \Delta\beta(\mathbf{q}) \left[\mathbf{w}^{(1)ad}(\mathbf{q}) - \boldsymbol{\nabla}_{\mathbf{q}}\beta_0(\mathbf{q})\right] \cdot d\mathbf{s} - \int_{\mathsf{V}} \Delta\beta(\mathbf{q}) \left[\sigma(\mathbf{q}) - \nabla^2_{\mathbf{q}}\beta_0(\mathbf{q})\right] d\mathbf{q} = 0 \tag{4.80}$$

where the integral over the boundary surface S is the sum of six individual integrals evaluated on the six boundary surfaces S_i, $i = 1$ through 6. The quantity inside square brackets in the second term of Eq. (4.80) is equal to zero since $\beta_0(\mathbf{q})$ is a solution of the Poisson equation [Eq. (4.69)]. We now expand the surface integral in the first term of that equation and write

$$I(\mathsf{S}) = \int_{\mathsf{S}} \Delta\beta(\mathbf{q}) \left[\mathbf{w}^{(1)ad}(\mathbf{q}) - \boldsymbol{\nabla}_{\mathbf{q}}\beta_0(\mathbf{q})\right] \cdot d\mathbf{s} = \sum_{i=1}^{6} I(\mathsf{S}_i) = 0 \tag{4.81}$$

where

$$I(\mathsf{S}_i) = \int_{\mathsf{S}_i} \Delta\beta(\mathbf{q}_{\mathsf{S}_i}) \left[\mathbf{w}^{(1)ad}(\mathbf{q}_{\mathsf{S}_i}) - \boldsymbol{\nabla}_{\mathbf{q}}\beta_0(\mathbf{q}_{\mathsf{S}_i})\right] \cdot d\mathbf{s}_i \tag{4.82}$$

are the surface integrals of interest on the six parts of the closed surface S. They can

be expressed as

$$
\begin{aligned}
I(\mathsf{S}_1) &= -\int_{\rho_{min}}^{\rho_{max}} \int_{\theta_{min}}^{\theta_{max}} \Delta\beta(\mathsf{S}_1) \left[\mathrm{w}_{\phi_\lambda}^{(1)ad}(\rho,\theta,\phi_{\lambda min}) - \left(\frac{1}{\rho \sin\theta} \frac{\partial \beta_0(\mathbf{q})}{\partial \phi_\lambda} \right)_{\phi_{\lambda min}} \right] \rho \; d\rho d\theta \\
I(\mathsf{S}_2) &= \int_{\rho_{min}}^{\rho_{max}} \int_{\theta_{min}}^{\theta_{max}} \Delta\beta(\mathsf{S}_2) \left[\mathrm{w}_{\phi_\lambda}^{(1)ad}(\rho,\theta,\phi_{\lambda max}) - \left(\frac{1}{\rho \sin\theta} \frac{\partial \beta_0(\mathbf{q})}{\partial \phi_\lambda} \right)_{\phi_{\lambda max}} \right] \rho \; d\rho d\theta \\
I(\mathsf{S}_3) &= -\int_{\rho_{min}}^{\rho_{max}} \int_{\phi_{\lambda min}}^{\phi_{\lambda max}} \Delta\beta(\mathsf{S}_3) \left[\mathrm{w}_{\theta}^{(1)ad}(\rho,\theta_{min},\phi_\lambda) - \left(\frac{1}{\rho} \frac{\partial \beta_0(\mathbf{q})}{\partial \theta} \right)_{\theta_{min}} \right] \rho \sin\theta_{min} \; d\rho d\phi_\lambda \\
I(\mathsf{S}_4) &= \int_{\rho_{min}}^{\rho_{max}} \int_{\phi_{\lambda min}}^{\phi_{\lambda max}} \Delta\beta(\mathsf{S}_4) \left[\mathrm{w}_{\theta}^{(1)ad}(\rho,\theta_{max},\phi_\lambda) - \left(\frac{1}{\rho} \frac{\partial \beta_0(\mathbf{q})}{\partial \theta} \right)_{\theta_{max}} \right] \rho \sin\theta_{max} \; d\rho d\phi_\lambda \\
I(\mathsf{S}_5) &= -\int_{\theta_{min}}^{\theta_{max}} \int_{\phi_{\lambda min}}^{\phi_{\lambda max}} \Delta\beta(\mathsf{S}_5) \left[\mathrm{w}_{\rho}^{(1)ad}(\rho_{min},\theta,\phi_\lambda) - \left(\frac{\partial \beta_0(\mathbf{q})}{\partial \rho} \right)_{\rho_{min}} \right] \rho_{min}^2 \sin\theta \; d\theta d\phi_\lambda \\
I(\mathsf{S}_6) &= \int_{\theta_{min}}^{\theta_{max}} \int_{\phi_{\lambda min}}^{\phi_{\lambda max}} \Delta\beta(\mathsf{S}_6) \left[\mathrm{w}_{\rho}^{(1)ad}(\rho_{max},\theta,\phi_\lambda) - \left(\frac{\partial \beta_0(\mathbf{q})}{\partial \rho} \right)_{\rho_{max}} \right] \rho_{max}^2 \sin\theta \; d\theta d\phi_\lambda
\end{aligned}
$$

Because of the Dirichlet conditions on S_1, S_2 and S_3 that resulted in Eqs. (4.75), $I(\mathsf{S}_1)$, $I(\mathsf{S}_2)$ and $I(\mathsf{S}_3)$ vanish. Eq. (4.81) requires that the sum of the remaining $I(\mathsf{S}_i)$ terms should vanish. Given the arbitrariness of the $\Delta\beta(\mathsf{S}_i)$ for i= 4 through 6, in order for that to happen, it is necessary that each of its terms vanish. This results in

$$
\left(\frac{\partial \beta_0(\mathbf{q})}{\partial \rho} \right)_{\rho_{min}} = \mathrm{w}_{\rho}^{(1)ad}(\rho_{min},\theta,\phi_\lambda) \tag{4.83}
$$

$$
\left(\frac{\partial \beta_0(\mathbf{q})}{\partial \rho} \right)_{\rho_{max}} = \mathrm{w}_{\rho}^{(1)ad}(\rho_{max},\theta,\phi_\lambda) \tag{4.84}
$$

$$
\left(\frac{\partial \beta_0(\mathbf{q})}{\partial \theta} \right)_{\theta_{max}} = \rho \; \mathrm{w}_{\theta}^{(1)ad}(\rho,\theta_{max},\phi_\lambda) \tag{4.85}
$$

These are the Neumann boundary conditions used at the ρ and θ boundaries as described in Sec. 4.2.4 in Eqs. (4.47) through (4.51). Together with Eqs. (4.71) they specify the boundary functions $\mathrm{B}_0(\mathbf{q}_\mathsf{S})$ and the nature of the associated boundary conditions, as indicated after Eq. (4.74). This physically acceptable choice of boundary conditions minimizes the average value of the magnitude of the coupling vector $\mathbf{w}_{tra}^{(1)ad}(\mathbf{q})$ over the important domain V and hence the extended domain U of internal nuclear configuration space.

Bibliography

[1] M. Born, Nachr. Akad. Wiss. Gött. Math.-Phys. Kl. Article No. 6, 1 (1951).

[2] M. Born and K. Huang, *Dynamical Theory of Crystal Lattices* (Oxford University Press, Oxford, 1954), pp. 166-177 and 402-407.

[3] H. C. Longuet-Higgins, Adv. Spectrosc. **2**, 429 (1961).

[4] G. Herzberg and H. C. Longuet-Higgins, Discussion Faraday Soc. **35**, 77 (1963).

[5] H. C. Longuet-Higgins, Proc. R. Soc. London, Ser. A **344**, 147 (1975).

[6] M. V. Berry, Proc. R. Soc. London, Ser. A **392**, 45 (1984).

[7] C. A. Mead, Chem. Phys. **49**, 23 (1980).

[8] C. A. Mead and D. G. Truhlar, J. Chem. Phys. **70**, 2284 (1979).

[9] A. Kuppermann, in *Dynamics of Molecules and Chemical Reactions*, edited by R. E. Wyatt and J. Z. H. Zhang (Marcel Dekker, New York, 1996), pp. 411-472.

[10] B. Kendrick and R. T. Pack, J. Chem. Phys. **104**, 7475 (1996).

[11] B. Kendrick and R. T. Pack, J. Chem. Phys. **104**, 7502 (1996).

[12] R. J. Buenker, G. Hirsch, S. D. Peyerimhoff, P. J. Bruna, J. Römelt, M. Bettendorff, and C. Petrongolo, in *Current Aspects of Quantum Chemistry*, Elsevier, New York, 1981, pp. 81-97.

[13] M. Desouter-Lecomte, C. Galloy, J. C. Lorquet, and M. V. Pires, J. Chem. Phys. **71**, 3661 (1979).

[14] B. H. Lengsfield, P. Saxe, and D. R. Yarkony, J. Chem. Phys. **81**, 4549 (1984).

[15] P. Saxe, B. H. Lengsfield, and D. R. Yarkony, Chem. Phys. Lett. **113**, 159 (1985).

[16] B. H. Lengsfield, and D. R. Yarkony, J. Chem. Phys. **84**, 348 (1986).

[17] J. O. Jensen and D. R. Yarkony, J. Chem. Phys. **89**, 3853 (1988).

[18] R. Abrol, A. Shaw, A. Kuppermann and D. R. Yarkony, J. Chem. Phys. **115**, 4640 (2001).

[19] P. M. Morse and H. Feshbach, *Methods of Theoretical Physics* (McGraw-Hill, New York, 1953), pp. 52-54, 1763.

[20] A. Thiel and H. Köppel, J. Chem. Phys. **110**, 9371 (1999).

[21] V. Sidis, in *State-selected and State-to-State Ion-Molecule Reaction Dynamics*: Part 2 Theory, Vol. 82, edited by M. Baer and C.-Y. Ng (Wiley, New York, 1992), pp. 73-134.

[22] F. T. Smith, Phys. Rev. **179**, 111 (1969).

[23] M. Baer, Chem. Phys. Lett. **35**, 112 (1975).

[24] C. A. Mead and D. G. Truhlar, J. Chem. Phys. **77**, 6090 (1982).

[25] T. Pacher, L. S. Cederbaum, and H. Köppel, J. Chem. Phys. **89**, 7367 (1988).

[26] T. Pacher, C. A. Mead, L. S. Cederbaum, and H. Köppel, J. Chem. Phys. **91**, 7057 (1989).

[27] M. Baer and R. Englman, Mol. Phys. **75**, 293 (1992).

[28] K. Ruedenberg and G. J. Atchity, J. Chem. Phys. **99**, 3799 (1993).

[29] M. Baer and R. Englman, Chem. Phys. Lett. **265** 105 (1997).

[30] M. Baer, J. Chem. Phys. **107** 2694 (1997).

[31] B. K. Kendrick, C. A. Mead, and D. G. Truhlar, J. Chem. Phys. **110**, 7594 (1999).

[32] M. Baer, R. Englman, and A. J. C. Varandas, Mol. Phys. **97**, 1185 (1999).

[33] D. R. Yarkony, J. Chem. Phys. **112**, 2111 (2000).

[34] D. R. Yarkony, J. Chem. Phys. **105**, 10456 (1996).

[35] D. R. Yarkony, J. Phys. Chem. A **101**, 4263 (1997).

[36] N. Matsunaga and D. R. Yarkony, J. Chem. Phys. **107**, 7825 (1997).

[37] N. Matsunaga and D. R. Yarkony, Mol. Phys. **93**, 79 (1998).

[38] R. G. Sadygov and D. R. Yarkony, J. Chem. Phys. **109**, 20 (1998).

[39] D. R. Yarkony, J. Chem. Phys. **110**, 701 (1999).

[40] C. A. Mead, J. Chem. Phys. **72**, 3839 (1980).

[41] B. Lepetit and A. Kuppermann, Chem. Phys. Lett. **166**, 581 (1990).

[42] Y.-S. M. Wu, A. Kuppermann, and B. Lepetit, Chem. Phys. Lett. **186**, 319 (1991).

[43] Y.-S. M. Wu and A. Kuppermann, Chem. Phys. Lett. **201**, 178 (1993).

[44] A. Kuppermann and Y.-S. M. Wu, Chem. Phys. Lett. **205**, 577 (1993).

[45] Y.-S. M. Wu and A. Kuppermann, Chem. Phys. Lett. **235**, 105 (1995).

[46] A. Kuppermann and Y.-S. M. Wu, Chem. Phys. Lett. **241**, 229 (1995).

[47] A. J. C. Varandas, F. B. Brown, C. A. Mead, D. G. Truhlar and N. C. Blais, J. Chem. Phys. **86**, 6258 (1987).

[48] M. Baer, Chem. Phys. **15**, 49 (1976).

[49] R. Englman, A. Yahalom, and M. Baer, Eur. Phys. J. D **8**, 1 (2000).

[50] R. Englman and M. Baer, J. Phys. Cond. Matt. **11**, 1059 (1999).

[51] A. Kuppermann, J. Phys. Chem. A **100**, 2621 (1996); **100**, 11202 (1996).

[52] A. Kuppermann, Chem. Phys. Lett. **32**, 374 (1975).

[53] L. M. Delves, Nucl. Phys. **9**, 391 (1959).

[54] L. M. Delves, Nucl. Phys. **20**, 275 (1960).

[55] D. Jepsen and J. O. Hirschfelder, Proc. Natl. Acad. Sci. U.S.A. **45**, 249 (1959).

[56] F. T. Smith, J. Math. Phys. **3**, 735 (1962).

[57] R. T. Ling and A. Kuppermann, in *Electronic and Atomic Collisions, Abstract of the 9th International Conference on the Physics of Electronic and Atomic Collisions, Seattle, Washington, 24-30 July 1975*, Vol. 1, edited by J. S. Riley and R. Geballe (Univ. Washington Press, Seattle, 1975), pp. 353-354.

[58] A. Kuppermann, in *Advances in Molecular Vibrations and Collision Dynamics*, edited by J. Bowman (JAI Press, Greenwich, CT, 1994), Vol. 2B, p. 117-186.

[59] Ref. [19], Eq. 1.4.8.

[60] J. C. Adams, Appl. Math. Comput. **43**, 79 (1991).

[61] J. C. Adams, Appl. Math. Comput. **34**, 113 (1989).

[62] B. Liu, J. Chem. Phys. **58**, 1925 (1973).

[63] P. Siegbahn and B. Liu, J. Chem. Phys. **68**, 2457 (1978).

[64] D. G. Truhlar and C. J. Horowitz, J. Chem. Phys. **68**, 2466 (1978); **71**, 1514 (1979) (E).

[65] S. Rogers, D. Wang, S. Walch, and A. Kuppermann, J. Phys. Chem. A **104**, 2308 (2000).

[66] Y.-S. M. Wu, A. Kuppermann, and J. B. Anderson, Phys. Chem. Chem. Phys. **6**, 929 (1999).

FIGURE CAPTIONS

Fig. 4.1 Mapping of a point P of a constant ρ hemisphere in the $OX_\lambda YZ_\lambda$ space onto a point Q on a plane tangent to that hemisphere at the intersection T of the OY axis with it, such that the length of the arc(TP) = TQ. The point P has θ, ϕ_λ polar angles in the $O\overline{X}_\lambda\overline{Y}_\lambda\overline{Z}$ space and $\omega_\lambda, \gamma_\lambda$ in the $OX_\lambda YZ_\lambda$ space. $\overline{\mathrm{P}}$ is the projection of point P on the $OX_\lambda Y$ plane.

Fig. 4.2 Boundary surface S for solving the Poisson Eq. (4.35) in the $O\overline{X}_\lambda\overline{Y}_\lambda\overline{Z}$ space of Fig. 4.1. The surface is not drawn to exact scale. Arc(DG) is part of a circle of radius 1.5 bohr; Arc(AF) is part of a circle of radius 10 bohr; $\angle$AOF = 60°; and $\angle$BOK = $\angle$EOK = 0.1°. The surface S is composed of 6 parts: ABCD surface S_1 (ϕ_λ = 0°, 0.1° $\leq \theta \leq$ 90°, 1.5 bohr $\leq \rho \leq$ 10 bohr); EFGH surface S_2 (ϕ_λ = 60°, 0.1° $\leq \theta \leq$ 90°, 1.5 bohr $\leq \rho \leq$ 10 bohr); BCHE surface S_3 (θ = 0.1°, 0° $\leq \phi_\lambda \leq$ 60°, 1.5 bohr $\leq \rho \leq$ 10 bohr); ADGF surface S_4 (θ = 90°, 0° $\leq \phi_\lambda \leq$ 60°, 1.5 bohr $\leq \rho \leq$ 10 bohr); CDGH surface S_5 (ρ = 1.5 bohr, 0.1° $\leq \theta \leq$ 90°, 0° $\leq \phi_\lambda \leq$ 60°); and ABEF surface S_6 (ρ = 10 bohr, 0.1° $\leq \theta \leq$ 90°, 0° $\leq \phi_\lambda \leq$ 60°).

Fig. 4.3 The quantity $\sin^2\theta\ \sigma(\rho, \theta, 3\phi_\lambda)$, in units of bohr^{-2}, with σ defined by Eq. (4.31), for the H_3 system as a function of θ and ϕ_λ, at: (a) ρ = 2 bohr, (b) ρ = 4 bohr, (c) ρ = 6 bohr, and (d) ρ = 8 bohr. The circles on the bottom face of each of the panels are constant θ circles, with the solid circle corresponding to θ = 90°, and radial lines are constant ϕ_λ lines whose values are displayed on the periphery of the solid circle. Equatorial views of $\sin^2\theta\ \sigma(\rho, \theta, 3\phi_\lambda)$ contours at: (e) ρ = 2 bohr, (f) ρ = 4 bohr, (g) ρ = 6 bohr, and (h) ρ = 8 bohr. See the first paragraph of Sec. 4.3.1 for the definition of the equatorial view.

Fig. 4.4 The diabatization angle $\beta(\rho, \theta, \phi_\lambda)$, in degrees, for the H_3 system at: (a) ρ = 2 bohr, (b) ρ = 4 bohr, (c) ρ = 6 bohr, and (d) ρ = 8 bohr. The bottom face of the panels are similar to those of the corresponding panels of Fig. 4.3. The equatorial view of β contours is also given at: (e) ρ = 2 bohr, (f) ρ = 4 bohr, (g) ρ = 6 bohr,

and (h) $\rho = 8$ bohr.

Fig. 4.5 Same as Fig. 4.4 for the $\gamma(\rho, \theta, 3\phi_\lambda)$ part of the diabatization angle $\beta(\rho, \theta, \phi_\lambda)$ defined by Eq. (4.36).

Fig. 4.6 Cuts of $\gamma(\rho, \theta, 3\phi_\lambda)$ (shown in Fig. 4.5) at three values of θ: 5° (solid line), 45° (dash-dotted line), and 90° (dotted line) for: (a) $\rho = 2$ bohr, (b) $\rho = 4$ bohr, (c) $\rho = 6$ bohr, and (d) $\rho = 8$ bohr and the corresponding cuts of $\gamma^{\mathrm{DMBE}}(\rho, \theta, 3\phi_\lambda)$ at the same three values of θ for: (e) $\rho = 2$ bohr, (f) $\rho = 4$ bohr, (g) $\rho = 6$ bohr, and (h) $\rho = 8$ bohr.

Fig. 4.7 Plots of Δ_γ, defined by Eq. (4.57), as a function of θ for four values of ρ: 2 bohr (solid line), 4 bohr (dashed line), 6 bohr (dash-dotted line), and 8 bohr (dotted line).

Fig. 4.8 Plots of γ_{6D}, the γ angle obtained from the solution of a Poisson equation using Dirichlet boundary conditions at all six boundaries. Panels (a) through (d) show the three-dimensional plots and panels (e) through (h) show the equatorial view of its contours similar to Fig. 4.4.

Fig. 4.9 Longitudinal (removable) part of the *ab initio* first-derivative coupling vector, $\mathbf{w}_{lon}^{(1)ad}(\rho, \theta, \phi_\lambda)$ as a function of ϕ_λ for $\rho = 4$ bohr, 6 bohr and 8 bohr and (a) $\theta = 1°$ (near-conical intersection geometries), (b) $\theta = 30°$, (c) $\theta = 60°$, and (d) $\theta = 90°$ (collinear geometries).

Fig. 4.10 Same as Fig. 4.9 for transverse (nonremovable) part of the *ab initio* first-derivative coupling vector, $\mathbf{w}_{tra}^{(1)ad}(\rho, \theta, \phi_\lambda)$.

Fig. 4.11 Same as Fig. 4.9 for transverse (nonremovable) part of the *ab initio* first-derivative coupling vector $\mathbf{w}_{tra,6D}^{(1)ad}(\rho, \theta, \phi_\lambda)$, obtained using the same Dirichlet boundary conditions as in Fig. 4.8.

Fig. 4.12 Longitudinal $\Phi_{lon}(\phi_\lambda; \rho, \theta)$ and transverse $\Phi_{tra}(\phi_\lambda; \rho, \theta)$ open-path phases

as a function of ϕ_λ for four values of θ: 1° (solid line), 30° (dashed line), 60° (dotted line), and 90° (dash-dotted line) for each of the four values of ρ: (a) and (e) 2 bohr, (b) and (f) 4 bohr, (c) and (g) 6 bohr, and (d) and (h) 8 bohr.

Fig. 4.13 (a) Adiabatic ground state (ε_1^{ad}) energy contours in the $X_\lambda Z_\lambda$ plane of Fig. 4.1 for a collinear approach ($\gamma_\lambda = 0°$or$180°$) of the H atom to the H_2 molecule; (b) Corresponding contours for the first-excited state (ε_2^{ad}) energies; (c) ε_1^{ad} contours in the YZ_λ plane of Fig. 4.1 for a perpendicular approach ($\gamma_\lambda = 90°$) of the H atom to the H_2 molecule; (d) Corresponding contours for ε_2^{ad}. All contour energies shown are in eV and correspond to the DSP fit to *ab initio* energies described in Chapter 3. The dashed lines in panels (c) and (d) correspond to conical intersection geometries.

Fig. 4.14 Same as for Fig. 4.13 except that the displayed energy contours correspond to the diagonal diabatic energies ε_{11}^d and ε_{22}^d.

Fig. 4.15 Contours corresponding to the off-diagonal diabatic energy ε_{12}^d in the $X_\lambda Z_\lambda$ plane of Fig. 4.1 for a collinear approach ($\gamma_\lambda = 0°$ or $180°$) of the H atom to the H_2 molecule. All contour energies shown are in eV.

Fig. 4.16 Conical intersection energies as a function of ρ for DSP (crosses), DMBE (circles), LSTH (squares), and EQMC (triangles) PESs. The DSP curve corresponds to $Z_\lambda = 0$ energies in panels (c) and (d) of Fig. 4.13.

Fig. 4.17 Adiabatic ground state (E_1) energy contours in an equatorial view (see text for definition) for: (a) $\rho = 2$ bohr, (b) $\rho = 4$ bohr, (c) $\rho = 6$ bohr, and (d) $\rho = 8$ bohr; and corresponding adiabatic first-excited state (E_2) energy contours for: (e) $\rho = 2$ bohr, (f) $\rho = 4$ bohr, (g) $\rho = 6$ bohr, and (h) $\rho = 8$ bohr. All contour energies shown are in eV.

Fig. 4.18 Same as for Fig. 4.17 except that the displayed energy contours correspond to the diagonal diabatic energies ε_{11}^d and ε_{22}^d.

Fig. 4.19 Contours corresponding to the off-diagonal diabatic energy ε_{12}^d in the equa-

torial view for: (a) $\rho = 2$ bohr, (b) $\rho = 4$ bohr, (c) $\rho = 6$ bohr, and (d) $\rho = 8$ bohr.

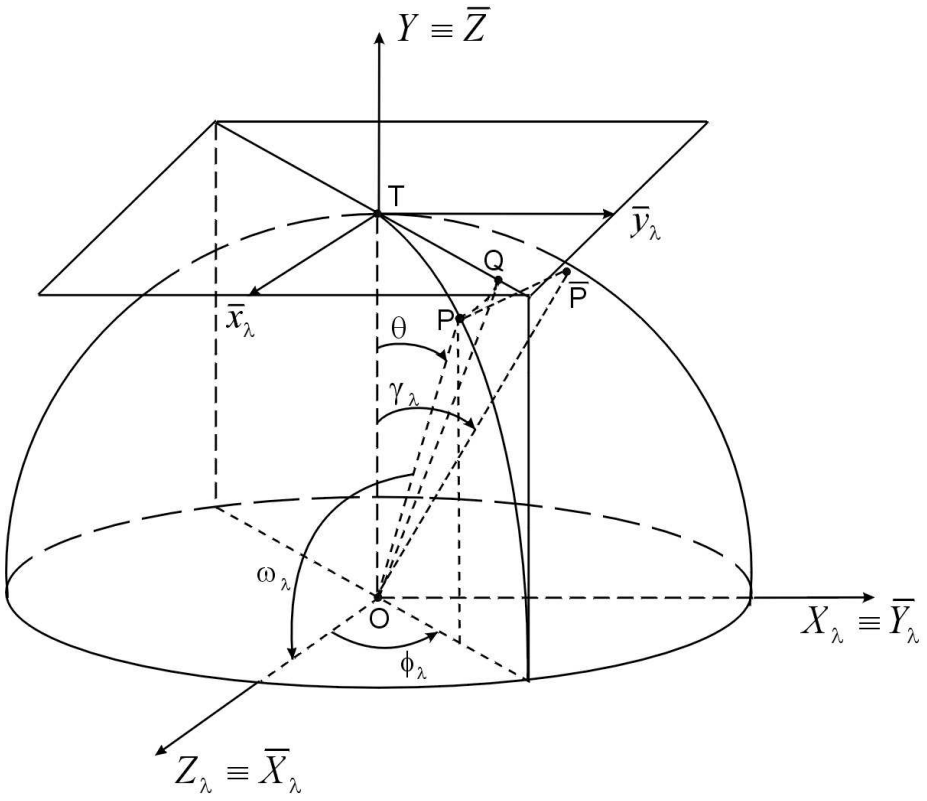
$Y \equiv \overline{Z}$
T
$\overline{y}_\lambda$
Q
$\overline{P}$
$\overline{x}_\lambda$
θ
P
γ_λ
ω_λ
O
$X_\lambda \equiv \overline{Y}_\lambda$
ϕ_λ
$Z_\lambda \equiv \overline{X}_\lambda$

Figure 4.1:

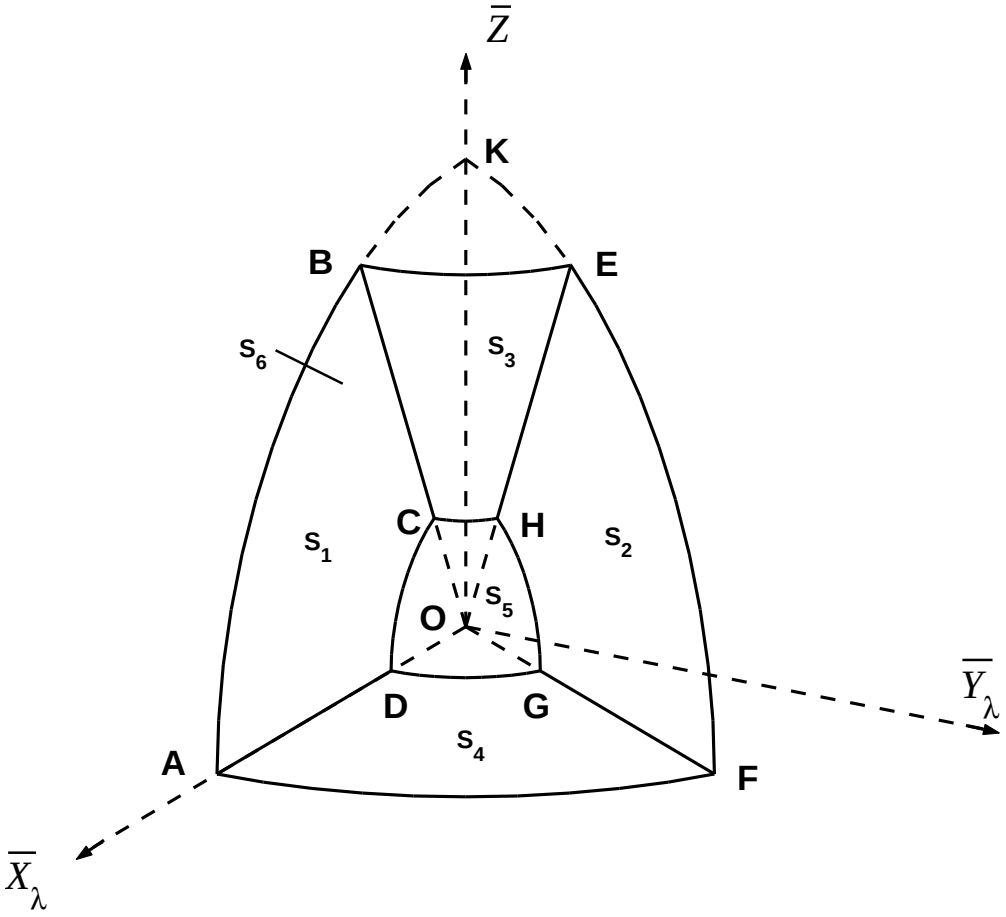
$\overline{Z}$
K
B
E
S_6
S_3
C
H
S_1
S_2
S_5
O
$\overline{Y}_\lambda$
D
G
S_4
A
F
$\overline{X}_\lambda$

Figure 4.2:

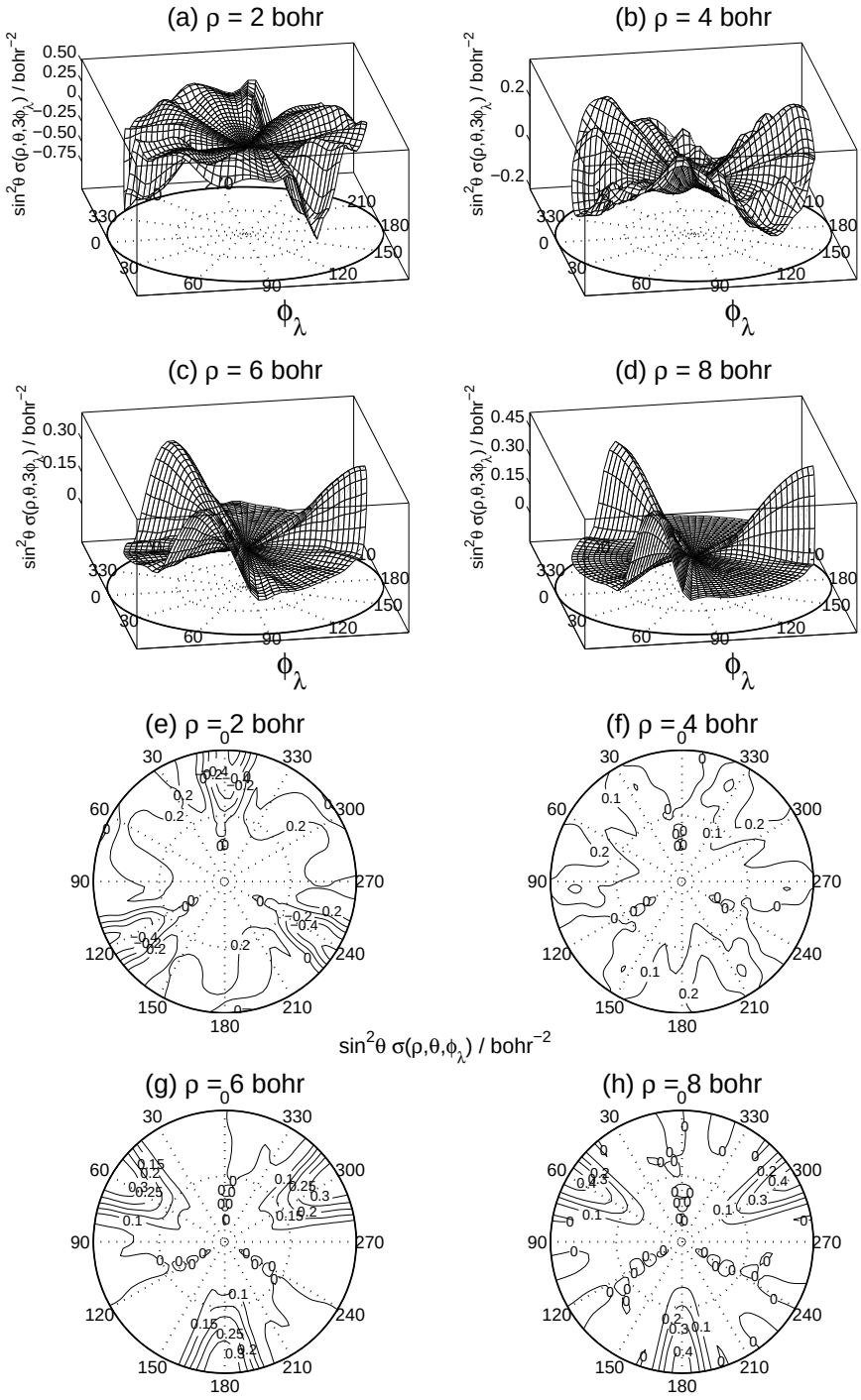
(a) ρ = 2 bohr
(b) ρ = 4 bohr
(c) ρ = 6 bohr
(d) ρ = 8 bohr
(e) ρ = 2 bohr
(f) ρ = 4 bohr
(g) ρ = 6 bohr
(h) ρ = 8 bohr
sin²θ σ(ρ,θ,3φλ) / bohr⁻²
φλ
sin²θ σ(ρ,θ,φλ) / bohr⁻²

Figure 4.3:

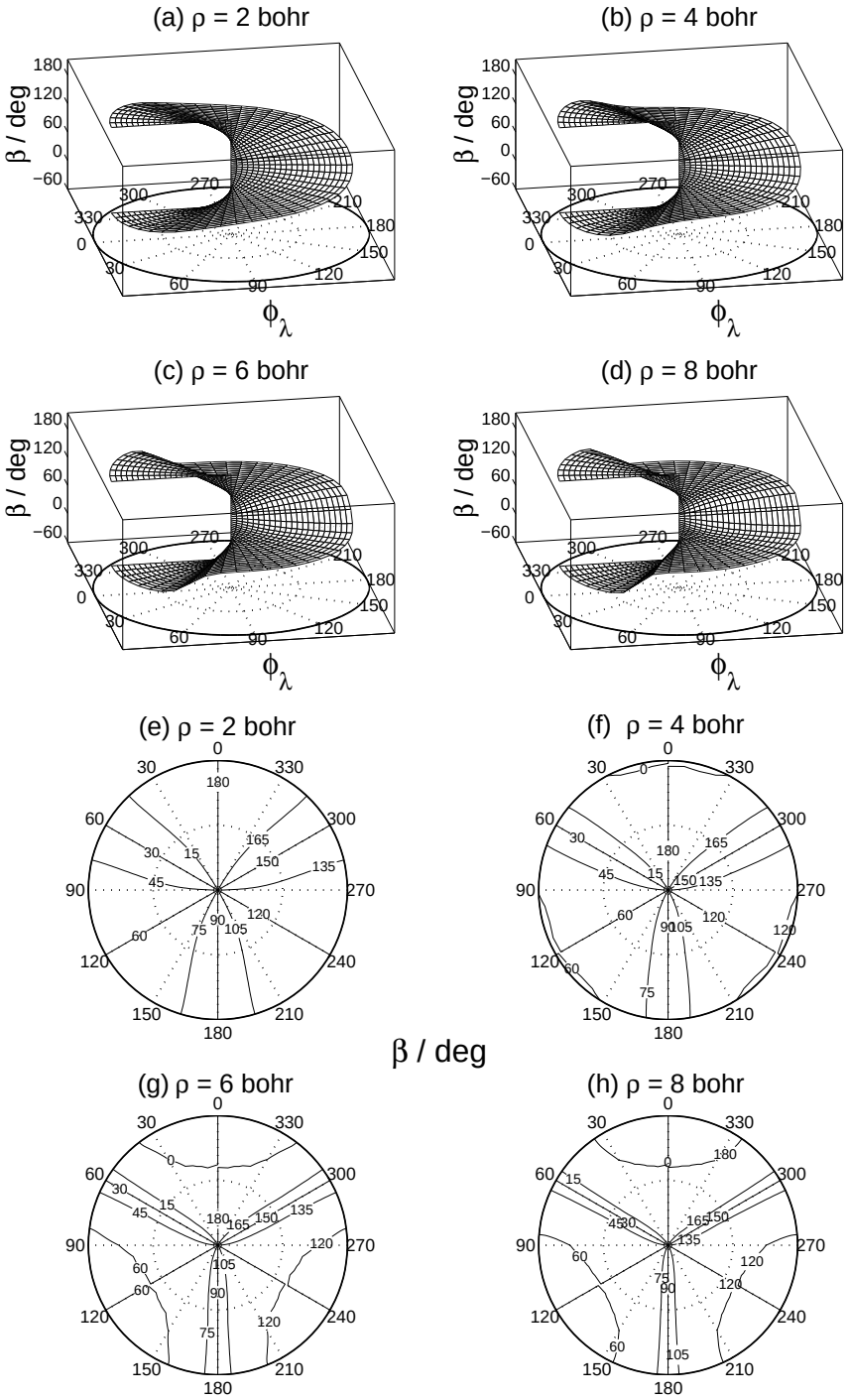
(a) ρ = 2 bohr
(b) ρ = 4 bohr
(c) ρ = 6 bohr
(d) ρ = 8 bohr
β / deg
ϕ_λ
(e) ρ = 2 bohr
(f) ρ = 4 bohr
β / deg
(g) ρ = 6 bohr
(h) ρ = 8 bohr

Figure 4.4:

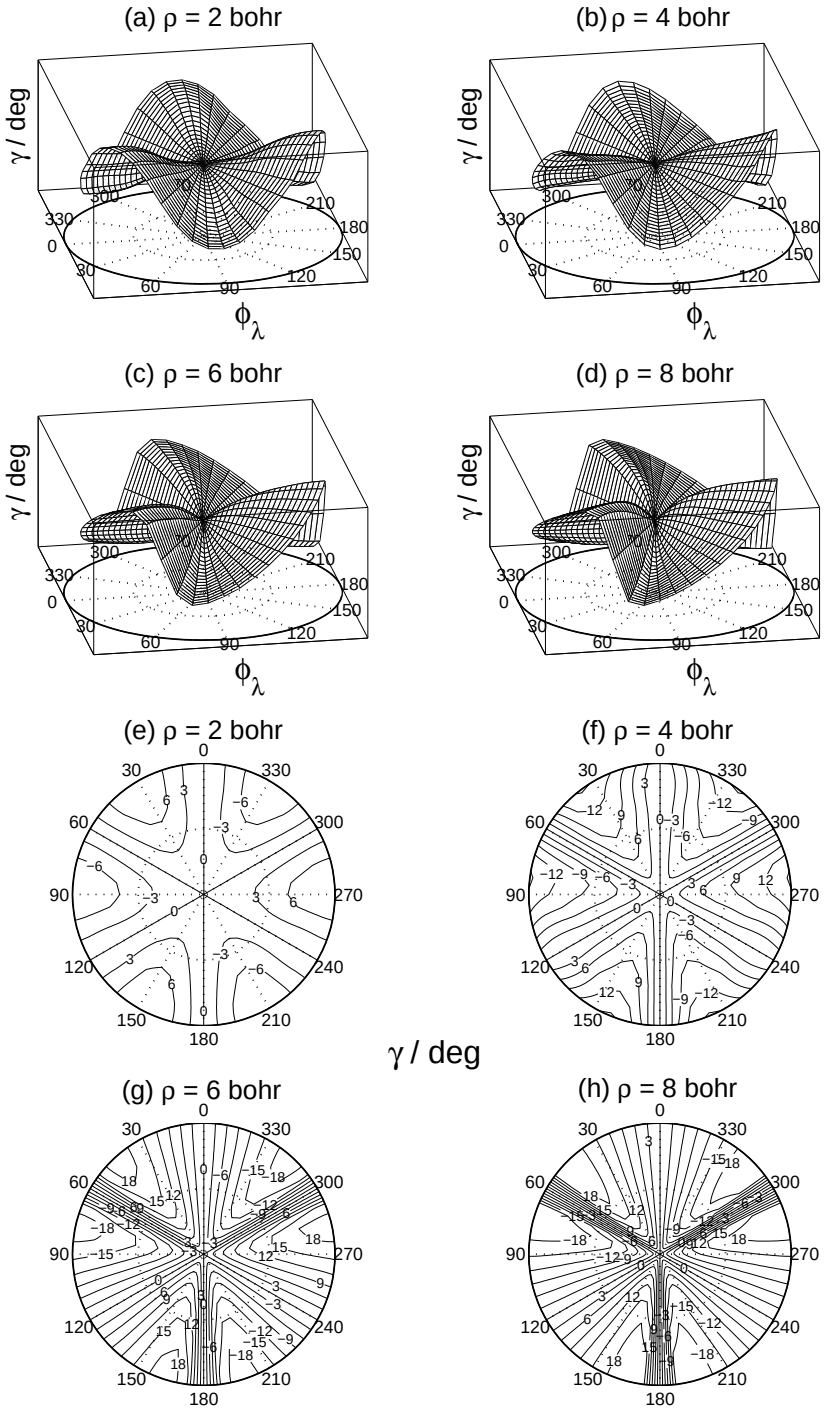
(a) ρ = 2 bohr
(b) ρ = 4 bohr
(c) ρ = 6 bohr
(d) ρ = 8 bohr
(e) ρ = 2 bohr
(f) ρ = 4 bohr
(g) ρ = 6 bohr
(h) ρ = 8 bohr
γ / deg
ϕ_λ

Figure 4.5:

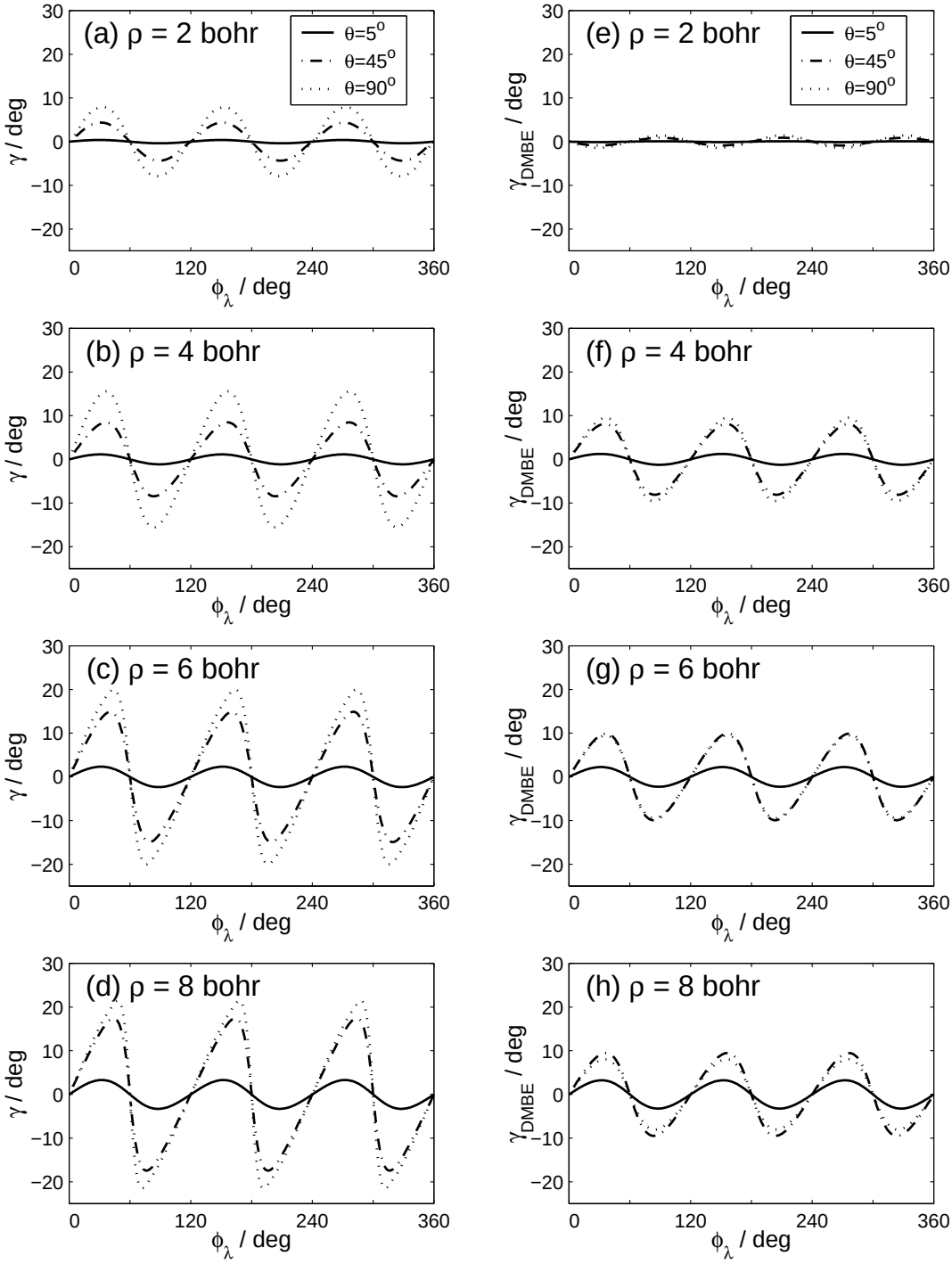
(a) ρ = 2 bohr
θ=5°
θ=45°
θ=90°
γ / deg
(e) ρ = 2 bohr
γDMBE / deg
(b) ρ = 4 bohr
(f) ρ = 4 bohr
(c) ρ = 6 bohr
(g) ρ = 6 bohr
(d) ρ = 8 bohr
(h) ρ = 8 bohr
φλ / deg
30
20
10
0
−10
−20
0
120
240
360

Figure 4.6:

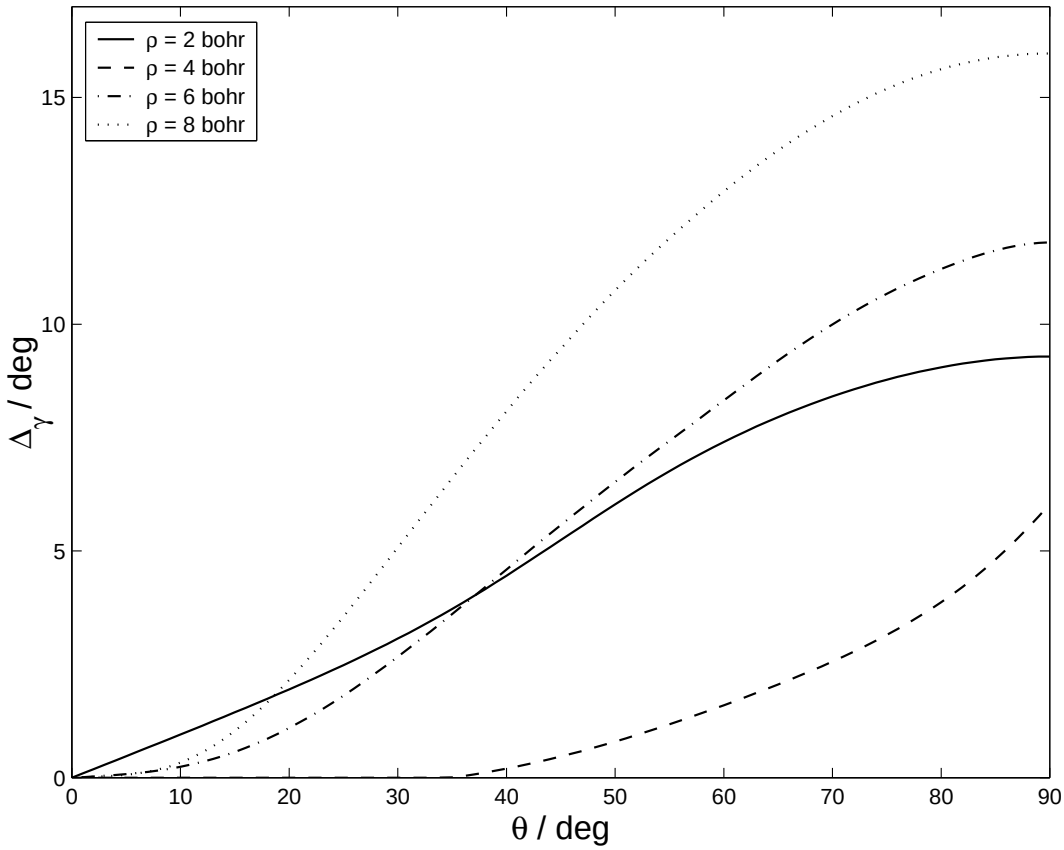
ρ = 2 bohr
ρ = 4 bohr
ρ = 6 bohr
ρ = 8 bohr
Δγ / deg
θ / deg
0
5
10
15
0
10
20
30
40
50
60
70
80
90

Figure 4.7:

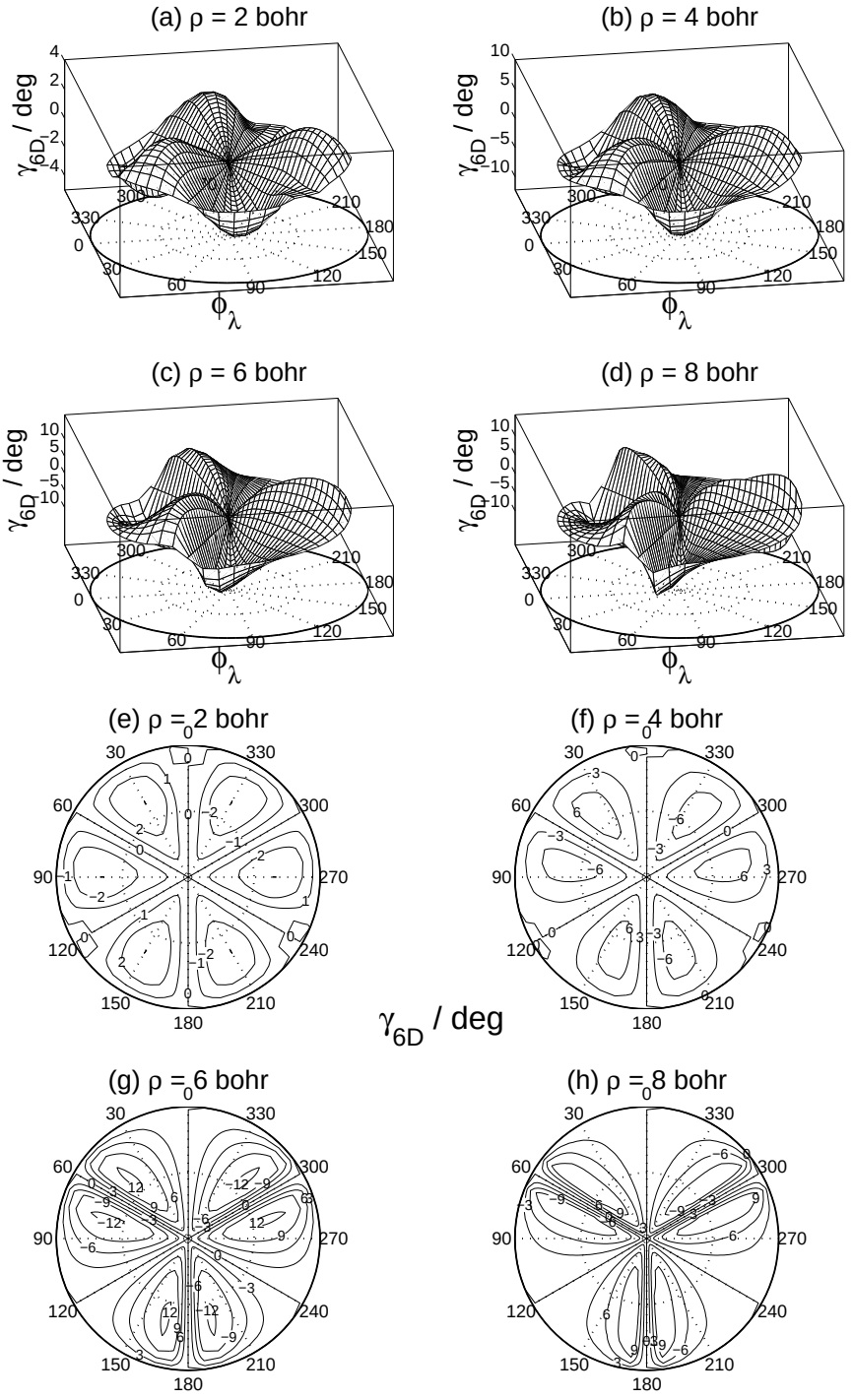
(a) ρ = 2 bohr
(b) ρ = 4 bohr
(c) ρ = 6 bohr
(d) ρ = 8 bohr
(e) ρ = 2 bohr
(f) ρ = 4 bohr
(g) ρ = 6 bohr
(h) ρ = 8 bohr
γ6D / deg
ϕλ

Figure 4.8:

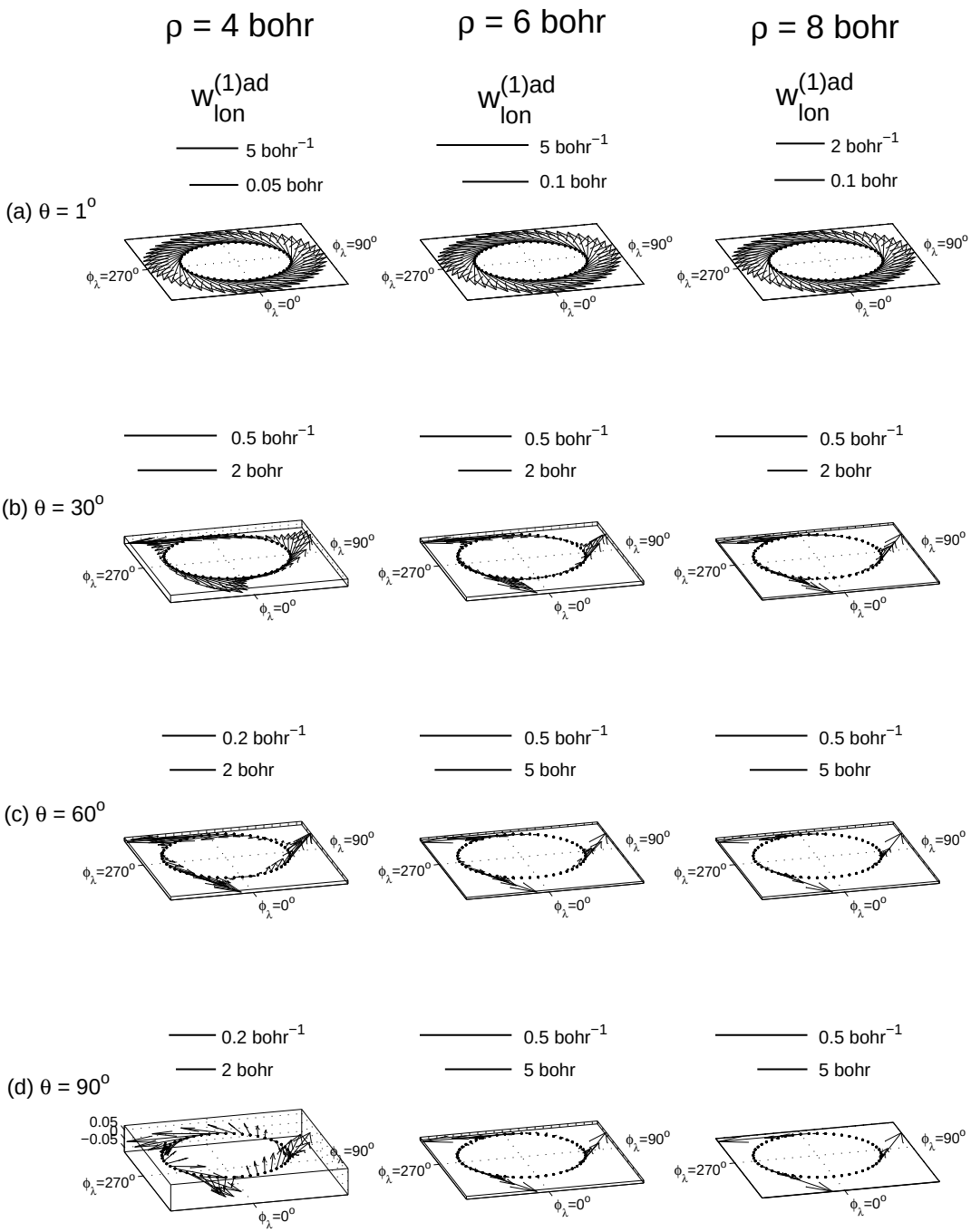
ρ = 4 bohr
ρ = 6 bohr
ρ = 8 bohr
$w^{(1)ad}_{lon}$
5 bohr^{-1}
0.05 bohr
0.1 bohr
2 bohr^{-1}
(a) θ = 1°
0.5 bohr^{-1}
2 bohr
(b) θ = 30°
0.2 bohr^{-1}
5 bohr
(c) θ = 60°
(d) θ = 90°
0.05
0
−0.05
ϕ_λ=0°
ϕ_λ=90°
ϕ_λ=270°

Figure 4.9:

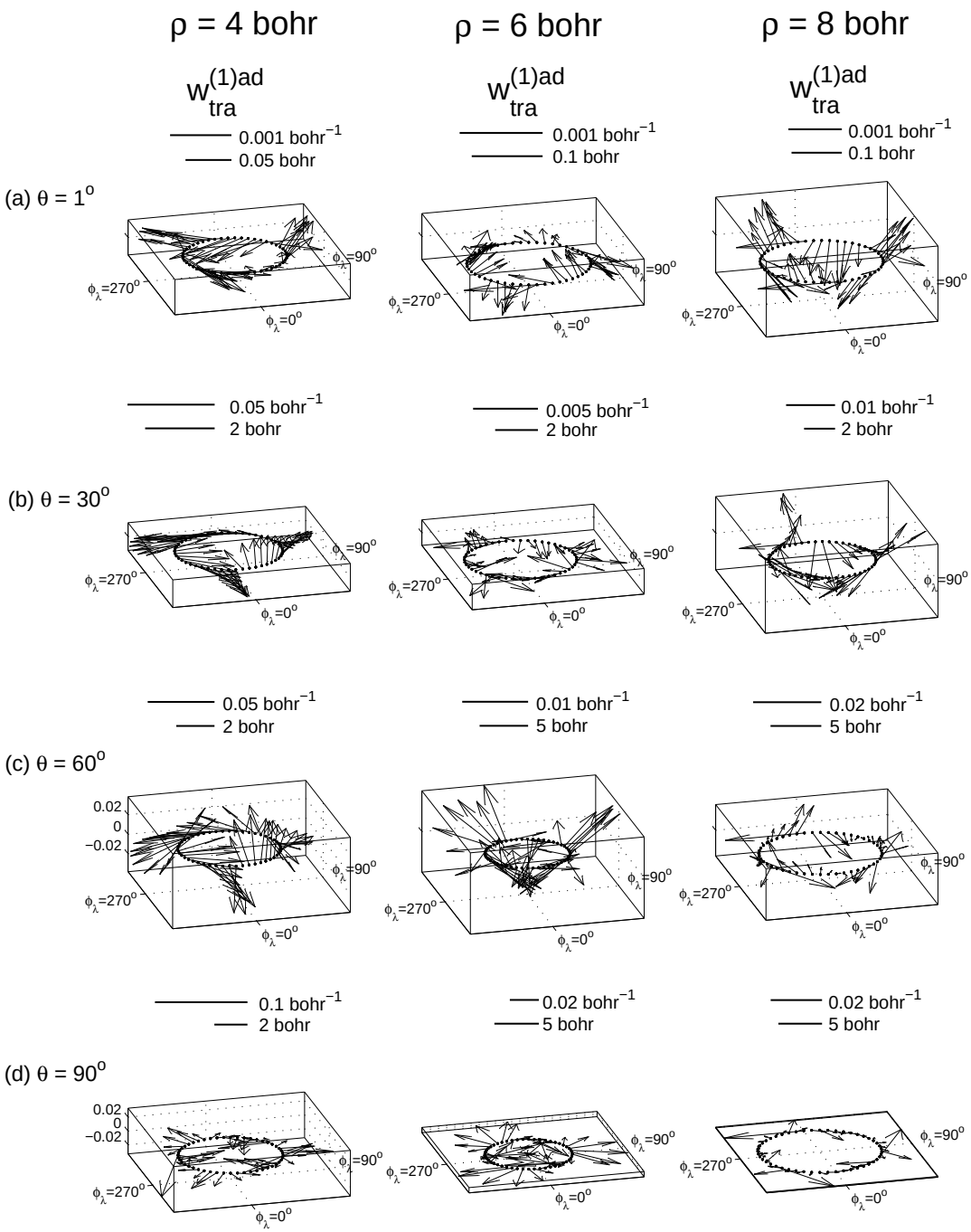
ρ = 4 bohr
ρ = 6 bohr
ρ = 8 bohr
$w^{(1)ad}_{tra}$
0.001 bohr^{-1}
0.05 bohr
0.1 bohr
(a) θ = 1°
0.05 bohr^{-1}
2 bohr
0.005 bohr^{-1}
0.01 bohr^{-1}
(b) θ = 30°
0.02 bohr^{-1}
5 bohr
(c) θ = 60°
0.1 bohr^{-1}
(d) θ = 90°
0.02
0
−0.02
ϕ_λ=0°
ϕ_λ=90°
ϕ_λ=270°

Figure 4.10:

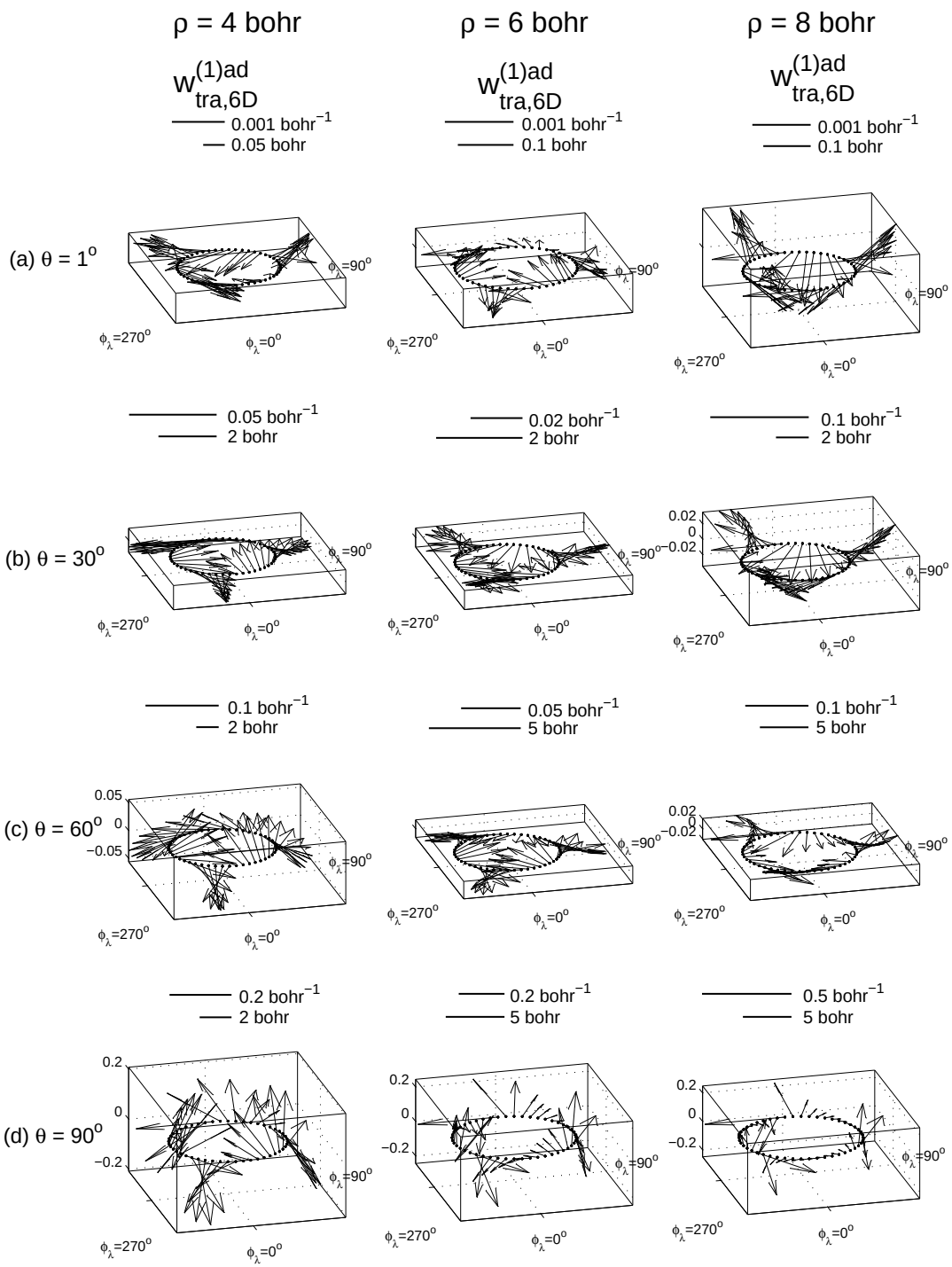
ρ = 4 bohr
ρ = 6 bohr
ρ = 8 bohr
$w^{(1)ad}_{tra,6D}$
0.001 bohr^{-1}
0.05 bohr
0.1 bohr
(a) θ = 1°
(b) θ = 30°
(c) θ = 60°
(d) θ = 90°
ϕ_λ=90°
ϕ_λ=270°
ϕ_λ=0°
0.05 bohr^{-1}
2 bohr
0.02 bohr^{-1}
0.1 bohr^{-1}
0.1 bohr^{-1}
5 bohr
0.05 bohr^{-1}
0.2 bohr^{-1}
0.5 bohr^{-1}

Figure 4.11:

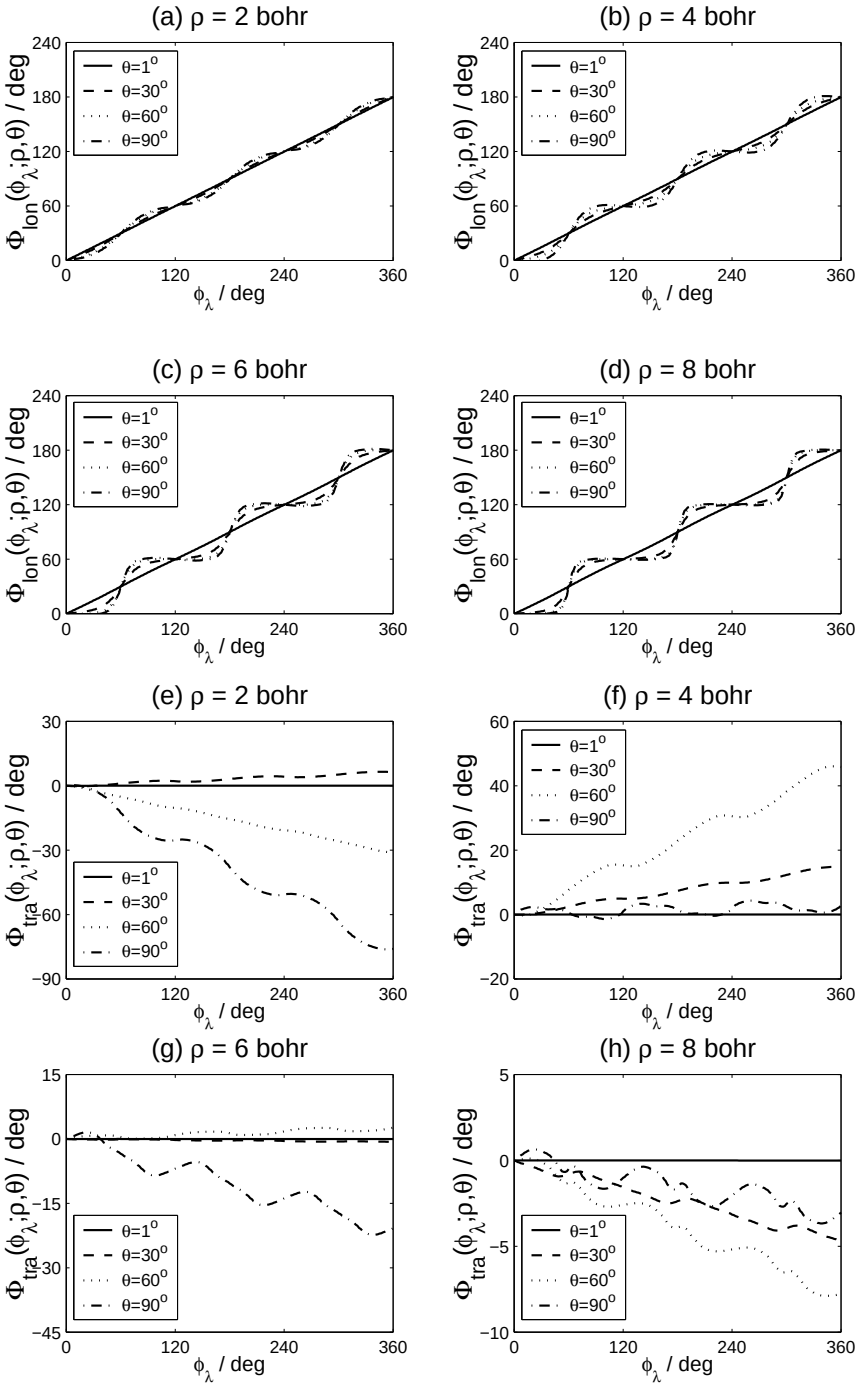
(a) ρ = 2 bohr
(b) ρ = 4 bohr
(c) ρ = 6 bohr
(d) ρ = 8 bohr
(e) ρ = 2 bohr
(f) ρ = 4 bohr
(g) ρ = 6 bohr
(h) ρ = 8 bohr
θ=1°
θ=30°
θ=60°
θ=90°
$\Phi_{lon}(\phi_\lambda;\rho,\theta)$ / deg
$\Phi_{tra}(\phi_\lambda;\rho,\theta)$ / deg
ϕ_λ / deg

Figure 4.12:

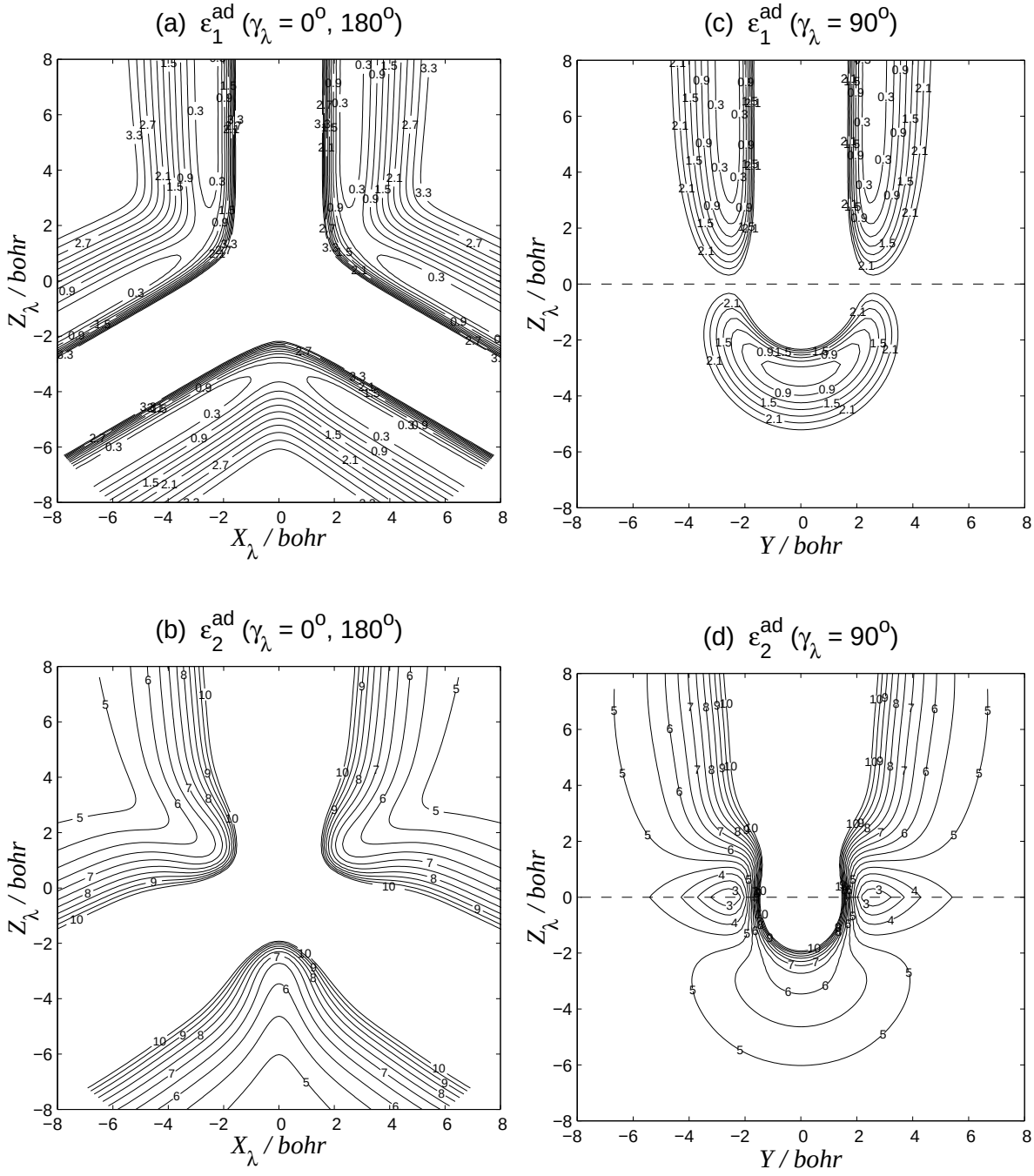
(a) ε_1^{ad} (γ_λ = 0°, 180°)
(c) ε_1^{ad} (γ_λ = 90°)
(b) ε_2^{ad} (γ_λ = 0°, 180°)
(d) ε_2^{ad} (γ_λ = 90°)
Z_λ / bohr
X_λ / bohr
Y / bohr

Figure 4.13:

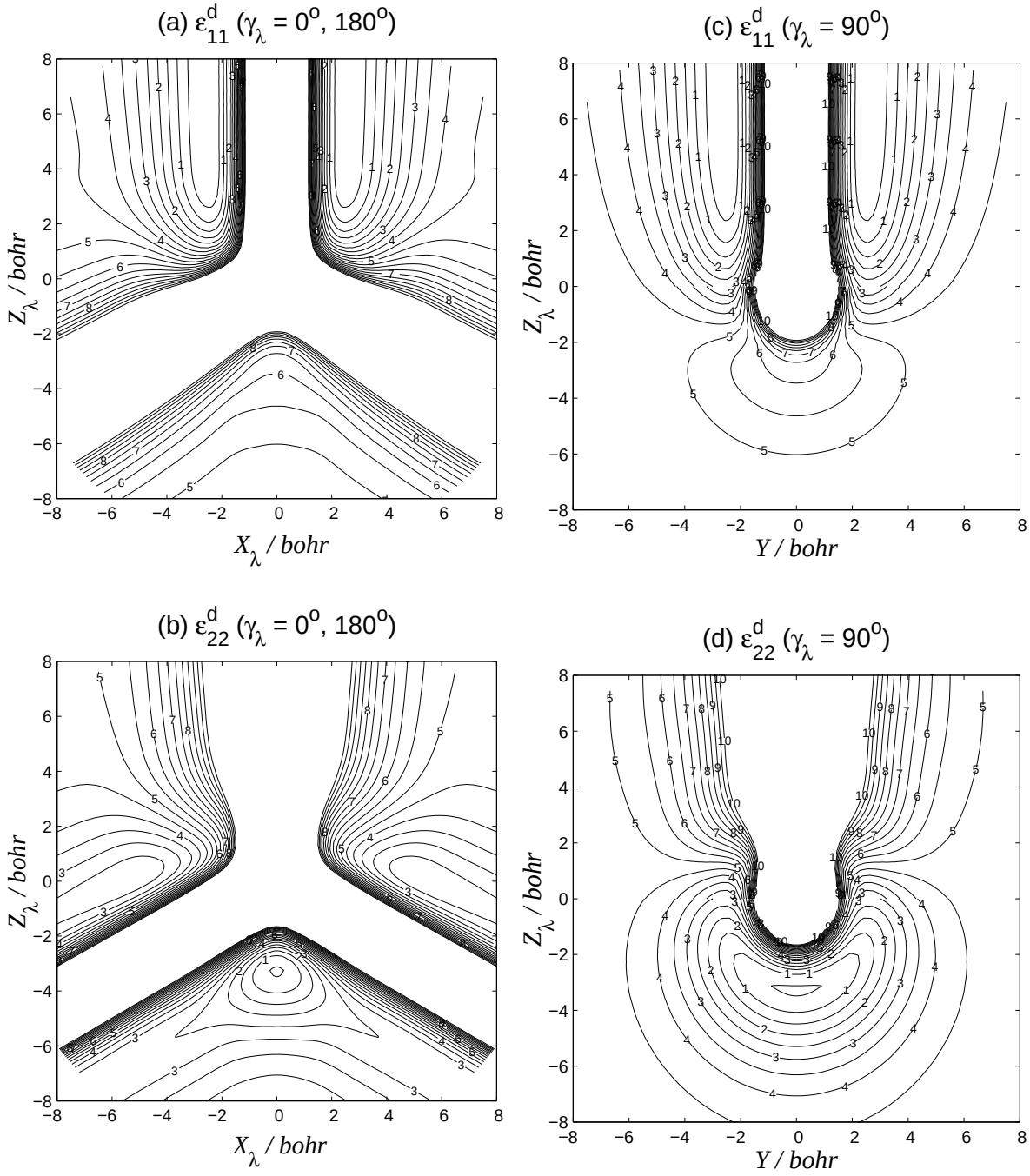
(a) ε^{d}_{11} (γ_λ = 0°, 180°)
(c) ε^{d}_{11} (γ_λ = 90°)
(b) ε^{d}_{22} (γ_λ = 0°, 180°)
(d) ε^{d}_{22} (γ_λ = 90°)
Z_λ / bohr
X_λ / bohr
Y / bohr

Figure 4.14:

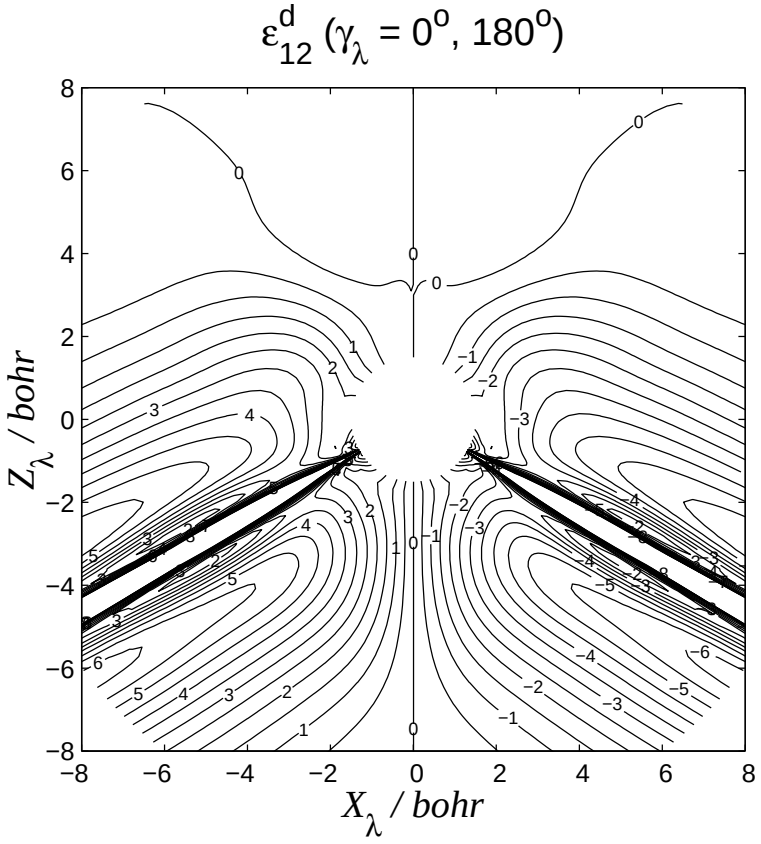
ε^{d}_{12} (γ_λ = 0°, 180°)
Z_λ / bohr
X_λ / bohr

Figure 4.15:

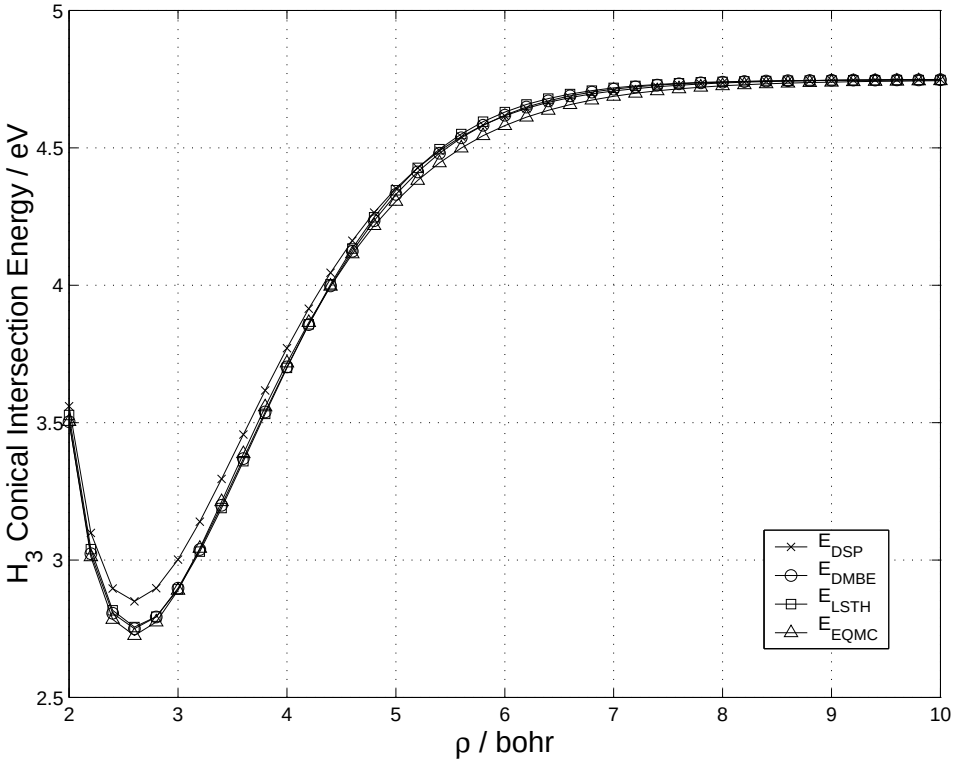
H3 Conical Intersection Energy / eV
ρ / bohr
E_DSP
E_DMBE
E_LSTH
E_EQMC
5
4.5
4
3.5
3
2.5
2
3
4
5
6
7
8
9
10

Figure 4.16:

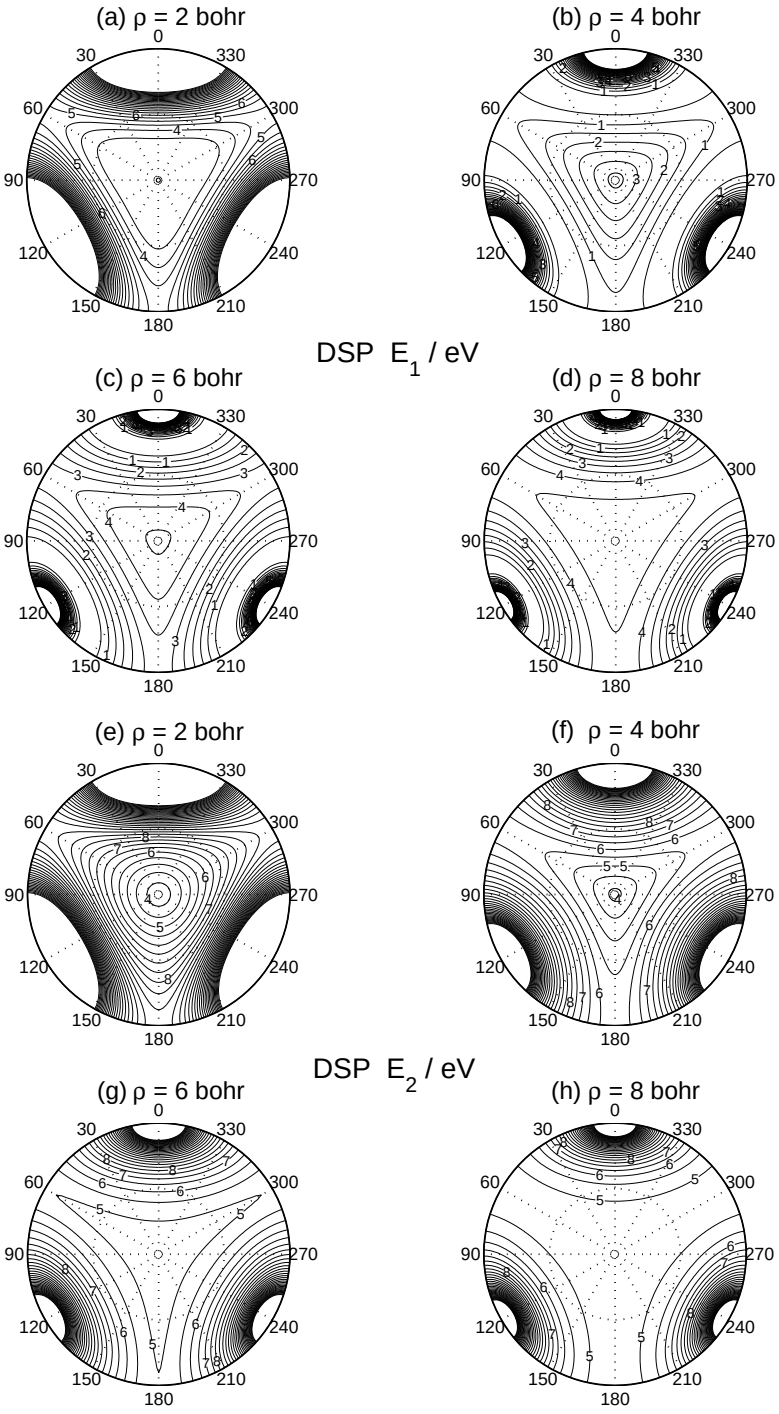
(a) ρ = 2 bohr
(b) ρ = 4 bohr
DSP E1 / eV
(c) ρ = 6 bohr
(d) ρ = 8 bohr
(e) ρ = 2 bohr
(f) ρ = 4 bohr
DSP E2 / eV
(g) ρ = 6 bohr
(h) ρ = 8 bohr
0
30
330
60
300
90
270
120
240
150
210
180

Figure 4.17:

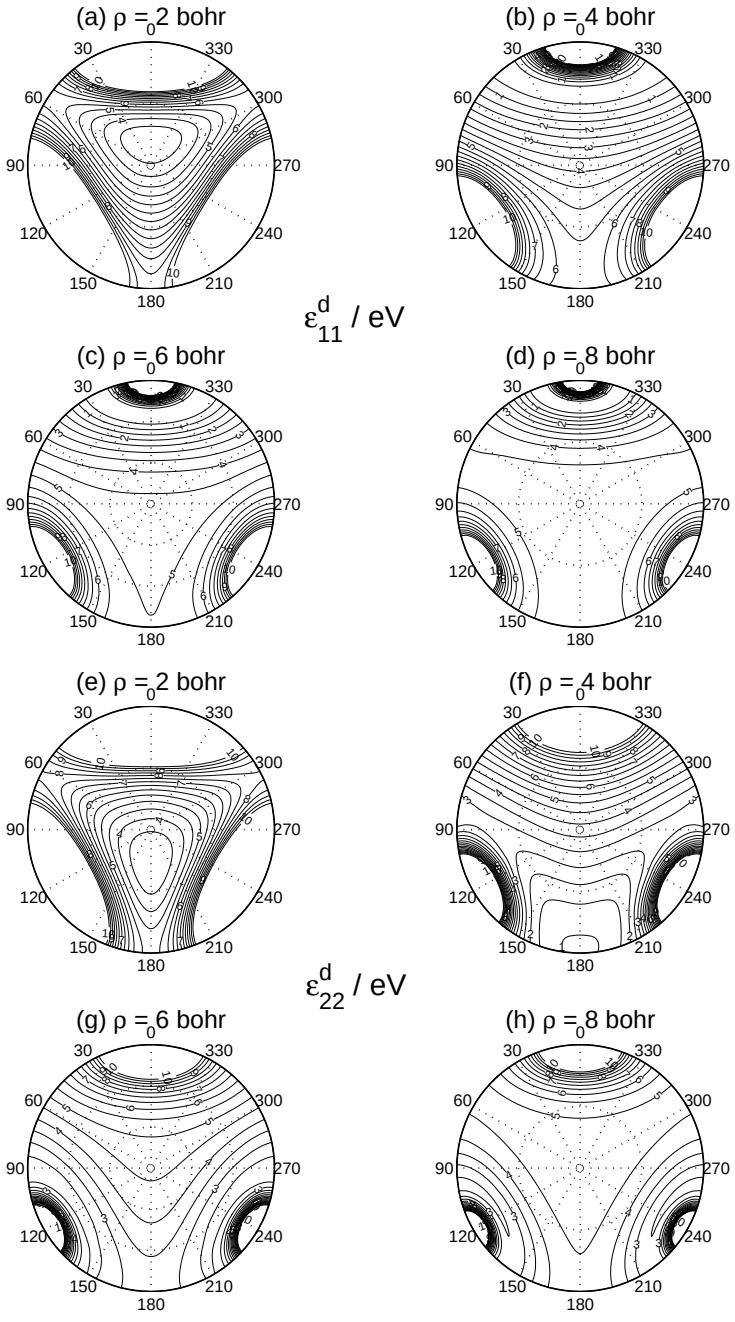
(a) ρ = 2 bohr
0
(b) ρ = 4 bohr
0
ε^d_11 / eV
(c) ρ = 6 bohr
0
(d) ρ = 8 bohr
0
(e) ρ = 2 bohr
0
(f) ρ = 4 bohr
0
ε^d_22 / eV
(g) ρ = 6 bohr
0
(h) ρ = 8 bohr
0
30
330
60
300
90
270
120
240
150
210
180

Figure 4.18:

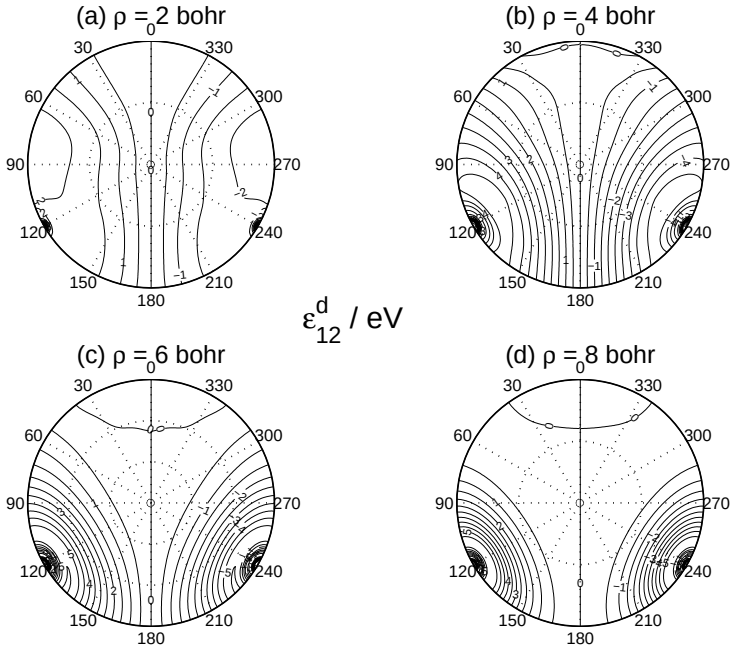

Figure 4.19:

Chapter 5 A two-electronic-state nonadiabatic quantum scattering formalism

5.1 Introduction

In most quantum descriptions of chemical reactions, the Born-Oppenheimer (BO) approximation [1] is invoked that restricts the motion of nuclei, during the course of the reaction, to a single electronically adiabatic state. Intersections (conical, parabolic or glancing) between neighboring adiabatic electronic states are very common in nature and nonadiabatic couplings between these states cannot be ignored in general. The past few years have witnessed a significant increase in theoretical interest aimed at understanding the nature of these nonadiabatic couplings and studying chemical reactions by invoking the Born-Huang (BH) expansion [2, 3] and using two or more degenerate electronic states to describe the reactions. A recent volume of *Advances in Chemical Physics* [4] deals with understanding the issues surrounding the role played by these degenerate electronic states in determining the mechanism and outcome of many chemical processes.

The presence of these degenerate electronic states is very common in polyatomic systems containing N atoms, where $N \geq 3$. A large majority of these states exhibit conical topologies in the internuclear geometric space in the vicinity of their degeneracies. Assuming the adiabatic electronic wave functions to be real, if the polyatomic system traverses a closed loop around a conical degeneracy in that geometric space, then the electronic wave function changes sign [5, 6]. This requires that the adiabatic nuclear wave functions also change sign to keep the total wave function single-valued

in the process inducing a geometric phase (GP) effect [7–9] into the system. This change of sign of the nuclear wave function, which is a special case of Berry's geometric phase [10], affects the nature of the solutions of the corresponding nuclear motion Schrödinger equation [11] and hence has important implications for the dynamics of the polyatomic system being considered.

The quantum-dynamical studies of chemical reactions on a single electronically adiabatic state have successfully covered triatomic [12–14] reactions over the last few decades and tetraatomic [15–17] reactions over the few years. In the last decade or so, these studies have included indirectly the effect of the first-excited adiabatic electronic state, that intersects conically with the ground state, by introducing the GP effect through appropriate boundary conditions on the adiabatic nuclear wave function corresponding to the ground electronic state [18–24]. The reaction rates (products of initial relative velocities by integral cross sections) for the D + H_2 reaction, obtained with the GP effect included [20], were in much better agreement with the experimental results [25–28] than those obtained with the GP effect excluded. Although the GP effect is certainly more pronounced at resonance energies [29], its importance for differential cross sections has been the topic of hot debate recently [23, 24].

Many studies have appeared in the last few years that include two or more excited electronic states and nonadiabatic couplings between them to study nonadiabatic behavior in chemical reactions. The effect of spin-orbit couplings on electronically nonadiabatic transitions has been demonstrated for many chemical systems [30–39]. The photodissociation of triatomic molecules like O_3 and H_2S has been studied on their conically intersecting potential energy surfaces (PESs) [40, 41]. The benchmark H + H_2 reaction has also been studied on its lowest two conically intersecting PESs, but only for total angular momentum quantum number $J = 0$ [42]. Most of these studies have been made possible due to the availability of realistic *ab initio* electronic PESs and their nonadiabatic couplings [43]. These nonadiabatic couplings have very interesting properties that have a forebearing on the behavior of molecular systems and are currently the topic of active interest [44]. The singular nature of these couplings at the

conical intersections of two adiabatic electronic states, introduces numerical difficulties in the solution of the corresponding coupled adiabatic nuclear motion Schrödinger equations. These difficulties can be circumvented by transforming the electronically adiabatic representation into a quasi-diabatic one [45–57], in which the nonadiabatic couplings still appear but are not singular.

In this chapter, we present a detailed two-electronic-state time-independent quantum reactive scattering formalism in both adiabatic and diabatic languages, to study the dynamics of a triatomic reaction. This approach, which has been briefly outlined elsewhere by us [58], is an extension of the one-electronic-state hyperspherical coupled-channel approach of Kuppermann and co-workers [18], used in the past for $H + H_2$ reaction and its isotopic variants with and without the inclusion of the GP effect [18–22]. A comparison of the cross sections obtained by this two-electronic-state formalism with the ones obtained using the one-electronic-state method is expected to provide for the first time an estimate of the energy range of validity of the one-electronic-state BO approximation. The first system that we plan to apply this formalism to is the prototypical $H + H_2$ reaction. Even though this simple reaction is the hydrogen atom of chemical reactions, it contains conically intersecting lowest two adiabatic electronic states that are degenerate for equilateral triangle geometries. This makes it an ideal case for the application of the formalism being presented for testing the validity of the BO approximation. Many *ab initio* PESs have appeared for its ground electronic state over the years [59–64]. Double many-body expansion (DMBE) analytical forms are available for its lowest two adiabatic electronic sheets [61] in addition to recent DMBE plus single polynomial (DSP) fits [65] to corresponding *ab initio* energies. Nonadiabatic first-derivative couplings and diabatic representations are also available in analytical [61] and fitted-*ab initio* [56,65] versions for H_3 system. Availability of lowest two adiabatic PESs, nonadiabatic couplings between them and a good diabatic representation [56] will facilitate the application of this formalism to $H + H_2$ reaction. The formalism being presented is a general one applicable to any triatomic reaction, but some details will be derived for the this

H_3 system utilising its symmetry with respect to the permutation of three identical nuclei.

A detailed review of the adiabatic and diabatic representations for polyatomic systems is given elsewhere [11, 58] and we will only mention the aspects needed for the discussion of the formalism. In Sec. 5.2, we introduce symmetrized hyperspherical coordinates for a triatomic system and the corresponding nuclear kinetic energy operator. In Sec. 5.3, we present in detail a method for solving the two-electronic-state version of the adiabatic nuclear motion Schrödinger equation with the GP effect included; since the GP effect needs to be built into the adiabatic language but not the diabatic one. In Sec. 5.4, we present its diabatic counterpart and discuss the various advantages and disadvantages of the two languages. Next chapter summarizes the work presented in the previous chapters along with the formalism discussed here.

5.2 Symmetrized hyperspherical coordinates

Consider a triatomic system with the three nuclei labelled A_α, A_β and A_γ. Let the arrangement channel $A_\lambda + A_\nu A_\kappa$ be called the λ arrangement channel, where $\lambda\nu\kappa$ is a cyclic permutation of $\alpha\beta\gamma$. After the separation of the center of mass coordinates, let $\mathbf{R}'_{\lambda_1}, \mathbf{R}'_{\lambda_2}$ be the Jacobi vectors associated with this arrangement channel λ, where $\mathbf{R}'_{\lambda_1}$ is the vector from A_ν to A_κ and $\mathbf{R}'_{\lambda_2}$ the vector from the center of mass of $A_\nu A_\kappa$ to A_λ. Let $\mathbf{R}_{\lambda_1}, \mathbf{R}_{\lambda_2}$ be the corresponding Delves mass-scaled coordinates [66, 67] defined by

$$\mathbf{R}_{\lambda_1} = \left(\frac{\mu_{\nu\kappa}}{\mu}\right)^{1/2} \mathbf{R}'_{\lambda_1} \qquad \text{and} \qquad \mathbf{R}_{\lambda_2} = \left(\frac{\mu_{\lambda,\nu\kappa}}{\mu}\right)^{1/2} \mathbf{R}'_{\lambda_2} \quad , \tag{5.1}$$

where $\mu_{\nu\kappa}$ is the reduced mass of $A_\nu A_\kappa$, $\mu_{\lambda,\nu\kappa}$ the reduced mass of the A_λ,$A_\nu A_\kappa$ pair, and μ the system's overall reduced mass given by

$$\mu = \left(\frac{m_\alpha m_\beta m_\gamma}{m_\alpha + m_\beta + m_\gamma}\right)^{1/2} \quad ,$$

m_λ being the mass of atom A_λ ($\lambda = \alpha, \beta, \gamma$). Let us define $\mathbf{R}_\lambda$ as the union of $\mathbf{R}_{\lambda_1}$ and $\mathbf{R}_{\lambda_2}$. So the nuclear motion kinetic energy operator in the six-dimensional $\mathbf{R}_\lambda$ space is given by

$$\widehat{T}_{nu}(\mathbf{R}_\lambda) = -\frac{\hbar^2}{2\mu}\nabla^2_{\mathbf{R}_\lambda} \tag{5.2}$$

So, the motion of the triatomic system in three-dimensional space gets replaced by that of a single particle of mass μ in a six-dimensional space.

It has been shown [68–73] that symmetrized hyperspherical body-fixed coordinates derived from $\mathbf{R}_\lambda$ are well suited for three-dimensional triatomic reactive scattering as these coordinates treat all three arrangement channels (λ, ν, κ) democratically. One frame of these hyperspherical coordinates include $\rho, \omega_\lambda, \gamma_\lambda$ [74, 75] besides the three Euler angles $(\delta_\lambda, \eta_\lambda, \zeta_\lambda)$, that rotate this body-fixed frame with respect to space-fixed one, and are given by

$$\rho = \left(R^2_{\lambda_1} + R^2_{\lambda_2}\right)^{1/2} \tag{5.3}$$

and

$$R_{\lambda_1} = \rho\ \sin(\omega_\lambda/2) \qquad R_{\lambda_2} = \rho\ \cos(\omega_\lambda/2) \qquad 0 \le \omega_\lambda \le \pi \tag{5.4}$$

where ρ is independent of the arrangement channel [66, 67].

The corresponding internal configuration space cartesian coordinates are defined by

$$\begin{aligned} X_\lambda &= \rho\ \sin\omega_\lambda\ \cos\gamma_\lambda \\ Y &= \rho\ \sin\omega_\lambda\ \sin\gamma_\lambda \\ Z_\lambda &= \rho\ \cos\omega_\lambda \end{aligned} \tag{5.5}$$

where γ_λ is the angle between $\mathbf{R}_{\lambda_1}$ and $\mathbf{R}_{\lambda_2}$ (or $\mathbf{R}'_{\lambda_1}$ and $\mathbf{R}'_{\lambda_2}$) in the 0 to π range and $\omega_\lambda, \gamma_\lambda$ are the polar angles of a point in this space. In an alternate internal configuration space frame, symmetrized hyperspherical coordinates θ, ϕ_λ are defined as the polar angles associated with the interchanged axes $\mathsf{O}\overline{X}_\lambda = \mathsf{O}Z_\lambda$, $\mathsf{O}\overline{Y}_\lambda = \mathsf{O}X_\lambda$,

and $\mathsf{O}\overline{Z}_\lambda = \mathsf{O}Y_\lambda$ for which

$$\begin{aligned} \overline{X}_\lambda &= Z_\lambda &&= \rho\ \sin\theta\ \cos\phi_\lambda \\ \overline{Y}_\lambda &= X_\lambda &&= \rho\ \sin\theta\ \sin\phi_\lambda \\ \overline{Z} &= Y &&= \rho\ \cos\theta \end{aligned} \tag{5.6}$$

The cartesian components of $\mathbf{R}_{\lambda_1}$ and $\mathbf{R}_{\lambda_2}$ in this body-fixed frame are given by

$$\begin{aligned} \mathbf{R}_{\lambda_1 X} &= -\rho\ \sin(\pi/4-\theta/2)\ \cos(\phi_\lambda/2) \\ \mathbf{R}_{\lambda_1 Y} &= 0 \\ \mathbf{R}_{\lambda_1 Z} &= \rho\ \cos(\pi/4-\theta/2)\ \sin(\phi_\lambda/2) \\ \mathbf{R}_{\lambda_2 X} &= \rho\ \sin(\pi/4-\theta/2)\ \sin(\phi_\lambda/2) \\ \mathbf{R}_{\lambda_2 Y} &= 0 \\ \mathbf{R}_{\lambda_2 Z} &= \rho\ \cos(\pi/4-\theta/2)\ \cos(\phi_\lambda/2) \end{aligned} \tag{5.7}$$

The coordinates ρ, θ and ϕ_λ are limited to the ranges

$$0 \le \rho < \infty \qquad 0 \le \theta \le \pi/2 \qquad 0 \le \phi_\lambda < 2\pi \tag{5.8}$$

The hyperangles θ and ϕ_λ describe the shape of the molecular triangle. Besides, $\theta = 0$ corresponds to symmetric top geometries and $\theta = \pi/2$ to collinear ones. The relation between θ, ϕ_λ and $\omega_\lambda, \gamma_\lambda$ is (using Eqs. (5.5) and (5.6))

$$\begin{aligned} \sin\theta\ \cos\phi_\lambda &= \cos\omega_\lambda \\ \sin\theta\ \sin\phi_\lambda &= \sin\omega_\lambda\ \cos\gamma_\lambda \\ \cos\theta &= \sin\omega_\lambda\ \sin\gamma_\lambda \end{aligned} \tag{5.9}$$

Let $Gx^{I\lambda}y^I z^{I\lambda}$ be a body-fixed frame $I\lambda$, whose axes are the principal axes of inertia of the three nuclei and whose Euler angles with respect to the space-fixed frame $Gx^{sf}y^{sf}z^{sf}$ are $a_\lambda, b_\lambda, c_\lambda$ with G being the center of mass of the three nuclei. The senses of these axes are chosen to result in a one-to-one correspondence between $\rho, \theta, \phi_\lambda, a_\lambda, b_\lambda, c_\lambda$ coordinates and the space-fixed cartesian coordinates of $\mathbf{R}_{\lambda_1}$ and

$\mathbf{R}_{\lambda_2}$. In addition, the $I\lambda$ axes are labelled so as to order the corresponding principal moments of inertia according to

$$I_z^\lambda \leq I_x^\lambda \leq I_y \tag{5.10}$$

Furthermore, let Υ_λ refer collectively to the five hyperangles $(\theta, \phi_\lambda, a_\lambda, b_\lambda, c_\lambda)$, $\mathbf{q}_\lambda$ to the three internal coordinates $(\rho, \theta, \phi_\lambda)$ and $\mathbf{R}_\lambda$ to all six hyperspherical coordinates.

The coordinates ρ, Υ_λ are called the principal axes of inertia symmetrized hyperspherical coordinates. They are very suitable for describing nuclear motion in the strong interaction regions as for any value of λ they treat these regions equally and basis sets based on them are very efficient. The nuclear kinetic energy operator in these coordinates is given by

$$\widehat{T}_{nu}(\mathbf{R}_\lambda) = -\frac{\hbar^2}{2\mu}\nabla^2_{\mathbf{R}_\lambda} = \widehat{T}_\rho(\rho) + \frac{\hat{\Lambda}^2(\Upsilon_\lambda)}{2\mu\rho^2} \tag{5.11}$$

where $\widehat{T}_\rho(\rho)$ is the hyperradial kinetic energy operator

$$\widehat{T}_\rho(\rho) = -\frac{\hbar^2}{2\mu}\frac{1}{\rho^5}\frac{\partial}{\partial\rho}\rho^5\frac{\partial}{\partial\rho} \tag{5.12}$$

and $\hat{\Lambda}^2(\Upsilon_\lambda)$ is the grand canonical angular momentum operator

$$\begin{aligned}
\hat{\Lambda}^2(\Upsilon_\lambda) \;=\; & \hat{\Lambda}^2_{\mathrm{o}}(\theta,\phi_\lambda) + \frac{4\hat{J}_z^{I\lambda^2}}{\cos^2\theta} \\
& + \frac{2}{1+\sin\theta}\left[\frac{\hat{J}^2 - \hat{J}_z^{I\lambda^2}}{2} + \frac{\hat{J}_+^{I\lambda^2} + \hat{J}_-^{I\lambda^2}}{4} - \hat{J}_z^{I\lambda^2}\right] \\
& + \frac{1}{\sin^2\theta}\left[\frac{\hat{J}^2 - \hat{J}_z^{I\lambda^2}}{2} - \frac{\hat{J}_+^{I\lambda^2} + \hat{J}_-^{I\lambda^2}}{4}\right] \\
& - 2\hbar\frac{\cos\theta}{\sin^2\theta}\left(\hat{J}_+^{I\lambda} - \hat{J}_-^{I\lambda}\right)\frac{\partial}{\partial\phi_\lambda}
\end{aligned} \tag{5.13}$$

where

$$\hat{\Lambda}^2_{\mathrm{o}}(\theta,\phi_\lambda) = -4\hbar^2\left(\frac{1}{\sin 2\theta}\frac{\partial}{\partial\theta}\sin 2\theta\frac{\partial}{\partial\theta} + \frac{1}{\sin^2\theta}\frac{\partial^2}{\partial\phi_\lambda^2}\right) \tag{5.14}$$

and

$$\hat{J}^{I\lambda}_{\pm} = \hat{J}^{I\lambda}_{x} \pm i\hat{J}^{I\lambda}_{y} \tag{5.15}$$

$\hat{J}^{I\lambda}_{x}$, $\hat{J}^{I\lambda}_{y}$ and $\hat{J}^{I\lambda}_{z}$ are the components of the total orbital angular momentum $\hat{\mathbf{J}}$ of the nuclei in the $I\lambda$ frame. The Euler angles $a_\lambda, b_\lambda, c_\lambda$ appear only in the $\hat{J}^2$, $\hat{J}^{I\lambda}_{z}$ and $\hat{J}^{I\lambda}_{\pm}$ angular momentum operators. We do not need their explicit expressions in terms of the partial derivatives of those Euler angles because we use Wigner rotation functions to expand our nuclear wave functions and the results of the effect of those operators on these rotation functions is analytically known [76]. This expansion is considered in the next section in detail.

The use of ρ, Υ_λ coordinates becomes inefficient for large values of ρ where the interaction between λ, ν, and κ arrangement channels becomes very weak. In these regions, the coordinates ρ and Ξ_λ, where $\Xi_\lambda \equiv (\omega_\lambda, \gamma_\lambda, \delta_\lambda, \eta_\lambda, \zeta_\lambda)$, have been used because it has been shown [70, 71] that basis sets based on these coordinates are very efficient. In this body-fixed Jacobi frame called bfλ, $\hat{\Lambda}^2(\Upsilon_\lambda)$ the grand canonical angular momentum operator mentioned above is given by

$$\hat{\Lambda}^2(\Xi_\lambda) = \hat{L}^2(\omega_\lambda) + \frac{\hat{j}^2_\lambda}{\sin^2\omega_\lambda} + \frac{\hat{l}^2_\lambda}{\cos^2\omega_\lambda} \tag{5.16}$$

where

$$\hat{L}^2(\omega_\lambda) = -4\hbar^2 \frac{1}{\sin^2\omega_\lambda}\frac{\partial}{\partial\omega_\lambda}\sin^2\omega_\lambda\frac{\partial}{\partial\omega_\lambda} \tag{5.17}$$

and $\hat{j}^2_\lambda$ and $\hat{l}^2_\lambda$ are the angular momentum operators corresponding to $\mathbf{R}_{\lambda_1}$ and $\mathbf{R}_{\lambda_2}$ respectively. The angular momenta associated with these operators are related to the total orbital angular momentum $\hat{\mathbf{J}}$ of the nuclei by

$$\hat{\mathbf{J}} = \hat{\mathbf{j}} + \hat{\mathbf{l}} \tag{5.18}$$

It is convenient to express $\hat{\Lambda}^2(\Xi_\lambda)$ in terms of $\partial/\partial\gamma_\lambda$ and $\hat{\mathbf{J}}$ instead of $\hat{\mathbf{j}}$ and $\hat{\mathbf{l}}$ using

their properties as

$$\begin{aligned}\hat{\Lambda}^2(\Xi_\lambda) &= \hat{L}^2(\omega_\lambda) + \frac{4}{\sin^2\omega_\lambda}\left[-\frac{\hbar^2}{\sin\gamma_\lambda}\frac{\partial}{\partial\gamma_\lambda}\sin\gamma_\lambda\frac{\partial}{\partial\gamma_\lambda} + \frac{1}{\sin^2\gamma_\lambda}\hat{J}_z^{\mathrm{bf}\lambda^2}\right] \\ &+ \frac{1}{\cos^2(\omega_\lambda/2)}\left\{\hat{J}^2 - 2\hat{J}_z^{\mathrm{bf}\lambda^2} + \left[\cot\gamma_\lambda\hat{J}_z^{\mathrm{bf}\lambda} - \hbar\left(\cot\gamma_\lambda + \frac{\partial}{\partial\gamma_\lambda}\right)\right]\hat{J}_-^{\mathrm{bf}\lambda}\right. \\ &+ \left.\left[\cot\gamma_\lambda\hat{J}_z^{\mathrm{bf}\lambda} + \hbar\left(\cot\gamma_\lambda + \frac{\partial}{\partial\gamma_\lambda}\right)\right]\hat{J}_+^{\mathrm{bf}\lambda}\right\} \qquad (5.19)\end{aligned}$$

where

$$\hat{J}_\pm^{\mathrm{bf}\lambda} = \hat{J}_x^{\mathrm{bf}\lambda} \pm \mathrm{i}\hat{J}_y^{\mathrm{bf}\lambda} \qquad (5.20)$$

$\hat{J}_x^{\mathrm{bf}\lambda}$, $\hat{J}_y^{\mathrm{bf}\lambda}$ and $\hat{J}_z^{\mathrm{bf}\lambda}$ are the components of $\hat{\mathbf{J}}$ in the bfλ frame. This Eq. (5.19) is used in place of Eq. (5.16) because the Euler angles $\delta_\lambda, \eta_\lambda, \zeta_\lambda$ of the bfλ frame appear only in $\hat{J}^2$, $\hat{J}_z^{\mathrm{bf}\lambda}$ and $\hat{J}_\pm^{\mathrm{bf}\lambda}$ and the action of these operators on the previously mentioned Wigner rotation functions are analytically known [76].

5.3 Adiabatic formalism

In a two-electronic-state approximation of the Born-Huang [2, 3] representation for a triatomic system involving electronically adiabatic states 1 (ground state) and 2 (first-excited state), system's total wave function is written as

$$\Psi^{\mathrm{O}}(\mathbf{r}, \mathbf{R}_\lambda) = \chi_1^{ad}(\mathbf{R}_\lambda)\psi_1^{el,ad}(\mathbf{r}; \mathbf{q}_\lambda) + \chi_2^{ad}(\mathbf{R}_\lambda)\psi_2^{el,ad}(\mathbf{r}; \mathbf{q}_\lambda) \qquad (5.21)$$

where $\mathbf{r}$ and $\mathbf{R}_\lambda$ are respectively the electronic and nuclear coordinates of the triatomic arrangement channel λ [11]. $\psi_1^{el,ad}(\mathbf{r}; \mathbf{q}_\lambda)$ and $\psi_2^{el,ad}(\mathbf{r}; \mathbf{q}_\lambda)$ are the adiabatic electronic wave functions satisfying the electronic Schrödinger equation

$$\widehat{H}^{el}(\mathbf{r}; \mathbf{q}_\lambda)\psi_n^{el,ad}(\mathbf{r}; \mathbf{q}_\lambda) = \varepsilon_n^{ad}(\mathbf{q}_\lambda)\psi_n^{el,ad}(\mathbf{r}; \mathbf{q}_\lambda) \qquad n = 1, 2 \qquad (5.22)$$

and $\chi_n^{ad}(\mathbf{R}_\lambda)$ $(n = 1, 2)$ are the corresponding adiabatic nuclear wave functions. $\varepsilon_n^{ad}(\mathbf{R}_\lambda)$ $(n = 1, 2)$ are the electronically adiabatic potential energy surfaces (PESs)

corresponding to the ground ($n = 1$) and first-excited ($n = 2$) adiabatic electronic states. If these surfaces exhibit a single conical intersection and the $\psi_n^{el,ad}$ are required to be real, then according to the geometric phase (GP) theorem [5–10],

$$\psi_n^{el,ad}(\mathbf{r};\mathbf{q}_\lambda) \rightarrow -\psi_n^{el,ad}(\mathbf{r};\mathbf{q}_\lambda) \qquad n = 1,2 \tag{5.23}$$

and

$$\chi_n^{ad}(\mathbf{R}_\lambda) \rightarrow -\chi_n^{ad}(\mathbf{R}_\lambda) \qquad n = 1,2 \tag{5.24}$$

when the polyatomic system traverses a closed loop in nuclear configuration space $\mathcal{Q}$ around that conical intersection (a so called pseudorotation). As a result, the nuclear wave functions $\chi_n^{ad}(\mathbf{R}_\lambda)$ are not single-valued functions of $\mathbf{R}_\lambda$, but behave in a way to make the total electro-nuclear wave function single-valued.

Let us define $\boldsymbol{\chi}^{ad}(\mathbf{R}_\lambda)$ as a two-dimensional column vector whose components are $\chi_1^{ad}(\mathbf{R}_\lambda)$ and $\chi_2^{ad}(\mathbf{R}_\lambda)$ such that

$$\boldsymbol{\chi}^{ad}(\mathbf{R}_\lambda) = \begin{pmatrix} \chi_1^{ad}(\mathbf{R}_\lambda) \\ \chi_2^{ad}(\mathbf{R}_\lambda) \end{pmatrix} \tag{5.25}$$

The Schrödinger equation satisfied by $\boldsymbol{\chi}^{ad}(\mathbf{R}_\lambda)$ is

$$\left[-\frac{\hbar^2}{2\mu}\left\{\mathbf{I}\nabla^2_{\mathbf{R}_\lambda} + 2\mathbf{W}^{(1)ad}(\mathbf{q}_\lambda)\cdot\boldsymbol{\nabla}_{\mathbf{R}_\lambda} + \mathbf{W}^{(2)ad}(\mathbf{q}_\lambda)\right\} + \left\{\boldsymbol{\varepsilon}^{ad}(\mathbf{q}_\lambda) - E\mathbf{I}\right\}\right]\boldsymbol{\chi}^{ad}(\mathbf{R}_\lambda) = \mathbf{0} \tag{5.26}$$

where $\mathbf{q}_\lambda$ represents the subset $\rho, \theta, \phi_\lambda$ of the six-dimensional set $\mathbf{R}_\lambda$ of nuclear coordinates. $\mathbf{I}$, $\mathbf{W}^{(1)ad}(\mathbf{q}_\lambda)$, $\mathbf{W}^{(2)ad}(\mathbf{q}_\lambda)$, and $\boldsymbol{\varepsilon}^{ad}(\mathbf{q}_\lambda)$ are 2×2 matrices and $\boldsymbol{\nabla}_{\mathbf{R}_\lambda}$ is a gradient operator in the six-dimensional nuclear configuration space mentioned earlier. $\mathbf{I}$ is the identity matrix and $\boldsymbol{\varepsilon}^{ad}(\mathbf{q}_\lambda)$ is the diagonal matrix whose diagonal elements are the PESs ε_1^{ad} and ε_2^{ad} mentioned earlier. The matrices $\mathbf{W}^{(1)ad}(\mathbf{q}_\lambda)$ and $\mathbf{W}^{(2)ad}(\mathbf{q}_\lambda)$ are the the first- and second-derivative [11, 43, 77–82] 2×2 coupling matrices whose elements

are defined by

$$\left.\begin{aligned} \mathbf{W}^{(1)ad}_{m,n}(\mathbf{q}_\lambda) &= \langle \psi^{el,ad}_m(\mathbf{r};\mathbf{q}_\lambda) \mid \boldsymbol{\nabla}_{\mathbf{R}_\lambda} \psi^{el,ad}_n(\mathbf{r};\mathbf{q}_\lambda)\rangle_{\mathbf{r}} \\ \mathrm{W}^{(2)ad}_{m,n}(\mathbf{q}_\lambda) &= \langle \psi^{el,ad}_m(\mathbf{r};\mathbf{q}_\lambda) \mid \nabla^2_{\mathbf{R}_\lambda} \psi^{el,ad}_n(\mathbf{r};\mathbf{q}_\lambda)\rangle_{\mathbf{r}} \end{aligned}\right\} m,n = 1,2 \tag{5.27}$$

and are respectively three-dimensional vectors ($\mathbf{W}^{(1)ad}_{m,n}(\mathbf{q}_\lambda)$) [56] and scalars ($\mathrm{W}^{(2)ad}_{m,n}(\mathbf{q}_\lambda)$). The matrix $\mathbf{W}^{(1)ad}(\mathbf{q}_\lambda)$ is in general skew-hermitian and, due to the requirement that electronic wave functions $\psi^{el,ad}_n(\mathbf{r};\mathbf{q}_\lambda)$ be real, is real and skew-symmetric and can be written as

$$\mathbf{W}^{(1)ad}(\mathbf{q}_\lambda) = \begin{pmatrix} 0 & \mathbf{W}^{(1)ad}_{1,2}(\mathbf{q}_\lambda) \\ -\mathbf{W}^{(1)ad}_{1,2}(\mathbf{q}_\lambda) & 0 \end{pmatrix} \tag{5.28}$$

We can now write Eq. (5.26) in explicit form as

$$\begin{aligned} \Bigg[-\tfrac{\hbar^2}{2\mu} \Bigg\{ \begin{pmatrix} 1 & 0 \\ 0 & 1 \end{pmatrix} \nabla^2_{\mathbf{R}_\lambda} + 2\mathbf{W}^{(1)ad}_{1,2}(\mathbf{q}_\lambda) \begin{pmatrix} 0 & 1 \\ -1 & 0 \end{pmatrix} \cdot \boldsymbol{\nabla}_{\mathbf{R}_\lambda} + \begin{pmatrix} \mathrm{W}^{(2)ad}_{1,1}(\mathbf{q}_\lambda) & \mathrm{W}^{(2)ad}_{1,2}(\mathbf{q}_\lambda) \\ \mathrm{W}^{(2)ad}_{2,1}(\mathbf{q}_\lambda) & \mathrm{W}^{(2)ad}_{2,2}(\mathbf{q}_\lambda) \end{pmatrix} \Bigg\} \\ + \Bigg\{ \begin{pmatrix} \varepsilon^{ad}_1(\mathbf{q}_\lambda) & 0 \\ 0 & \varepsilon^{ad}_2(\mathbf{q}_\lambda) \end{pmatrix} - E \begin{pmatrix} 1 & 0 \\ 0 & 1 \end{pmatrix} \Bigg\} \Bigg] \begin{pmatrix} \chi^{ad}_1(\mathbf{R}_\lambda) \\ \chi^{ad}_2(\mathbf{R}_\lambda) \end{pmatrix} = \begin{pmatrix} 0 & 0 \\ 0 & 0 \end{pmatrix} \end{aligned} \tag{5.29}$$

In this two-electronic-state adiabatic nuclear motion Schrödinger equation, the nuclear wave functions corresponding to ground ($\chi^{ad}_1(\mathbf{R}_\lambda)$) and first-excited ($\chi^{ad}_2(\mathbf{R}_\lambda)$) adiabatic electronic states are coupled by two terms: one containing the first-derivative coupling vector $\mathbf{W}^{(1)ad}_{1,2}(\mathbf{q}_\lambda)$ and the other containing the second-derivative coupling elements $\mathrm{W}^{(2)ad}_{1,2}(\mathbf{q}_\lambda)$ and $\mathrm{W}^{(2)ad}_{2,1}(\mathbf{q}_\lambda)$. Depending on the total energy of the system, these nonadiabatic coupling terms can allow the nuclei to sample the first-excited electronic state during the course of the reaction and affect its mechanism and final outcome. It should be stressed that the effect of the geometric phase (if present) on Eqs. (5.29) must be added by either appropriate boundary conditions [11, 18] or the introduction of an appropriate vector potential [8, 11, 83]. It is interesting to point

out that in one-electronic-state BO approximation, Eq. (5.29) reduces to

$$\left[-\frac{\hbar^2}{2\mu}\left\{\nabla^2_{\mathbf{R}_\lambda}+\mathrm{W}^{(2)ad}_{1,1}(\mathbf{q}_\lambda)\right\}+\left\{\varepsilon^{ad}_1(\mathbf{q}_\lambda)-E\right\}\right]\chi^{ad}_1(\mathbf{R}_\lambda)=0 \tag{5.30}$$

This equation contains a second-derivative self-coupling term $\mathrm{W}^{(2)ad}_{1,1}(\mathbf{q}_\lambda)$ which is generally assumed to be small and dropped in all one-electronic-state dynamical calculations. Only recently has any interest been shown in studying the effect of this term on dynamical properties of molecules. This term appears as an additive term in Eq. (5.30), and even though small it can alter the PESs of reactive systems by tens or even hundreds of wavenumbers [84]. It can become especially important when trying to predict dynamical phenomenon that can be verified experimentally.

5.3.1 Partial wave expansion

We can rewrite the adiabatic two-electronic-state nuclear motion Schrödinger equation [Eq. (5.26)] as

$$\left[-\frac{\hbar^2}{2\mu}\left\{\mathbf{I}\nabla^2_{\mathbf{R}_\lambda}+2\mathbf{W}^{(1)ad}(\mathbf{q}_\lambda)\cdot\boldsymbol{\nabla}_{\mathbf{R}_\lambda}\right\}+\left\{\overline{\boldsymbol{\varepsilon}}^{ad}(\mathbf{q}_\lambda)-E\mathbf{I}\right\}\right]\boldsymbol{\chi}^{ad}(\mathbf{R}_\lambda)=\mathbf{0} \tag{5.31}$$

where we have added the second-derivative coupling matrix $\mathbf{W}^{(2)ad}$, which is just an additive term, to the adiabatic energy matrix $\boldsymbol{\varepsilon}^{ad}(\mathbf{q}_\lambda)$ using

$$\overline{\boldsymbol{\varepsilon}}^{ad}(\mathbf{q}_\lambda)=\boldsymbol{\varepsilon}^{ad}(\mathbf{q}_\lambda)-\frac{\hbar^2}{2\mu}\mathbf{W}^{(2)ad}(\mathbf{q}_\lambda)=\begin{pmatrix}\overline{\varepsilon}^{ad}_{11}(\mathbf{q}_\lambda) & \overline{\varepsilon}^{ad}_{12}(\mathbf{q}_\lambda)\\ \overline{\varepsilon}^{ad}_{21}(\mathbf{q}_\lambda) & \overline{\varepsilon}^{ad}_{22}(\mathbf{q}_\lambda)\end{pmatrix} \tag{5.32}$$

where

$$\begin{aligned}
\overline{\varepsilon}^{ad}_{11}(\mathbf{q}_\lambda) &= \varepsilon^{ad}_1(\mathbf{q}_\lambda)-\tfrac{\hbar^2}{2\mu}\mathbf{W}^{(2)ad}_{11}(\mathbf{q}_\lambda)\\
\overline{\varepsilon}^{ad}_{12}(\mathbf{q}_\lambda) &= -\tfrac{\hbar^2}{2\mu}\mathbf{W}^{(2)ad}_{12}(\mathbf{q}_\lambda)\\
\overline{\varepsilon}^{ad}_{21}(\mathbf{q}_\lambda) &= -\tfrac{\hbar^2}{2\mu}\mathbf{W}^{(2)ad}_{21}(\mathbf{q}_\lambda)\\
\overline{\varepsilon}^{ad}_{22}(\mathbf{q}_\lambda) &= \varepsilon^{ad}_2(\mathbf{q}_\lambda)-\tfrac{\hbar^2}{2\mu}\mathbf{W}^{(2)ad}_{22}(\mathbf{q}_\lambda)
\end{aligned} \tag{5.33}$$

The two adiabatic nuclear wave functions $\chi^{ad}_1(\mathbf{R}_\lambda)$ and $\chi^{ad}_2(\mathbf{R}_\lambda)$, which are the

components of the column vector $\boldsymbol{\chi}^{ad}(\mathbf{R}_\lambda)$ (see Eq. 5.25), can be expressed as linear combinations of auxiliary nuclear wave functions $\chi_1^{ad,JM\Pi\Gamma}(\mathbf{R}_\lambda)$ and $\chi_2^{ad,JM\Pi\Gamma}(\mathbf{R}_\lambda)$, respectively as

$$\begin{pmatrix} \chi_1^{ad}(\mathbf{R}_\lambda) \\ \chi_2^{ad}(\mathbf{R}_\lambda) \end{pmatrix} = \sum_{J=0}^{\infty} \sum_{M=-J}^{M=J} C_\lambda^{JM} \sum_{\Pi=0}^{1} \sum_{\Gamma} \begin{pmatrix} \chi_1^{ad,JM\Pi\Gamma}(\mathbf{R}_\lambda) \\ \chi_2^{ad,JM\Pi\Gamma}(\mathbf{R}_\lambda) \end{pmatrix} \tag{5.34}$$

If $\chi_1^{ad,JM\Pi\Gamma}(\mathbf{R}_\lambda)$ and $\chi_2^{ad,JM\Pi\Gamma}(\mathbf{R}_\lambda)$ are defined as components of the column vector $\boldsymbol{\chi}^{ad,JM\Pi\Gamma}(\mathbf{R}_\lambda)$, then we can write Eq. (5.34) as

$$\boldsymbol{\chi}^{ad}(\mathbf{R}_\lambda) = \sum_{J=0}^{\infty} \sum_{M=-J}^{M=J} C_\lambda^{JM} \sum_{\Pi=0}^{1} \sum_{\Gamma} \boldsymbol{\chi}^{ad,JM\Pi\Gamma}(\mathbf{R}_\lambda) \tag{5.35}$$

The linear combinations are referred to as partial wave expansions and the individual wave functions $\chi_1^{ad,JM\Pi\Gamma}(\mathbf{R}_\lambda)$ and $\chi_2^{ad,JM\Pi\Gamma}(\mathbf{R}_\lambda)$ are referred to as partial waves. $\boldsymbol{\chi}^{ad,JM\Pi\Gamma}$ is a simultaneous eigenfunction of the adiabatic nuclear motion Hamiltonian matrix $\widehat{\mathbf{H}}^{ad}(\mathbf{R}_\lambda)$ given by

$$\widehat{\mathbf{H}}^{ad}(\mathbf{R}_\lambda) = \left[-\frac{\hbar^2}{2\mu} \left\{ \mathbf{I} \nabla^2_{\mathbf{R}_\lambda} + 2\mathbf{W}^{(1)ad}(\mathbf{q}_\lambda) \cdot \boldsymbol{\nabla}_{\mathbf{R}_\lambda} \right\} + \overline{\boldsymbol{\varepsilon}}^{ad}(\mathbf{q}_\lambda) \right], \tag{5.36}$$

of the square of the total nuclear orbital angular momentum $\hat{\mathbf{J}}$, of its space-fixed z-component $\hat{\mathbf{J}}_z$ and of the inversion operator $\hat{I}$ of the nuclei through their center of mass according to the expressions

$$\begin{aligned} \widehat{\mathbf{H}}^{ad}\boldsymbol{\chi}^{ad,JM\Pi\Gamma} &= E\boldsymbol{\chi}^{ad,JM\Pi\Gamma} \\ \hat{J}^2\boldsymbol{\chi}^{ad,JM\Pi\Gamma} &= J(J+1)\hbar^2\boldsymbol{\chi}^{ad,JM\Pi\Gamma} \\ \hat{J}_z\boldsymbol{\chi}^{ad,JM\Pi\Gamma} &= M\hbar\boldsymbol{\chi}^{ad,JM\Pi\Gamma} \\ \hat{I}\boldsymbol{\chi}^{ad,JM\Pi\Gamma} &= (-1)^{\Pi}\boldsymbol{\chi}^{ad,JM\Pi\Gamma} \end{aligned} \tag{5.37}$$

In these equations, J and M are quantum numbers associated with the angular momentum operators $\hat{J}^2$ and $\hat{J}_z$, respectively. $\Pi = 0,\ 1$ is a parity quantum number that specifies the symmetry or antisymmetry of the $\boldsymbol{\chi}^{ad,JM\Pi\Gamma}(\mathbf{R}_\lambda)$ column vector

with respect to the inversion of the nuclei through their center of mass. Note that the same parity quantum number Π appears for $\chi_1^{ad,JM\Pi\Gamma}(\mathbf{R}_\lambda)$ and $\chi_2^{ad,JM\Pi\Gamma}(\mathbf{R}_\lambda)$ in Eq. (5.34). Also, the same irreducible representation symbol Γ in these two components of $\boldsymbol{\chi}^{ad,JM\Pi\Gamma}(\mathbf{R}_\lambda)$ appears. This does not mean that these adiabatic nuclear wave functions transform according to the irreducible representation Γ. Its meaning instead is as follows. The electronuclear Hamiltonian of the system is invariant under the group of permutations of identical $A_\lambda A_\nu A_\kappa$ atoms. For A_3 it is the P_3 group, for A_2B it is the P_2 group and for three distinct atoms ABC it is the trivial identity group. As a result, the $\Psi^{\mathrm{O}}(\mathbf{r},\mathbf{R}_\lambda)$ that appears in Eq. (5.21) must transform according to an irreducible representation Γ of the corresponding permutation group. The superscript Γ signifies that the transformation properties of $\boldsymbol{\chi}^{ad,JM\Pi\Gamma}$ are such that when taken together with the transformation properties of $\boldsymbol{\psi}^{el,ad}(\mathbf{r};\mathbf{q}_\lambda)$, they make $\Psi^{\mathrm{O}}(\mathbf{r},\mathbf{R}_\lambda)$ belong to Γ. The separate factors $\chi_i^{ad,JM\Pi\Gamma}$ and $\psi_i^{el,ad}(\mathbf{r};\mathbf{q}_\lambda)$ may not individually belong to Γ but their product does. In addition, it is important to stress that this adiabatic nuclear wave function vector $\boldsymbol{\chi}^{ad,JM\Pi\Gamma}(\mathbf{R}_\lambda)$ may not be single-valued, due to the GP effect mentioned in the introduction. We will use this boundary condition to chose appropriate basis functions, in the absence or presence of the conical intersection, for the expansion of the nuclear wave functions as will be discussed next. The procedure mentioned next will be applied to H_3 system as an example to obtain Π,Γ basis sets in the next section.

As mentioned in Sec. 5.2, we will use ρ,Υ_λ coordinates in the strong interaction region and ρ,Ξ_λ in the weak interaction and asymptotic regions. For the following discussion, we will refer to the five-dimensional Υ_λ set or the Ξ_λ set of coordinates using the symbol ξ_λ. Let us now expand the two nuclear motion partial waves $\chi_1^{ad,JM\Pi\Gamma}$ and $\chi_2^{ad,JM\Pi\Gamma}$ according to the following column vector equation

$$\begin{pmatrix} \chi_1^{ad,JM\Pi\Gamma,\mathbf{n}'_\lambda\Omega'_\lambda}(\rho,\xi_\lambda) \\ \chi_2^{ad,JM\Pi\Gamma,\mathbf{n}'_\lambda\Omega'_\lambda}(\rho,\xi_\lambda) \end{pmatrix} = \rho^{-5/2}\sum_{\Omega_\lambda} D^{J\Pi}_{M\Omega_\lambda}(\xi_\lambda^{(1)}) \begin{pmatrix} \sum_{n_{1_\lambda}} b^{ad,J\Pi\Gamma\mathbf{n}'_\lambda\Omega'_\lambda}_{1,n_{1_\lambda},\Omega_\lambda}(\rho;\bar{\rho})\Phi^{ad,\Pi\Gamma}_{1,n_{1_\lambda},\Omega_\lambda}(\xi_\lambda^{(2)};\bar{\rho}) \\ \sum_{n_{2_\lambda}} b^{ad,J\Pi\Gamma\mathbf{n}'_\lambda\Omega'_\lambda}_{2,n_{2_\lambda},\Omega_\lambda}(\rho;\bar{\rho})\Phi^{ad,\Pi\Gamma}_{2,n_{2_\lambda},\Omega_\lambda}(\xi_\lambda^{(2)};\bar{\rho}) \end{pmatrix} \tag{5.38}$$

where $\xi_\lambda^{(1)}$ refers to one of the two sets of three Euler angles and $\xi_\lambda^{(2)}$ refers to one

of the two sets of two hyperangles (θ, ϕ_λ) or $(\omega_\lambda, \gamma_\lambda)$. Ω_λ is the absolute magnitude of the quantum number for the projection of the total angular momentum onto the body-fixed $Gz^{I\lambda}$ axis, such that

$$\begin{aligned} \Omega_\lambda &= 0, 1, ..., J \qquad \text{for} \quad J+\Pi \quad \text{even} \\ &= 1, 2, ..., J \qquad \text{for} \quad J+\Pi \quad \text{odd} \end{aligned} \tag{5.39}$$

Furthermore, the $D^{J\Pi}_{M\Omega_\lambda}(\xi^{(1)}_\lambda)$ are the parity-symmetrized Wigner rotation functions defined as [18]

$$D^{J\Pi}_{M\Omega_\lambda}(\xi^{(1)}_\lambda) = \left\{ \frac{2J+1}{16\pi^2[1+(-1)^{J+\Pi}\delta_{\Omega_\lambda,0}]} \right\}^{1/2} \left[D^J_{M\Omega_\lambda}(\xi^{(1)}_\lambda) + (-1)^{J+\Pi+\Omega_\lambda} D^J_{M,-\Omega_\lambda}(\xi^{(1)}_\lambda) \right] \tag{5.40}$$

where $D^J_{M\Omega_\lambda}(\xi^{(1)}_\lambda)$ is a Wigner rotation function of the Euler angles $\xi^{(1)}_\lambda$ [76]. The symmetrized Wigner functions have been orthonormalized according to

$$\int D^{J'\Pi'}_{M'\Omega'_\lambda}(\xi^{(1)}_\lambda) D^{J\Pi}_{M\Omega_\lambda}(\xi^{(1)}_\lambda) d\tau = \delta^{J'\Pi'M'\Omega'_\lambda}_{J\Pi M\Omega_\lambda} \tag{5.41}$$

where $d\tau$ is the volume element for the Euler angles $\xi^{(1)}_\lambda$.

In Eq. (5.38), $\Phi^{ad,\Pi\Gamma}_{1,n_{1_\lambda},\Omega_\lambda}(\xi^{(2)}_\lambda;\bar{\rho})$ and $\Phi^{ad,\Pi\Gamma}_{2,n_{2_\lambda},\Omega_\lambda}(\xi^{(2)}_\lambda;\bar{\rho})$ are the adiabatic two-dimensional local hyperspherical surface functions (LHSFs) that depend parametrically on $\bar{\rho}$ and are defined as the eigenfunctions of an adiabatic reference Hamiltonian matrix $\hat{\mathbf{h}}^{\Omega_\lambda}_{ad}(\xi^{(2)}_\lambda;\bar{\rho})$. This matrix can be chosen to be block diagonal, i.e.,

$$\hat{\mathbf{h}}^{\Omega_\lambda}_{ad}(\xi^{(2)}_\lambda;\bar{\rho}) = \frac{\hat{\Lambda}^2_1(\xi^{(2)}_\lambda)}{2\mu\bar{\rho}^2} \begin{pmatrix} 1 & 0 \\ 0 & 1 \end{pmatrix} + \begin{pmatrix} \overline{\varepsilon}^{ad}_{11}(\bar{\rho},\xi^{(2)}_\lambda) & 0 \\ 0 & \overline{\varepsilon}^{ad}_{22}(\bar{\rho},\xi^{(2)}_\lambda) \end{pmatrix} \tag{5.42}$$

or have the off-diagonal nonadiabatic couplings built in, i.e.,

$$\hat{\mathbf{h}}^{\Omega_\lambda}_{ad}(\xi^{(2)}_\lambda;\bar{\rho}) = \frac{\hat{\Lambda}^2_1(\xi^{(2)}_\lambda)}{2\mu\bar{\rho}^2} \begin{pmatrix} 1 & 0 \\ 0 & 1 \end{pmatrix} + \begin{pmatrix} \overline{\varepsilon}^{ad}_{11}(\bar{\rho},\xi^{(2)}_\lambda) & \overline{\varepsilon}^{ad}_{12}(\bar{\rho},\xi^{(2)}_\lambda) \\ \overline{\varepsilon}^{ad}_{21}(\bar{\rho},\xi^{(2)}_\lambda) & \overline{\varepsilon}^{ad}_{22}(\bar{\rho},\xi^{(2)}_\lambda) \end{pmatrix} \tag{5.43}$$

In Eqs. (5.42) and (5.43), $\hat{\Lambda}^2(\xi_\lambda^{(2)})$ refers to

$$\begin{aligned}\hat{\Lambda}_1^2(\theta,\phi_\lambda) &= \hat{\Lambda}_o^2(\theta,\phi_\lambda)+\frac{4\Omega_\lambda^2\hbar^2}{\cos^2\theta}\\ &= -4\hbar^2\left(\frac{1}{\sin 2\theta}\frac{\partial}{\partial\theta}\sin 2\theta\frac{\partial}{\partial\theta}+\frac{1}{\sin^2\theta}\frac{\partial^2}{\partial\phi_\lambda^2}\right)+\frac{4\Omega_\lambda^2\hbar^2}{\cos^2\theta} \qquad (5.44)\end{aligned}$$

in the strong interaction region of the potential or to

$$\begin{aligned}\hat{\Lambda}_1^2(\omega_\lambda,\gamma_\lambda) &= \hat{L}^2(\omega_\lambda)+\frac{4}{\sin^2\omega_\lambda}\left[\frac{-\hbar^2}{\sin\gamma_\lambda}\frac{\partial}{\partial\gamma_\lambda}\sin\gamma_\lambda\frac{\partial}{\partial\gamma_\lambda}+\frac{\Omega_\lambda^2\hbar^2}{\sin^2\gamma_\lambda}\right] \qquad (5.45)\\ &= -4\hbar^2\frac{1}{\sin^2\omega_\lambda}\frac{\partial}{\partial\omega_\lambda}\sin^2\omega_\lambda\frac{\partial}{\partial\omega_\lambda}+\frac{4}{\sin^2\omega_\lambda}\left[\frac{-\hbar^2}{\sin\gamma_\lambda}\frac{\partial}{\partial\gamma_\lambda}\sin\gamma_\lambda\frac{\partial}{\partial\gamma_\lambda}+\frac{\Omega_\lambda^2\hbar^2}{\sin^2\gamma_\lambda}\right]\end{aligned}$$

in the weak interaction and asymptotic regions [18, 72].

For the $\hat{\mathbf{h}}_{ad}^{\Omega_\lambda}(\xi_\lambda^{(2)};\bar{\rho})$ matrix in Eq. (5.42), $\Phi_{1,n_{1_\lambda},\Omega_\lambda}^{ad,\Pi\Gamma}(\xi_\lambda^{(2)};\bar{\rho})$ and $\Phi_{2,n_{2_\lambda},\Omega_\lambda}^{ad,\Pi\Gamma}(\xi_\lambda^{(2)};\bar{\rho})$ are solutions of uncoupled second-order partial differential equations, whereas for the $\hat{\mathbf{h}}_{ad}^{\Omega_\lambda}(\xi_\lambda^{(2)};\bar{\rho})$ matrix in Eq. (5.43), they are solutions of coupled differential equations and therefore their calculation requires a larger computational effort than to obtain the former. Since, however, that reference Hamiltonian matrix is independent of the total energy E of the system, the LHSFs need to be evaluated only once whereas the resulting scattering equations given by Eq. (5.71) (derived later on) must be solved for many values of E. As the off-diagonal couplings are built into Eq. (5.43), a smaller number of the corresponding LHSFs will be needed for convergence of the solutions of the scattering equations, as opposed to the ones resulting from Eq. (5.42), which don't have these terms built in. Given the fact that the computational effort for solving those scattering scattering equations scales with the cube of the number of LHSFs used, it is desirable to use LHSFs obtained from Eq. (5.43) rather than Eq. (5.42).

With either of these adiabatic reference Hamiltonians, the LHSFs satisfy the eigenvalue equation

$$\hat{\mathbf{h}}_{ad}^{\Omega_\lambda}(\xi_\lambda^{(2)};\bar{\rho})\begin{pmatrix}\Phi_{1,n_{1_\lambda},\Omega_\lambda}^{ad,\Pi\Gamma}(\xi_\lambda^{(2)};\bar{\rho})\\ \Phi_{2,n_{2_\lambda},\Omega_\lambda}^{ad,\Pi\Gamma}(\xi_\lambda^{(2)};\bar{\rho})\end{pmatrix}=\begin{pmatrix}\epsilon_{1,n_{1_\lambda},\Omega_\lambda}^{ad,\Pi\Gamma}(\bar{\rho})\Phi_{1,n_{1_\lambda},\Omega_\lambda}^{ad,\Pi\Gamma}(\xi_\lambda^{(2)};\bar{\rho})\\ \epsilon_{2,n_{2_\lambda},\Omega_\lambda}^{ad,\Pi\Gamma}(\bar{\rho})\Phi_{2,n_{2_\lambda},\Omega_\lambda}^{ad,\Pi\Gamma}(\xi_\lambda^{(2)};\bar{\rho})\end{pmatrix} \qquad (5.46)$$

The adiabatic LHSFs are not allowed to diverge anywhere on the half-sphere of fixed radius $\bar{\rho}$. This boundary condition furnishes the quantum numbers n_{1_λ} and n_{2_λ}, each of which is two-dimensional since the reference Hamiltonian $\hat{\mathbf{h}}_{ad}^{\Omega_\lambda}$ has two angular degrees of freedom. The superscripts $\mathbf{n}'_\lambda, \Omega'_\lambda$ in Eq. (5.38), with $\mathbf{n}'_\lambda$ referring to the union of n'_{1_λ} and n'_{2_λ}, indicate that the number of linearly independent solutions of Eqs. (5.37) is equal to the number of adiabatic LHSFs used in the expansions of Eq. (5.38).

In the strong interaction region, the adiabatic functions $\Phi^{ad,\Pi\Gamma}_{i,n_{i_\lambda},\Omega_\lambda}(\theta,\phi_\lambda;\bar{\rho})$, $(i = 1,2)$, which are eigenfunctions of the reference Hamiltonian given by Eqs. (5.42) or (5.43) and Eq. (5.44), are obtained by expanding them in a body-fixed basis $\overline{\Phi}^{ad,\Pi\Gamma}_{i,n_{i_\lambda},\Omega_\lambda}(\theta,\phi_\lambda)$ constructed from direct products of simple analytical functions [18,72]

$$\overline{\Phi}^{ad,\Pi\Gamma}_{i,n_{i_\lambda},\Omega_\lambda}(\theta,\phi_\lambda) = f^{\Omega_\lambda}_{n_{i\theta_\lambda},n_{i\phi_\lambda}}(\theta)\; g^{ad,\Pi\Gamma}_{i,n_{i\phi_\lambda}\Omega_\lambda}(\phi_\lambda) \tag{5.47}$$

where $n_{i_\lambda} \equiv (n_{i\theta_\lambda}, n_{i\phi_\lambda})$. $g^{ad,\Pi\Gamma}_{i,n_{i\phi_\lambda}\Omega_\lambda}$ are chosen to be simple trigonometric functions of ϕ_λ and $f^{\Omega_\lambda}_{n_{i\theta_\lambda},n_{i\phi_\lambda}}$ are chosen as Jacobi polynomials in $\cos 2\theta$, such that the resulting adiabatic nuclear wave functions transform under the operations of the permutation symmetry group of identical atoms in the way described after Eqs. (5.37). Eqs. (5.46) are then transformed into an algebraic eigenvalue eigenvector equation involving the coefficients of these expansions, which is solved numerically by linear algebra methods. Appendix 5.A describes the procedure to obtain trigonometric functions in ϕ_λ needed to obtain adiabatic electronuclear functions with P_3 permutation symmetries, in the presence and absence of the conical intersection, which correspond to different boundary conditions.

The reference Hamiltonian in the strong interaction region given by Eqs. (5.42) and (5.44) contains the kinetic energy operator piece $\hat{\Lambda}_1^2(\theta,\phi_\lambda)$, which has singularities at $\theta = 0$ (symmetric top geometries) and at $\theta = \pi/2$ (collinear geometries). The full Hamiltonian given by Eqs. (5.36), (5.11) and (5.13) contains the $\hat{\Lambda}^2(\theta,\phi_\lambda,a_\lambda,b_\lambda,c_\lambda)$ part that also shows similar singularities at $\theta = 0$ and $\theta = \pi/2$. The choice of

Jacobi polynomials for $f^{\Omega_\lambda}_{n_{i\theta_\lambda},n_{i\phi_\lambda}}$ mentioned above for expanding the adiabatic surface functions should in principle be a good one as it will make the adiabatic surface functions and hence the nuclear wave functions behave properly at those singularities. In reality, it is not a good choice for the singularity at $\theta = 0$, if $n_{i\phi_\lambda} = 0$ is an allowed value. Since we have built the second-derivative couplings, that diverge at this value of θ as $1/\sin^2\theta$, into the reference Hamiltonian given by Eqs. (5.42) or (5.43), the abovementioned choice of Jacobi polynomials still might turn out to be appropriate. This remains to be tested. An alternate approach to solve this problem is to replace the reference Hamiltonian by one that contains the full $\hat{\Lambda}^2(\theta, \phi_\lambda, a_\lambda, b_\lambda, c_\lambda)$ operator and the associated hyperspherical harmonics, which have been obtained recently for tetraatomic [85] and triatomic systems [86].

In the weak interaction region, where the coordinates $(\rho, \omega_\lambda, \gamma_\lambda)$ of Eq. (5.5) are used, the adiabatic LHSFs $\Phi^{ad,\Pi\Gamma}_{i,n_{i_\lambda},\Omega_\lambda}(\omega_\lambda, \gamma_\lambda; \bar{\rho})$, $(i = 1, 2)$ are eigenfunctions of the reference Hamiltonian given by Eqs. (5.42) or (5.43) and Eq. (5.46). These weak interaction region LHSFs are expanded in a body-fixed basis $\overline{\Phi}^{ad,\Pi\Gamma}_{i,n_{i_\lambda},\Omega_\lambda}(\omega_\lambda, \gamma_\lambda)$ constructed from the direct product of special functions

$$\overline{\Phi}^{ad,\Pi\Gamma}_{i,n_{i_\lambda},\Omega_\lambda}(\omega_\lambda, \gamma_\lambda) = f^{\Omega_\lambda}_{n_{i\gamma_\lambda}}(\gamma_\lambda) g^{ad,\Pi\Gamma}_{i,n_{i\omega_\lambda},\Omega_\lambda}(\omega_\lambda) \tag{5.48}$$

where $f^{\Omega_\lambda}_{n_{i\gamma_\lambda}}(\gamma_\lambda)$ are the associated Legendre functions of $\cos\gamma_\lambda$ and $g^{ad,\Pi\Gamma}_{i,n_{i\omega_\lambda},\Omega_\lambda}(\omega_\lambda)$ are a set of functions of ω_λ determined by the numerical solution of a one-dimensional eigenfunction equation in ω_λ using Gegenbauer polynomials [87] in $\cos\omega_\lambda$. The $\hat{\Lambda}^2_1(\omega_\lambda, \gamma_\lambda)$ operator in Eq. (5.46) has singularities at $\omega_\lambda = 0$ and $\omega_\lambda = \pi$. The Gegenbauer polynomials are well behaved at $\omega_\lambda = 0$ and the $\omega_\lambda = \pi$ region is not accessible in the weak interaction region. The $\gamma_\lambda = 0$ and $\gamma_\lambda = \pi$ singularities don't affect the LHSFs either, as the abovementioned associated Legendre functions of $\cos\gamma_\lambda$ are well behaved at these nuclear configurations.

Once the adiabatic LHSFs are known, they provide the basis of functions in terms of which the expansion in Eq. (5.38) is defined. The adiabatic nuclear wave function column vector of that equation is then inserted into the first equation of Eqs. (5.37)

to yield

$$\widehat{\mathbf{H}}^{ad}\sum_{\Omega_\lambda} D^{J\Pi}_{M\Omega_\lambda}(\xi^{(1)}_\lambda)\begin{pmatrix} \sum_{n_{1_\lambda}} b^{ad,J\Pi\Gamma\mathbf{n}'_\lambda\Omega'_\lambda}_{1,n_{1_\lambda},\Omega_\lambda}(\rho;\bar{\rho})\Phi^{ad,\Pi\Gamma}_{1,n_{1_\lambda},\Omega_\lambda}(\xi^{(2)}_\lambda;\bar{\rho}) \\ \sum_{n_{2_\lambda}} b^{ad,J\Pi\Gamma\mathbf{n}'_\lambda\Omega'_\lambda}_{2,n_{2_\lambda},\Omega_\lambda}(\rho;\bar{\rho})\Phi^{ad,\Pi\Gamma}_{2,n_{2_\lambda},\Omega_\lambda}(\xi^{(2)}_\lambda;\bar{\rho}) \end{pmatrix} = E\sum_{\Omega_\lambda} D^{J\Pi}_{M\Omega_\lambda}(\xi^{(1)}_\lambda)\begin{pmatrix} \sum_{n_{1_\lambda}} b^{ad,J\Pi\Gamma\mathbf{n}'_\lambda\Omega'_\lambda}_{1,n_{1_\lambda},\Omega_\lambda}(\rho;\bar{\rho})\Phi^{ad,\Pi\Gamma}_{1,n_{1_\lambda},\Omega_\lambda}(\xi^{(2)}_\lambda;\bar{\rho}) \\ \sum_{n_{2_\lambda}} b^{ad,J\Pi\Gamma\mathbf{n}'_\lambda\Omega'_\lambda}_{2,n_{2_\lambda},\Omega_\lambda}(\rho;\bar{\rho})\Phi^{ad,\Pi\Gamma}_{2,n_{2_\lambda},\Omega_\lambda}(\xi^{(2)}_\lambda;\bar{\rho}) \end{pmatrix} \tag{5.49}$$

where $\widehat{\mathbf{H}}^{ad}$ is the adiabatic Hamiltonian matrix operator of Eq. (5.36). Use of the orthonormality of the symmetrized Wigner functions [Eq. (5.41)] and integration over the two-dimensional adiabatic LHSFs in θ, ϕ_λ hyperangles for the strong interaction region yields a set of coupled hyperradial second-order ordinary differential equations (also called coupled-channel equations) in the coefficients $b^{ad,J\Pi\Gamma\mathbf{n}'_\lambda\Omega'_\lambda}_{1,n_{1_\lambda},\Omega_\lambda}(\rho;\bar{\rho})$ and $b^{ad,J\Pi\Gamma\mathbf{n}'_\lambda\Omega'_\lambda}_{2,n_{2_\lambda},\Omega_\lambda}(\rho;\bar{\rho})$ given by

$$\begin{aligned}
&\left[-\tfrac{\hbar^2}{2\mu}\begin{pmatrix}1&0\\0&1\end{pmatrix}\tfrac{\partial^2}{\partial\rho^2}+\begin{pmatrix}\mathcal{A}^{ad,\Pi\Gamma,\Omega_\lambda}_{11,n_{1_\lambda}}(\rho;\bar{\rho})&0\\0&\mathcal{A}^{ad,\Pi\Gamma,\Omega_\lambda}_{22,n_{2_\lambda}}(\rho;\bar{\rho})\end{pmatrix}\right]\begin{pmatrix} b^{ad,J\Pi\Gamma\mathbf{n}'_\lambda\Omega'_\lambda}_{1,n_{1_\lambda},\Omega_\lambda}(\rho;\bar{\rho}) \\ b^{ad,J\Pi\Gamma\mathbf{n}'_\lambda\Omega'_\lambda}_{2,n_{2_\lambda},\Omega_\lambda}(\rho;\bar{\rho})\end{pmatrix} \\
&+\begin{pmatrix} \sum_{n'_{1_\lambda}}\left[\mathcal{B}^{ad,\Pi\Gamma,\Omega_\lambda}_{11,n_{1_\lambda},n'_{1_\lambda}}(\rho;\bar{\rho})+\mathcal{C}^{ad,\Pi\Gamma,\Omega_\lambda}_{11,n_{1_\lambda},n'_{1_\lambda}}(\rho;\bar{\rho})\right] b^{ad,J\Pi\Gamma\mathbf{n}'_\lambda\Omega'_\lambda}_{1,n'_{1_\lambda},\Omega_\lambda}(\rho;\bar{\rho}) \\ \sum_{n'_{2_\lambda}}\left[\mathcal{B}^{ad,\Pi\Gamma,\Omega_\lambda}_{22,n_{2_\lambda},n'_{2_\lambda}}(\rho;\bar{\rho})+\mathcal{C}^{ad,\Pi\Gamma,\Omega_\lambda}_{22,n_{2_\lambda},n'_{2_\lambda}}(\rho;\bar{\rho})\right] b^{ad,J\Pi\Gamma\mathbf{n}'_\lambda\Omega'_\lambda}_{2,n'_{2_\lambda},\Omega_\lambda}(\rho;\bar{\rho})\end{pmatrix} \\
&+\begin{pmatrix} \sum_{n'_{1_\lambda}}\left[\mathcal{D}^{ad,\Pi\Gamma,\Omega_\lambda}_{11,n_{1_\lambda},n'_{1_\lambda},\Omega_\lambda\pm1}(\rho;\bar{\rho})b^{ad,J\Pi\Gamma\mathbf{n}'_\lambda\Omega'_\lambda}_{1,n'_{1_\lambda},\Omega_\lambda\pm1}(\rho;\bar{\rho})+\mathcal{E}^{ad,\Pi\Gamma,\Omega_\lambda}_{11,n_{1_\lambda},n'_{1_\lambda},\Omega_\lambda\pm2}(\rho;\bar{\rho})b^{ad,J\Pi\Gamma\mathbf{n}'_\lambda\Omega'_\lambda}_{1,n'_{1_\lambda},\Omega_\lambda\pm2}(\rho;\bar{\rho})\right] \\ \sum_{n'_{2_\lambda}}\left[\mathcal{D}^{ad,\Pi\Gamma,\Omega_\lambda}_{22,n_{2_\lambda},n'_{2_\lambda},\Omega_\lambda\pm1}(\rho;\bar{\rho})b^{ad,J\Pi\Gamma\mathbf{n}'_\lambda\Omega'_\lambda}_{2,n'_{2_\lambda},\Omega_\lambda\pm1}(\rho;\bar{\rho})+\mathcal{E}^{ad,\Pi\Gamma,\Omega_\lambda}_{22,n_{2_\lambda},n'_{2_\lambda},\Omega_\lambda\pm2}(\rho;\bar{\rho})b^{ad,J\Pi\Gamma\mathbf{n}'_\lambda\Omega'_\lambda}_{2,n'_{2_\lambda},\Omega_\lambda\pm2}(\rho;\bar{\rho})\right]\end{pmatrix} \\
&+\begin{pmatrix} \sum_{n'_{2_\lambda}}\left[\mathcal{F}^{ad,\Pi\Gamma,\Omega_\lambda}_{12,n_{1_\lambda},n'_{2_\lambda}}(\rho;\bar{\rho})b^{ad,J\Pi\Gamma\mathbf{n}'_\lambda\Omega'_\lambda}_{2,n'_{2_\lambda},\Omega_\lambda}(\rho;\bar{\rho})+\mathcal{G}^{ad,\Pi\Gamma,\Omega_\lambda}_{12,n_{1_\lambda},n'_{2_\lambda},\Omega_\lambda\pm1}(\rho;\bar{\rho})b^{ad,J\Pi\Gamma\mathbf{n}'_\lambda\Omega'_\lambda}_{2,n'_{2_\lambda},\Omega_\lambda\pm1}(\rho;\bar{\rho})\right] \\ -\sum_{n'_{1_\lambda}}\left[\mathcal{F}^{ad,\Pi\Gamma,\Omega_\lambda}_{21,n_{2_\lambda},n'_{1_\lambda}}(\rho;\bar{\rho})b^{ad,J\Pi\Gamma\mathbf{n}'_\lambda\Omega'_\lambda}_{1,n'_{1_\lambda},\Omega_\lambda}(\rho;\bar{\rho})+\mathcal{G}^{ad,\Pi\Gamma,\Omega_\lambda}_{21,n_{2_\lambda},n'_{1_\lambda},\Omega_\lambda\pm1}(\rho;\bar{\rho})b^{ad,J\Pi\Gamma\mathbf{n}'_\lambda\Omega'_\lambda}_{1,n'_{1_\lambda},\Omega_\lambda\pm1}(\rho;\bar{\rho})\right]\end{pmatrix} \\
&+\begin{pmatrix} \sum_{n'_{1_\lambda}}\mathcal{H}^{ad,\Pi\Gamma,\Omega_\lambda}_{11,n_{1_\lambda},n'_{1_\lambda}}(\rho;\bar{\rho})b^{ad,J\Pi\Gamma\mathbf{n}'_\lambda\Omega'_\lambda}_{1,n'_{1_\lambda},\Omega_\lambda}(\rho;\bar{\rho})+\sum_{n'_{2_\lambda}}\mathcal{H}^{ad,\Pi\Gamma,\Omega_\lambda}_{12,n_{1_\lambda},n'_{2_\lambda}}(\rho;\bar{\rho})b^{ad,J\Pi\Gamma\mathbf{n}'_\lambda\Omega'_\lambda}_{2,n'_{2_\lambda},\Omega_\lambda}(\rho;\bar{\rho}) \\ \sum_{n'_{1_\lambda}}\mathcal{H}^{ad,\Pi\Gamma,\Omega_\lambda}_{21,n_{2_\lambda},n'_{1_\lambda}}(\rho;\bar{\rho})b^{ad,J\Pi\Gamma\mathbf{n}'_\lambda\Omega'_\lambda}_{1,n'_{1_\lambda},\Omega_\lambda}(\rho;\bar{\rho})+\sum_{n'_{2_\lambda}}\mathcal{H}^{ad,\Pi\Gamma,\Omega_\lambda}_{22,n_{2_\lambda},n'_{2_\lambda}}(\rho;\bar{\rho})b^{ad,J\Pi\Gamma\mathbf{n}'_\lambda\Omega'_\lambda}_{2,n'_{2_\lambda},\Omega_\lambda}(\rho;\bar{\rho})\end{pmatrix} \\
&+\begin{pmatrix} \sum_{n'_{2_\lambda}}\mathcal{J}^{ad,\Pi\Gamma,\Omega_\lambda}_{12,n_{1_\lambda},n'_{2_\lambda}}(\rho;\bar{\rho})\partial b^{ad,J\Pi\Gamma\mathbf{n}'_\lambda\Omega'_\lambda}_{2,n'_{2_\lambda},\Omega_\lambda}(\rho;\bar{\rho})/\partial\rho \\ -\sum_{n'_{1_\lambda}}\mathcal{J}^{ad,\Pi\Gamma,\Omega_\lambda}_{21,n_{2_\lambda},n'_{1_\lambda}}(\rho;\bar{\rho})\partial b^{ad,J\Pi\Gamma\mathbf{n}'_\lambda\Omega'_\lambda}_{1,n'_{1_\lambda},\Omega_\lambda}(\rho;\bar{\rho})/\partial\rho\end{pmatrix} = E\begin{pmatrix} b^{ad,J\Pi\Gamma\mathbf{n}'_\lambda\Omega'_\lambda}_{1,n_{1_\lambda},\Omega_\lambda}(\rho;\bar{\rho}) \\ b^{ad,J\Pi\Gamma\mathbf{n}'_\lambda\Omega'_\lambda}_{2,n_{2_\lambda},\Omega_\lambda}(\rho;\bar{\rho})\end{pmatrix}
\end{aligned} \tag{5.50}$$

where for $i,j = 1,2$ and in θ,ϕ_λ coordinates denoting $\Phi^{ad,\Pi\Gamma}_{i,n_{i_\lambda},\Omega_\lambda}(\theta,\phi_\lambda;\bar{\rho})$ simply as $\Phi^{ad,\Pi\Gamma}_{i,n_{i_\lambda},\Omega_\lambda}$,

$$\mathcal{A}^{ad,\Pi\Gamma,\Omega_\lambda}_{i,n_{i_\lambda}}(\rho;\bar{\rho}) = \frac{15\hbar^2}{8\mu\rho^2} + \frac{\overline{\rho}^2}{\rho^2}\epsilon^{ad,\Pi\Gamma}_{i,n_{i_\lambda},\Omega_\lambda}(\bar{\rho}) \tag{5.51}$$

$$\mathcal{B}^{ad,\Pi\Gamma,\Omega_\lambda}_{ii,n_{i_\lambda},n'_{i_\lambda}}(\rho;\bar{\rho}) = \langle\Phi^{ad,\Pi\Gamma}_{i,n_{i_\lambda},\Omega_\lambda}|\varepsilon^{ad}_i(\rho,\theta,\phi_\lambda) - \frac{\overline{\rho}^2}{\rho^2}\varepsilon^{ad}_i(\bar{\rho},\theta,\phi_\lambda)|\Phi^{ad,\Pi\Gamma}_{i,n'_{i_\lambda},\Omega_\lambda}\rangle \tag{5.52}$$

$$\begin{aligned}\mathcal{C}^{ad,\Pi\Gamma,\Omega_\lambda}_{ii,n_{i_\lambda},n'_{i_\lambda}}(\rho;\bar{\rho}) = \tfrac{\hbar^2}{2\mu\rho^2}\Big[&J(J+1)\langle\Phi^{ad,\Pi\Gamma}_{i,n_{i_\lambda},\Omega_\lambda}|\left(\tfrac{1}{1+\sin\theta}+\tfrac{1}{2\sin^2\theta}\right)|\Phi^{ad,\Pi\Gamma}_{i,n'_{i_\lambda},\Omega_\lambda}\rangle\\ &-{\Omega_\lambda}^2\langle\Phi^{ad,\Pi\Gamma}_{i,n_{i_\lambda},\Omega_\lambda}|\left(\tfrac{3}{1+\sin\theta}+\tfrac{1}{2\sin^2\theta}\right)|\Phi^{ad,\Pi\Gamma}_{i,n'_{i_\lambda},\Omega_\lambda}\rangle\Big]\end{aligned} \tag{5.53}$$

$$\begin{aligned}\mathcal{D}^{ad,\Pi\Gamma,\Omega_\lambda}_{ii,n_{i_\lambda},n'_{i_\lambda},\Omega_\lambda\pm1}(\rho;\bar{\rho}) = \tfrac{\hbar^2}{\mu\rho^2}\Big[&-\zeta_+(J,\Omega_\lambda)\tfrac{N_{J,\Omega_\lambda+1}}{N_{J,\Omega_\lambda}}\langle\Phi^{ad,\Pi\Gamma}_{i,n_{i_\lambda},\Omega_\lambda}|\tfrac{\cos\theta}{\sin^2\theta}|\partial\Phi^{ad,\Pi\Gamma}_{i,n'_{i_\lambda},\Omega_\lambda+1}/\partial\phi_\lambda\rangle\\ &+\zeta_-(J,\Omega_\lambda)\tfrac{N_{J,\Omega_\lambda-1}}{N_{J,\Omega_\lambda}}\langle\Phi^{ad,\Pi\Gamma}_{i,n_{i_\lambda},\Omega_\lambda}|\tfrac{\cos\theta}{\sin^2\theta}|\partial\Phi^{ad,\Pi\Gamma}_{i,n'_{i_\lambda},\Omega_\lambda-1}/\partial\phi_\lambda\rangle\Big]\end{aligned} \tag{5.54}$$

$$\begin{aligned}\mathcal{E}^{ad,\Pi\Gamma,\Omega_\lambda}_{ii,n_{i_\lambda},n'_{i_\lambda},\Omega_\lambda\pm2}(\rho;\bar{\rho}) = \tfrac{\hbar^2}{4\mu\rho^2}\Big[&\zeta_+(J,\Omega_\lambda)\zeta_+(J,\Omega_\lambda+1)\tfrac{N_{J,\Omega_\lambda+2}}{N_{J,\Omega_\lambda}}\langle\Phi^{ad,\Pi\Gamma}_{i,n_{i_\lambda},\Omega_\lambda}|\tfrac{1}{1+\sin\theta}-\tfrac{1}{2\sin^2\theta}|\Phi^{ad,\Pi\Gamma}_{i,n'_{i_\lambda},\Omega_\lambda+2}\rangle\\ &+\zeta_-(J,\Omega_\lambda)\zeta_-(J,\Omega_\lambda-1)\tfrac{N_{J,\Omega_\lambda-2}}{N_{J,\Omega_\lambda}}\langle\Phi^{ad,\Pi\Gamma}_{i,n_{i_\lambda},\Omega_\lambda}|\tfrac{1}{1+\sin\theta}-\tfrac{1}{2\sin^2\theta}|\Phi^{ad,\Pi\Gamma}_{i,n'_{i_\lambda},\Omega_\lambda-2}\rangle\Big]\end{aligned} \tag{5.55}$$

$$\mathcal{F}^{ad,\Pi\Gamma,\Omega_\lambda}_{ij,n_{i_\lambda},n'_{j_\lambda},\Omega_\lambda\pm2}(\rho;\bar{\rho}) = -\frac{\hbar^2}{\mu}\langle\Phi^{ad,\Pi\Gamma}_{i,n_{i_\lambda},\Omega_\lambda}|\widehat{W}^{ad(1)}_{1,2}(\rho,\theta,\phi_\lambda)|\Phi^{ad,\Pi\Gamma}_{j,n'_{j_\lambda},\Omega_\lambda}\rangle \tag{5.56}$$

$$\begin{aligned}\mathcal{G}^{ad,\Pi\Gamma,\Omega_\lambda}_{ij,n_{i_\lambda},n'_{j_\lambda},\Omega_\lambda\pm1}(\rho;\bar{\rho}) = \tfrac{\hbar^2}{\mu\rho}\Big[&\zeta_+(J,\Omega_\lambda)\tfrac{N_{J,\Omega_\lambda+1}}{N_{J,\Omega_\lambda}}\langle\Phi^{ad,\Pi\Gamma}_{i,n_{i_\lambda},\Omega_\lambda}|\cot\theta\ \mathrm{W}^{ad(1)}_{1,2,\phi_\lambda}(\mathbf{q}_\lambda)|\Phi^{ad,\Pi\Gamma}_{j,n'_{j_\lambda},\Omega_\lambda+1}\rangle\\ &-\zeta_-(J,\Omega_\lambda)\tfrac{N_{J,\Omega_\lambda-1}}{N_{J,\Omega_\lambda}}\langle\Phi^{ad,\Pi\Gamma}_{i,n_{i_\lambda},\Omega_\lambda}|\cot\theta\ \mathrm{W}^{ad(1)}_{1,2,\phi_\lambda}(\mathbf{q}_\lambda)|\Phi^{ad,\Pi\Gamma}_{j,n'_{j_\lambda},\Omega_\lambda-1}\rangle\Big]\end{aligned} \tag{5.57}$$

$$\mathcal{H}^{ad,\Pi\Gamma,\Omega_\lambda}_{ij,n_{i_\lambda},n'_{j_\lambda}}(\rho;\bar{\rho}) = -\frac{\hbar^2}{2\mu}\langle\Phi^{ad,\Pi\Gamma}_{i,n_{i_\lambda},\Omega_\lambda}|\mathrm{W}^{ad(2)}_{i,j}(\rho,\theta,\phi_\lambda)|\Phi^{ad,\Pi\Gamma}_{j,n'_{j_\lambda},\Omega_\lambda}\rangle \tag{5.58}$$

$$\mathcal{J}^{ad,\Pi\Gamma,\Omega_\lambda}_{ij,n_{i_\lambda},n'_{j_\lambda}}(\rho;\bar{\rho}) = -\frac{\hbar^2}{\mu}\langle\Phi^{ad,\Pi\Gamma}_{i,n_{i_\lambda},\Omega_\lambda}|\mathrm{W}^{ad(1)}_{1,2,\rho}(\rho,\theta,\phi_\lambda)|\Phi^{ad,\Pi\Gamma}_{j,n'_{j_\lambda},\Omega_\lambda}\rangle \tag{5.59}$$

In Eq. (5.56), $\widehat{W}^{ad(1)}_{1,2}(\rho,\theta,\phi_\lambda)$ is the operator defined as

$$\widehat{W}^{ad(1)}_{1,2}(\rho,\theta,\phi_\lambda) = -\frac{5}{2\rho}\mathrm{W}_{1,2,\rho}(\rho,\theta,\phi_\lambda)+\frac{1}{\rho}\mathrm{W}^{ad(1)}_{1,2,\theta}(\rho,\theta,\phi_\lambda)\frac{\partial}{\partial\theta}+\frac{1}{\rho\sin\theta}\mathrm{W}^{ad(1)}_{1,2,\phi_\lambda}(\rho,\theta,\phi_\lambda)\frac{\partial}{\partial\phi_\lambda} \tag{5.60}$$

In this equation, $\mathrm{W}^{(ad(1)}_{1,2,\rho}$, $\mathrm{W}^{ad(1)}_{1,2,\theta}$ and $\mathrm{W}^{ad(1)}_{1,2,\phi_\lambda}$ are the ρ, θ and ϕ_λ components of the first-derivative coupling vector $\mathbf{W}^{ad(1)}_{1,2}$ [65]. In Eqs. (5.54), (5.55) and (5.57), N_{J,Ω_λ} is the normalization constant of Eq. (5.40), and $\zeta_\pm(J,\Omega_\lambda)$ are coupling constants given

by

$$\zeta_{\pm}(J,\Omega_\lambda) = [J(J+1) - \Omega_\lambda(\Omega_\lambda \pm 1)]^{1/2} \tag{5.61}$$

We can follow the same procedure for the weak interaction region by integrating over the two-dimensional adiabatic LHSFs in $\omega_\lambda, \gamma_\lambda$ hyperangles to obtain the corresponding coupled-channel equations in the coefficients $b^{ad,J\Pi\Gamma\mathbf{n}'_\lambda\Omega'_\lambda}_{1,n_{1_\lambda},\Omega_\lambda}(\rho;\bar{\rho})$ and $b^{ad,J\Pi\Gamma\mathbf{n}'_\lambda\Omega'_\lambda}_{2,n_{2_\lambda},\Omega_\lambda}(\rho;\bar{\rho})$ to obtain

$$\begin{aligned}
&\left[-\frac{\hbar^2}{2\mu}\begin{pmatrix}1&0\\0&1\end{pmatrix}\frac{\partial^2}{\partial\rho^2} + \begin{pmatrix}\mathcal{A}^{ad,\Pi\Gamma,\Omega_\lambda}_{1,n_{1_\lambda}}(\rho;\bar{\rho}) & 0\\ 0 & \mathcal{A}^{ad,\Pi\Gamma,\Omega_\lambda}_{2,n_{2_\lambda}}(\rho;\bar{\rho})\end{pmatrix}\right]\begin{pmatrix} b^{ad,J\Pi\Gamma\mathbf{n}'_\lambda\Omega'_\lambda}_{1,n_{1_\lambda},\Omega_\lambda}(\rho;\bar{\rho})\\ b^{ad,J\Pi\Gamma\mathbf{n}'_\lambda\Omega'_\lambda}_{2,n_{2_\lambda},\Omega_\lambda}(\rho;\bar{\rho})\end{pmatrix}\\
&+\begin{pmatrix}\sum_{n'_{1_\lambda}}\left[\mathcal{B}^{ad,\Pi\Gamma,\Omega_\lambda}_{11,n_{1_\lambda},n'_{1_\lambda}}(\rho;\bar{\rho}) + \mathcal{C}^{ad,\Pi\Gamma,\Omega_\lambda}_{11,n_{1_\lambda},n'_{1_\lambda}}(\rho;\bar{\rho})\right] b^{ad,J\Pi\Gamma\mathbf{n}'_\lambda\Omega'_\lambda}_{1,n'_{1_\lambda},\Omega_\lambda}(\rho;\bar{\rho})\\ \sum_{n'_{2_\lambda}}\left[\mathcal{B}^{ad,\Pi\Gamma,\Omega_\lambda}_{22,n_{2_\lambda},n'_{2_\lambda}}(\rho;\bar{\rho}) + \mathcal{C}^{ad,\Pi\Gamma,\Omega_\lambda}_{22,n_{2_\lambda},n'_{2_\lambda}}(\rho;\bar{\rho})\right] b^{ad,J\Pi\Gamma\mathbf{n}'_\lambda\Omega'_\lambda}_{2,n'_{2_\lambda},\Omega_\lambda}(\rho;\bar{\rho})\end{pmatrix}\\
&+\begin{pmatrix}\sum_{n'_{1_\lambda}}\mathcal{D}^{ad,\Pi\Gamma,\Omega_\lambda}_{11,n_{1_\lambda},n'_{1_\lambda},\Omega_\lambda\pm1}(\rho;\bar{\rho}) b^{ad,J\Pi\Gamma\mathbf{n}'_\lambda\Omega'_\lambda}_{1,n'_{1_\lambda},\Omega_\lambda\pm1}(\rho;\bar{\rho})\\ \sum_{n'_{2_\lambda}}\mathcal{D}^{ad,\Pi\Gamma,\Omega_\lambda}_{22,n_{2_\lambda},n'_{2_\lambda},\Omega_\lambda\pm1}(\rho;\bar{\rho}) b^{ad,J\Pi\Gamma\mathbf{n}'_\lambda\Omega'_\lambda}_{2,n'_{2_\lambda},\Omega_\lambda\pm1}(\rho;\bar{\rho})\end{pmatrix}\\
&+\begin{pmatrix}\sum_{n'_{2_\lambda}}\left[\mathcal{F}^{ad,\Pi\Gamma,\Omega_\lambda}_{12,n_{1_\lambda},n'_{2_\lambda}}(\rho;\bar{\rho}) b^{ad,J\Pi\Gamma\mathbf{n}'_\lambda\Omega'_\lambda}_{2,n'_{2_\lambda},\Omega_\lambda}(\rho;\bar{\rho}) + \mathcal{G}^{ad,\Pi\Gamma,\Omega_\lambda}_{12,n_{1_\lambda},n'_{2_\lambda},\Omega_\lambda\pm1}(\rho;\bar{\rho}) b^{ad,J\Pi\Gamma\mathbf{n}'_\lambda\Omega'_\lambda}_{2,n'_{2_\lambda},\Omega_\lambda\pm1}(\rho;\bar{\rho})\right]\\ -\sum_{n'_{1_\lambda}}\left[\mathcal{F}^{ad,\Pi\Gamma,\Omega_\lambda}_{21,n_{2_\lambda},n'_{1_\lambda}}(\rho;\bar{\rho}) b^{ad,J\Pi\Gamma\mathbf{n}'_\lambda\Omega'_\lambda}_{1,n'_{1_\lambda},\Omega_\lambda}(\rho;\bar{\rho}) + \mathcal{G}^{ad,\Pi\Gamma,\Omega_\lambda}_{21,n_{2_\lambda},n'_{1_\lambda},\Omega_\lambda\pm1}(\rho;\bar{\rho}) b^{ad,J\Pi\Gamma\mathbf{n}'_\lambda\Omega'_\lambda}_{1,n'_{1_\lambda},\Omega_\lambda\pm1}(\rho;\bar{\rho})\right]\end{pmatrix}\\
&+\begin{pmatrix}\sum_{n'_{1_\lambda}}\mathcal{H}^{ad,\Pi\Gamma,\Omega_\lambda}_{11,n_{1_\lambda},n'_{1_\lambda}}(\rho;\bar{\rho}) b^{ad,J\Pi\Gamma\mathbf{n}'_\lambda\Omega'_\lambda}_{1,n'_{1_\lambda},\Omega_\lambda}(\rho;\bar{\rho}) + \sum_{n'_{2_\lambda}}\mathcal{H}^{ad,\Pi\Gamma,\Omega_\lambda}_{12,n_{1_\lambda},n'_{2_\lambda}}(\rho;\bar{\rho}) b^{ad,J\Pi\Gamma\mathbf{n}'_\lambda\Omega'_\lambda}_{2,n'_{2_\lambda},\Omega_\lambda}(\rho;\bar{\rho})\\ \sum_{n'_{1_\lambda}}\mathcal{H}^{ad,\Pi\Gamma,\Omega_\lambda}_{21,n_{2_\lambda},n'_{1_\lambda}}(\rho;\bar{\rho}) b^{ad,J\Pi\Gamma\mathbf{n}'_\lambda\Omega'_\lambda}_{1,n'_{1_\lambda},\Omega_\lambda}(\rho;\bar{\rho}) + \sum_{n'_{2_\lambda}}\mathcal{H}^{ad,\Pi\Gamma,\Omega_\lambda}_{22,n_{2_\lambda},n'_{2_\lambda}}(\rho;\bar{\rho}) b^{ad,J\Pi\Gamma\mathbf{n}'_\lambda\Omega'_\lambda}_{2,n'_{2_\lambda},\Omega_\lambda}(\rho;\bar{\rho})\end{pmatrix}\\
&+\begin{pmatrix}\sum_{n'_{2_\lambda}}\mathcal{J}^{ad,\Pi\Gamma,\Omega_\lambda}_{12,n_{1_\lambda},n'_{2_\lambda}}(\rho;\bar{\rho})\partial b^{ad,J\Pi\Gamma\mathbf{n}'_\lambda\Omega'_\lambda}_{2,n'_{2_\lambda},\Omega_\lambda}(\rho;\bar{\rho})/\partial\rho\\ -\sum_{n'_{1_\lambda}}\mathcal{J}^{ad,\Pi\Gamma,\Omega_\lambda}_{21,n_{2_\lambda},n'_{1_\lambda}}(\rho;\bar{\rho})\partial b^{ad,J\Pi\Gamma\mathbf{n}'_\lambda\Omega'_\lambda}_{1,n'_{1_\lambda},\Omega_\lambda}(\rho;\bar{\rho})/\partial\rho\end{pmatrix} = E\begin{pmatrix} b^{ad,J\Pi\Gamma\mathbf{n}'_\lambda\Omega'_\lambda}_{1,n_{1_\lambda},\Omega_\lambda}(\rho;\bar{\rho})\\ b^{ad,J\Pi\Gamma\mathbf{n}'_\lambda\Omega'_\lambda}_{2,n_{2_\lambda},\Omega_\lambda}(\rho;\bar{\rho})\end{pmatrix}
\end{aligned} \tag{5.62}$$

where for $i,j=1,2$ and in $\omega_\lambda,\gamma_\lambda$ coordinates denoting $\Phi^{ad,\Pi\Gamma}_{i,n_{i_\lambda},\Omega_\lambda}(\omega_\lambda,\gamma_\lambda;\bar{\rho})$ simply as $\Phi^{ad,\Pi\Gamma}_{i,n_{i_\lambda},\Omega_\lambda}$,

$$\mathcal{A}^{ad,\Pi\Gamma,\Omega_\lambda}_{i,n_{i_\lambda}}(\rho;\bar{\rho}) = \frac{15\hbar^2}{8\mu\rho^2} + \frac{\overline{\rho}^2}{\rho^2}\epsilon^{ad,\Pi\Gamma}_{i,n_{i_\lambda},\Omega_\lambda}(\bar{\rho}) \tag{5.63}$$

$$\mathcal{B}^{ad,\Pi\Gamma,\Omega_\lambda}_{ii,n_{i_\lambda},n'_{i_\lambda}}(\rho;\bar{\rho}) = \langle\Phi^{ad,\Pi\Gamma}_{i,n_{i_\lambda},\Omega_\lambda}|\varepsilon^{ad}_i(\rho,\omega_\lambda,\gamma_\lambda) - \frac{\overline{\rho}^2}{\rho^2}\varepsilon^{ad}_i(\bar{\rho},\omega_\lambda,\gamma_\lambda)|\Phi^{ad,\Pi\Gamma}_{i,n'_{i_\lambda},\Omega_\lambda}\rangle \tag{5.64}$$

$$\mathcal{C}^{ad,\Pi\Gamma,\Omega_\lambda}_{ii,n_{i_\lambda},n'_{i_\lambda}}(\rho;\bar{\rho}) = \tfrac{\hbar^2}{2\mu\rho^2}\Big[J(J+1)\langle\Phi^{ad,\Pi\Gamma}_{i,n_{i_\lambda},\Omega_\lambda}|\tfrac{1}{\cos^2\omega_\lambda/2}|\Phi^{ad,\Pi\Gamma}_{i,n'_{i_\lambda},\Omega_\lambda}\rangle - 2{\Omega_\lambda}^2\langle\Phi^{ad,\Pi\Gamma}_{i,n_{i_\lambda},\Omega_\lambda}|\tfrac{1}{\cos^2\omega_\lambda/2}|\Phi^{ad,\Pi\Gamma}_{i,n'_{i_\lambda},\Omega_\lambda}\rangle\Big] \tag{5.65}$$

$$\begin{aligned}\mathcal{D}^{ad,\Pi\Gamma,\Omega_\lambda}_{ii,n_{i_\lambda},n'_{i_\lambda},\Omega_\lambda\pm1}(\rho;\bar{\rho}) &= \tfrac{\hbar^2}{2\mu\rho^2}\Big[\zeta_+(J,\Omega_\lambda)\tfrac{N_{J,\Omega_\lambda+1}}{N_{J,\Omega_\lambda}}\langle\Phi^{ad,\Pi\Gamma}_{i,n_{i_\lambda},\Omega_\lambda}|\hat{D}^{\Omega_\lambda}_1(\omega_\lambda,\gamma_\lambda)|\Phi^{ad,\Pi\Gamma}_{i,n'_{i_\lambda},\Omega_\lambda+1}\rangle \\ &\quad +\zeta_-(J,\Omega_\lambda)\tfrac{N_{J,\Omega_\lambda-1}}{N_{J,\Omega_\lambda}}\langle\Phi^{ad,\Pi\Gamma}_{i,n_{i_\lambda},\Omega_\lambda}|\hat{D}^{\Omega_\lambda}_2(\omega_\lambda,\gamma_\lambda)|\Phi^{ad,\Pi\Gamma}_{i,n'_{i_\lambda},\Omega_\lambda-1}\rangle\Big] \\ \text{with}\quad \hat{D}^{\Omega_\lambda}_1(\omega_\lambda,\gamma_\lambda) &= \tfrac{1}{\cos^2\omega_\lambda/2}\left\{(\Omega_\lambda+2)\cot\gamma_\lambda+\tfrac{\partial}{\partial\gamma_\lambda}\right\} \\ \text{and}\quad \hat{D}^{\Omega_\lambda}_2(\omega_\lambda,\gamma_\lambda) &= \tfrac{1}{\cos^2\omega_\lambda/2}\left\{(\Omega_\lambda-2)\cot\gamma_\lambda-\tfrac{\partial}{\partial\gamma_\lambda}\right\}\end{aligned} \tag{5.66}$$

$$\mathcal{F}^{ad,\Pi\Gamma,\Omega_\lambda}_{ij,n_{i_\lambda},n'_{j_\lambda},\Omega_\lambda\pm2}(\rho;\bar{\rho}) = -\frac{\hbar^2}{\mu}\langle\Phi^{ad,\Pi\Gamma}_{i,n_{i_\lambda},\Omega_\lambda}|\widehat{W}^{ad(1)}_{1,2}(\rho,\omega_\lambda,\gamma_\lambda)|\Phi^{ad,\Pi\Gamma}_{j,n'_{j_\lambda},\Omega_\lambda}\rangle \tag{5.67}$$

$$\mathcal{G}^{ad,\Pi\Gamma,\Omega_\lambda}_{ij,n_{i_\lambda},n'_{j_\lambda},\Omega_\lambda\pm1}(\rho;\bar{\rho}) = \tfrac{-\hbar^2}{2\mu\rho}\Big[\zeta_+(J,\Omega_\lambda)\tfrac{N_{J,\Omega_\lambda+1}}{N_{J,\Omega_\lambda}}\langle\Phi^{ad,\Pi\Gamma}_{i,n_{i_\lambda},\Omega_\lambda}|\tfrac{1}{\cos^2\omega_\lambda/2}\ \mathrm{W}^{ad(1)}_{1,2,\gamma_\lambda}(\mathbf{q}_\lambda)|\Phi^{ad,\Pi\Gamma}_{j,n'_{j_\lambda},\Omega_\lambda+1}\rangle - \zeta_-(J,\Omega_\lambda)\tfrac{N_{J,\Omega_\lambda-1}}{N_{J,\Omega_\lambda}}\langle\Phi^{ad,\Pi\Gamma}_{i,n_{i_\lambda},\Omega_\lambda}|\tfrac{1}{\cos^2\omega_\lambda/2}\ \mathrm{W}^{ad(1)}_{1,2,\gamma_\lambda}(\mathbf{q}_\lambda)|\Phi^{ad,\Pi\Gamma}_{j,n'_{j_\lambda},\Omega_\lambda-1}\rangle\Big] \tag{5.68}$$

$$\mathcal{H}^{ad,\Pi\Gamma,\Omega_\lambda}_{ij,n_{i_\lambda},n'_{j_\lambda}}(\rho;\bar{\rho}) = -\frac{\hbar^2}{2\mu}\langle\Phi^{ad,\Pi\Gamma}_{i,n_{i_\lambda},\Omega_\lambda}|\mathrm{W}^{ad(2)}_{i,j}(\rho,\omega_\lambda,\gamma_\lambda)|\Phi^{ad,\Pi\Gamma}_{j,n'_{j_\lambda},\Omega_\lambda}\rangle \tag{5.69}$$

$$\mathcal{J}^{ad,\Pi\Gamma,\Omega_\lambda}_{ij,n_{i_\lambda},n'_{j_\lambda}}(\rho;\bar{\rho}) = -\frac{\hbar^2}{\mu}\langle\Phi^{ad,\Pi\Gamma}_{i,n_{i_\lambda},\Omega_\lambda}|\mathrm{W}^{ad(1)}_{1,2,\rho}(\rho,\omega_\lambda,\gamma_\lambda)|\Phi^{ad,\Pi\Gamma}_{j,n'_{j_\lambda},\Omega_\lambda}\rangle \tag{5.70}$$

In Eq. (5.67), $\widehat{W}^{ad(1)}_{1,2}(\rho,\omega_\lambda,\gamma_\lambda)$ is the $\omega_\lambda,\gamma_\lambda$ equivalent of Eq. (5.60). In Eqs. (5.68) and (5.70), $\mathrm{W}^{ad(1)}_{i,j,\rho}$ and $\mathrm{W}^{ad(1)}_{1,2,\gamma_\lambda}$ are the ρ and γ_λ components of the first-derivative coupling vector in $\rho,\omega_\lambda,\gamma_\lambda$ coordinates.

Now if we define the column vectors $\mathbf{b}_i^{ad,J\Pi\Gamma\mathbf{n}'_\lambda\Omega'_\lambda}(\rho;\bar{\rho})$ $(i=1,2)$ as the vectors whose elements are scanned by $n_{i_\lambda},\Omega_\lambda$ considered as a single row index. Let us also define a matrix $\mathbf{B}^{ad,J\Pi\Gamma}(\rho;\bar{\rho})$ whose $\mathbf{n}'_\lambda,\Omega'_\lambda$ column vector is obtained by stacking the vector $\mathbf{b}_2^{ad,J\Pi\Gamma\mathbf{n}'_\lambda\Omega'_\lambda}(\rho;\bar{\rho})$ under the vector $\mathbf{b}_1^{ad,J\Pi\Gamma\mathbf{n}'_\lambda\Omega'_\lambda}(\rho;\bar{\rho})$. These vectors, for different $\mathbf{n}'_\lambda,\Omega'_\lambda$, are then placed side-by-side thereby generating a square matrix $\mathbf{B}^{ad,J\Pi\Gamma}$ whose dimensions are the total number of LHSFs (channels) used. The coupled hyperradial equation satisfied by this matrix has the form

$$\left[-\frac{\hbar^2}{2\mu}\mathbf{I}\frac{d^2}{d\rho^2}+\mathbf{V}^{ad,J\Pi\Gamma}(\rho;\bar{\rho})\right]\mathbf{B}^{ad,J\Pi\Gamma}(\rho;\bar{\rho}) = E\mathbf{B}^{ad,J\Pi\Gamma}(\rho;\bar{\rho}) \tag{5.71}$$

using either Eq. (5.50) or (5.62) and ignoring its $\mathcal{J}^{ad,\Pi\Gamma,\Omega_\lambda}_{ij,n_{i_\lambda},n'_{j_\lambda}}(\rho;\bar{\rho})$ term given by Eq. (5.59)

or (5.70) as it appears with a first derivative with respect to ρ of the expansion coefficients and is expected to be small. It can be introduced later in a perturbative treatment to assess its effect. $\mathbf{V}^{ad,J\Pi\Gamma}(\rho;\bar{\rho})$ is the interaction potential matrix obtained by this derivation procedure and which encompasses $\overline{\boldsymbol{\epsilon}}^{ad}(\bar{\rho})$ and the matrices with parts defined in Eq. (5.51) through Eq. (5.59) or Eq. (5.63) through Eq. (5.70):

$$\mathbf{V}^{ad,J\Pi\Gamma}(\rho;\bar{\rho}) = \begin{pmatrix} \mathbf{V}_{11}^{ad,J\Pi\Gamma}(\rho;\bar{\rho}) & \mathbf{V}_{12}^{ad,J\Pi\Gamma}(\rho;\bar{\rho}) \\ \mathbf{V}_{21}^{ad,J\Pi\Gamma}(\rho;\bar{\rho}) & \mathbf{V}_{22}^{ad,J\Pi\Gamma}(\rho;\bar{\rho}) \end{pmatrix} \tag{5.72}$$

Its dimensions are those of $\mathbf{B}^{ad,J\Pi\Gamma}(\rho;\bar{\rho})$.

5.3.2 Propagation scheme and asymptotic analysis

The strong and weak interaction regions of the internal configuration space is divided into a certain number of spherical hyperradial shells. The two-dimensional adiabatic LHSFs are determined at the center $\bar{\rho}_i$ of each shell i, whose boundaries are given by $\bar{\rho}_{i,i+1}$. These LHSFs are then used to obtain the coupling matrix $\mathbf{V}^{ad,J\Pi\Gamma}(\rho;\bar{\rho}_i)$ given above in Eq. (5.72). The continuity of the nuclear wave function and its first derivative with respect to ρ is imposed at the boundary $\rho_{i,i+1}$ with the help of the overlap matrix $\mathcal{O}^{\Pi\Gamma}$ defined below. The corresponding continuity conditions on $\mathbf{B}^{ad,J\Pi\Gamma}$ and its ρ derivative are

$$\mathbf{B}_{\mathbf{n}_\lambda\Omega_\lambda}^{ad,J\Pi\Gamma\mathbf{m}'_\lambda\Omega'_\lambda}(\rho_{i,i+1};\bar{\rho}_{i+1}) = \sum_{\mathbf{n}'_\lambda} \mathbf{B}_{\mathbf{n}'_\lambda\Omega_\lambda}^{ad,J\Pi\Gamma\mathbf{m}'_\lambda\Omega'_\lambda}(\rho_{i,i+1};\bar{\rho}_i)[\mathcal{O}^{\Pi\Gamma\Omega_\lambda}]_{\mathbf{n}_\lambda}^{\mathbf{n}'_\lambda}(\bar{\rho}_{i+1},\bar{\rho}_i) \tag{5.73}$$

and

$$\left(\frac{\partial \mathbf{B}_{\mathbf{n}_\lambda\Omega_\lambda}^{ad,J\Pi\Gamma\mathbf{m}'_\lambda\Omega'_\lambda}(\rho;\bar{\rho}_{i+1})}{\partial\rho}\right)_{\rho\to\rho_{i,i+1}^+} = \sum_{\mathbf{n}'_\lambda} \left(\frac{\partial \mathbf{B}_{\mathbf{n}'_\lambda\Omega_\lambda}^{ad,J\Pi\Gamma\mathbf{m}'_\lambda\Omega'_\lambda}(\rho;\bar{\rho}_i)}{\partial\rho}\right)_{\rho\to\rho_{i,i+1}^-} [\mathcal{O}^{\Pi\Gamma\Omega_\lambda}]_{\mathbf{n}_\lambda}^{\mathbf{n}'_\lambda}(\bar{\rho}_{i+1},\bar{\rho}_i) \tag{5.74}$$

The overlap matrix $\mathcal{O}^{\Pi\Gamma}$ has elements defined as

$$[\mathcal{O}^{\Pi\Gamma\Omega_\lambda}]^{\mathbf{n}'_\lambda}_{\mathbf{n}_\lambda}(\bar{\rho}_{i+1},\bar{\rho}_i) = \langle \Phi^{ad,\Pi\Gamma\Omega_\lambda}_{\mathbf{n}_\lambda}(\xi^{(2)}_\lambda;\bar{\rho}_{i+1})|\Phi^{ad,\Pi\Gamma\Omega_\lambda}_{\mathbf{n}'_\lambda}(\xi^{(2)}_\lambda;\bar{\rho}_i)\rangle \tag{5.75}$$

where $\Phi^{ad,\Pi\Gamma\Omega_\lambda}_{\mathbf{n}_\lambda}(\xi^{(2)}_\lambda;\bar{\rho}_i)$ is a column vector

$$\Phi^{ad,\Pi\Gamma\Omega_\lambda}_{\mathbf{n}_\lambda}(\xi^{(2)}_\lambda;\bar{\rho}_i) = \begin{pmatrix} \Phi^{ad,\Pi\Gamma\Omega_\lambda}_{1,n_{1\lambda}}(\xi^{(2)}_\lambda;\bar{\rho}_i) \\ \Phi^{ad,\Pi\Gamma\Omega_\lambda}_{2,n_{2\lambda}}(\xi^{(2)}_\lambda;\bar{\rho}_i) \end{pmatrix} \tag{5.76}$$

whose two components are defined in Eq. (5.46). At the switchover hyperradius (ρ_s) that separates the strong and weak interaction regions, the overlap matrix is calculated by first projecting the two-dimensional (θ,ϕ_λ) LHSFs in the last sector of the strong interaction region onto the $\omega_\lambda,\gamma_\lambda$ space and then computing its overlap with the two-dimensional (θ,ϕ_λ) LHSFs in the first sector of the weak interaction region.

The coupled hyperradial equations in Eq. (5.71) are transformed into the coupled first-order non-linear Bessel-Ricatti logarithmic matrix differential equation

$$\frac{d\mathbf{F}^{ad,J\Pi\Gamma}(\rho;\bar{\rho})}{d\rho} + [\mathbf{F}^{ad,J\Pi\Gamma}(\rho;\bar{\rho})]^2 + \frac{2\mu}{\hbar^2}[E\mathbf{I} - \mathbf{V}^{ad,J\Pi\Gamma}(\rho;\bar{\rho})] = \mathbf{0} \tag{5.77}$$

where

$$\mathbf{F}^{ad,J\Pi\Gamma}(\rho;\bar{\rho}) = [(d/d\rho)\mathbf{B}^{ad,J\Pi\Gamma}(\rho;\bar{\rho})][\mathbf{B}^{ad,J\Pi\Gamma}(\rho;\bar{\rho})]^{-1} \tag{5.78}$$

is the logarithmic derivative matrix and associated with $\mathbf{B}^{ad,J\Pi\Gamma}$. Eq. (5.77) is integrated from the beginning of each sector to its end using a highly efficient fourth-order logarithmic-derivative method [90–92], and matched smoothly from one shell to another by using

$$\mathbf{F}^{ad,J\Pi\Gamma}(\rho;\bar{\rho}_{i+1}) = [\mathcal{O}^{\Pi\Gamma}(\bar{\rho}_{i+1},\bar{\rho}_i)]^{-1}\mathbf{F}^{ad,J\Pi\Gamma}(\rho;\bar{\rho}_i)\mathcal{O}^{\Pi\Gamma}(\bar{\rho}_{i+1},\bar{\rho}_i) \tag{5.79}$$

which is obtained by using Eqs. (5.73), (5.74) and (5.78).

Using this method, the $\mathbf{F}^{ad,J\Pi\Gamma}$ matrix is propagated from a very small value of $\rho = \rho_o$, where a WKB solution is applicable, through a value ρ_s which separates the strong and weak interaction regions, to an asymptotic value $\rho = \rho_a$ where the interactions between different arrangement channels λ have become negligible. At this asymptotic ρ_a, the adiabatic $\boldsymbol{\chi}^{ad,JM\Pi\Gamma}$ is matched to the asymptotic atom-diatom wave functions. This asymptotic analysis furnishes the reactance matrix $\mathsf{R}^{J\Pi\Gamma}$ and from it the scattering matrix $\mathsf{S}^{J\Pi\Gamma}$ [69–71]. For total energies E at which no electronically excited states of the isolated atoms or diatomic molecules are open, the elements of the open parts of these matrices correspond to the ground electronic atom and diatom products only. This is done for all Γ and both parities ($\Pi = 0, 1$) and for a sufficiently large number of values of J (i.e., of partial waves) for the resulting differential and integral cross sections to be converged.

5.4 Diabatic formalism

Total orbital electronuclear wavefunction of Eq. (5.21) can also be expanded in terms of two diabatic electronic wave functions $\psi_1^{el,d}(\mathbf{r};\mathbf{q}_\lambda)$ and $\psi_2^{el,d}(\mathbf{r};\mathbf{q}_\lambda)$ as

$$\Psi^{\mathrm{O}}(\mathbf{r},\mathbf{R}_\lambda) = \chi_1^d(\mathbf{R}_\lambda)\psi_1^{el,d}(\mathbf{r};\mathbf{q}_\lambda) + \chi_2^d(\mathbf{R}_\lambda)\psi_2^{el,d}(\mathbf{r};\mathbf{q}_\lambda) \tag{5.80}$$

where the coefficients of the expansion are the diabatic nuclear motion wave functions $\chi_1^d(\mathbf{R}_\lambda)$ and $\chi_2^d(\mathbf{R}_\lambda)$. The diabatic electronic wave functions can be obtained from the uniquely known adiabatic ones through a unitary transformation

$$\begin{pmatrix} \psi_i^d(\mathbf{r};\mathbf{R}_\lambda) \\ \\ \psi_j^d(\mathbf{r};\mathbf{R}_\lambda) \end{pmatrix} = \widetilde{\mathbf{U}}[\beta(\mathbf{q}_\lambda)] \begin{pmatrix} \psi_i^{ad}(\mathbf{r};\mathbf{R}_\lambda) \\ \\ \psi_j^{ad}(\mathbf{r};\mathbf{R}_\lambda) \end{pmatrix} \tag{5.81}$$

where $\widetilde{\mathbf{U}}[\beta(\mathbf{q}_\lambda)]$ is the transpose of the adiabatic-to-diabatic transformation matrix

$$\mathbf{U}[\beta(\mathbf{q}_\lambda)] = \begin{pmatrix} \cos\beta(\mathbf{q}_\lambda) & -\sin\beta(\mathbf{q}_\lambda) \\ \sin\beta(\mathbf{q}_\lambda) & \cos\beta(\mathbf{q}_\lambda) \end{pmatrix} \tag{5.82}$$

and $\beta(\mathbf{q}_\lambda)$ is called the diabatization or mixing angle obtained by solving a Poisson equation [56, 58, 88] involving the first-derivative nonadiabatic coupling vector $\mathbf{W}_{1,2}^{(1)ad}(\mathbf{q}_\lambda)$. Diabatization is done in most cases to avoid the singular nonadiabatic couplings of the adiabatic representation. An ideal diabatic basis would be one in which the first-derivative coupling vanishes [89]. This can happen only if the complete set of electronic states are included in the Born-Huang expansion of the electronuclear wave function, which is not a practical proposition. The solution is to include only a few excited electronic states and follow an optimal diabatization procedure [56, 58], which minimizes the magnitude of the first-derivative couplings in the diabatic representation over the entire internal nuclear configuration space.

The diabatic nuclear wave functions are related to their adiabatic counterparts by

$$\boldsymbol{\chi}^d(\mathbf{R}_\lambda) = \widetilde{\mathbf{U}}[\beta(\mathbf{q}_\lambda)]\boldsymbol{\chi}^{ad}(\mathbf{R}_\lambda) \tag{5.83}$$

where $\boldsymbol{\chi}^d(\mathbf{R}_\lambda)$ is the two-dimensional column vector whose two elements are $\chi_1^d(\mathbf{R}_\lambda)$ and $\chi_2^d(\mathbf{R}_\lambda)$ and is written as

$$\boldsymbol{\chi}^d(\mathbf{R}_\lambda) = \begin{pmatrix} \chi_1^d(\mathbf{R}_\lambda) \\ \chi_2^d(\mathbf{R}_\lambda) \end{pmatrix} \tag{5.84}$$

Replacement of Eq. (5.83) into Eq. (5.26) yields the diabatic nuclear motion scattering equation

$$\left[-\frac{\hbar^2}{2\mu}\left\{\mathbf{I}\nabla^2_{\mathbf{R}_\lambda} + 2\mathbf{W}^{(1)d}(\mathbf{q}_\lambda)\cdot\boldsymbol{\nabla}_{\mathbf{R}_\lambda} + \mathbf{W}^{(2)d}(\mathbf{q}_\lambda)\right\} + \left\{\boldsymbol{\varepsilon}^d(\mathbf{q}_\lambda) - E\mathbf{I}\right\}\right]\boldsymbol{\chi}^d(\mathbf{R}_\lambda) = \mathbf{0}. \tag{5.85}$$

The elements of the first-derivative $\mathbf{W}^{(1)d}(\mathbf{q}_\lambda)$ and second-derivative $\mathbf{W}^{(2)d}(\mathbf{q}_\lambda)$ cou-

pling diabatic matrices are analogous to their adiabatic counterparts. In particular, $\mathbf{W}^{(1)d}(\mathbf{q}_\lambda)$ is equal to the transverse part $\mathbf{W}^{(1)ad}_{tra}(\mathbf{q}_\lambda)$ of the adiabatic coupling vector $\mathbf{W}^{(1)ad}(\mathbf{q}_\lambda)$ [56,88]. If the adiabatic couplings display a singularity for special nuclear geometries, e.g., displayed at the equilateral triangle geometries for H_3, their diabatic counterparts (both first- and second-derivative couplings) don't display these singularities. This is one of the main advantages of using a diabatic representation. In Eq. (5.85), $\boldsymbol{\varepsilon}^d(\mathbf{q}_\lambda)$ is a 2×2 diabatic energy matrix which is obtained from the adiabatic one $\boldsymbol{\varepsilon}^{ad}(\mathbf{q}_\lambda)$ using

$$\boldsymbol{\varepsilon}^d(\mathbf{q}_\lambda) = \widetilde{\mathbf{U}}[\beta(\mathbf{q}_\lambda)]\ \boldsymbol{\varepsilon}^{ad}(\mathbf{q}_\lambda)\ \mathbf{U}[\beta(\mathbf{q}_\lambda)] \tag{5.86}$$

We can now write Eq. (5.85) in explicit form similar to its adiabatic counterpart [Eq. (5.29)]

$$\begin{aligned}\Bigg[-\frac{\hbar^2}{2\mu}\Bigg\{\begin{pmatrix}1 & 0\\ 0 & 1\end{pmatrix}\nabla^2_{\mathbf{R}_\lambda} + 2\mathbf{W}^{(1)d}_{1,2}(\mathbf{q}_\lambda)\begin{pmatrix}0 & 1\\ -1 & 0\end{pmatrix}\cdot\boldsymbol{\nabla}_{\mathbf{R}_\lambda} + \begin{pmatrix}\mathrm{W}^{(2)d}_{1,1}(\mathbf{q}_\lambda) & \mathrm{W}^{(2)d}_{1,2}(\mathbf{q}_\lambda)\\ \mathrm{W}^{(2)d}_{2,1}(\mathbf{q}_\lambda) & \mathrm{W}^{(2)d}_{2,2}(\mathbf{q}_\lambda)\end{pmatrix}\Bigg\}\\ + \Bigg\{\begin{pmatrix}\varepsilon^d_{11}(\mathbf{q}_\lambda) & \varepsilon^d_{12}(\mathbf{q}_\lambda)\\ \varepsilon^d_{21}(\mathbf{q}_\lambda) & \varepsilon^d_{22}(\mathbf{q}_\lambda)\end{pmatrix} - E\begin{pmatrix}1 & 0\\ 0 & 1\end{pmatrix}\Bigg\}\Bigg]\begin{pmatrix}\chi^d_1(\mathbf{R}_\lambda)\\ \chi^d_2(\mathbf{R}_\lambda)\end{pmatrix} = \begin{pmatrix}0 & 0\\ 0 & 0\end{pmatrix}\end{aligned} \tag{5.87}$$

In this two-state diabatic nuclear motion Schrödinger equation, the nuclear wave functions are coupled by the first-derivative and second-derivative couplings and the diabatic energy matrix. Since all diabatic representations are obtained by some type of mixing of the adiabatic states, the diabatic nuclear wave functions are expected to be intrinsically coupled to each other. The diabatization procedure mentioned earlier also gaurantees that the diabatic electronic wave functions are single-valued upon a pseudorotation and the GP effect is not required to be imposed on diabatic nuclear wave functions.

5.4.1 Partial wave expansion

As we did in the adiabatic case, we can write the diabatic nuclear motion Schrödinger Eq. (5.85) as

$$\left[-\frac{\hbar^2}{2\mu}\left\{\mathbf{I}\nabla^2_{\mathbf{R}_\lambda}+2\mathbf{W}^{(1)d}(\mathbf{q}_\lambda)\cdot\boldsymbol{\nabla}_{\mathbf{R}_\lambda}\right\}+\left\{\overline{\boldsymbol{\varepsilon}}^d(\mathbf{q}_\lambda)-E\mathbf{I}\right\}\right]\boldsymbol{\chi}^d(\mathbf{R}_\lambda)=\mathbf{0} \tag{5.88}$$

The modified diabatic energy matrix $\overline{\boldsymbol{\varepsilon}}^d(\mathbf{q}_\lambda)$ that appears in Eq. (5.88) is given by

$$\overline{\boldsymbol{\varepsilon}}^d(\mathbf{q}_\lambda)=\boldsymbol{\varepsilon}^d(\mathbf{q}_\lambda)-\frac{\hbar^2}{2\mu}\mathbf{W}^{(2)d}(\mathbf{q}_\lambda)=\begin{pmatrix}\overline{\varepsilon}^d_{11}(\mathbf{q}_\lambda) & \overline{\varepsilon}^d_{12}(\mathbf{q}_\lambda)\\ \overline{\varepsilon}^d_{21}(\mathbf{q}_\lambda) & \overline{\varepsilon}^d_{22}(\mathbf{q}_\lambda)\end{pmatrix} \tag{5.89}$$

where

$$\overline{\varepsilon}^d_{ij}(\mathbf{q}_\lambda)=\varepsilon^d_{ij}(\mathbf{q}_\lambda)-\frac{\hbar^2}{2\mu}\mathbf{W}^{(2)d}_{ij}(\mathbf{q}_\lambda)\quad i,j=1,2 \tag{5.90}$$

The two diabatic nuclear wave functions $\chi^d_1(\mathbf{R}_\lambda)$ and $\chi^d_2(\mathbf{R}_\lambda)$ can be expressed as linear combinations of auxiliary nuclear wave functions $\chi^{d,JM\Pi\Gamma}_1(\mathbf{R}_\lambda)$ and $\chi^{d,JM\Pi\Gamma}_2(\mathbf{R}_\lambda)$ respectively similar to their adiabatic counterparts (the linear combinations referred to as partial wave expansions and the individual $\chi^{d,JM\Pi\Gamma}_1$ and $\chi^{d,JM\Pi\Gamma}_2$ referred to as partial waves),

$$\begin{pmatrix}\chi^d_1(\mathbf{R}_\lambda)\\ \chi^d_2(\mathbf{R}_\lambda)\end{pmatrix}=\sum_{J=0}^{\infty}\sum_{M=-J}^{M=J}C^{JM}_\lambda\sum_{\Pi=0}^{1}\sum_{\Gamma}\begin{pmatrix}\chi^{d,JM\Pi\Gamma}_1(\mathbf{R}_\lambda)\\ \chi^{d,JM\Pi\Gamma}_2(\mathbf{R}_\lambda)\end{pmatrix} \tag{5.91}$$

If $\chi^{d,JM\Pi\Gamma}_1(\mathbf{R}_\lambda)$ and $\chi^{d,JM\Pi\Gamma}_2(\mathbf{R}_\lambda)$ are defined as components of the column vector $\boldsymbol{\chi}^{d,JM\Pi\Gamma}(\mathbf{R}_\lambda)$, then we can write Eq. (5.91) as

$$\boldsymbol{\chi}^d(\mathbf{R}_\lambda)=\sum_{J=0}^{\infty}\sum_{M=-J}^{M=J}C^{JM}_\lambda\sum_{\Pi=0}^{1}\sum_{\Gamma}\boldsymbol{\chi}^{d,JM\Pi\Gamma}(\mathbf{R}_\lambda) \tag{5.92}$$

If we define another nuclear wave function column vector

$$\boldsymbol{\chi}^{d,JM\Pi\Gamma}(\mathbf{R}_\lambda) = \begin{pmatrix} \chi_1^{d,JM\Pi\Gamma}(\mathbf{R}_\lambda) \\ \chi_2^{d,JM\Pi\Gamma}(\mathbf{R}_\lambda) \end{pmatrix} \tag{5.93}$$

then $\boldsymbol{\chi}^{d,JM\Pi\Gamma}$ is a simultaneous eigenfunction of the diabatic matrix $\widehat{\mathbf{H}}^d(\mathbf{R}_\lambda)$ expressed as

$$\widehat{\mathbf{H}}^d(\mathbf{R}_\lambda) = \left[-\frac{\hbar^2}{2\mu} \left\{ \mathbf{I}\nabla^2_{\mathbf{R}_\lambda} + 2\mathbf{W}^{(1)d}(\mathbf{q}_\lambda) \cdot \boldsymbol{\nabla}_{\mathbf{R}_\lambda} \right\} + \overline{\boldsymbol{\varepsilon}}^d(\mathbf{q}_\lambda) \right], \tag{5.94}$$

of the square of the total nuclear orbital angular momentum $\hat{\mathbf{J}}$, of its space-fixed z-component $\hat{\mathbf{J}}_z$ and of the inversion operator $\hat{I}$ of the nuclei through their center of mass according to the expressions

$$\begin{aligned} \widehat{\mathbf{H}}^{nu}\boldsymbol{\chi}^{d,JM\Pi\Gamma} &= E\boldsymbol{\chi}^{d,JM\Pi\Gamma} \\ \hat{J}^2\boldsymbol{\chi}^{d,JM\Pi\Gamma} &= J(J+1)\hbar^2\boldsymbol{\chi}^{d,JM\Pi\Gamma} \\ \hat{J}_z\boldsymbol{\chi}^{d,JM\Pi\Gamma} &= M\hbar\boldsymbol{\chi}^{d,JM\Pi\Gamma} \\ \hat{I}\boldsymbol{\chi}^{d,JM\Pi\Gamma} &= (-1)^{\Pi}\boldsymbol{\chi}^{d,JM\Pi\Gamma} \end{aligned} \tag{5.95}$$

In these equations, J, M, Π, Γ carry the same definitions as they did in the adiabatic language. The irreducible representation Γ again refers to the fact that $\boldsymbol{\chi}^{d,JM\Pi\Gamma}$ leads to an electronuclear wave function which transforms according to that representation of the system's permutation group.

Let us now expand the two nuclear motion partial waves $\chi_1^{d,JM\Pi\Gamma}$ and $\chi_2^{d,JM\Pi\Gamma}$ according to the following vector equation

$$\begin{pmatrix} \chi_1^{d,JM\Pi\Gamma,\mathbf{n}'_\lambda\Omega'_\lambda}(\rho,\xi_\lambda) \\ \chi_2^{d,JM\Pi\Gamma,\mathbf{n}'_\lambda\Omega'_\lambda}(\rho,\xi_\lambda) \end{pmatrix} = \rho^{-5/2} \sum_{\Omega_\lambda} D^{J\Pi}_{M\Omega_\lambda}(\xi_\lambda^{(1)}) \begin{pmatrix} \sum_{n_{1_\lambda}} b^{d,J\Pi\Gamma\mathbf{n}'_\lambda\Omega'_\lambda}_{1,n_{1_\lambda},\Omega_\lambda}(\rho;\bar{\rho}) \Phi^{d,\Pi\Gamma}_{1,n_{1_\lambda},\Omega_\lambda}(\xi_\lambda^{(2)};\bar{\rho}) \\ \sum_{n_{2_\lambda}} b^{d,J\Pi\Gamma\mathbf{n}'_\lambda\Omega'_\lambda}_{2,n_{2_\lambda},\Omega_\lambda}(\rho;\bar{\rho}) \Phi^{d,\Pi\Gamma}_{2,n_{2_\lambda},\Omega_\lambda}(\xi_\lambda^{(2)};\bar{\rho}) \end{pmatrix} \tag{5.96}$$

In Eq. (5.96), $\Phi^{d,\Pi\Gamma}_{1,n_{1_\lambda},\Omega_\lambda}(\xi_\lambda^{(2)};\bar{\rho})$ and $\Phi^{d,\Pi\Gamma}_{2,n_{2_\lambda},\Omega_\lambda}(\xi_\lambda^{(2)};\bar{\rho})$ are the diabatic two-dimensional local hyperspherical surface functions (LHSFs) that depend parametrically on $\bar{\rho}$ and are defined as the eigenfunctions of a diabatic reference Hamiltonian matrix $\hat{\mathbf{h}}_d^{\Omega_\lambda}(\xi_\lambda^{(2)};\bar{\rho})$.

Similar to the adiabatic langiage, this matrix can be chosen to be block diagonal, i.e.,

$$\hat{\mathbf{h}}_d^{\Omega_\lambda}(\xi_\lambda^{(2)};\bar{\rho}) = \frac{\hat{\Lambda}_1^2(\xi_\lambda^{(2)})}{2\mu\bar{\rho}^2}\begin{pmatrix} 1 & 0 \\ 0 & 1 \end{pmatrix} + \begin{pmatrix} \overline{\boldsymbol{\varepsilon}}_{11}^d(\bar{\rho},\xi_\lambda^{(2)}) & 0 \\ 0 & \overline{\boldsymbol{\varepsilon}}_{22}^d(\bar{\rho},\xi_\lambda^{(2)}) \end{pmatrix} \tag{5.97}$$

or have the off-diagonal nonadiabatic couplings built in, i.e.,

$$\hat{\mathbf{h}}_d^{\Omega_\lambda}(\xi_\lambda^{(2)};\bar{\rho}) = \frac{\hat{\Lambda}_1^2(\xi_\lambda^{(2)})}{2\mu\bar{\rho}^2}\begin{pmatrix} 1 & 0 \\ 0 & 1 \end{pmatrix} + \begin{pmatrix} \overline{\boldsymbol{\varepsilon}}_{11}^d(\bar{\rho},\xi_\lambda^{(2)}) & \overline{\boldsymbol{\varepsilon}}_{12}^d(\bar{\rho},\xi_\lambda^{(2)}) \\ \overline{\boldsymbol{\varepsilon}}_{21}^d(\bar{\rho},\xi_\lambda^{(2)}) & \overline{\boldsymbol{\varepsilon}}_{22}^d(\bar{\rho},\xi_\lambda^{(2)}) \end{pmatrix} \tag{5.98}$$

In Eqs. (5.97) and (5.98), $\hat{\Lambda}^2(\xi_\lambda^{(2)})$ refers to angular operators in θ,ϕ_λ coordinates [Eq. (5.44)] in the strong interaction region or $\omega_\lambda,\gamma_\lambda$ coordinates [Eq. (5.46)] in the weak interaction and asymptotic regions [18, 72].

For the $\hat{\mathbf{h}}_d^{\Omega_\lambda}(\xi_\lambda^{(2)};\bar{\rho})$ matrix in Eq. (5.97), $\Phi^{d,\Pi\Gamma}_{1,n_{1_\lambda},\Omega_\lambda}(\xi_\lambda^{(2)};\bar{\rho})$ and $\Phi^{d,\Pi\Gamma}_{2,n_{2_\lambda},\Omega_\lambda}(\xi_\lambda^{(2)};\bar{\rho})$ are solutions of uncoupled second-order partial differential equations, whereas for the $\hat{\mathbf{h}}_d^{\Omega_\lambda}(\xi_\lambda^{(2)};\bar{\rho})$ matrix in Eq. (5.98), they are solutions of coupled differential equations. Like their adiabatic partners, their calculation requires a larger computational effort than to obtain the former and as the off-diagonal couplings are built into Eq. (5.98), a smaller number of the corresponding LHSFs will be needed for convergence of the solutions of the scattering equations, as opposed to the ones resulting from Eq. (5.97), which don't have these terms built in. Here also it is desirable to use LHSFs obtained from Eq. (5.98) rather than Eq. (5.97).

With either of these diabatic reference Hamiltonians, the LHSFs satisfy the eigenvalue equation

$$\hat{\mathbf{h}}_d^{\Omega_\lambda}(\xi_\lambda^{(2)};\bar{\rho})\begin{pmatrix} \Phi^{d,\Pi\Gamma}_{1,n_{1_\lambda},\Omega_\lambda}(\xi_\lambda^{(2)};\bar{\rho}) \\ \Phi^{d,\Pi\Gamma}_{2,n_{2_\lambda},\Omega_\lambda}(\xi_\lambda^{(2)};\bar{\rho}) \end{pmatrix} = \begin{pmatrix} \epsilon^{d,\Pi\Gamma}_{1,n_{1_\lambda},\Omega_\lambda}(\bar{\rho})\Phi^{d,\Pi\Gamma}_{1,n_{1_\lambda},\Omega_\lambda}(\xi_\lambda^{(2)};\bar{\rho}) \\ \epsilon^{d,\Pi\Gamma}_{2,n_{2_\lambda},\Omega_\lambda}(\bar{\rho})\Phi^{d,\Pi\Gamma}_{2,n_{2_\lambda},\Omega_\lambda}(\xi_\lambda^{(2)};\bar{\rho}) \end{pmatrix} \tag{5.99}$$

The diabatic LHSFs are not allowed to diverge anywhere on the half-sphere of fixed radius $\bar{\rho}$. This boundary condition furnishes the quantum numbers n_{1_λ} and n_{2_λ}, each of which is two-dimensional since the reference Hamiltonian $\hat{\mathbf{h}}_d^{\Omega_\lambda}$ has two angular

degrees of freedom. The superscripts $\mathbf{n}'_\lambda, \Omega'_\lambda$ in Eq. (5.96), with $\mathbf{n}'_\lambda$ referring to the union of n'_{1_λ} and n'_{2_λ}, indicate that the number of linearly independent solutions of Eqs. (5.95) is equal to the number of diabatic LHSFs used in the expansions of Eq. (5.96).

In the strong interaction region, the diabatic functions $\Phi^{d,\Pi\Gamma}_{i,n_{i_\lambda},\Omega_\lambda}(\theta,\phi_\lambda;\bar{\rho})$, $(i = 1,2)$, which are eigenfunctions of the reference Hamiltonian given by Eqs. (5.97) or (5.98) and Eq. (5.44), are obtained using the same body-fixed basis $\overline{\Phi}^{d,\Pi\Gamma}_{i,n_{i_\lambda},\Omega_\lambda}(\theta,\phi_\lambda)$ used in the adiabatic representation,

$$\overline{\Phi}^{d,\Pi\Gamma}_{i,n_{i_\lambda},\Omega_\lambda}(\theta,\phi_\lambda) = f^{\Omega_\lambda}_{n_{i\theta_\lambda}}(\theta)\; g^{d,\Pi\Gamma}_{i,n_{i\phi_\lambda},\Omega_\lambda}(\phi_\lambda) \tag{5.100}$$

where $n_{i_\lambda} \equiv (n_{i\theta_\lambda}, n_{i\phi_\lambda})$. $g^{d,\Pi\Gamma}_{i,n_{i\phi_\lambda},\Omega_\lambda}$ are again chosen to be simple trigonometric functions of ϕ_λ and $f^{\Omega_\lambda}_{n_{i\theta_\lambda}}$ are chosen as Jacobi polynomials in $\cos\theta$, such that the resulting diabatic nuclear wave functions transform under the operations of the permutation symmetry group of identical atoms in the way described after Eqs. (5.95). Eqs. (5.99) are then transformed into an algebraic eigenvalue eigenvector equation involving the coefficients of these expansions, which is solved numerically by linear algebra methods. As was the case in the adiabatic treatment, the singularities in the $\hat{\Lambda}^2_1$ operator of Eq. (5.97) or Eq. (5.98) at $\theta = 0$ and $\theta = \pi/2$ need to be handled carefully. With the reference Hamiltonian mentioned above, the Jacobi polynomials are unable to handle the pole at $\theta = 0$. Besides, in the current diabatic case, the second-derivative coupling element, that has been added to the diabatic energies [see Eq. (5.89)], is not singular at $\theta = 0$. This might require using the full $\hat{\Lambda}^2$ operator and related hyperspherical harmonics [85, 86]. Appendix 5.A describes a method to obtain trigonometric functions in ϕ_λ that provide diabatic electronuclear functions with P_3 permutation symmetries, in the presence and absence of the conical intersection.

In the weak interaction region, where the coordinates $(\rho, \omega_\lambda, \gamma_\lambda)$ of Eq. (5.5) are used, the diabatic LHSFs $\Phi^{d,\Pi\Gamma}_{i,n_{i_\lambda},\Omega_\lambda}(\omega_\lambda,\gamma_\lambda;\bar{\rho})$, $(i = 1,2)$ are eigenfunctions of the reference Hamiltonian given by Eqs. (5.97) or (5.98) and Eq. (5.46). These weak in-

teraction region diabatic LHSFs are expanded in a body-fixed basis $\overline{\Phi}^{d,\Pi\Gamma}_{i,n_{i_\lambda},\Omega_\lambda}(\omega_\lambda,\gamma_\lambda)$, used in the adiabatic language and constructed from the direct product of the associated Legendre functions of $\cos\gamma_\lambda$ and at a set of functions of ω_λ determined by the numerical solution of a one-dimensional eigenfunction equation in ω_λ using Gegenbauer polynomials [87] in $\cos\omega_\lambda$. As in the adiabatic case, the $\omega_\lambda = 0$ singularity in $\hat{\Lambda}_1^2$ operator is compensated by the well-behaved Gegenbauer polynomials.

Once the diabatic LHSFs are known, they provide the basis of functions in terms of which the expansion in Eq. (5.96) is defined. The diabatic nuclear wave function vector of that equation is then inserted into the first equation of Eqs. (5.95). Use of the orthonormality of the symmetrized Wigner functions [Eq. (5.41)] and integration over the two-dimensional diabatic LHSFs, yields a set of coupled hyperradial second-order ordinary differential equations (also called coupled-channel equations) in the coefficients $b^{d,J\Pi\Gamma\mathbf{n}'_\lambda\Omega'_\lambda}_{1,n_{1_\lambda},\Omega_\lambda}(\rho;\bar{\rho})$ and $b^{d,J\Pi\Gamma\mathbf{n}'_\lambda\Omega'_\lambda}_{2,n_{2_\lambda},\Omega_\lambda}(\rho;\bar{\rho})$ analogous to the adiabatic Eq. (5.50). Let us define the diabatic column vectors $\mathbf{b}_i^{d,J\Pi\Gamma\mathbf{n}'_\lambda\Omega'_\lambda}(\rho;\bar{\rho})$ $(i=1,2)$ as the vectors whose elements are scanned by $n_{i_\lambda},\Omega_\lambda$ considered as a single row index. Let us also define a matrix $\mathbf{B}^{d,J\Pi\Gamma}(\rho;\bar{\rho})$ whose $\mathbf{n}'_\lambda,\Omega'_\lambda$ column vector is obtained by stacking the vector $\mathbf{b}_2^{d,J\Pi\Gamma\mathbf{n}'_\lambda\Omega'_\lambda}(\rho;\bar{\rho})$ under the vector $\mathbf{b}_1^{d,J\Pi\Gamma\mathbf{n}'_\lambda\Omega'_\lambda}(\rho;\bar{\rho})$. These vectors, for different $\mathbf{n}'_\lambda,\Omega'_\lambda$, are then placed side by side thereby generating a square matrix $\mathbf{B}^{d,J\Pi\Gamma}$ whose dimensions are the total number of LHSFs (channels) used. The coupled hyperradial equation satisfied by this matrix has the form

$$\left[-\frac{\hbar^2}{2\mu}\mathbf{I}\frac{d^2}{d\rho^2}+\mathbf{V}^{d,J\Pi\Gamma}(\rho;\bar{\rho})\right]\mathbf{B}^{d,J\Pi\Gamma}(\rho;\bar{\rho})=E\mathbf{B}^{d,J\Pi\Gamma}(\rho;\bar{\rho}) \tag{5.101}$$

where $\mathbf{V}^{d,J\Pi\Gamma}(\rho;\bar{\rho})$ is the interaction potential matrix obtained by this derivation procedure and which encompasses $\overline{\boldsymbol{\epsilon}}^d(\bar{\rho})$:

$$\mathbf{V}^{d,J\Pi\Gamma}(\rho;\bar{\rho})=\begin{pmatrix}\mathbf{V}^{d,J\Pi\Gamma}_{11}(\rho;\bar{\rho}) & \mathbf{V}^{d,J\Pi\Gamma}_{12}(\rho;\bar{\rho})\\ \mathbf{V}^{d,J\Pi\Gamma}_{21}(\rho;\bar{\rho}) & \mathbf{V}^{d,J\Pi\Gamma}_{22}(\rho;\bar{\rho})\end{pmatrix} \tag{5.102}$$

Its dimensions are those of $\mathbf{B}^{d,J\Pi\Gamma}(\rho;\bar{\rho})$.

5.4.2 Propagation scheme and asymptotic analysis

The strong and weak interaction regions of the internal configuration space is divided into a certain number of spherical hyperradial shells. The two-dimensional diabatic LHSFs are determined at the center $\bar{\rho}$ of each shell. These LHSFs are then used to obtain the coupling matrix $\mathbf{V}^{d,J\Pi\Gamma}(\rho;\bar{\rho})$ given above in Eq. (5.102). The coupled hyperradial equations in Eq. (5.101) are transformed into the coupled first-order nonlinear Bessel-Ricatti logarithmic matrix differential equation

$$\frac{d\mathbf{F}^{d,J\Pi\Gamma}(\rho;\bar{\rho})}{d\rho} + [\mathbf{F}^{d,J\Pi\Gamma}(\rho;\bar{\rho})]^2 + \frac{2\mu}{\hbar^2}[E\mathbf{I} - \mathbf{V}^{d,J\Pi\Gamma}(\rho;\bar{\rho})] = \mathbf{0} \tag{5.103}$$

where

$$\mathbf{F}^{d,J\Pi\Gamma}(\rho;\bar{\rho}) = [(d/d\rho)\mathbf{B}^{d,J\Pi\Gamma}(\rho;\bar{\rho})][\mathbf{B}^{d,J\Pi\Gamma}(\rho;\bar{\rho})]^{-1} \tag{5.104}$$

is the logarithmic derivative matrix and associated with $\mathbf{B}^{d,J\Pi\Gamma}$. Eq. (5.103) is integrated from the beginning of each sector to its end using a highly efficient fourth-order logarithmic-derivative method [90–92], and matched smoothly from one shell to another.

Using this method, the $\mathbf{F}^{d,J\Pi\Gamma}$ matrix is propagated from a very small value of $\rho = \rho_o$, where a WKB solution is applicable, through a value ρ_s which separates the strong and weak interaction regions, to an asymptotic value $\rho = \rho_a$ where the interactions between different arrangement channels λ have become negligible. This diabatic log-derivative matrix is transformed smoothly from one sector to the next and across the switchover hyperradius ρ_s in the same way that the adiabatic one is transformed as discussed in Sec. 5.3.2. At this asymptotic ρ_a, the diabatic $\boldsymbol{\chi}^{d,JM\Pi\Gamma}$ is transformed to its adiabatic representation using the adiabatic-to-diabatic matrix and matched to the asymptotic atom-diatom wave functions. This asymptotic analysis furnishes the reactance matrix $\mathsf{R}^{J\Pi\Gamma}$ and from it the scattering matrix $\mathsf{S}^{J\Pi\Gamma}$ [69–71]. For total energies E at which no electronically excited states of the isolated atoms or diatomic molecules are open, the elements of the open parts of these matrices correspond to the ground electronic atom and diatom products only. This is done for

all Γ and both parities ($\Pi = 0, 1$) and for a sufficiently large number of values of J (i.e., of partial waves) for the resulting differential and integral cross sections to be converged.

5.4.3 Adiabatic vs. diabatic approaches

We recall the adiabatic and diabatic nuclear motion Schrödinger Eqs. (5.26) and (5.85):

Adiabatic:

$$\left[-\frac{\hbar^2}{2\mu}\left\{\mathbf{I}\nabla^2_{\mathbf{R}_\lambda} + 2\mathbf{W}^{(1)ad}(\mathbf{q}_\lambda)\cdot\boldsymbol{\nabla}_{\mathbf{R}_\lambda} + \mathbf{W}^{(2)ad}(\mathbf{q}_\lambda)\right\} + \left\{\boldsymbol{\varepsilon}^{ad}(\mathbf{q}_\lambda) - E\mathbf{I}\right\}\right]\boldsymbol{\chi}^{ad}(\mathbf{R}_\lambda) = \mathbf{0} \tag{5.105}$$

Diabatic:

$$\left[-\frac{\hbar^2}{2\mu}\left\{\mathbf{I}\nabla^2_{\mathbf{R}_\lambda} + 2\mathbf{W}^{(1)d}(\mathbf{q}_\lambda)\cdot\boldsymbol{\nabla}_{\mathbf{R}_\lambda} + \mathbf{W}^{(2)d}(\mathbf{q}_\lambda)\right\} + \left\{\boldsymbol{\varepsilon}^{d}(\mathbf{q}_\lambda) - E\mathbf{I}\right\}\right]\boldsymbol{\chi}^{d}(\mathbf{R}_\lambda) = \mathbf{0} \tag{5.106}$$

In the molecular systems that exhibit a conical intersection for some special geometries between their neighboring adiabatic electronic states, both first-derivative ($\mathbf{W}^{(1)ad}(\mathbf{q}_\lambda)$) and second-derivative ($\mathbf{W}^{(2)ad}(\mathbf{q}_\lambda)$) nonadiabatic coupling terms are singular at those geometries. Even in the cases where singularities are absent, the presence of the gradient term ($\mathbf{W}^{(1)ad}(\mathbf{q}_\lambda)\cdot\boldsymbol{\nabla}_{\mathbf{R}_\lambda}$) in Eq. (5.105) makes its numerical solution inefficient and requires a special treatment of the pole in $\mathbf{W}^{(1)ad}$ at conical intersection geometries. These problems can be avoided by constructing a diabatic representation, in which the coupling terms ($\mathbf{W}^{(1)d}(\mathbf{q}_\lambda)$ and $\mathbf{W}^{(2)d}(\mathbf{q}_\lambda)$) do not contain singularities. If the optimal diabatization procedure is followed [56], the magnitude of $\mathbf{W}^{(1)d}(\mathbf{q}_\lambda)$ over the entire dynamically important internal nuclear configuration space can be minimized. This enables the dropping of the gradient containing term ($\mathbf{W}^{(1)d}(\mathbf{q}_\lambda)\cdot\boldsymbol{\nabla}_{\mathbf{R}_\lambda}$), to a good first approximation, from the diabatic Schrödinger equation and facilitates the use of efficient propagation methods available in the absence of such a gradient term. To test the quality of this approximation, this term can be

reintroduced perturbatively into the scattering equations to assess its effect on the reaction cross sections.

In the adiabatic representation of a system containing singular couplings at the conical intersection geometries, the second-derivative couplings have a second-order pole compared to the first-derivative couplings. In energy units this translates to nuclear wave functions not sampling the conical intersection geometries or their very near vicinity where the second-derivative coupling might still be large. These second-derivative couplings decay faster than the first-derivative ones as we move away from the conical intersection point, and the presence of the first-derivative couplings in the gradient term mentioned above will still make the solution of the adiabatic equations inefficient. A quantum scattering study using both representations can resolve these issues more quantitatively.

Appendix 5.A - Geometric phase boundary conditions for the adiabatic and diabatic nuclear wave function basis sets

Consider a triatomic nuclear geometry described by a point P in the six-dimensional hyperspherical coordinate space $\rho, \theta, \phi_\lambda, a_\lambda, b_\lambda, c_\lambda$. If this point P is taken along a closed loop that encircles a conical intersection geometry, its coordinates change to $\rho, \theta, \phi_\lambda + 2\pi, (\pi + a_\lambda) \bmod 2\pi, \pi - b_\lambda, (\pi - c_\lambda) \bmod 2\pi$. This is called a pseudorotation. The Wigner rotation functions given by Eq. (5.40) undergo the following change upon this pseudorotation:

$$D^{J\Pi}_{M\Omega_\lambda}((\pi + a_\lambda) \bmod 2\pi, \pi - b_\lambda, (\pi - c_\lambda) \bmod 2\pi) = (-1)^\Pi D^{J\Pi}_{M\Omega_\lambda}(a_\lambda, b_\lambda, c_\lambda) \quad (5.107)$$

Since the only other piece of the nuclear wave function that undergoes a change upon this pseudorotation is the $g^{\Pi\Gamma}_{i,n_{i\phi_\lambda},\Omega_\lambda}(\phi_\lambda)$ piece, we can incorporate its effect on Wigner functions mentioned above into boundary conditions on $g^{\Pi\Gamma}_{i,n_{i\phi_\lambda}\Omega_\lambda}(\phi_\lambda)$.

In the absence of a conical intersection, the adiabatic or diabatic nuclear wave functions don't change upon a pseudorotation, as the corresponding electronic wave functions are single-valued. This leads to the following no-geometric-phase (NGP) boundary conditions for the adiabatic and diabatic ϕ_λ functions:

$$g^{ad,\Pi\Gamma}_{i,p_\lambda\Omega_\lambda}(\phi_\lambda + 2\pi) = (-1)^\Pi g^{ad,\Pi\Gamma}_{i,p_\lambda\Omega_\lambda}(\phi_\lambda) \quad (5.108)$$

$$g^{d,\Pi\Gamma}_{i,p_\lambda\Omega_\lambda}(\phi_\lambda + 2\pi) = (-1)^\Pi g^{d,\Pi\Gamma}_{i,p_\lambda\Omega_\lambda}(\phi_\lambda) \quad (5.109)$$

where $i = 1, 2$ and $p_\lambda = n_{i\phi_\lambda}$.

In the presence of a conical intersection, the adiabatic nuclear wave functions change sign upon a pseudorotation [see Eq. (5.24)] leading to the following geometric-phase (GP) boundary condition on adiabatic ϕ_λ functions:

$$g^{ad,\Pi\Gamma}_{i,p_\lambda\Omega_\lambda}(\phi_\lambda + 2\pi) = -(-1)^\Pi g^{ad,\Pi\Gamma}_{i,p_\lambda\Omega_\lambda}(\phi_\lambda) \quad (5.110)$$

The diabatic nuclear wave functions, on the other hand, are constructed such that they don't change upon the pseudorotation leading to the following GP boundary condition for diabatic ϕ_λ functions:

$$g^{d,\Pi\Gamma}_{i,p_\lambda\Omega_\lambda}(\phi_\lambda + 2\pi) = (-1)^{\Pi} g^{d,\Pi\Gamma}_{i,p_\lambda\Omega_\lambda}(\phi_\lambda) \tag{5.111}$$

For H_3 system, which belongs to the P_3 permutation group, in the absence of a conical intersection, the ground ($i = 1$) adiabatic electronic wave function belongs to the A_1 irreducible representation and the first-excited ($i = 2$) one belongs to the A_2 representation of the P_3 group. In the presence of a conical intersection, these adiabatic states belong to the E irreducible representation of the P_3 group. Using projection operators from group theory [93] and symmetry operations of this P_3 group, different ϕ_λ functions can be obtained that belong to A_1, A_2 or E representations and satisfy the boundary conditions given by Eqs. (5.108) through (5.111). These functions are given in Tables 5.I and 5.II for adiabatic basis sets and Tables 5.I and 5.III for diabatic basis sets for different choices of Π and Ω_λ quantum numbers.

Table 5.I: Adiabatic ($g^{ad,\Pi\Gamma}_{i,p_\lambda\Omega_\lambda}$) and diabatic ($g^{d,\Pi\Gamma}_{i,p_\lambda\Omega_\lambda}$) basis sets in ϕ_λ for P_3 permutation group in the absence of a conical intersection[a]

Ω_λ	Γ	$g^{ad,0\Gamma}_{1,p_\lambda\Omega_\lambda}$ or $g^{d,0\Gamma}_{1,p_\lambda\Omega_\lambda}$	$g^{ad,1\Gamma}_{1,p_\lambda\Omega_\lambda}$ or $g^{d,1\Gamma}_{1,p_\lambda\Omega_\lambda}$
Even	A_1	$\cos[3p_\lambda\phi_\lambda]$	$\cos[(3p_\lambda+3/2)\phi_\lambda]$
	A_2	$\sin[3p_\lambda\phi_\lambda]$	$\sin[(3p_\lambda+3/2)\phi_\lambda]$
	E	$\cos[(3p_\lambda\pm1)\phi_\lambda]$	$\cos[(3p_\lambda\pm1/2)\phi_\lambda]$
Odd	A_1	$\sin[3p_\lambda\phi_\lambda]$	$\sin[(3p_\lambda+3/2)\phi_\lambda]$
	A_2	$\cos[3p_\lambda\phi_\lambda]$	$\cos[(3p_\lambda+3/2)\phi_\lambda]$
	E	$\sin[(3p_\lambda\pm1)\phi_\lambda]$	$\sin[(3p_\lambda\pm1/2)\phi_\lambda]$

Ω_λ	Γ	$g^{ad,0\Gamma}_{2,p_\lambda\Omega_\lambda}$ or $g^{d,0\Gamma}_{2,p_\lambda\Omega_\lambda}$	$g^{ad,1\Gamma}_{2,p_\lambda\Omega_\lambda}$ or $g^{d,1\Gamma}_{2,p_\lambda\Omega_\lambda}$
Even	A_1	$\sin[3p_\lambda\phi_\lambda]$	$\sin[(3p_\lambda+3/2)\phi_\lambda]$
	A_2	$\cos[3p_\lambda\phi_\lambda]$	$\cos[(3p_\lambda+3/2)\phi_\lambda]$
	E	$\sin[(3p_\lambda\pm1)\phi_\lambda]$	$\sin[(3p_\lambda\pm1/2)\phi_\lambda]$
Odd	A_1	$\cos[3p_\lambda\phi_\lambda]$	$\cos[(3p_\lambda+3/2)\phi_\lambda]$
	A_2	$\sin[3p_\lambda\phi_\lambda]$	$\sin[(3p_\lambda+3/2)\phi_\lambda]$
	E	$\cos[(3p_\lambda\pm1)\phi_\lambda]$	$\cos[(3p_\lambda\pm1/2)\phi_\lambda]$

[a] $p_\lambda \geq 0$, $3p_\lambda - 1 > 0$ and $3p_\lambda - 1/2 > 0$

Table 5.II: Adiabatic basis sets $g^{ad,\Pi\Gamma}_{i,p_\lambda\Omega_\lambda}$ $(i = 1, 2)$ in ϕ_λ for P_3 permutation group in the presence of a conical intersection[b]

Ω_λ	Γ	$g^{ad,0\Gamma}_{1,p_\lambda\Omega_\lambda}$	$g^{ad,1\Gamma}_{1,p_\lambda\Omega_\lambda}$
Even	A_1	$\cos[(3p_\lambda + 3/2)\phi_\lambda]$	$\cos(3p_\lambda\phi_\lambda)$
	A_2	$\sin[(3p_\lambda + 3/2)\phi_\lambda]$	$\sin(3p_\lambda\phi_\lambda)$
	E	$\cos[(3p_\lambda \pm 1/2)\phi_\lambda]$	$\cos[(3p_\lambda \pm 1)\phi_\lambda]$
Odd	A_1	$\sin[(3p_\lambda + 3/2)\phi_\lambda]$	$\sin(3p_\lambda\phi_\lambda)$
	A_2	$\cos[(3p_\lambda + 3/2)\phi_\lambda]$	$\cos(3p_\lambda\phi_\lambda)$
	E	$\sin[(3p_\lambda \pm 1/2)\phi_\lambda]$	$\sin[(3p_\lambda \pm 1)\phi_\lambda]$

Ω_λ	Γ	$g^{ad,0\Gamma}_{2,p_\lambda\Omega_\lambda}$	$g^{ad,1\Gamma}_{2,p_\lambda\Omega_\lambda}$
Even	A_1	$\sin[(3p_\lambda + 3/2)\phi_\lambda]$	$\sin(3p_\lambda\phi_\lambda)$
	A_2	$\cos[(3p_\lambda + 3/2)\phi_\lambda]$	$\cos(3p_\lambda\phi_\lambda)$
	E	$\sin[(3p_\lambda \pm 1/2)\phi_\lambda]$	$\sin[(3p_\lambda \pm 1)\phi_\lambda]$
Odd	A_1	$\cos[(3p_\lambda + 3/2)\phi_\lambda]$	$\cos(3p_\lambda\phi_\lambda)$
	A_2	$\sin[(3p_\lambda + 3/2)\phi_\lambda]$	$\sin(3p_\lambda\phi_\lambda)$
	E	$\cos[(3p_\lambda \pm 1/2)\phi_\lambda]$	$\cos[(3p_\lambda \pm 1)\phi_\lambda]$

[b] $p_\lambda \geq 0$, $3p_\lambda - 1 > 0$ and $3p_\lambda - 1/2 > 0$

Table 5.III: Diabatic basis sets $g^{d,\Pi\Gamma}_{i,p_\lambda\Omega_\lambda}$ in ϕ_λ for P_3 group in the presence of a conical intersection[c]

Ω_λ	Γ	$g^{d,0\Gamma}_{1,p_\lambda\Omega_\lambda}$	$g^{d,1\Gamma}_{1,p_\lambda\Omega_\lambda}$
Even	A_1	$\cos[(3p_\lambda+1)\phi_\lambda]$	$\cos[(3p_\lambda-1/2)\phi_\lambda]$
	A_2	$\sin[(3p_\lambda+2)\phi_\lambda]$	$\sin[(3p_\lambda+1/2)\phi_\lambda]$
	E	$\cos[\{(3p_\lambda+1)\pm 1\}\phi_\lambda]$	$\cos[\{(3p_\lambda+1)\pm 1/2\}\phi_\lambda]$
Odd	A_1	$\sin[(3p_\lambda+1)\phi_\lambda]$	$\sin[(3p_\lambda-1/2)\phi_\lambda]$
	A_2	$\cos[(3p_\lambda+2)\phi_\lambda]$	$\cos[(3p_\lambda+1/2)\phi_\lambda]$
	E	$\sin[\{(3p_\lambda+1)\pm 1\}\phi_\lambda]$	$\sin[\{(3p_\lambda+1)\pm 1/2\}\phi_\lambda]$

Ω_λ	Γ	$g^{d,0\Gamma}_{2,p_\lambda\Omega_\lambda}$	$g^{d,1\Gamma}_{2,p_\lambda\Omega_\lambda}$
Even	A_1	$\sin[(3p_\lambda+1)\phi_\lambda]$	$\sin[(3p_\lambda-1/2)\phi_\lambda]$
	A_2	$\cos[(3p_\lambda+2)\phi_\lambda]$	$\cos[(3p_\lambda+1/2)\phi_\lambda]$
	E	$\sin[\{(3p_\lambda+1)\pm 1\}\phi_\lambda]$	$\sin[\{(3p_\lambda+1)\pm 1/2\}\phi_\lambda]$
Odd	A_1	$\cos[(3p_\lambda+1)\phi_\lambda]$	$\cos[(3p_\lambda-1/2)\phi_\lambda]$
	A_2	$\sin[(3p_\lambda+2)\phi_\lambda]$	$\sin[(3p_\lambda+1/2)\phi_\lambda]$
	E	$\cos[\{(3p_\lambda+1)\pm 1\}\phi_\lambda]$	$\cos[\{(3p_\lambda+1)\pm 1/2\}\phi_\lambda]$

[c] $p_\lambda \geq 0$ and $3p_\lambda - 1/2 > 0$

Bibliography

[1] M. Born and J. R. Oppenheimer, Ann. Phys. (Leipzig) **84**, 457 (1927).

[2] M. Born, Nachr. Akad. Wiss. Gött. Math.-Phys. Kl. Article No. 6, 1 (1951).

[3] M. Born and K. Huang, *Dynamical Theory of Crystal Lattices* (Oxford University Press, Oxford, 1954), pp. 166-177 and 402-407.

[4] *The Role of Degenerate States in Chemistry: A Special Volume of Advances in Chemical Physics*, eds. M. Baer and G. D. Billing (Wiley-Interscience, New York, 2002), Vol. 124.

[5] G. Herzberg and H. C. Longuet-Higgins, Discussion Faraday Soc. **35**, 77 (1963).

[6] H. C. Longuet-Higgins, Proc. R. Soc. London A **344**, 147 (1975).

[7] H. C. Longuet-Higgins, Adv. Spectrosc. **2**, 429 (1961).

[8] C. A. Mead and D. G. Truhlar, J. Chem. Phys. **70**, 2284 (1979).

[9] C. A. Mead, Chem. Phys. **49**, 23 (1980).

[10] M. V. Berry, Proc. Roy. Soc. London, Ser. A **392**, 45 (1984).

[11] A. Kuppermann, in *Dynamics of Molecules and Chemical Reactions*, edited by R. E. Wyatt and J. Z. H. Zhang (Marcel Dekker, New York, 1996), pp. 411-472.

[12] *Theory of Chemical Reaction Dynamics* Vols. I and II, edited by M. Baer (CRC Press, Boca Raton (Florida), 1985).

[13] *Dynamics of Molecules and Chemical Reactions*, edited by R. E. Wyatt and J. Z. H. Zhang (Marcel Dekker, New York, 1996).

[14] G. Nyman and H.-G. Yu, Rep. Prog. Phys. **63**, 1001 (2000).

[15] J. Z. H. Zhang, J. Q. Dai, and W. Zhu, J. Phys. Chem. A **101**, 2746 (1997).

[16] S. K. Pogrebnya, J. Palma, D. C. Clary, and J. Echave, Phys. Chem. Chem. Phys. **2**, 693 (2000).

[17] D. H. Zhang, M. A. Collins and S. Y. Lee, Science **290**, 961 (2000).

[18] Y.-S. M. Wu, A. Kuppermann, and B. Lepetit, Chem. Phys. Lett. **186**, 319 (1991).

[19] Y.-S. M. Wu and A. Kuppermann, Chem. Phys. Lett. **201**, 178 (1993).

[20] A. Kuppermann and Y.-S. M. Wu, Chem. Phys. Lett. **205**, 577 (1993).

[21] Y.-S. M. Wu and A. Kuppermann, Chem. Phys. Lett. **235**, 105 (1995).

[22] A. Kuppermann and Y.-S. M. Wu, Chem. Phys. Lett. **241**, 229 (1995).

[23] B. K. Kendrick, J. Chem. Phys. **112**, 5679 (2000); **114**, 4335 (2001) (E).

[24] A. Kuppermann and Y.-S. M. Wu, Chem. Phys. Lett. **349**, 537 (2001).

[25] D. A. V. Kliner, K. D. Rinen, and R. N. Zare, Chem. Phys. Lett. **166**, 107 (1990).

[26] D. A. V. Kliner, D. E. Adelman and R. N. Zare, J. Chem. Phys. **95**, 1648 (1991).

[27] D. Neuhauser, R. S. Judson, D. J. Kouri, D. E. Adelman, N. E. Shafer, D. A. V. Kliner and R. N. Zare, Science **257**, 519 (1992).

[28] D. E. Adelman, N. E. Shafer, D. A. V. Kliner and R. N. Zare, J. Chem. Phys. **97**, 7323 (1992).

[29] F. Fernandez-Alonso and R. N. Zare, Ann. Rev. Phys. Chem. **53**, 67 (2002).

[30] M. Gilbert and M. Baer, J. Phys. Chem. **98**, 12822 (1994).

[31] G. C. Schatz, J. Phys. Chem. **99**, 7522 (1995).

[32] C. S. Maierle, G. C. Schatz, M. S. Gordon, P. McCabe, and J. N. L. Connor, J. Chem. Soc. Faraday Trans. **93**, 709 (1997).

[33] G. C. Schatz, P. McCabe, and J. N. L. Connor, Faraday Discuss. **110**, 139 (1997).

[34] A. J. Dobbyn, J. N. L. Connor, N. A. Besley, P. J. Knowles, and G. C. Schatz, Phys. Chem. Chem. Phys. **2**, 549 (2000).

[35] T. W. J. Whiteley, A. J. Dobbyn, J. N. L. Connor and G. C. Schatz, Phys. Chem. Chem. Phys. **2**, 549 (2000).

[36] M. H. Alexander, H.-J. Werner, and D. E. Manolopoulos, J. Chem. Phys. **109**, 5710 (1998).

[37] M. H. Alexander, D. E. Manolopoulos and H.-J. Werner, J. Chem. Phys. **113**, 11084 (2000).

[38] T. Takayanagi and Y. Kurosaki, J. Chem. Phys. **113**, 7158 (2000).

[39] V. Aquilanti, S. Cavalli, D. De Fazio, and A. Volpi, Int. J. Quant. Chem. **85**, 368 (2001).

[40] H. Flöthmann, C. Beck, R. Schinke, C. Woywod and W. Domcke, J. Chem. Phys. **107**, 7296 (1997).

[41] D. Simah, B. Hartke and H.-J. Werner, J. Chem. Phys. **111**, 4523 (1999).

[42] S. Mahapatra, H. Köppel and L. S. Cederbaum, J. Phys. Chem. A **105**, 2321 (2001).

[43] B. H. Lengsfield and D.R. Yarkony, in State-selected and State-to-State Ion-Molecule Reaction Dynamics: Part 2 Theory, Vol. 82, edited by M. Baer and C.-Y. Ng (Wiley, New York, 1992), pp. 1-71.

[44] M. Baer, Phys. Rep. **358**, 75 (2002).

[45] T. Pacher, L. S. Cederbaum, and H. Köppel, J. Chem. Phys. **89**, 7367 (1988).

[46] T. Pacher, C. A. Mead, L. S. Cederbaum, and H. Köppel, J. Chem. Phys. **91**, 7057 (1989).

[47] V. Sidis, in *State-selected and State-to-State Ion-Molecule Reaction Dynamics*: Part 2 Theory, Vol. 82, edited by M. Baer and C.-Y. Ng (Wiley, New York, 1992), pp. 73-134.

[48] M. Baer and R. Englman, Mol. Phys. **75**, 293 (1992).

[49] K. Ruedenberg and G. J. Atchity, J. Chem. Phys. **99**, 3799 (1993).

[50] M. Baer and R. Englman, Chem. Phys. Lett. **265** 105 (1997).

[51] M. Baer, J. Chem. Phys. **107** 2694 (1997).

[52] B. K. Kendrick, C. A. Mead, and D. G. Truhlar, J. Chem. Phys. **110**, 7594 (1999).

[53] M. Baer, R. Englman, and A. J. C. Varandas, Mol. Phys. **97**, 1185 (1999).

[54] A. Thiel and H. Köppel, J. Chem. Phys. **110**, 9371 (1999).

[55] D. R. Yarkony, J. Chem. Phys. **112**, 2111 (2000).

[56] R. Abrol and A. Kuppermann, J. Chem. Phys. **116**, 1035 (2002).

[57] H. Nakamura and D. G. Truhlar, J. Chem. Phys. **117**, 5576 (2002).

[58] A. Kuppermann and R. Abrol, in Ref. [4], pp. 283-322.

[59] P. Siegbahn and B. Liu, J. Chem. Phys. **68**, 2457 (1978).

[60] D. G. Truhlar and C. J. Horowitz, **68**, 2466 (1978); **71**, 1514 (1979) (E).

[61] A. J. C. Varandas, F. B. Brown, C. A. Mead, D. G. Truhlar, and N. C. Blais, J. Chem. Phys. **86**, 6258 (1987).

[62] A. I. Boothroyd, W. J. Keogh, P. G. Martin, and M. R. Peterson, J. Chem. Phys. **104**, 7139 (1996).

[63] Y.-S. M. Wu, A. Kuppermann, and J. B. Anderson, Phys. Chem. Chem. Phys. **1**, 929 (1999).

[64] S. L. Mielke, B. C. Garrett, and K. A. Peterson, J. Chem. Phys. **116**, 4142 (2002).

[65] R. Abrol, A. Shaw, A. Kuppermann and D. R. Yarkony, J. Chem. Phys. **115**, 4640 (2001).

[66] L. M. Delves, Nucl. Phys. **9**, 391 (1959).

[67] L. M. Delves, Nucl. Phys. **20**, 275 (1960).

[68] A. Kuppermann and P. G. Hipes, J. Chem. Phys. **84**, 5962 (1986).

[69] P. G. Hipes and A. Kuppermann, Chem. Phys. Lett. **133**, 1 (1987).

[70] S. A. Cuccaro, P. G. Hipes and A. Kuppermann, Chem. Phys. Lett. **154**, 155 (1989).

[71] S. A. Cuccaro, P. G. Hipes and A. Kuppermann, Chem. Phys. Lett. **157**, 440 (1989).

[72] J. M. Launay and M. Le Dourneuf, Chem. Phys. Lett. **163**, 178 (1989).

[73] Y.-S. M. Wu, S. A. Cuccaro, P. G. Hipes and A. Kuppermann, Chem. Phys. Lett. **168**, 429 (1990).

[74] A. Kuppermann, Chem. Phys. Lett. **32**, 374 (1975).

[75] A. Kuppermann, in *Advances in Molecular Vibrations and Collision Dynamics*, edited by J. Bowman (JAI Press, Greenwich, CT, 1994), Vol. 2B, pp. 117-186.

[76] A. S. Davydov, *Quantum Mechanics, 2nd Ed.*, Pergamon Press, Oxford, UK, 1976, p. 151.

[77] R. J. Buenker, G. Hirsch, S. D. Peyerimhoff, P. J. Bruna, J. Römelt, M. Bettendorff, and C. Petrongolo, in *Current Aspects of Quantum Chemistry*, Elsevier, New York, 1981, pp. 81-97.

[78] M. Desouter-Lecomte, C. Galloy, J. C. Lorquet, and M. V. Pires, J. Chem. Phys. **71**, 3661 (1979).

[79] B. H. Lengsfield, P. Saxe, and D. R. Yarkony, J. Chem. Phys. **81**, 4549 (1984).

[80] P. Saxe, B. H. Lengsfield, and D. R. Yarkony, Chem. Phys. Lett. **113**, 159 (1985).

[81] B. H. Lengsfield, and D. R. Yarkony, J. Chem. Phys. **84**, 348 (1986).

[82] J. O. Jensen and D. R. Yarkony, J. Chem. Phys. **89**, 3853 (1988).

[83] B. Kendrick and R. T. Pack, J. Chem. Phys. **104**, 7475 (1996).

[84] S. Garashchuk, J. C. Light and V. A. Rassolov, Chem. Phys. Lett. **333**, 459 (2001).

[85] D. Wang and A. Kuppermann, J. Chem. Phys. **115**, 9184 (2001).

[86] D. Wang and A. Kuppermann, unpublished results.

[87] M. Abramowitz and I. A. Stegun, *Handbook of Mathematical Functions* (Dover, New York, 1970), pp. 773-802.

[88] R. G. Sadygov and D. R. Yarkony, J. Chem. Phys. **109**, 20 (1998).

[89] F. T. Smith, Phys. Rev. **179**, 111 (1969).

[90] B. R. Johnson, J. Comput. Phys. **13**, 445 (1973).

[91] D. E. Manolopoulos, J. Chem. Phys. **85**, 6425 (1986).

[92] D. E. Manolopoulos, M. J. Jamieson, and A. D. Pradhan, J. Comput. Phys. **105**, 169 (1993).

[93] M. Hamermesh, *Group Theory and its Applications to Physical Problems* (Addison-Wesley, Reading, MA, 1962), pp. 113 and 182.

Chapter 6 Summary and conclusions

A general Born-Huang treatment of quantum dynamics for multiple interacting electronic states is considered for a polyatomic system. In the adiabatic representation, the n-electronic-state nuclear motion Schrödinger equation is presented along with the structure of the first-derivative and second-derivative nonadiabatic coupling matrices. In this representation, the geometric phase must be introduced separately and the presence of nonadiabatic couplings introduces numerical inefficiencies for the solution of that Schrödinger equation, even if those couplings are not singular at electronically-degenerate nuclear geometries. This makes it desirable to go to a diabatic representation, which incorporates automatically the geometric phase effect. In addition, appropriate boundary conditions can be chosen so as to impart desired properties on the diabatic version of the n-electronic-state nuclear motion Schrödinger equation. One such property is the minimization of the magnitude of the nonadiabatic couplings. If a complete (infinite) set of adiabatic electronic wave functions is used in a Born-Huang expansion of the system's electronuclear wave function (which is not possible in practice), this term vanishes automatically. In practice, a finite number n of adiabatic states are included for the treatment of chemical reactions. For this case, a residual coupling term survives in the diabatic representation as a *nonremovable* coupling term, which however does not diverge at conical intersection geometries. A general method is presented that minimizes this *nonremovable* coupling term over the entire internal nuclear configuration space, leading to an optimal diabatization. As a very good first approximation, this term can be ignored in the diabatic nuclear motion Schrödinger equation. Since that term is obtained as a part of the diabatization process, its effect on the reaction cross sections can be studied subsequently by perturbative or other methods. This treatment is then applied to the benchmark H_3 system in the presence of its lowest two adiabatic electronic states

$1\ ^2A'$ and $2\ ^2A'$.

The results of accurate calculations of the first-derivative coupling vector between these two states of H_3 are presented. These calculations are performed over the entire internal nuclear configuration space of this system of possible importance for its reactive scattering, up to total energies of about 5 eV. In addition, a fit (DSP) to its ground and first-excited electronic energies obtained by *ab initio* methods is given. The couplings are found to be non-negligible even away from the conical intersection between these states, and can be used to obtain their longitudinal (removable) and transverse (nonremovable) parts. We have also compared our results with the analytical ones, obtained by a double many-body expansion (DMBE) method [Varandas et al. *J. Chem. Phys.* **86**, 6258 (1987)], which have built into them the right physical behavior in the vicinity of the conical intersection geometries. The DMBE ground-state electronic energies agree well with the DSP fit to the *ab initio* energies, while the first-excited ones show some significant differences. The DMBE couplings are purely longitudinal and hence fully *removable* upon an adiabatic to diabatic transformation. They compare well with the *ab initio* ones only in the neighborhood of the conical intersection, as expected.

We have also investigated the line integrals (along closed paths around the conical intersection between these electronic states) of the *ab initio* couplings over the entire nuclear configuration space considered. We found large deviations of the topological phase $\Phi_{\mathsf{T}}(\rho,\theta)$ from π suggesting the existence of conical intersections between the $2\ ^2A'$ and $3\ ^2A'$ states and/or the presence of non-negligible derivative couplings involving excluded electronic states. Electronic energy calculations for the $3\ ^2A'$ state and its first-derivative couplings with the $2\ ^2A'$ state could lead to a quantitative correlation between the topological phase between the $1\ ^2A'$ and $2\ ^2A'$ states and the locus of possible intersection geometries between the $2\ ^2A'$ and $3\ ^2A'$ states.

We have reported the first global optimal diabatic basis, obtained from accurate *ab initio* first-derivative couplings between the $1\ ^2A'$ and $2\ ^2A'$ adiabatic PESs of H_3. These couplings were used in a three-dimensional Poisson equation for the dia-

batization angle, over the entire dynamically important domain U of internal nuclear configuration space, together with a combination of Neumann and Dirichlet boundary conditions. These conditions were chosen so as to minimize the average value of the magnitude of the transverse (*nonremovable*) part of the first-derivative coupling vector over that domain. Since that is the only part of that vector that appears in the diabatic nuclear motion Schrödinger equation, the result is an optimal diabatic basis. The minimization was measured quantitatively by solving the Poisson equation with only Dirichlet boundary conditions and comparing the average magnitude of the transverse coupling vector obtained from this solution with that obtained from the optimal solution. The transverse vector was found to be about 80 % smaller than the original first-derivative vector, indicating that the minimization provided by the Neumann boundary conditions used in the latter was very significant.

The diabatization angle was calculated over the full U domain. The resulting diagonal and off-diagonal components of the diabatic potential energy matrix were obtained and their importance for the reactive scattering process was discussed. The longitudinal and transverse parts of the full first-derivative coupling vector were calculated and a detailed analysis of their relative magnitudes in the dynamically important regions of nuclear configuration space was presented. In a first but good approximation to the nuclear motion diabatic scattering equations, the transverse part can be neglected (as well as the small second-derivative diabatic coupling matrix correction to the diabatic PESs). Since, however, it is now known, it can be introduced perturbatively at a later stage to assess its importance for the two-electronic-state scattering calculations. It is expected to have only a small effect on the scattering dynamics, but just how small remains to be determined.

A quantum scattering formalism for a triatomic reaction on two interacting electronic states is presented in both adiabatic and diabatic representations. Advantages and disadvantages of the two approaches are discussed and compared. This formalism is an extension of the time-independent coupled-channel hyperspherical method for one adiabatic electronic state. The extended formalism involves obtaining adia-

batic or diabatic local hyperspherical surface functions (LHSFs) for each hyperradial shell. The partial wave adiabatic or diabatic nuclear wave functions are expanded in terms of these surface functions and the coefficients of the expansion propagated to an asymptotic value of the hyperradius. Here the adiabatic nuclear wave function is directly matched to asymptotic diatom rovibrational states, whereas the diabatic nuclear wave function needs to be first transformed to its adiabatic counterpart and then matched to asymptotic diatom rovibrational states. This asymptotic analysis of the nuclear wave function gives the partial wave scattering matrices needed to obtain the desired differential and integral cross sections. This formalism enables the calculation of these cross sections over a broader energy range that sample the first-excited adiabatic electronic sheet in particular. It also allows for a comparison of the cross sections obtained using this two-electronic-state formalism with those obtained using only the adiabatic ground electronic state (with the geometric phase included), which should provide an estimation of the energy range of validity of the one-electronic-state Born-Oppenheimer approximation.